4-25-2012 12:00 AM

Structural Motifs of Novel Metallothionein Proteins

Duncan E K Sutherland
The University of Western Ontario

Supervisor
Dr. Martin J. Stillman
The University of Western Ontario

Graduate Program in Chemistry
A thesis submitted in partial fulfillment of the requirements for the degree in Doctor of Philosophy

Structural Motifs of Novel Metallothionein Proteins

(Spine title: Structural Motifs of Metallothionein)

(Thesis format: Integrated-Article)

By

Duncan Ewan Keith Sutherland

Graduate Program in Chemistry

Submitted in partial fulfillment of the requirements for the degree of
Doctor of Philosophy

School of Graduate and Postdoctoral Studies
The University *of* Western Ontario
London, Ontario, Canada
April, 2012

School of Graduate and Postdoctoral Studies

The University *of* Western Ontario

CERTIFICATE OF EXAMINATION

Supervisor	Examiners
_____	_____
Dr. Martin Stillman	Dr. Yining Huang
	_____
	Dr. John Honek
	_____
	Dr. Ken K.-C. Yeung
	_____
	Dr. Graeme Hunter

The thesis by

Duncan Ewan Keith Sutherland

entitled:

Structural Motifs of Novel Metallothionein Proteins

is accepted in partial fulfillment of the requirements for the degree of

Doctor of Philosophy

Date_____ _____

Chair of the Thesis Examination Board

ABSTRACT

Metallothioneins (MT) are a family of small cysteine rich proteins, which since their discovery in 1957, have been implicated in a range of roles including toxic metal detoxification, protection against oxidative stress, and as a metallochaperone involved in the homeostasis of both essential zinc and copper. The most well studied member of the family is the mammalian MT, which consists of two domains: a β-domain with 9 cysteine residues, which sequesters 3 Cd^{2+}/Zn^{2+} or 6 Cu^{+} ions, and an α-domain with 11 cysteine residues, which sequesters 4 Cd^{2+}/Zn^{2+} or 6 Cu^{+} ions. Despite over half a century of research, the exact functions of MT are still unknown but must be related to its metalation status. Several areas that are not well studied, but that could lead to the assignment of function include 1) the determination of the exact mechanism of metalation and the structural characterization of 2) submetalated and 3) supermetalated forms of MT. Together these three areas of study will provide a more comprehensive understanding of the potential metalation chemistries of MT *in vivo*.

Towards this goal, the following thesis presents electrospray ionization mass spectrometric (ESI MS) data showing that the mechanism of metalation of MT is noncooperative. That is metalation events occur independently of each other, allowing for partially metalated species to exist *in vivo*. Further metalation studies using the isolated domains of MT as metal ion competitors against the full MT protein have yielded evidence that a new Zn_5-MT exists in which both domains 'coalesce.' In addition, NMR and CD spectroscopy, coupled with ESI mass spectrometric data, have shown the existence of a new 'supermetalated' Cd_8-MT, which also results in a 'coalescence' of both domains. Taken together these results indicate that 1) partially metalated forms of the protein are in fact stable and 2) the traditional structural view of MT, where both domains act in isolation, is in fact the exceptional case and that under conditions of metal ion deficiency and excess, both domains interact with each other.

Keywords: Metallothionein, cadmium, zinc, mechanism of metalation, competitive metalation, metal-induced folding, supermetalated metallothionein, ESI mass spectrometry, NMR spectroscopy, CD spectroscopy

CO-AUTHORSHIP STATEMENT

The following thesis contains material from previously published manuscripts. Dr. Martin Stillman is coauthor of all the published papers and was responsible for supervising Duncan Sutherland. For all chapters in which a portion has been published, Duncan Sutherland wrote the first draft of the paper. Dr. Martin Stillman was involved in all levels of publication having major roles in both editing and revising the published manuscripts.

For Chapter 2 and 3, Duncan Sutherland was solely responsible for acquiring all cadmium metalation data. Ms. Kelly Summers is gratefully acknowledged for acquiring zinc metalation data (Chapter 4), as well as her help with the preparation of related figures. Further, Duncan Sutherland was responsible for all experimental considerations and training of Ms. Kelly Summers, who acquired the ESI MS data and was a coauthor of the manuscript published.

For Chapter 5 and 6, Dr. Mathew Willans (NMR facility manager, UWO) is gratefully acknowledged for his role in determining the parameters for and helping to acquire data from ^{113}cadmium-NMR samples. For his contribution, Dr. Mathew Willans is listed as a coauthor on all associated manuscripts. Duncan Sutherland was responsible for all sample preparation, interpretation of data, figure development and writing of manuscripts.

ACKNOWLEDGEMENTS

I would like to acknowledge my parents, Ian and Katherine Sutherland, as well as my brother, Thomas Sutherland, for their support of my education (both graduate and undergraduate). Without their unwaivering encouragement, none of this would have been possible.

I would also like to thank members of the Stillman bioinorganic group, both past and present for being exceptional labmates. Specifically Thanh Ngu for being my role model in graduate school, Michael Tiedemann for being a great friend and as a great resource in both undergraduate and graduate school, Kelly Summers for her collaborative work, and finally Tyler Pinter for his novel experimental approach and unique mechanical abilities.

Many thanks are also given to the staff of the Electronic Shop (John Vanstone, Warren Lindsay, Barakat Misk and Jon Aukema) and the Chemstore staff (Marylou Hart, Sherrie McPhee and DonYakobchuk). I am greatly indebted to Doug Hairsine for training and advice on the ESI MS and the Department of Chemistry (and its entire staff) for my experience as a both an undergraduate and gradute student.

Last but not least, I would like to thank Professor Martin Stillman for his support of my research efforts and the opportunities he gave me to collaborate with other research groups, involve myself as a volunteer for a series of international chemistry conferences (CanBIC-1, -2 and -3) and many international conference opportunities.

TABLE OF CONTENTS

LIST OF FIGURES

LIST OF TABLES

LIST OF ABBREVIATIONS AND DEFINITIONS

AAS	Atomic absorption spectroscopy
α–hMT	α domain of human metallothionein 1a
βh-MT	β domain of human metallothionein 1a
βα–hMT	two-domain βα human metallothionein 1a
apo-MT	metal-free metallothionein
holo-MT	fully metalated or native metallothionein
CD	circular dichroism
CRM	charged residue model
DNA	deoxyribonucleic acid
ε	molar absorptivity or molar extinction coefficient
E. coli	*Escherichia coli*
EPR	Electron paramagnetic resonance spectroscopy
ESI	electrospray ionization
EXAFS	Extended X-ray absorption fine structure
in vitro	in an aqueous environment in a test tube
in vivo	in a biological or cellular environment
IPTG	isopropyl-β-D-thiogalactoside
K_F	association constant
LMCT	Ligand-to-metal charge transfer band
m/z	mass-to-charge ratio
Magic Number	the stoichiometric ratios that appear to represent stable saturated clusters

MD	molecular dynamics
MM	molecular mechanics
MM3/MD	molecular dynamics with energy minimization by molecular mechanics with Allinger's MM3 force field
mRNA	messenger ribonucleic acid
MS	mass spectrometry
MT	metallothionein
MT-1a	metallothionein isoform 1a
MTF-1	Metal regulatory transcription factor 1
NMR	nuclear magnetic resonance spectroscopy
NOE	Nuclear Overhauser Effect
pET	plasmid for expression by T7 RNA polymerase
rfMT	recombinant *Fucus vesiculosus* metallothionein
rhMT	recombinant human metallothionein
rlMT	rabbit liver metallothionein
TOF	time-of-flight
Tris	tris(hydroxymethyl)aminomethane buffer
XANES	X-ray absorption near edge structure
XAS	X-ray absorption spectroscopy

Chapter 1. Introduction[1]

1.1 Metallothionein

Metallothioneins (MTs) are a group of metalloproteins characterized by their small size (~6,000 – 7,000 Da), high cysteine content, an absence of disulfide bonds, and a lack of aromatic amino acids (*1*). Metallothioneins bind strongly to the monovalent Group 11 and the divalent Group 12, d^{10} metals. The effect of binding to these soft Group 11 and 12 metals on the cysteinyl thiols is to reduce the pK_a of the cysteines by up 6 orders of magnitude. As a consequence, the cysteine sulphurs bind to the metals as thiolates. Key to the discussion is that the formation of these metal-thiolate (cysteine) bonds dominates the secondary structure of the protein, so that we may describe the secondary and tertiary structures present in the native metalated protein as arising primarily as a result of metal-induced folding.

MT was initially isolated by Margoshes and Vallee in 1957 from samples of horse kidney cortex that through progressive purification showed an increase in relative cadmium content (*2*). The protein was named metallothionein for its unusually high metal (metallo) and sulphur (thiol) content (*3*). Since its discovery, members of the MT family have been isolated from a wide array of sources including all animal phyla, fungi, plants, as well as cyanobacteria (*4*). Owing to both the high cysteine content of these proteins (~30%) and their presence in all organisms, MT is implicated in a number of physiological processes. The most commonly cited processes are metal ion homeostasis, toxic metal detoxification, and protection against oxidative stress.

Mammalian MTs comprises 20 cysteine residues that act to encapsulate two metal-thiolate cores (β and α) using a combination of bridging and terminal thiolates (where terminal defines coordination to only a single metal ion) from the cysteinyl residues (Figure 1-1). The two separate domains form a dumb-bell-like structure in the crystal first described from analysis of the X-ray diffraction data from rat liver MT (*5*). The β-

[1] A version of this work has been published:

domain with 9 cysteine residues is capable of binding 3 Cd^{2+} or Zn^{2+}, or 6 Cu^{+} and an α-domain with 11 cysteine residues capable of binding 4 Cd^{2+} or Zn^{2+}, or 6 Cu^{+}. Molecular modeling and later experimental data from solution studies suggests that the two domains are not isolated but rather somewhat coalesced. MT binds a wide range of metals with similar stoichiometries, but we may consider them not to be 'natural'. We describe these additional binding motifs below. A common thread in the mammalian MTs is, however, the formation of the two metal-thiolate clusters where a mixture of metals can bind in each domain and where the metals in either domain can be different. The question of the extent of domain interaction in the function of MTs is a current topic of intense research.

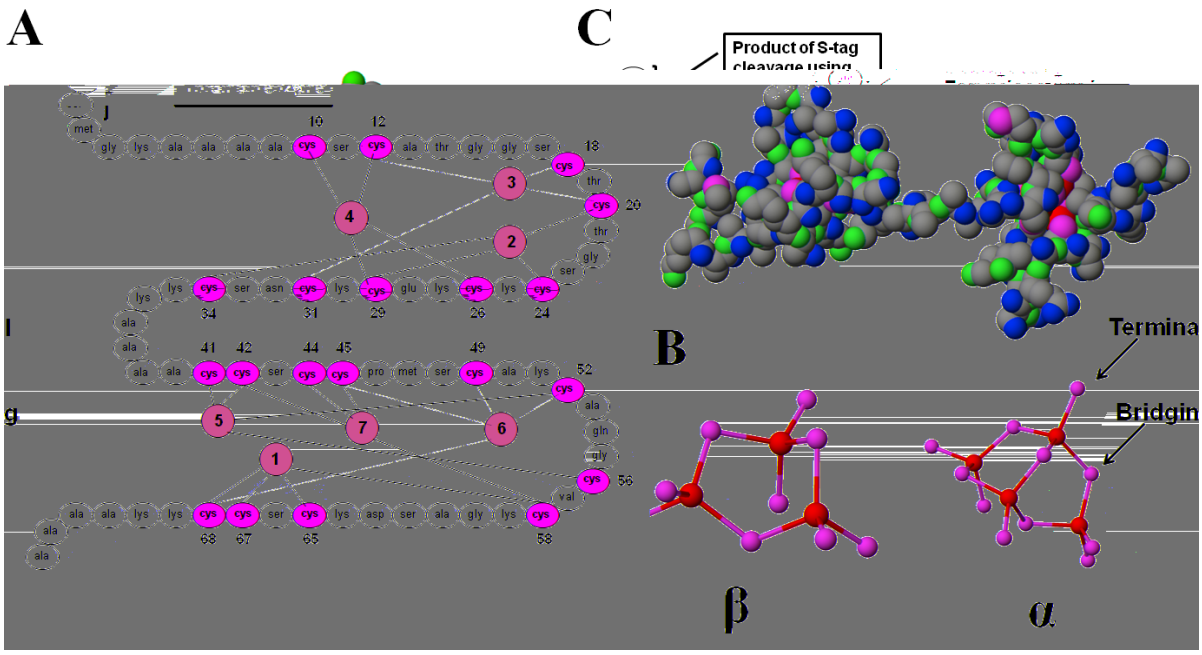

Figure 1-1. Molecular model structure of Cd_7-βα-rhMT. (A) Space filling structure of cadmium metalated recombinant human MT-1a (Cd_7-βα-rhMT 1a) calculated using molecular modeling. The N-terminal β domain is located on the left hand side, while the C-terminal α domain is located on the right-hand side. (B) The cadmium-cysteinyl-thiolate connections, both terminal and bridging, in Cd_7-βα-rhMT 1a are presented as a ball-and-stick model: β domain (left) and α domain (right). The α domain has one bridging and one terminal thiolate labeled to clearly illustrate the different modes of coordination. (C) Connectivity diagram of human metallothionein 1a, which shows that each of the seven cadmium atoms is connected to exactly four cysteine amino acids in a tetrahedral arrangement. In the nomenclature used here, the 'recombinant' source is noted by a prefix of 'r', and the origin of the sequence is indicated by the second prefix, here 'h' for human. Molecular modeling data from Chan *et al.* (6).

The MT family contains a number of isoforms (and subisoforms) where the complement of these is organism dependent. In particular, mammals contain four MT subfamilies that have been proposed to exhibit specific roles (*7*): MT-1 and MT-2 in the liver and kidneys, which are induced by a number of stimuli including metal ions, glucocorticoids, cytokines and oxidative stress (*4*, *8*-*9*), MT-3, primarily found in the central nervous system (*10*), and MT-4, found in certain stratified squamous epithelial tissues (*11*). While a number of stimuli can induce expression of both MT-1 and MT-2, the expression of MT-3 and MT-4 is more strictly controlled. Presumably, differences in expression are the result of both MT-3 and MT-4 having specific biological functions. To support the proposal for specificity of function, disruption of the natural expression of MT-3, through ectopic expression in mice, has been shown to cause pancreatic acinar cell necrosis and death (*12*).

1.2 Function

1.2.1 Metal ion homeostasis

Naturally occurring MTs are usually isolated as either Zn-MT, Cu-MT or as the mixed metal species Zn,Cu-MT and Zn,Cd-MT. In the case of mammals, Zn-MT is the dominant form (*13*), however, Cu-MT has been isolated from several sources including fetal liver MT (*14*-*15*), bovine calf liver MT (*16*), rat kidney (*17*), as well as brain specific MT-3 (*10*). Elevated Cu-MT levels have also been found in patients suffering from Wilson's disease (*18*). While in the case of yeast and fungi, Cu-MT is the dominant species (*19*).

At the cellular level both toxic and nontoxic metals are tightly controlled and estimates of free Cu^{+} and Zn^{2+} suggest that neither is available in the cytosol (*20*-*21*). The absence of freely available Cu^{+} and Zn^{2+} suggests that an organism is able to exist in this state by using metallochaperones to transport these ions in a controlled manner. MT is considered one such metallochaperone, which is capable of transporting essential Zn^{2+} and Cu^{+} to apo-enzymes (*22*-*25*). Indeed metal exchange experiments have been conducted in which Zn^{2+} from Zn_7-βα-MT has been transferred to Zn-dependent enzymes, for example, m-aconitase (*22*), carbonic anhydrase (*23*), and the prototypical transcription factor (*24*),

Gal4. Removal of Zn^{2+} from the zinc finger-containing transcription factor Sp1 demonstrates that MT may also act as a Zn^{2+} acceptor (*25*). It should be noted that zinc fingers are structural motifs that coordinate one or more Zn^{2+} ions to stabilize their protein fold. Thus this natural association of MT with the biologically essential Zn^{2+} and Cu^{+} has suggested that one of the functions of MT is the maintenance of metal ion homeostasis. While metal exchange to apo-enzymes requiring these metals has been reported, no mechanistic details have emerged yet about how the metal transfer takes place.

Support for the role of MT as a metallochaperone is found in the transcription of DNA to RNA, which has been shown to be strongly controlled by exposure to metal ions, for example in yeast (*26-27*), *Drosophila (28)* and mammals (*29-31*). In the case of mammals, of the four isoforms (MT-1 to -4) only two (MT-1 and MT-2) are strongly upregulated by metal ions. Induction of inducible MT isoforms requires both the interaction of a metal response element (MRE) with a metal response element binding transcription factor 1 (MTF-1). MREs are cis-acting DNA sequences necessary and sufficient for metallothionein expression under heavy metal load (*29, 32*). MTF-1 is a zinc binding protein that contains six Cys_2-His_2 zinc fingers, the presence of these zinc fingers, along with differences in their respective affinity, make MTF-1 exquisitely sensitive to changes in the concentration of zinc in a cell (*33-34*). Cell free transcription experiments have shown a number of stresses, including exposure to Cd^{2+}, Cu^{+} and H_2O_2 function by displacing naturally bound Zn^{2+} from MT (*35*). These free Zn^{2+} ions bind to MTF-1 leading to a translocation of MTF-1 from the cytoplasm to the nucleus where the Zn-MTF-1 interacts with MREs leading to upregulation of MT. In this way, MT is capable of countering and deactivating a wide range of insults in order to return an organism to homeostatic balance.

1.2.2 Toxic metal detoxification

The proposed detoxifying properties of MT were inferred from metal analysis of samples isolated from human kidneys (*36*). These samples contained significant amounts of excess Cd^{2+} and some Hg^{2+}, the presence of Hg^{2+} being traced back to the use of therapeutic mercurial diuretics. In addition to Cd^{2+} and Hg^{2+}, MT is generally understood

to coordinate all the group 11 and 12 metals, and is also capable of binding to other metals including: Co^{2+}, Pb^{2+}, $Pt^{2+/4+}$, Fe^{2+}, As^{3+}, Bi^{3+} and Tc^{5+} (*37-41*). The binding affinities of MT for metal ions follows closely with the association constant of metal ions for inorganic thiolate ligands ($Hg^{2+} > Cu^{+} > Cd^{2+} > Zn^{2+}$). Thus MT preferentially coordinates many toxic metals and ultimately this coordination leads to the release of Zn^{2+}, which acts to upregulate the production of MT and returns an organism to homeostatic balance.

The requirement for and the toxicological effects of excess Zn^{2+} have been well documented (*42*). MT knockout studies have highlighted the importance of this protein in the homeostasis of Zn^{2+} (*43*). For example, MT-null mouse pups fed severely deficient Zn^{2+} diets, showed delays in kidney development when compared to wild-type controls. These pups lacked a hepatic reservoir of zinc critical for proper development. On the other hand, MT-null adult mice challenged with increased Zn^{2+} showed a greater incidence of pancreatic acinar cell degeneration. In this case, MT is able to act as a temporary sink to accommodate the influx of Zn^{2+}. These results demonstrate that MT is critical in protecting an organism from the extremes of Zn^{2+} exposure, acting as both a source and a sink for Zn^{2+} during deficiency and excess, respectively.

Copper toxicity is also of considerable interest, because unlike zinc, free copper is able to catalyze the formation of hydroxyl radicals through Haber-Weiss and Fenton reactions (*42*). Significant regulation of copper transport in humans relies on two homologous copper transport proteins: namely, ATP7A and ATP7B (*44*). Mutations to ATP7A result in Menkes disease, where copper accumulates in the kidneys and intestinal wall, while the brain, serum and liver do not receive adequate amounts (*45*). A murine model of Menkes disease involving MT-1 and -2 knockout mice demonstrated that in the absence of inducible MT, knockout mice were more susceptible to copper toxicity (*46*). The second disorder, Wilson's disease, resulting from mutations to ATP7B, is characterized by the accumulation of copper in the liver leading to cellular damage and release of free copper into the blood serum (*44*). Cellular damage is somewhat mitigated by the accumulation of copper in the form of Cu-MT (*18, 47*). In this manner, MT is able to sequester Cu^{+}, and with 20 thiol groups can act as a reducing agent to further protect against oxidative stress (*48-49*).

Chronic cadmium poisoning significantly affects the kidneys. Traditionally, the nephrotoxicity of Cd^{2+} exposure was thought to be the result of a transfer of Cd-MT from the liver to the kidneys with subsequent degradation leading to a high local concentration of Cd^{2+}. Indeed liver transplant studies aimed at monitoring Cd-MT levels have shown a time dependent decrease in Cd-MT present in the liver with concomitant increase of Cd-MT present in the kidneys (*50*). Further complicating the problem, recent studies have demonstrated that MT knockout mice are hypersensitive to Cd^{2+}, while only accumulating 7% Cd^{2+} compared to their wild-type mice. However, it is not a paradox that MT-knockout mice only accumulate little Cd^{2+}, but are sensitive to Cd^{2+}. Little accumulation in knockout mice would suggest that free Cd^{2+} is travelling directly to the kidneys and subsequently harming the organ. These results indicated that MT enhances the accumulation of Cd^{2+} in the kidneys but that it also significantly reduces the associated toxic effects (*51*). It should be noted at this point that retention of Cd^{2+} in humans is primarily attributed to MT and that the biological half-life of Cd^{2+} in the human body is on the order of several decades (*52-53*).

MT knockout mice, in which both MT-1 and MT-2 were inactivated, experience enhanced hepatic Cd^{2+} poisoning, but under control conditions these MT-null mice were viable and reproduced normally (*54*). These results suggest that MT acts to buffer the toxic effects of Cd^{2+} to an organism by sequestering the Cd^{2+}, likely leading to the release of Zn^{2+}, which would act to upregulate MT. To further support the buffering role of MT, wild-type mice given increasing doses of Cd^{2+} developed a tolerance to Cd^{2+} lethality, as evidenced by a 7-fold increase in the LD_{50} (*55*). While under the same conditions, the LD_{50} of MT-null mice was unaffected. These pretreatment experiments underscore the importance of not only MT in toxic metal detoxification, but also the total MT pool in an organism.

The ability of methylmercury ($MeHg^{+}$) to induce neurotoxic effects in a cell is related to the amount of MT present, with increasing amounts directly attenuating the associated toxic effects. The astrocyte is thought to play a pivotal role in $MeHg^{+}$ mediated death, because it expresses three times as much MT as its associated neurons and could potentially function as a buffer to protect these neurons, and consequently the organism, from toxic insult (8-9, 56). Surprisingly $MeHg^{+}$ is not capable of directly inducing MT in

spite of its large affinity for thiol groups. We consider that MT, binding metals in a noncooperative fashion, will coordinate $MeHg^{+}$ through the available thiols found in any of the partially metalated forms (57-59).

1.2.3 Protection against oxidative stress

The high thiol content of MT makes it an ideal molecule to interact with and inhibit reactive oxygen species (ROS). Indeed, animal studies, in which cardiac specific MT is overexpressed, have shown that MT functions to protect against oxidative stress, specifically in the inhibition of ischemia-reperfusion induced myocardial injury (*60-61*). MT is upregulated by ROS through the antioxidant response element (ARE), a promoter region on the MT gene, ARE-binding transcription factors, as well as MTF-1. Perhaps the most well known reactivity of MT is that with air leading to oxidation of the cysteine residues and subsequent formation of sulfonic acid and disulfide bonds. Metal free (apo-) MT is particularly susceptible to oxygen, and metalation experiments should be carried out under strictly anaerobic conditions.

Nitric oxide has also been shown to increase the intracellular release of Zn^{2+} through the oxidation of Zn-MT in mouse lung fibroblasts (*62*). *In vitro* analysis of the oxidation products of the three isoforms (MT -1, -2, and -3), suggests the mechanism of oxidation of each is different. In the case of mouse MT-1, the β-domain metals are exclusively released (*63*), while the products from the oxidation of rabbit MT-2 show a more distributed release pattern (*64*), and finally, for human MT-3 a long lived Cd_2-α-domain intermediate exists when nitric oxide induces oxidation of the protein (*65*). It is probable that these differences in metal release are the result of the distinct functions of each isoform under nitrosative stress. Both cell free and cell culture studies of Zn-MT in the presence of H_2O_2 have also shown that MT is capable of acting as an antioxidant leading to release of Zn^{2+}, which acts to upregulate MT through MTF-1 (*35, 66-67*).

Metal ions are a significant source of ROS cellular chemistry with both copper and iron capable of producing hydroxyl radicals (*68*). Zn-MT is capable of inhibiting the production of copper catalyzed hydroxyl radicals *in vitro*. With 20 cysteine residues, MT is capable of reducing Cu^{2+} to Cu^{+}, after which it can be coordinated with high affinity to MT.

As a reducing agent that readily coordinates Zn^{2+}, a proposed function of MT is sensing the presence of incoming oxidants. In this redox cycle, an ROS oxidizes MT leading to Zn^{2+} release (*49, 69*). This Zn^{2+} is responsible for upregulating Zn-dependent proteins through MTF-1. Either reduction of the previously oxidized MT with glutathione, or complete replacement with *de novo* MT then leads to a reestablishment of zinc homeostasis. In this manner, MT may either directly interact with the ROS, or in cases where ROS production is the result of a metal ion that readily coordinates MT, such as copper, MT may act to sequester the metal ion and effectively neutralize ROS activity.

1.3 Structural Characterization

X-ray diffraction results have been reported from just two crystals, the first successful example was for rat Cd_5Zn_2-MT-2 (*5*), and the second was for yeast Cu_8-MT (*70*). It should be noted that MT has been described as being notoriously difficult to crystallize, and much of our structural knowledge is the result of the many NMR-based studies reported. Structures based on analyses of the NMR data have been reported from several mammalian sources (*71-74*). These structures provide the absolute connectivities of all atoms and their spatial relationship with the metal-thiolate core but not the alignment of the linkage between the two domains. The domain alignments were determined from the X-ray diffraction studies for the rat liver Cd_5,Zn_2-MT (*5*). In the case of the X-ray crystal structure of rat Cd_5Zn_2-MT-2 species, all metal centres were tetrahedrally coordinated by cysteinyl-thiolates; later, when compared to the NMR structure, both showed identical molecular architectures (*75*). A comparison of the NMR-based structures of human Cd_7- and Zn_7-MT-2 has shown overall maintenance of cluster geometry and demonstrated that MT can accommodate metal ions of varying size (*76*). The ability of Cd^{2+} to replace Zn^{2+} isomorphously is exploited in many experiments due to several advantageous properties of the cadmium-thiolate cluster, such as the availability of $^{113/111}$Cd NMR active isotopes, as well as the red shifted ligand-to-metal charge transfer band in the optical spectrum.

Copper(I) is capable of coordinating with a range of geometries depending on the Cu(I) : MT stoichiometric ratio. Digonal and trigonal geometries were found in the X-ray diffraction structure of the Cu-MT from yeast (*70*). While no mammalian Cu-MT X-ray diffraction structure exists, spectroscopic data have demonstrated the existence of

both a Cu_{12}-MT and a Cu_{15}-MT for the two-domain, rabbit liver MT 2a, the former likely being mainly copper coordinated in a trigonal geometry, while the latter is likely a mixture of trigonal and digonal geometries (*77*). In addition to these fully metalated structures, a copper folding intermediate in the β-domain, Cu_4-MT, has been isolated for both rat liver MT-1 and mouse MT-3 but is of unknown coordination geometry (*78*). It is probable that this intermediate is related to the mixed metal species, Cu_4Zn_4-MT-3, thought to a critical product in controlling the oxidative damage caused by the Cu^+/Cu^{2+} redox cycle in Alzheimer's disease (*79*). Previous NMR metal exchange experiments, in which Cd^{2+} was reacted with calf liver Zn_4,Cu_3-MT-1 and -2 have shown that cadmium ions could only displace the zinc ions (*16*). Based on the NMR chemical shifts, it was concluded that these zinc ions were almost exclusively located in the α-domain, while the copper ions were located preferentially in the β-domain. From these results it has been proposed that MT is capable of separating metal types into different domains, essentially isolating the chemistry of both essential zinc and copper.

While NMR spectroscopy and X-ray diffraction studies have yielded the most significant information about the structure of MT, other techniques have also greatly contributed including CD, emission and Raman spectroscopy. In the case of CD spectroscopy, the ligand-to-metal charge transfer is strongly affected by the chirality of the protein and changes to the chirality can affect the signal observed (*80-81*). For example, due to exciton coupling in mammalian MT, a typical spectrum has the cross-over of the derivative envelope centered at ~250 nm, however upon supermetalation exciton coupling is broken and a CD band maximum at ~250 nm is now observed (*82-83*). In this way, one is able to infer that the metal coordination of both clusters is symmetric and that supermetalation results in a loss of this symmetry. Emission spectroscopy is also useful and in the case of copper emission is most intense when 12 equivalents of Cu^+ have been added forming Cu_{12}-MT. Loss of emission intensity past 12 equivalents of Cu^+ added to rabbit liver MT demonstrates that the protein is opening and assuming a less compact and more porous form (*84*). Raman spectroscopy is also gaining interest because of its ability to determine the oxidation state of cysteine residues, the identity of coordinating ligands and finally identification of cysteine residues that could be modified by radical attack (*85*). These techniques, while not as structurally

specific as NMR spectroscopy, X-ray absorption spectroscopic methods or X-ray diffraction studies, provide useful information that help in the determination of the dynamic structures of MT and further our understanding of its overall function(s).

1.4 Zinc and Cadmium binding to MT

Zinc is critical to the continued health of an organism and is required for the proper functioning of a number of enzymes and transcription factors. With 5-20% of all cellular Zn associated with MT, structural motifs of Zn-MT are of critical importance (*86*). Exposure of an organism to cadmium will negatively affect the health of an individual, including both liver and kidney damage. Cadmium is also a known carcinogen, capable of both inhibiting several DNA repair systems, as well as indirectly producing ROS to further DNA damage (*87-88*). Perhaps the most well known disease associated with cadmium poisoning is Itai-Itai, made famous by mass cadmium poisoning in Toyama Prefecture, Japan, and most strikingly characterized by an increase in bone brittleness leading to an increased incidence of fractures (*89*). While it may seem initially odd to include Zn^{2+}, an essential element, with Cd^{2+}, a toxic metal, both share similar coordination geometries. This is best demonstrated by NMR spectroscopy that has shown an almost identical protein fold when either metal is bound and a significant portion of the structural information known is derived from Cd-MT (*76*).

For both Zn^{2+} and Cd^{2+}, the most well characterized form of MT is mammalian, with an N-terminal β-domain containing 9 cysteine residues and a C-terminal α-domain containing 11 cysteine residues. The traditional number of metals bound to the full protein are 7 metal ions, 3 in the β-domain (Zn_3- or Cd_3-β-MT) and 4 in the α-domain (Zn_4- or Cd_4-α-MT). More recent evidence points towards a new supermetalated form of the protein that is discussed in Chapters 5 and 6.

Several studies have together provided compelling evidence that the two domains of mammalian MT are structurally independent. To illustrate, the ^{113}Cd chemical shifts of the isolated α-domain are remarkably similar to those of the full protein indicating that the complete loss of the β-domain does not affect, to a large extent, the environment of the α-domain (*90*). While NMR structural studies from several MT sources, including mouse (*74*) and human (*72*), show a lack of interdomain peaks associated with the

nuclear overhauser effect (NOEs), which would strongly suggest that the fully metalated domains are independent of each other. It is possible that the independence of the two domains is critical to the function of MT.

The initial proton NMR studies of MT demonstrated that in the absence of metal binding the structure was a random coil (although we note that proposed models of the apo-MT support the presence of a motif-like structure), however, upon addition of either Cd^{2+} or Zn^{2+} the structure became significantly more rigid (*91-93*). Further analysis of the chemical shifts of cadmium atoms, as well as the splitting pattern, lead to the determination of the stoichiometry of the polynuclear clusters: Cd_3S_9 and Cd_4S_{11} (*90, 94-97*). Since these initial studies, solution structures have been determined from a number of MT sources including mammalian (human, rat, rabbit and mouse) (*71-76*), plant (*98*) and cyanobacteria (*99*). The critical step in the determination of the overall structure of mammalian MT was the X-ray crystallographic structure showing an identical molecular architecture to the previously determined NMR structure but with the alignment of the two domains now defined (*5*).

1.5 Copper binding to MT

Copper is vital for the continued health of all organisms. Copper induced toxicity is of considerable interest and its dyshomeostasis can lead to a number of diseases including Wilson's disease and Menkes disease (*44*). Unlike zinc, free copper is redox active and able to catalyze the formation of hydroxyl radicals through Haber-Weiss and Fenton reactions (*42*). A murine model of Menkes disease involving MT-1 and MT-2 null mice have shown enhanced sensitivity to copper toxicity (*46*). In the case of Wilson's disease, a marked increase in Cu-MT has been demonstrated (*18, 47*). These two examples emphasize the importance of MT in maintaining health through the control of transient fluctuations in Cu^{+} availability (*42, 100*).

In the case of copper, it has been reported that there exists a preference for its accumulation in the β-domain of mammalian MT before binding under thermodynamic control in the α-domain. In essence, this would allow simultaneous involvement of both Zn^{2+} and Cu^{+} in the homeostatic functioning of the organism. This dual nature of the metal-binding properties of MTs could be critical to the brain specific MT-3 and its

interactions with the protein $A\beta_{1-40}$-Cu^{2+}, a producer of reactive oxygen critical to Alzheimer's disease (*79, 101*). In this fashion Zn_7-MT-3 is capable of deactivating $A\beta_{1-40}$-Cu^{2+} by exchanging Cu^{2+} for Zn^{2+}. Following this exchange Cu^{2+} is reduced and sequestered specifically into the β domain of MT-3.

Emission spectroscopy has been particularly useful in studying Cu^+ binding to MT. The first such study was for the fungus *Neurospora crassa* (102). Since this initial study, both equilibrium and kinetic emission data have been reported for both Cu^+ and Ag^+ binding to different MTs. In these studies, excitation of Cu^+ at 300 nm leads to a spin forbidden transition of $3d^{10} \rightarrow 3d^9 4s^1$, or alternatively $3d^{10} \rightarrow 3d^9 4p^1$, with subsequent emission from a long-lived state at a wavelength significantly red shifted from the initial excitation band (near 600 nm for Cu^+ and 570 nm for Ag^+). Because the emission intensity is dependent on the environment of the metal ion, any changes in this intensity as a function of metal stoichiometry is the result of the dynamics of protein folding.

The spectroscopic data (absorption, CD and emission) indicate that for the two-domain βα-MT-2a protein that there exist two significant saturation points, the "magic numbers" of copper binding, with Cu(I) : MT ratios (i) of 12 and (ii) of 15 (*77*). Each domain is independently capable of binding 6 Cu^+ ions leading to the formation of metal clusters with the stoichiometry Cu_6S_9 and Cu_6S_{11} for the β- and α-domains, respectively (*103-104*). Domain mixing experiments have shown the fluctionality of these clusters as Cu^+ ions located in the α-domain migrate to the β-domain displacing metal ions of weaker affinity in the process. Interestingly, the emission of Cu_{12}-βα-MT formed by the stepwise addition of Cu^+ to a solution of Zn_7-βα-MT is very time and temperature sensitive (*77, 84*). These results demonstrate that the initial Cu^+ binding is distributive without particular preference for either the α- or β-domain, which is the kinetic product of metalation. Given sufficient time and thermal energy, rearrangement of the protein leads to preferential accumulation of Cu^+ in the β-domain.

An unusual species was identified during titrations of Cd_7-MT 2 with Cu^+. The spectroscopic maxima were found for a mixed metal species with 12 Cu^+ and four Cd^{2+}, Cd_4Cu_{12}-MT. It was proposed that the 4 Cd^{2+} were mixed with 6 Cu^+ in the α domain and the remaining 6 Cu^+ were bound in the β domain (*77*). Like Hg_{18}-MT 2 (see below), it is possible that this species is in fact a single domain species.

To summarize, "the magic numbers" of the metalation of MT with Cu^{+} are 6 for the isolated β- and α-domains and 12 and 15 for the full protein. When multiple metals are present both Cu_9Zn_2-MT and $Cu_{12}Cd_4$-MT form. Interestingly, Cu^{+} has a preference of the β-domain, which has been used to interpret the location of Cu^{+} in many of these species.

1.6 Mercury binding to MT

Mercury has no known physiological role and environmental exposure can come in several forms including elemental mercury (Hg^0), inorganic mercury (Hg^{2+} and Hg_2^{2+}) and organic forms of mercury, such as methylmercury (CH_3Hg^{+}), and toxicity is greatest for the alkylated species. Mercury has long been associated with MT, with early copurification attributed, in part, to the therapeutic use of mercurials (*36*). MT-null mice have been instrumental in demonstrating the protective role of MT against Hg induced toxicity (*105-108*). It should be noted that like CH_3Hg^{+}, Hg^0 is lipid soluble and can cross the blood brain barrier, where it can be oxidized to Hg^{2+} with catalase and H_2O_2 (*109*). MT has a critically important role in protecting an organism against methylmercury poisoning, and pretreatment experiments in which administration of MT inducers (Zn^{2+} and Cd^{2+}) caused an increase in the tolerance of astrocytes against toxic methylmercury insult (*56, 110-111*). The above examples highlight the importance of MT in the maintenance of neurological health.

A significant body of work has been produced describing not only the structurally significant stoichiometries of Hg-MT, but also the factors that influence their formation, such as time, temperature, presence of MT coordinated metals and the identity of the counter ions used in Hg^{2+} addition (*112-115*). Four saturation points have been spectroscopically observed including Hg_7-, Hg_{11}-, Hg_{18}-, and Hg_{20}-MT. The latter, having a very weak CD spectrum, is likely the result of a complete unwinding of the protein leading to a random coil with Hg^{2+} coordinated in a linear fashion. The most notable technique used in titrations of MT with Hg^{2+} to date is CD spectroscopy. The technique measures the difference between left and right circularly polarized light caused by the chirality of the chromophore. In this case, the chirality of the ligand-to-metal charge transfer of each mercury-thiolate cluster is measured. Because the metals that

bind MT form predefined structures that exhibit specific chirality, CD spectroscopy is extremely sensitive in monitoring the metalation of MT. The CD bands specifically probes the metal-cysteine binding site structure because the chirality arises from a combination of the chiral wrapping of the peptide chain around the binding site and the exact energy of the ligand-to-metal charge transfer band (LMCT band). The energies of the LMCT depend on the coordination number of the Hg^{2+} and, therefore, on the structure adopted at a each specific Hg(II) : MT stoichiometric ratio. Changes in the wavelength of bands and the band morphologies in the CD spectrum as a function of Hg^{2+} loading indicate changes in binding site geometry as a function of the Hg^{2+} stoichiometric ratio.

While the metalation reactions of MT by Hg^{2+} have been studied for apo-MT, Zn-MT and Cd-MT, the importance of MT in zinc chemistry suggests that the displacement of Zn^{2+} by Hg^{2+} in MT is the most biologically relevant. It should be noted that: 1) displacement of Cd^{2+} in Cd-MT is the result of a distributive metalation, in which Hg^{2+} binds statistically to both the β- and α- domain, and 2) the metalation of apo-MT with Hg^{2+} follows a very similar pattern to that measured when Hg^{2+} is added to Zn-MT with the singular exception that in the early stages of the reaction no isolated $HgSR_4$ units are observed.

Hg_{18}-βα-MT-2 from rabbit liver has been reported to be a structurally significant species, where it was proposed that each Hg^{2+} atom adopts a pseudotetrahedral structure, each with two bridging thiolates and outlying chloride anions (*113, 115*). The necessity for Hg^{2+} to be coordinated to two cysteine residues and chloride ions has been confirmed by XAFS measurements (*116*). In this way, each Hg^{2+} atom is effectively stacked on the others leading to the formation of one large domain instead of two smaller ones. Interestingly this species may only be formed from isoform 2, unless isoform 1 is first lyophilized and then dissolved in acid. Formation of Hg_{18}-βα-MT-2 has been attributed to residues 38-40, where the unique presence of two consecutive proline residues allows the twisting of the protein to accommodate a single domain structure. In the case of lyophilized protein, breaking of the solvent-protein bonds allows an alternate conformation to be adopted in acid, which upon addition of Hg^{2+} leads to the formation of Hg_{18}-βα-MT-1. We will return to the formation of a single-domain species in Chapter 6, but to summarize the "magic numbers" of Hg^{2+} to MT binding are 7, 11 and 18.

1.7 The mechanism of metalation of MT

In recent years there has been considerable debate regarding the mechanism of metalation of MT (*57-59, 117-118*). Specifically, do the metals bind in a noncooperative manner, that is one at a time, or do they bind in a cooperative manner, that is all-or-nothing? Briefly a noncooperative mechanism of metalation implies that the binding of one metal ion is independent of the others, and as such, throughout metalation a decrease in the association constants is related to a decrease in the number of available sites. While a cooperative mechanism of metalation implies that binding of one metal facilitates the binding of further metals leading to an increase in the association constants. The mechanism of metalation has significant consequences for our understanding of the protein and its interactions with the cellular environment. For example, several MT polymorphisms have been linked to the longevity of certain human groups, with both low Zn-MT levels and satisfactory Zn^{2+} bioavailability being good markers for human health (*119-121*). Exposure of this mutant MT to nitric oxide, resulted in less Zn^{2+} release compared to the wild-type. If the Zn^{2+} binds to MT in a cooperative fashion, then one can infer that the mutant is inherently less reactive, however if Zn^{2+} binds to MT in a noncooperative fashion, then there is potential that a large pool of partially oxidized MT exists. In both cases, the mechanism of metalation, and the potential for partially metalated species taking part in cellular chemistry has significant consequences in the understanding of the relationship between Zn^{2+} bioavailability, MT and the overall health of an individual.

Early research supported a cooperative mechanism of metalation. For example, a titration of $^{113}Cd^{2+}$ with MT, as monitored by ^{113}Cd-NMR, demonstrated the apperance of only fully metalated MT and no intermediates (*118*). If the metals were to bind sequentially, then one would have predicted the appearance and disappearance, as a function of the amount of $^{113}Cd^{2+}$ added to solution, of ^{113}Cd-NMR signals associated with isolated tetrahedral cadmium-thiolates. The absence of those signals, and the presence of only signals associated with fully metalated Cd_7-MT, would suggest a cooperative mechanism of metalation. However, this assumes that the isolated tetrahedral cadmium-thiolate units are not significantly mobile.

A significant problem with studying metalation reactions with metals that are biologically relevant to the chemistry of MT, such as Zn^{2+}, Cd^{2+} and Cu^{+}, is that these are d^{10} metals, and consequently are chromophorically silent in many spectroscopies. In such cases, researchers have, until recently, been limited to the ligand-to-metal charge transfer bands in the optical spectrum (using absorption, emission, circular dichroism (CD) and magnetic circular dichroism (MCD) techniques) making their coordination properties difficult to study. One way to overcome this problem, involves using Co^{2+} as a spectroscopic probe for Zn^{2+}. The metalation of apo-MT to form Co_7-MT is of interest, because the results indicate that for the binding of at least the first three Co^{2+} atoms, the spectroscopic signature indicates the presence of isolated Co-tetrathiolate units within the MT binding site. As further Co^{2+} is added, both electronic absorption, EPR and ^{1}H NMR spectra indicate thiolate bridging occurs as the coordination remains tetrahedral by sulphur (*122-123*). These results are significant in that if MT were to bind metal ions in a cooperative fashion then cluster formation would be immediate upon addition of Co^{2+} leaving a significant fraction of the protein in the unmetalated apo-MT state. The experimental data indicate that cluster formation requires the addition of several equivalents, and consequently binds Co^{2+} in a noncoooperative manner.

Recently the technique of ESI-mass spectrometry, which detects each unique protein species with a different mass-to-charge ratio, has allowed the study of dilute protein solutions as a function of metal loading; data that complements the optical spectroscopic data. Using this technique, two papers have provided evidence for the mechanism of metalation of MT to occur in a noncooperative fashion. Specifically, the addition of Cd^{2+} to MT-3 (*59*), the brain specific isoform, and the α-domain of MT-1 (*58*). This data, however, cannot be immediately generalized to all mammalian MTs, because unlike MT-1, -2 and -4, MT-3 has an additional threonine (Thr5) in a TCPCP motif, and a glutamate-rich hexapeptide near the C-terminal that have both been shown to be critical to its function (*124-125*). Consequently, the mechanism of MT-1 or -2 will need to be determined.

1.8 Scope of the Thesis

The metalation chemistry of MT has typically focused on its fully metalated states, that is Zn_7- and Cd_7-MT. Consequently the overall structure of this state is well known, but such questions as the mechanism of metalation and the mechanism of metal exchange have been largely overlooked. In addition, the respective structures of these submetalated and metal exchange intermediates have not been characterized.

This thesis is composed of seven Chapters. The first Chapter gives on overview of MT, both its functions and its metalation chemistry, with an emphasis placed on the wide array of metals that are capable of binding. Chapter two gives a complete description of the recombinant preparation methods of the MT, both the full protein and its isolated domains, as well as a brief description of the instrumental techniques (UV absorption, CD and NMR spectroscopy, as well as ESI-mass spectrometry and molecular mechanics/dynamics) used to probe the metalation reactions of MT. The remainder of this thesis focuses on determining the mechanism of metalation, as well as the metalated structures that may exist *in vivo*.

Chapter three describes an equilibrium study in which the cooperative nature of the metal binding mechanism is explored by examination of the speciation of both the isolated β-domain, as well as the full MT protein, using electrospray ionization mass spectrometry. While Chapter four describes the first ever competition reaction between the isolated domains and the full MT protein, as well as provide metalation evidence for a new Zn_5-MT structure that may be a partially metalated stable intermediate. The results from this study are necessary to allow for a generalization of the noncooperative mechanism of metalation to all mammalian MT isoforms.

Chapter five discusses the structural determination of a new Cd_4-β-rhMT-1a structure by examination of the domain speciation under metal ion excess. This novel cluster arrangement is characterized by CD and UV absorption spectroscopy, ESI mass spectrometry and ^{113}Cd NMR spectroscopy. Chapter six extends these excess metal ion studies to the full MT protein, and provides evidence for the existence of a novel Cd_8-βα-rhMT-1a structure, in which both domains act to coordinate the eighth metal ion.

Finally, Chapter seven draws together the result of these studies, presented in Chapter three through six, and discusses them with respect to the known functions of MT.

1.9 References

1. Kojima, Y. (1991) Definitions and Nomenclature of Metallothioneins, In *Methods in Enzymology: Metallobiochemistry Part B Metallothionein and Related Molecules* (Riordan, J. F., and Vallee, B. L., Eds.), Academic Press, Inc., San Diego.
2. Margoshes, M., and Vallee, B. L. (1957) A cadmium protein from equine kidney cortex, *J. Am. Chem. Soc. 79*, 4813-4814.
3. Kagi, J. H. R., and Vallee, B. L. (1960) Metallothionein: A cadmium- and zinc-containing protein from equine renal cortex, *J. Biol. Chem. 235*, 3460-3465.
4. Kagi, J. H. R. (1993) Evolution, structure and chemical acitivity of class I metallothioneins: An overview., In *Metallothionein III: Biological roles and medical implications* (Suzuki, K. T., Imura, N., and Kimura, M., Eds.), Birkhauser-Verlag, Berlin.
5. Robbins, A. H., McRee, D. E., Williamson, M., Collett, S. A., Xuong, N. H., Furey, W. F., Wang, B. C., and Stout, C. D. (1991) Refined crystal structure of Cd, Zn metallothionein at 2.0 Å resolution, *J. Mol. Biol. 221*, 1269-1293.
6. Chan, J., Huang, Z., Watt, I., Kille, P., and Stillman, M. J. (2007) Characterization of the conformational changes in recombinant human metallothioneins using ESI-MS and molecular modeling, *Can. J. Chem. 85*, 898-912.
7. Binz, P.-A., and Kagi, J. H. R. (1999) Metallothionein: Molecular evolution and classification, In *Metallothionein IV* (Klaassen, C. D., Ed.), pp 7-13, Birkhauser, Berlin.
8. Kramer, K. K., Zoelle, J. T., and Klaassen, C. D. (1996) Induction of metallothionein mRNA and protein in primary murine neuron cultures, *Toxicol. Appl. Pharmacol. 141*, 1-7.
9. Kramer, K. K., Liu, J., Choudhuri, S., and Klaassen, C. D. (1996) Induction of metallothionein mRNA and protein in murine astrocyte cultures, *Toxicol. Appl. Pharmacol. 136*, 94-100.
10. Uchida, Y., Takio, K., Titani, K., Ihara, Y., and Tomonaga, M. (1991) The growth inhibitory factor that is deficient in the Alzheimer's Disease brain is a 68 amino acid metallothionein-like protein, *Neuron 337-347*.
11. Quaife, C. J., Findley, S. D., Erickson, J. C., Froelick, G. J., Kelly, E. J., Zambrowicz, B. P., and Palmiter, R. D. (1994) Induction of a new metallothionein isoform (MT-IV) occurs during differentiation of stratified squamous epithelia, *Biochemistry 33*, 7250-7259.
12. Quaife, C. J., Kelly, E. J., Masters, B. A., Brinster, R. L., and Palmiter, R. D. (1998) Ectopic expression of metallothionein-III causes pancreatic acinar cell necrosis in transgenic mice, *Toxicol. Appl. Pharmacol. 148*, 148-157.
13. Li, Y., and Maret, W. (2008) Human metallothionein metallomics, *J. Anal. At. Spectrom. 23*, 1055-1062.
14. Ryden, L., and Deutsch, H. F. (1978) Preparation and properties of the major copper-binding component in human fetal liver: Its identification as metallothionein, *J. Biol. Chem. 253*, 519-524.

15. Hartmann, H. J., and Weser, U. (1977) Copper-thionein from fetal bovine liver, *Biochim. Biophys. Acta 491*, 211-222.
16. Briggs, R. W., and Armitage, I. M. (1982) Evidence for site-selective metal binding in calf liver metallothionein, *J. Biol. Chem. 257*, 1259-1262.
17. Szymanska, J. A., Zelazowski, A. J., and Stillman, M. J. (1983) Spectroscopic characterization of rat kidney Hg,Cu-metallothionein, *Biochem. Biophys. Res. Commun. 115*, 167-173.
18. Stillman, M. J., Gasyna, Z., and Zelazowski, A. J. (1989) A luminescence probe for metallothionein in liver tissue: Emission intensity measured directly from copper metallothionein induced in rat liver, *FEBS Lett. 257*, 283-286.
19. Dolderer, B., Hartmann, H.-J., and Weser, U. (2009) Metallothioneins in Yeast and Fungi, *Met. Ions Life Sci. 5*, 83-105.
20. Outten, C. E., and O'Halloran, T. V. (2001) Femtomolar sensitivity of metalloregulatory proteins controlling zinc homeostasis, *Science 292*, 2488-2492.
21. Rae, T. D., Schmidt, P. J., Pufahl, R. A., Culotta, V. C., and O'Halloran, T. V. (1999) Undetectable intracellular free copper: The requirement of a copper chaperone for superoxide dismutase, *Science 284*, 805-808.
22. Feng, W., Cai, J., Pierce, W. M., Franklin, R. B., Maret, W., Benz, F. W., and Kang, Y. J. (2005) Metallothionein transfers zinc to mitochondrial aconitase through a direct interaction in mouse hearts, *Biochem. Biophys. Res. Commun. 332*, 853-858.
23. Mason, A. Z., Perico, N., Moeller, R., Thrippleton, K., Potter, T., and Lloyd, D. (2004) Metal donation and apo-metalloenzyme activation by stable isotopically labeled metallothionein, *Mar. Environ. Res. 58*, 371-375.
24. Maret, W., Larsen, K. S., and Vallee, B. L. (1997) Coordination dynamics of biological zinc "clusters" in metallothioneins and in the DNA-binding domain of the transcription factor Gal4, *Proc. Natl. Acad. Sci. U.S.A 94*, 2233-2237.
25. Zeng, J., Heuchel, R., Schaffner, W., and Kagi, J. H. R. (1991) Thionein (apometallothionein) can modulate DNA binding and transcription activation by zinc finger containing factor Sp1, *FEBS Lett. 279*, 310-312.
26. Ecker, D. J., Butt, T. R., Sternberg, E. J., Neeper, M. P., Debouck, C., Gorman, J. A., and Crooke, S. T. (1986) Yeast metallothionein function in metal ion detoxification, *J. Biol. Chem. 261*, 16895-16900.
27. Butt, T. R., Sternberg, E. J., Gorman, J. A., Clark, P., Hamer, D., Rosenberg, M., and Crooke, S. T. (1984) Copper metallothionein of yeast, structure of the gene, and regulation of expression, *Proc. Natl. Acad. Sci. U.S.A 81*.
28. Bonneton, F., Theodore, L., Silar, P., Maroni, G., and Wegnez, M. (1996) Response of *Drosophila* metallothionein promoters to metallic, heat shock and oxidative stresses, *FEBS Lett. 380*, 33-38.
29. Stuart, G. W., Searle, P. F., Chen, H. Y., Brinster, R. L., and Palmiter, R. D. (1984) A 12-base-pair DNA motif that is repeated several times in metallothionein gene promoters confers metal regulation to a heterologous gene, *Proc. Natl. Acad. Sci. U.S.A 81*, 7318-7322.

30. Carter, A. D., Felber, B. K., Walling, M., Jubier, M.-F., Schmidt, C. J., and Hamer, D. H. (1984) Duplicated heavy metal control sequences of the mouse metallothionein-I gene, *Proc. Natl. Acad. Sci. U.S.A 81*, 1984.
31. Andrews, G. K. (2000) Regulation of metallothionein gene expression by oxidative stress and metal ions, *Biochem. Pharmacol. 59*, 95-104.
32. Stuart, G. W., Searle, P. F., and Palmiter, R. D. (1985) Identification of multiple metal regulatory elements in mouse metallothionein-I promoter by assaying synthetic sequences, *Nature 317*, 828-831.
33. Chen, X., Chu, M., and Giedroc, D. P. (1999) MRE-binding transcription factor-1: Weak zinc-binding finger domains 5 and 6 modulate the structure, affinity, and specificity of the metal-response element complex, *Biochemistry 38*, 12915-12925.
34. Giedroc, D. P., Chen, X., Pennella, M. A., and LiWang, A. C. (2001) Conformational heterogeneity in the C-terminal zinc fingers of human MTF-1, *J. Biol. Chem. 276*, 42322-42332.
35. Zhang, B., Georgiev, O., Hagmann, M., Gunes, C., Cramer, M., Faller, P., Vasak, M., and Schaffner, W. (2003) Activity of metal-responsive transcription factor 1 by toxic heavy metals and H_2O_2 in vitro is modulated by metallothionein, *Mol. Cell. Biol. 23*, 8471-8485.
36. Pulido, P., Kagi, J. H. R., and Vallee, B. L. (1966) Isolation and some properties of human metallothionein, *Biochemistry 5*, 1768-1777.
37. Nielson, K. B., Atkin, C. L., and Winge, D. R. (1985) Distinct metal-binding configurations in metallothionein, *J. Biol. Chem. 260*, 5342-5350.
38. Good, M., and Vasak, M. (1986) Iron(II)-substituted metallothionein: Evidence for the existence of iron-thiolate clusters, *Biochemistry 25*, 8353-8356.
39. Morelock, M. M., Cormier, T. A., and Tolman, G. L. (1988) Technetium metallothioneins, *Inorg. Chem. 27*, 3137-3140.
40. Ngu, T. T., Krecisz, S., and Stillman, M. J. (2010) Bismuth binding studies to the human metallothionein using electrospray mass spectrometry, *Biochem. Biophys. Res. Commun. 396*, 206-212.
41. Vasak, M. (1980) Spectroscopic studies on cobalt(II) metallothionein: Evidence for pseudotetrahedral metal coordination, *J. Am. Chem. Soc. 102*, 3953-3955.
42. Cai, L., Li, X.-K., Song, Y., and Cherian, M. G. (2005) Essentiality, toxicology and chelation therapy of zinc and copper, *Curr. Med. Chem. 12*, 2753-2763.
43. Kelly, E. J., Quaife, C. J., Froelick, G. J., and Palmiter, R. D. (1996) Metallothionein I and II protects against zinc deficiency and zinc toxicity in mice, *J. Nutr. 126*, 1782-1790.
44. Kodama, H., and Fujisawa, C. (2009) Copper metabolism and inherited copper transport disorders: molecular mechanisms, screening, and treatment, *Metallomics 1*, 42-52.
45. Suzuki-Kurasaki, M., Okabe, M., and Kurasaki, M. (1997) Copper-metallothionein in the kidney of macular mice: A model for menkes disease, *J. Histochem. Cytochem. 45*, 1493-1501.
46. Kelly, E. J., and Palmiter, R. D. (1996) A murine model of Menkes disease reveals a physiological function of metallothionein, *Nat. Genet. 126*, 1782-1790.

47. Nartey, N. O., Frei, J. V., and Cherian, M. G. (1987) Hepatic copper and metallothionein distribution in Wilson's disease (hepatolenticular degeneration), *Lab. Invest. 57*, 397-401.
48. Chiaverini, N., and DeLey, M. (2010) Protective effect of metallothionein on oxidative stress-induced DNA damage, *Free Radical Res. 44*, 605-613.
49. Kang, Y. J. (2006) Metallothionein redox cycle and function, *Exp. Biol. Med. 231*, 1459-1467.
50. Chan, H. M., Zhu, L.-F., Zhong, R., Grant, D., Goyer, R. A., and Cherian, M. G. (1993) Nephrotoxicity in rats following liver transplantation from cadmium-exposed rats, *Toxicol. Appl. Pharmacol. 123*, 89-96.
51. Liu, J., Liu, Y., Habeebu, S. S., and Klaassen, C. D. (1998) Susceptibility of MT-null mice to chronic $CdCl_2$-induced nephrotoxicity indicates that renal injury is not mediated by the CdMT complex, *Toxicol. Sci. 46*, 197-203.
52. Klaassen, C. D., Liu, J., and Diwan, B. A. (2009) Metallothionein protection of cadmium toxicity, *Toxicol. Appl. Pharmacol. 238*, 215-220.
53. Suwazono, Y., Kido, T., Nakagawa, H., Nishijo, M., Honda, R., Kobayashi, E., Dochi, M., and Nogawa, K. (2009) Biological half-life of cadmium in the urine of inhabitants after cessation of cadmium exposure, *Biomarkers 14*, 77-81.
54. Masters, B. A., Kelly, E. J., Quaife, C. J., Brinster, R. L., and Palmiter, R. D. (1994) Targeted disruption of metallothionein I and II genes increases sensitivity to cadmium, *Proc. Natl. Acad. Sci. U.S.A 91*, 584-588.
55. Park, J. D., Liu, Y., and Klaassen, C. D. (2001) Protective effect of metallothionein against the toxicity of cadmium and other metals, *Toxicology 163*, 93-100.
56. West, A. K., Hidalgo, J., Eddins, D., Levin, E. D., and Aschner, M. (2008) Metallothionein in the central nervous system: Roles in protection, regeneration and cognition, *Neurotoxicology 29*, 488-502.
57. Sutherland, D. E. K., and Stillman, M. J. (2008) Noncooperative cadmium(II) binding to human metallothionein 1a, *Biochem. Biophys. Res. Commun. 372*, 840-844.
58. Rigby-Duncan, K. E., and Stillman, M. J. (2007) Evidence for noncooperative metal binding to the α domain of human metallothionein, *FEBS J. 274*, 2253-2261.
59. Palumaa, P., Eriste, E., Njunkova, O., Pokras, L., Jornvall, H., and Sillard, R. (2002) Brain-specific metallothionein-3 has higher metal-binding capacity than ubiquitous metallothioneins and binds metals noncooperatively, *Biochemistry 41*, 6158-6163.
60. Kang, Y. J., Li, G., and Saari, J. T. (1999) Metallothionein inhibits ischemia-reperfusion injury in mouse heart, *Am. J. Physiol. Heart Circ. Physiol. 276*, H993-H997.
61. Kang, Y. J., Li, Y., Sun, X., and Sun, X. (2003) Antiapoptotic effect and inhibition of ischemia/reperfusion-induced myocardial injury in metallothionein-overexpressing transgenic mice, *Am. J. Pathol. 163*, 1579-1586.
62. St.Croix, C. M., Wasserloos, K. J., Dineley, K. E., Reynolds, I. J., Levitan, E. S., and Pitt, B. R. (2002) Nitric oxide-induced changes in intracellular zinc

homeostasis are mediated by metallothionein/thionein, *Am. J. Physiol. Lung Cell Mol. Physiol. 282*, L185-L192.

63. Zangger, K., Oz, G., Haslinger, E., Kunert, O., and Armitage, I. M. (2001) Nitric oxide selectively releases metals from the amino-terminal domain of metallothioneins: potential role at inflammatory sites, *FASEB J. 15*, 1303-1305.
64. Khatai, L., Goessler, W., Lorencova, H., and Zangger, K. (2004) Modulation of nitric oxide-mediated metal release from metallothionein by the redox state of glutathione *in vitro*, *Eur. J. Biochem. 271*, 2408-2416.
65. Wang, H., Li, H., Cai, B., Huang, Z.-X., and Sun, H. (2008) The effect of nitric oxide on metal release from metallothionein-3: gradual unfolding of the protein, *J. Biol. Inorg. Chem. 13*, 411-419.
66. Elgohary, W. G., Sidhu, S., Krezoski, S. O., Petering, D. H., and Byrnes, R. W. (1998) Protection of DNA in HL-60 cells from damage generated by hydroxyl radicals produced by reaction of H_2O_2 with cell iron by zinc-metallothionein, *Chem.-Biol. Interact. 115*, 85-107.
67. Quesada, A. R., Byrnes, R. W., Krezoski, S. O., and Petering, D. H. (1996) Direct reaction of H_2O_2 with sulfhydryl groups in HL-60 cells: Zinc-metallothionein and other sites, *Arch. Biochem. Biophys. 334*, 241-250.
68. Cai, L., Koropatnick, J., and Cherian, M. G. (1995) Metallothionein protects DNA from copper-induced but not iron-induced cleavage in vitro, *Chem.-Biol. Interact. 96*, 143-155.
69. Maret, W. (2008) Metallothionein redox biology in the cytoprotective and cytotoxic functions of zinc, *Exp. Gerontol. 43*, 363-369.
70. Calderone, V., Dolderer, B., Hartmann, H.-J., Echner, H., Luchinat, C., Bianco, C. D., Mangani, S., and Weser, U. (2005) The crystal structure of yeast copper thionein: The solution of a long-lasting enigma, *Proc. Natl. Acad. Sci. U.S.A 102*, 51-56.
71. Arseniev, A., Schultze, P., Worgotter, E., Braun, W., Wagner, G., Vasak, M., Kagi, J. H. R., and Wuthrich, K. (1988) Three-dimensional structure of rabbit liver [Cd_7]metallothionein-2a in aqueous solution determined by nuclear magnetic resonance, *J. Mol. Biol. 201*, 637-657.
72. Messerle, B. A., Schaffer, A., Vasak, M., Kagi, J. H. R., and Wuthrich, K. (1990) Three-dimensional structure of human [$^{113}Cd_7$]metallothionein-2 in solution determined by nuclear magnetic resonance spectroscopy, *J. Mol. Biol. 214*, 765-779.
73. Schultze, P., Worgotter, E., Braun, W., Wagner, G., Vasak, M., Kagi, J. H. R., and Wuthrich, K. (1988) Conformation of [Cd_7]-metallothionein-2 from rat liver in aqueous solution determined by nuclear magnetic resonance spectroscopy, *J. Mol. Biol. 203*, 251-268.
74. Zangger, K., Oz, G., Otvos, J. D., and Armitage, I. M. (1999) Three-dimensional solution structure of mouse [Cd_7]-metallothionein-1 by homonuclear and heteronuclear NMR spectroscopy, *Protein Sci. 8*, 2630-2638.
75. Braun, W., Vasak, M., Robbins, A. H., Stout, C. D., Wagner, G., Kagi, J. H. R., and Wuthrich, K. (1992) Comparison of the NMR solution structure and the x-ray crystal structure of rat metallothionein-2, *Proc. Natl. Acad. Sci. U.S.A 89*, 10124-10128.

76. Messerle, B. A., Schaffer, A., Vasak, M., Kagi, J. H. R., and Wuthrich, K. (1992) Comparison of the solution conformations of human [Zn_7]-metallothionein-2 and [Cd_7]-metallothionein-2 using nuclear magnetic resonance spectroscopy, *J. Mol. Biol. 225*, 433-443.
77. Presta, A., Green, A. R., Zelazowski, A., and Stillman, M. J. (1995) Copper binding to rabbit liver metallothionein: Formation of a continuum of copper(I)-thiolate stoichiometric species, *Eur. J. Biochem. 227*, 226-240.
78. Jensen, L. T., Peltier, J. M., and Winge, D. R. (1998) Identification of a four copper folding intermediate in mammalian copper metallothionein by electrospray ionization mass spectrometry, *J. Biol. Inorg. Chem. 3*, 627-631.
79. Meloni, G., Faller, P., and Vasak, M. (2007) Redox silencing of copper in metal-linked neurodegenerative disorders: Reaction of Zn_7metallothionein-3 with Cu^{2+} ions, *J. Biol. Chem. 282*, 16068-16078.
80. Stillman, M. J. (1992) Optical Spectroscopy of Metallothioneins, In *Metallothioneins: Synthesis, structure and properties of metallothioneins, phytochelatines and metal-thiolate complexes* (Stillman, M. J., Shaw-III, C. F., and Suzuki, K. T., Eds.), pp 55-120, VCH Publishers, New York.
81. Rupp, H., and Weser, U. (1978) Circular dichroism of metallothioneins. A structural approach, *Biochim. Biophys. Acta 533*, 209-226.
82. Sutherland, D. E. K., Willans, M. J., and Stillman, M. J. (2010) Supermetalation of the β domain of human metallothionein 1a, *Biochemistry 49*, 3593-3601.
83. Rigby-Duncan, K. E., Kirby, C. W., and Stillman, M. J. (2008) Metal exchange in metallothioneins - a novel structurally significant Cd_5 species in the alpha domain of human metallothionein 1a *FEBS J. 275*, 2227-2239.
84. Green, A. R., Presta, A., Gasyna, Z., and Stillman, M. J. (1994) Luminescent probe of copper-thiolate cluster formation within mammalian metallothionein, *Inorg. Chem. 33*, 4159-4168.
85. Torreggiani, A., and Tinti, A. (2010) Raman spectroscopy a promising technique for investigations of metallothioneins, *Metallomics 2*, 246-260.
86. Balamurugan, K., and Schaffner, W. (2009) Regulation of metallothionein gene expression, *Met. Ions Life Sci. 5*, 31-49.
87. Giaginis, C., Gatzidou, E., and Theocharis, S. (2006) DNA repair systems as targets of cadmium toxicity, *Toxicol. Appl. Pharmacol. 213*, 282-290.
88. Liu, J., Qu, W., and Kadiiska, M. B. (2009) Role of oxidative stress in cadmium toxicity and carcinogenesis, *Toxicol. Appl. Pharmacol. 238*, 209-214.
89. Jarup, L., and Akesson, A. (2009) Current status of cadmium as an envrionmental health problem, *Toxicol. Appl. Pharmacol. 238*, 201-208.
90. Boulanger, Y., Armitage, I. M., Miklossy, K.-A., and Winge, D. R. (1982) ^{113}Cd NMR study of a metallothionein fragment: Evidence for a two-domain structure, *J. Biol. Chem. 257*, 13717-13719.
91. Galdes, A., Vasak, M., Hill, H. A. O., and Kagi, J. H. R. (1978) ^{1}H NMR spectra of metallothioneins, *FEBS Lett. 92*, 17-21.
92. Rupp, H., Voelter, W., and Weser, U. (1974) 270 MHz proton magnetic resonance spectra of metallothionein, *FEBS Lett. 40*, 176-179.

93. Vasak, M., Galdes, A., Hill, H. A. O., Kagi, J. H. R., Bremner, I., and Young, B. W. (1980) Investigation of the structure of metallothioneins by proton nuclear magnetic resonance spectroscopy, *Biochemistry 19*, 416-425.
94. Otvos, J. D., and Armitage, I. M. (1980) Structure of the metal clusters in rabbit liver metallothionein, *Proc. Natl. Acad. Sci. U.S.A 77*, 7094-7098.
95. Otvos, J. D., and Armitage, I. M. (1979) ^{113}Cd NMR of metallothionein: Direct evidence for the existence of polynuclear metal binding sites, *J. Am. Chem. Soc. 101*, 7734-7736.
96. Sadler, P. J., Bakka, A., and Beynon, P. J. (1978) ^{113}Cd nuclear magnetic resonance of metallothionein: Non-equivalent CdS_4 sites, *FEBS Lett. 94*, 315-318.
97. Hunt, C. T., Boulanger, Y., Fesik, S. W., and Armitage, I. M. (1984) NMR analysis of the structure and metal sequestering properties of metallothioneins, *Environ. Health Perspect. 54*, 135-145.
98. Peroza, E. A., Schmucki, R., Guntert, P., Freisinger, E., and Zerbe, O. (2009) The β_E-domain of wheat E_c-1 metallothionein: a metal-binding domain with a distinctive structure *J. Mol. Biol. 387*, 207-218.
99. Blindauer, C. A., Harrison, M. D., Parkinson, J. A., Robinson, A. K., Cavet, J. S., Robinson, N. J., and Sadler, P. J. (2001) A metallothionein containing a zinc finger within a four-metal cluster protects a bacterium from zinc toxicity, *Proc. Natl. Acad. Sci. U.S.A 98*, 9593-9598.
100. Prohaska, J. R. (2008) Role of copper transporters in copper homeostasis, *Am. J. Clin. Nutr. 88*, 826S-829S.
101. Meloni, G., Sonois, V., Delaine, T., Guilloreau, L., Gillet, A., Teissie, J., Faller, P., and Vasak, M. (2008) Metal swap between Zn_7-metallothionein-3 and amyloid-β-Cu protects against amyloid-β toxicity, *Nat. Chem. Biol. 4*, 366-372.
102. Beltramini, M., and Lerch, K. (1981) Luminescence properties of *Neurospora* copper metallothionein, *FEBS Lett. 127*, 201-203.
103. Salgado, M. T., and Stillman, M. J. (2004) Cu^+ distribution in metallothionein fragments, *Biochem. Biophys. Res. Commun. 318*, 73-80.
104. Li, Y.-J., and Weser, U. (1992) Circular dichroism, luminescence, and electronic absorption of copper binding sites in metallothionein and its chemically synthesized α and β domains, *Inorg. Chem. 31*, 5526-5533.
105. Yoshida, M., Watanabe, C., Horie, K., Satoh, M., Sawada, M., and Shimada, A. (2005) Neurobehavioral changes in metallothionein-null mice prenatally exposed to mercury vapor, *Toxicol. Lett. 155*, 361-368.
106. Yoshida, M., Watanabe, C., Satoh, M., Yasutake, A., Sawada, M., Ohtsuka, Y., Akama, Y., and Tohyama, C. (2004) Susceptibility of metallothionein-null mice to the behavioral alterations caused by exposure to mercury vapor at human-relevant concentration, *Toxicol. Sci. 80*, 69-73.
107. Yoshida, M., Watanabe, C., Kishimoto, M., Yasutake, A., Satoh, M., Sawada, M., and Akama, Y. (2006) Behavioral changes in metallothionein-null mice after the cessation of long-term, low-level exposure to mecury vapor, *Toxicol. Lett. 161*, 210-218.

108. Satoh, M., Nishimura, N., Kanayama, Y., Naganuma, A., Suzuki, T., and Tohyama, C. (1997) Enhanced renal toxicity by inorganic mercury in metallothionein-null mice, *J. Pharmacol. Exp. Ther. 283*, 1529-1533.
109. Rooney, J. P. K. (2007) The role of thiols, dithiols, nutritional factors and interacting ligands in the toxicology of mercury, *Toxicology 234*, 145-156.
110. Aschner, M., Conklin, D. R., Yao, C. P., Allen, J. W., and Tan, K. H. (1998) Induction of astrocyte metallothioneins (MTs) by zinc confers resistance against the acute cytotoxic effects of methylmercury on cell swelling, Na^+ uptake, and K^+ release, *Brain Res. 813*, 254-261.
111. Rising, L., Vitarella, D., Kimelberg, H. K., and Aschner, M. (1995) Metallothionein induction in neonatal rat primary astrocyte cultures protects against methylmercury cytotoxicity, *J. Neurochem. 65*, 1562-1568.
112. Lu, W., and Stillman, M. J. (1993) Mercury-thiolate clusters in metallothionein. Analysis of circular dichroism spectra of complexes formed between α-metallothionein, apometallothionein, zinc metallothionein, and cadmium metallothionein and Hg^{2+}, *J. Am. Chem. Soc. 115*, 3291-3299.
113. Lu, W., Zelazowski, A. J., and Stillman, M. J. (1993) Mercury binding to metallothioneins: Formation of the Hg_{18}-MT species, *Inorg. Chem. 32*, 919-926.
114. Leiva-Presa, A., Capdevila, M., and Gonzalez-Duarte, P. (2004) Mercury(II) binding to metallothioneins: Variables governing the formation and structural features of the mammalian Hg-MT species, *Eur. J. Biochem. 271*, 4872-4880.
115. Cai, W., and Stillman, M. J. (1988) Hg_{18}-metallothionein, *J. Am. Chem. Soc. 110*, 7872-7873.
116. Jiang, D. T., Heald, S. M., Sham, T. K., and Stillman, M. J. (1994) Structures of the cadmium, mercury, and zinc thiolate clusters in metallothionein: XAFS study of Zn_7-MT, Cd_7-MT, Hg_7-MT, and Hg_{18}-MT formed from rabbit liver metallothionein 2, *J. Am. Chem. Soc. 116*, 11004-11013.
117. Gehrig, P. M., You, C., Dallinger, R., Gruber, C., Brouwer, M., Kagi, J. H. R., and Hunziker, P. E. (2000) Electrospray ionization mass spectrometry of zinc, cadmium, and copper metallothioneins: Evidence for metal-binding cooperativity, *Protein Sci. 9*, 395-402.
118. Good, M., Hollenstein, R., Sadler, P. J., and Vasak, M. (1988) ^{113}Cd NMR studies on metal-thiolate cluster formation in rabbit Cd(II)-metallothionein: Evidence for a pH dependence, *Biochemistry 27*, 7163-7166.
119. Mocchegiani, E., Giacconi, R., Muti, E., Cipriano, C., Costarelli, L., Tesei, S., Gasparini, N., and Malavolta, M. (2007) Zinc-bound metallothioneins and immune plasticity: Lessons from very old mice and humans, *Immun. Ageing 4*, doi:10.1186/1742-4933-1184-1187.
120. Giacconi, R., Bonfigli, A. R., Testa, R., Sirolla, C., Cipriano, C., Marra, M., Muti, E., Malavolta, M., Costarelli, L., Piacenza, F., Tesei, S., and Mocchegiani, E. (2008) +647 A/C and +1245 MT1A polymorphisms in the susceptibility of diabetes mellitus and cardiovascular complications, *Mol. Gen. Metab. 94*, 98-104.
121. Maret, W. (2008) A role for metallothionein in the pathogenesis of diabetes and its cardiovascular complications, *Mol. Gen. Metab. 94*, 1-3.

122. Bertini, I., Luchinat, C., Messori, L., and Vasak, M. (1989) Proton NMR studies of the cobalt(II)-metallothionein system, *J. Am. Chem. Soc. 111*, 7296-7300.
123. Vasak, M., and Kagi, J. H. R. (1981) Metal thiolate clusters in cobalt(II)-metallothionein, *Proc. Natl. Acad. Sci. U.S.A 78*, 6709-6713.
124. Romero-Isart, N., Jensen, L. T., Zerbe, O., Winge, D. R., and Vasak, M. (2002) Engineering of metallothionein-3 neuroinhibitory activity into the inactive isoform metallothionein-1, *J. Biol. Chem. 277*, 37023-37028.
125. Sewell, A. K., Jensen, L. T., Erickson, J. C., Palmiter, R. D., and Winge, D. R. (1995) Bioactivity of metallothionein-3 correlates with its novel β domain sequence rather than metal binding properties, *Biochemistry 34*, 4740-4747.

Chapter 2. Methods for Preparation and Characterization of Recombinant MT[2]

2.1 Introduction

Metallothionein (MT) was first isolated from horse kidney cortex in 1957. This first isolation of MT relied upon retaining the cadmium content present in kidney homogenate following a series of purifications. In fact, early *in vitro* studies of MT relied upon purification from natural sources, the most well studied of which were those from mammalian sources including, human, rabbit, and horse. These purification protocols relied upon rigorous and time consuming metal ion injection procedures, where the lab animal was euthanized and the organ of interest, usually the liver or the kidney, was isolated with subsequent MT extraction. Studies on human MT were further complicated by the necessity to isolate MT from cadavers. The above described procedure, while inefficient, is well suited for studying MT isoforms -1 and -2, because both can be induced by a number of stimuli including metal ions, glucocorticoids, cytokines and oxidative stress. However expression of other MT isoforms, MT-3 and MT-4, are more strictly controlled. This restriction is a contributing factor to their relatively late isolation and discovery.

Modern studies rely heavily on recombinant protein expression systems, where the MT of interest is grown and isolated from a non natural source, for example human MT grown and purified from *Escherichia coli* (*E. coli*). In these systems, the MT gene has been inserted into a host organism, which will produce significant quantities of the protein. There are several advantages when compared to isolation from natural sources, including enhanced purity and efficiency. MT from natural sources is composed of a mixture of isoform that must be separated using lengthy chromatographic methods. Since only a single isoform is inserted into the host system, these purification steps are avoided. By using recombinant protein expression systems, unusual MT proteins have

[2] A version of this work has been published:

been designed, including single domain studies (β or α-rhMT) and different domain combinations (αβ-, ββ-, βββ-, αα- and ααα- rhMT). There are, however, several disadvantages to these systems including necessary alterations of the MT-protein sequence to enhance expression and addition of peptide sequences, for example S-tag purification system, to the protein in order to allow for efficient purification from the cell lysate. Finally, there is also the potential for post-translational modifications that may significantly alter the chemical properties of the protein.

In this Chapter, the recombinant protein preparation is described for the production of the isolated β- and α-domains, and full MT protein of isoform 1a referred to as β-rhMT, α-rhMT and βα-rhMT, respectively. A brief description of the instrumental techniques used to characterize MT and its domains are also provided.

2.2 Recombinant Expression and Purification of MT 1a

2.2.1 Materials and solution preparation

Materials

Table 2-1 provides a list of the chemicals and biological agents used in the preparation of MT and its isolated domains. All experiments described throughout this thesis used these compounds.

Solutions preparation

All solutions were prepared with deionized water (di-H_2O) with a resistivity greater than 14 MΩ•cm (Barnstead, Dubuque, IL, USA). The kanamycin antibiotic solution was prepared by adding di-H_2O to 0.5 g of solid kanamycin to a final volume of 10 mL (50 mg/mL final conc.). Large particulate was then removed by filtering the kanamycin solution through 0.2 μm syringe filters. The filtrate was separated into 1 mL aliquots in sterile Eppendorf tubes and stored in a freezer at -20 °C. The isopropyl-β-D-thiogalactoside (IPTG) was prepared by adding di-H_2O to 2.38 g of solid IPTG to a final volume of 10 mL (1 M final conc.). This solution was then separated into 0.7 mL aliquots in sterile Eppendorf tubes and stored in a freezer at -20 °C. The LB Miller Broth was prepared by adding 25 g to each of the 4-Fernbach flasks containing 1 L of di-H_2O and lightly sealed with aluminum foil. The LB Agar gel was prepared by adding di-H_2O

to 4 g of agar to a final volume of 100 mL. This solution was lightly sealed with aluminum foil. In order to sterilize the solutions, both the LB Miller Broth and Agar were autoclaved for 20 min at 121 °C. When the LB Agar was warm to the touch, kanamycin antiboitc solution was added (final conc. 50 μg/mL). The LB Agar was poured into disposable sterile Petri dishes and the gel was allowed to solidify to room temperature. These dishes were parafilmed and stored in a fridge at 4 °C.

Table 2-1. Chemical and biological reagents used.

CHEMICAL	F. W. (g/mol)	GRADE	SUPPLIER
Ammonium Formate, NH_4COOH	63.06	Reagent	J. T. Baker
Ammonium Hydroxide, NH_4OH	35.05	Reagent	Caledon
BL21(DE3) Strain of *E. coli*		Biotech	
Cadmium sulfate, $3CdSO_4•8H_2O$	769.56	ACS	Fisher
Cadmium(113)chloride, $^{113}CdCl_2$	183.9	>96%	Trace Sciences International
Formic Acid (88%), HCOOH	46.03	Reagent	Caledon
Hydrochloric Acid, HCl	36.46	Reagent	Caledon
Isopropyl-β-D-thiogalactoside	238.31	Biotech	Fisher
Kanamycine, monosulfate, $C_{18}H_{36}N_4O_{11}•H_2SO_4$	582.58	Biotech	EMD
LB Agar, Miller		Biotech	Difco Laboratories
LB Broth, Miller		Biotech	Fluka Analytical
Sephadex G-25 Fine		Biotech	Amersham Biosciences
Thrombin CleanCleave™ Kit		Biotech	Sigma-Aldrich
Tris(2-carboxyethyl)phosphine (TCEP), $C_9H_{15}O_6P$	286.65	Reagent	Sigma-Aldrich
Tris(hydroxymethyl)aminomethane (Tris), $(CH_2OH)_3CNH_2$	121.14	Reagent	EMD
Zinc sulfate, $3ZnSO_4•7H_2O$	287.56	ACS	Caledon

MT was purified from the cell homogenate by using an SP ion exchange column and required four solutions: 10 mM Tris-HCl, pH 7.4 (Solution A), 10 mM Tris-HCl + 1 M NaCl, pH 7.4 (Solution B), 350 mM ammonium formate (Solution C), and di-H_2O

(Solution D). All four buffers were prepared by dissolving the appropriate amount of chemical into di-H_2O and the pH was adjusted using either concentrated hydrochloric, formic acid, or ammonium hydroxide. The pH of the solutions was monitored using a pH meter (Accumet Basic AB15, Fisher Scientific, Ottawa, ON, Canada) with an Accumet Semimicro pH electrode. MT can readily oxidize upon exposure to oxygen. To impede oxidation of the cysteine residues to disulfide bonds by oxygen, all solutions were rigorously evacuated and argon saturated.

Metallothionein Transformed Bacterial Cells

The MT DNA was provided by Peter Kille (Cardiff, Wales) and transformed by Jayna Chan, Christie Vermieren and Thanh Ngu (U.W.O). The following sections briefly discuss the MT construct and describe in detail, the growth, isolation and purification of MT from bacterial cells.

The DNA constructs of the isolated β- and α-domains and the full MT protein engineered from human MT 1a (Table 2-2). The pET-29a plasmids (Novagen/EMD Biosciences, San Diego, CA, USA), which the MT protein and its isolated domains were transformed into, contained a kanamycin-resistance gene allowing selective growth of bacteria that have taken up the plasmid. This plasmid contains an S-tag™ (Novagen/EMD Biosciences) upstream of the MT DNA sequence. Consequently, all expressed protein will be S-tag fusion proteins with the tag attached to the N-terminus. Plasmids were transformed into competent *E. coli* BL21(DE3) cells (Novagen/EMD Biosciences). All transformed cell lines were grown to an optical density of 0.6 and stored in a 50% (v/v) solution of glycerol at -80 °C.

Table 2-2. Amino acid sequences used in study. Amino acid sequence of human MT 1a (hMT-1a), recombinant human MT 1a (rhMT-1a), the isolated β-domain of human MT 1a (β-rhMT-1a), the isolated α-domain of human MT 1a (α-rhMT-1a) and finally the S-tag used to stabilize the expression of the MT protein. The N-terminus is located on the left hand side, while the C-terminus is located on the right. Colour legend: Red – cysteine residues, Green – inserts to align sequences of different lengths, blue – modified amino acids found in constructs.

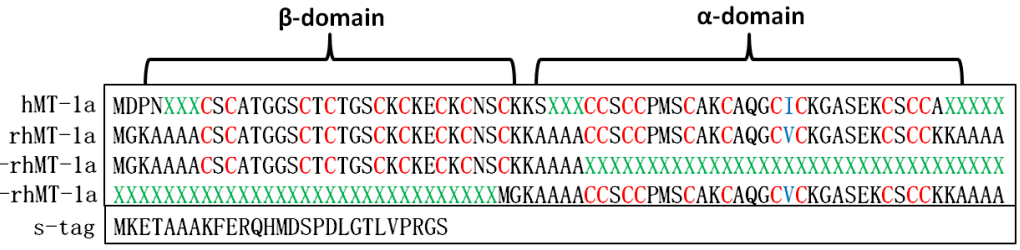

2.2.2 Overexpression of Recombinant Cd-Metallothionein

The protocol for MT, and its isolated domains, preparation is presented in Figure 2-1. It should be noted that this protocol allows for the production of metalated Cd-MT, specifically Cd_7-βα-rhMT, Cd_3-β-rhMT and Cd_4-α-rhMT. From the glycerol stocks, a small portion of frozen cells were plated onto room temperature agar plates containing 50 μg/mL (final conc.) kanamycin sulfate. The presence of the antibiotic ensures that only cells that have been transformed with the MT plasmid will grow. These plates were kept overnight at 37 °C. To four 2 L Fernbach flasks, 1 L of sterilized LB liquid media was added, as well as kanamycin and $CdSO_4$ to a final concentration of 50 μg/mL and 50 μM, respectively. The $CdSO_4$ was added to ensure that any MT grown prior to induction would be stabilized and it also provided a secondary selective pressure for bacteria that express MT. The cells were transferred into the LB liquid media and placed in an incubator-shaker at 37 °C and 150 rpm to facilitate aeration of the cells. Protein expression was induced at an optical density of 0.5-0.6 at 600 nm, which corresponds to the mid-log phase of the bacterial growth cycle. At this point, IPTG was added to a final concentration 0.7 mM to induce MT expression. The cells were allowed to express MT for 30 min, at which point additional $CdSO_4$ was added to solution to a final total $CdSO_4$ concentration of 200 μM.

2.2.3 Isolation and purification of recombinant Cd-metallothionein

Following growth, the cells were isolated by centrifugation at 8,983 *g* for 15 min using an Avanti J-series centrifuge (Beckman-Coulter, Mississauga, ON, Canada) with a JLA-9.1000 rotor. At this point the LB broth supernatant was discarded and the cell pellet was resuspended in a deoxygenated 10 mM Tris-HCl solution, pH 7.4. The cells were lysed using a French press and were centrifuged at 20,442 *g* for 1 hr using a JLA-25.50 rotor to remove the cellular debris. Typical yields were 10 mg of protein per 1 L of LB broth.

The supernatant was loaded onto a Hi Trap™ SP Sepharose™ HP cation exchange chromatographic cartridge. The elution was monitored using the ligand-to-metal charge transfer (LMCT) transition of S→Cd of MT by UV absorption spectroscopy. The cartridges were washed with solution A that had been argon saturated to remove the cellular components that were weakly associated to the column. Following this wash, a stepwise increase in the amount of solution B from 0% to 5% in 1% increments removed more tightly bound complexes. Cd-MT elutes at 5% (50 mM) NaCl. At this point, the salt concentration is increased to 30% in order to remove the protein in as small a volume as possible. A small aliquot of the protein was desalted into 5 mM ammonium formate in order to determine the purity by electrospray ionization mass spectrometry. The protein was subsequently concentrated to an 8 mL fraction using the stirred ultrafiltration cell (Amicon Bioseparations/Millipore, Bedford, MA, USA) with a YM-3 cellulose membrane (3,000 MWCO) under pressure by an inert gas (in this case nitrogen) to avoid oxidation of the protein through oxygen exposure.

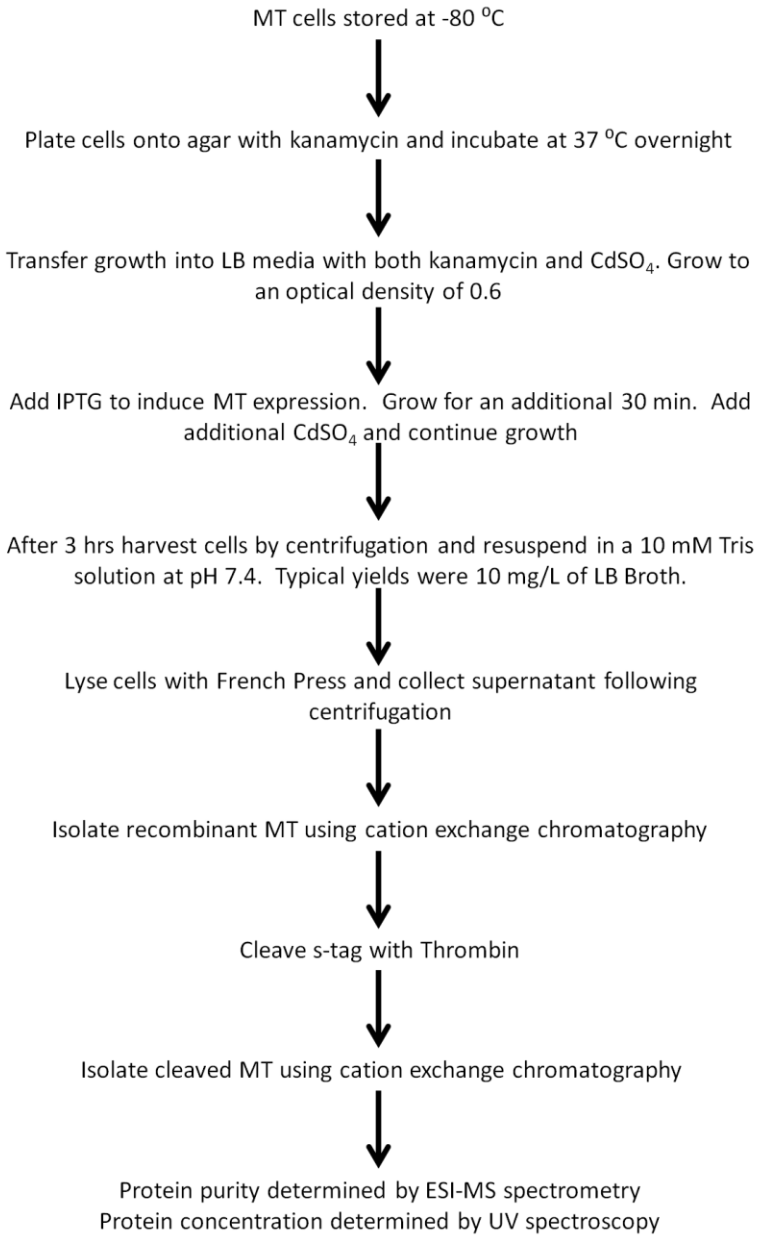

Figure 2-1. Protein preparation protocol for all metallothioneins used.

2.2.4 Cleavage of the S-tag from recombinant Cd-metallothionein

Both the isolated domains, and the full MT protein, were expressed with a 27 amino acid S-tag (Table 2-2 Figure 2-2) attached to the N-terminus of the recombinant protein. This tag has been observed to aid in the stability of the MT protein during expression (personal communication with Professor Peter Kille). For all subsequent experiments, the S-tag is cleaved using a Thrombin CleanCleave™ Kit. This kit contains bovine

Thrombin immobilized onto agarose beads. There are two optimal cleavage sites for the thrombin enzyme: The first is P4-P3-Pro-Arg/Lys•P1'-P2', where P4 and P3 are hydrophobic residues and both P1' and P2' are non-acidic residues. The scissile bond is the Arg/Lys•P1'. The second is P2-Arg/Lys•P1', where P2 or P1' is a glycine residue and Arg/Lys•P1'is the scissile bond. Figure 2-2 shows that the Thrombin enzyme cleaves M_7-βα-rhMT 1a at an Arg-Gly bond. One consequence of this cleavage site is that there remain 2 amino acids, glycine and serine, from the S-tag.

The thrombin suspension was purchased as immobilized agarose beads (Thrombin CleanCleave™, Sigma) to facilitate separation from the recombinant protein without the need for chromatographic steps. The thrombin-agarose slurry was stored at -20 °C in a 50 % (v/v) solution of glycerol and 20 mM Tris-HCl, pH 8.0. Use of the thrombin-agarose beads requires two cleavage buffers, 500 mM Tris-HCl, pH 8.0, 100 mM $CaCl_2$ (10X cleavage buffer) and a 50 mM Tris-HCl, pH 8.0, 10 mM $CaCl_2$ (1X cleavage buffer), both of which were rigorously bubbled with argon and evacuated immediately prior to use. The resin was washed by pelleting the beads by centrifugation at 500 *g* for 5 min using an Eppendorf centrifuge 5418 (Eppendorf North America, Inc., Westbury, NY). The supernatant was removed and the beads were resuspended in an equal volume of 1X cleavage buffer. The cells were again pelleted and resuspended in 1X cleavage buffer to insure complete removal of glycerol.

To the resuspended beads, 10% (v/v) of 10X deoxygenated cleavage buffer was added directly to the Thrombin slurry. The protein and a magnetic stir bar were added to the Thrombin solution, evacuated and sealed under Argon. The mixture was stirred at 4 °C overnight. The beads were removed by centrifugation at 500 g for 5 min and were washed with deoxygenated 1X cleavage to ensure complete removal of the beads. The supernatant from both the initial cleavage and the wash, which contained the protein and the S-tag, were pooled.

A fine G-25 Sephadex size-exclusion column was equilibrated with deoxygenated 10 mM Tris-HCl, pH 7.4. The protein solution was loaded onto this column and desalted. The protein/S-tag mixture was subsequently loaded onto the SP ion exchange column at a rate of 3 mL/min. All solutions used for the SP ion exchange column are identical to those used to purify the recombinant MT from the cell homogenate. The column was

washed with solution A and monitored using UV absorption spectroscopy. While MT requires a solution of 10 mM Tris, pH 7.4 and 50 mM NaCl to elute from the column, the S-tag does not adhere strongly and can be eluted by simply washing the column with solution A. Once the UV absorption profile showed that no peptide was being eluted, the composition of solution B in the eluent was increased from 0% to 5%, with a concomitant decrease in the composition of solution A from 100% to 95%. This increase facilitates the removal of any remaining S-tag, as well as other proteins that may bind weakly to the column. At 5% solution B both the full MT protein, or the isolated fragments, begin to elute from the column. This is observed by an increase in the absorption at 250 nm corresponding to the LMCT of the S → Cd bonds in the metal-thiolate clusters. The composition of solution B in the eluent is immediately increased to 30%. This allows complete removal of either MT or its isolated clusters in a minimum volume. The cleaved protein collected from the SP column was concentrated using stirred ultrafiltration cell model 8200 (Amicon Bioseparations/Millipore) with the YM-3 membrane (3,000 MWCO) to 8 mL.

All cleaved protein was subjected to both mass spectrometric and UV absorption spectroscopic analysis. In the former, electrospray ionization mass spectrometry provided the mass of the protein plus any bound Cd^{2+} ions. The observed mass always corresponded well with the theoretical mass. There were several instances in which a loss of amino acids was observed. In these cases, ESI-mass spectrometric analysis revealed the identity of the missing amino acids. UV absorption spectroscopy provided an estimate of the concentration of either of the isolated domains, or the full MT protein.

2.2.5 Preparation of metal-free recombinant metallothionein

A sample of thrombin cleaved metal-free (apo-) MT was prepared by decreasing the pH of metalated Cd_3-β-, Cd_4-α- and Cd_7-βα-rhMT to 2 through the stepwise addition of concentrated HCl. The pH was monitored using pHydrion® pH paper (Micro Essential Laboratory, Inc.). A deoxygenated fine G-25 Sephadex size-exclusion column was used to remove the previously bound Cd^{2+} ions. The eluent buffer was chosen to suit the final experiment. For example, apo-MT prepared for electrospray mass spectrometry, was exchanged into di-H_2O pH adjusted to 2.7 with concentrated formic acid. Unlike Cd-

bound MT, apo-MT has no LMCT and metal free fractions were monitored by UV absorption at 220 nm. A small aliquot of buffer exchanged MT was remetalated using $CdSO_4$ and the LMCT was monitored in order to determine the apo-protein concentration. The demetalated MT was subsequently evacuated, capped and backfilled with argon in order to remove the bulk of oxygen in the sample. Exposure to oxygen oxidizes MT and samples prepared in this manner may last for up to several weeks.

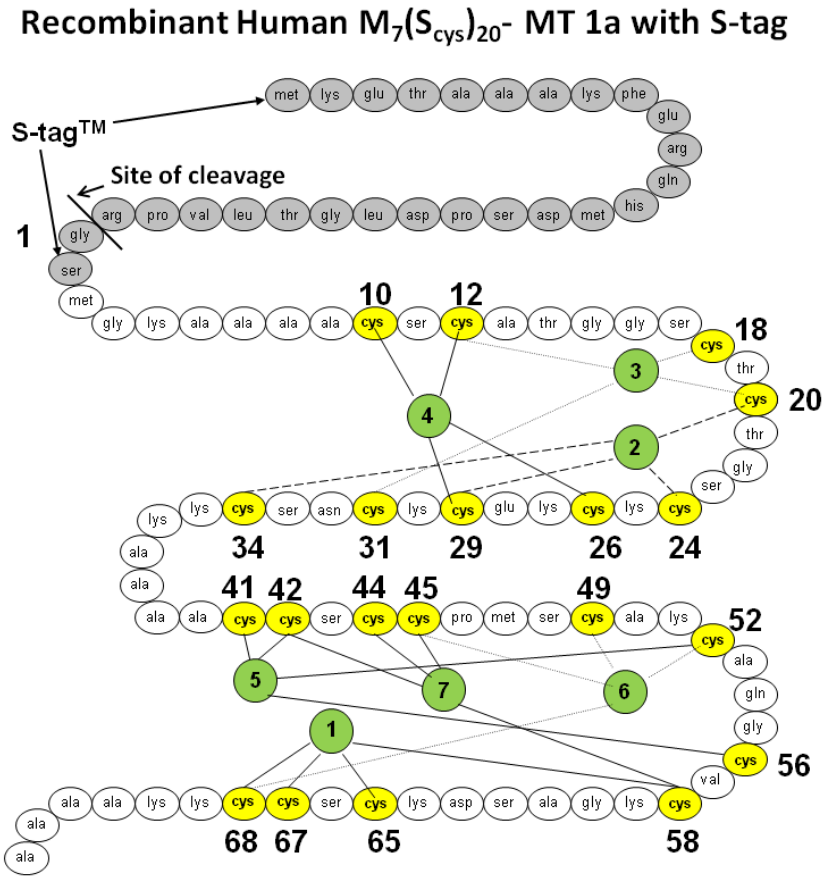

Figure 2-2 A connectivity diagram of MT 1a. This shows that each of the seven cadmium atoms is connected to exactly four cysteine amino acids. The connectivity diagram has been renumbered to accommodate the amino acids glycine and serine, both of which are a product of S-tag cleavage with Thrombin, located on the N-terminal of the β-domain.

2.2.6 Preparation of ^{113}Cd-recombinant metallothionein

To a sample of deoxygenated metal-free (apo-) MT 1a, solid $^{113}CdCl_2$ was added directly to the solution at a ratio that would lead to complete metalation for either of the

isolated domains (3 or 4 Cd^{2+} per β or α-rhMT, respectively), or the full MT protein (7 Cd^{2+} per βα-rhMT 1a). The solution was neutralized by the stepwise addition of deoxygenated concentrated ammonium hydroxide. MT spontaneously remetalates when neutralized. The solution is then rigorously evacuated to remove any oxygen that may have entered the solution. A fine G-25 Sephadex size-exclusion column was buffer equilibrated with 5 mM ammonium formate that had been pH adjusted to 7.4 with deoxygenated concentrated ammonium hydroxide. The isotopically enriched MT sample was then desalted into the 5 mM ammonium formate solution, pH 7.4 in order to remove any excess salt of $^{113}Cd^{2+}$ ions that may be present. The solution was then concentrated to 8 mL using an Amicon stirred ultrafiltration cell model 8200. The MT solution was further concentrated to 1-2 mL using an Amicon stirred ultrafiltration cell model 8010. The final concentration was determined by UV absorption spectroscopy through a thousand fold dilution of an aliquot of the isotopically enriched MT sample.

2.3 Instrumental Techniques

Metallothionein binds a wide array of metals, ranging from physiologically crucial metals, such as Zn^{2+} and Cu^{+}, to the toxic metals, such as Cd^{2+} and Hg^{2+}. We outline several techniques, which have been critical to the understanding of metal binding. Critical to this thesis include UV absorption, circular dichroism and nuclear magnetic resonance spectroscopy, as well as electrospray ionization mass spectrometry. A brief overview of these techniques and the information that can be extracted from them is discussed. A section describing the computational modeling that was used to calculate the qualitative models of supermetalated MT is also presented.

2.3.1 UV absorption spectroscopy

Metallothionein exhibits a number of characteristic spectroscopic signatures that depend on the type of metal bound. Because of the lack of either aromatic amino acids or a defined secondary structure, such a β sheet or an α helix, in the apo-form (*1-2*) it is far easier to measure spectroscopic properties that are entirely dependent on both the type and number of metals bound, than is the case with many metalloproteins (*3-5*). UV-visible absorption and circular dichroism spectroscopies have been the key techniques in

the determination of the relative affinities of metallothioneins for metal ions, the mode of metal coordination and possible stoichiometries of these metals. In particular, the lack of aromatic amino acid residues allows UV absorption spectroscopy to monitor the ligand-to-metal charge transfer bands above 220 nm without interference. These techniques are widely used to monitor metalation reactions of d^{10} metals, such as Zn^{2+}, Cd^{2+}, Hg^{2+}, Cu^{+} and Ag^{+} (*6-11*). Typically, a titration with a metal ion leads to a change in the UV absorption spectrum of the solution demonstrating either binding of the metal to the metal free protein, or, alternatively displacement of an already present metal. The former is used to determine binding stoichiometries for high affinity metals, while the latter can be used to determine binding affinity and possible mixed metal species. If, however, the incoming metal ion has a low binding affinity, then caution should be taken in directly correlating a spectroscopically-determined maximum with a particular metal binding stoichiometry.

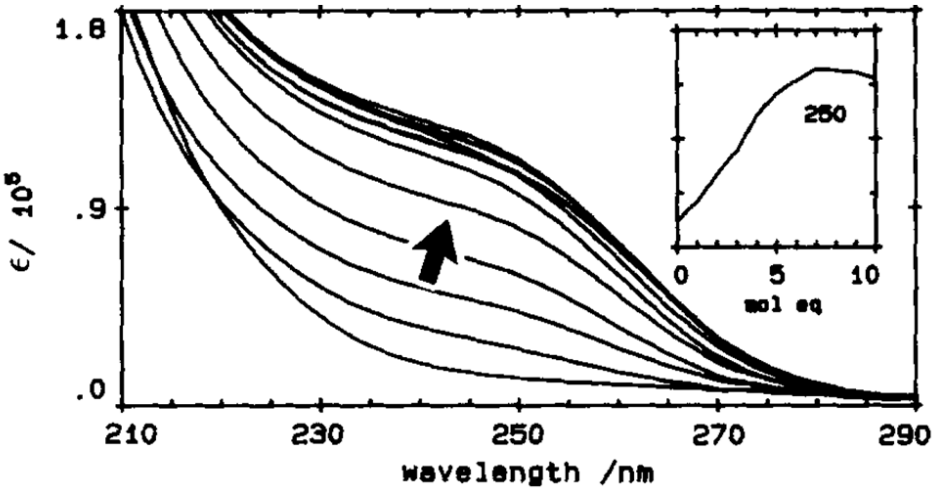

Figure 2-3. **UV absorption spectroscopy of rabbit liver metallothionein 2 (βα-rlMT-2) as a function of increasing additions of aliquots of Cd^{2+}.** The concentration of protein was 10 μM, while spectra were recorded at pH 7. There are 11 lines: line 1, apo-βα-rlMT-2 at pH 2; line 2, apo-βα-rlMT-2 at pH 7; lines 3-11 for apo-βα-rlMT-2 with different concentrations of Cd^{2+} (1.06, 2.14, 3.5, 5.0, 5.95, 6.05, 6.92, 7.61, and 8.82 molar equivalent). It should be noted that as the amount of Cd^{2+} added to the solution increases, the absorbance at 250 nm increases as well. The inset represents changes in the intensity as monitored by the ligand-to-metal charge transfer band of cadmium thiolate at 250 nm, as a function of molar equivalents of Cd^{2+} added. Adapted from (12) with permission from ASBMB Copyright 1987.

Figure 2-3 shows a classical titration of rabbit liver apoMT-2 with Cd^{2+} monitored by UV-absorption spectroscopy between 210 and 290 nm (*12*). Initially, the absorbance is associated with the protein backbone, the metal-free apo-MT. However, upon addition of Cd^{2+} a shoulder forms at 250 nm, which corresponds to the ligand-to-metal charge transfer of cadmium-thiolate bonds. The UV absorbance at 250 nm is at a maximum at 7 Cd^{2+} atoms, corresponding to fully metalated Cd_7-βα-MT-2. Complete binding of the Cd^{2+} ions is the result of the high affinity of cysteinyl sulfurs for Cd^{2+}, $6.0x10^{21} – 10^{25.6}$ M^{-1} (*13-14*). While the stoichiometry of metal binding may be extracted from UV absorption spectra, it is the CD spectra that clearly show changes in the metal-binding sites indicative of a transition from individual CdS_4 sites to the formation of the polynuclear clusters (*15*). The maximum of seven Cd^{2+} per βα-MT has been confirmed by ESI-MS measurements for MTs from many different mammalian sources, for example, human MT (*16-17*). In the case shown in Figure 2-3, we see a slight reduction in absorbance at 250 nm, which has been interpreted as due to non-specific Cd^{2+} associating with the protein. That these ions do not change the CD band envelope morphology is strong evidence that the Cd_7S_{20} domain structure is not directly affected.

While metallothionein is key in the cellular homeostasis of both Zn^{2+} and Cu^{+}, as d^{10} metals, their spectroscopic signatures are essentially limited to the ligand-to-metal charge transfer bands (thiolate to Zn^{2+} and thiolate to Cu^{+}). On the other hand, metalation of metallothionein using metal ions with an incomplete d shell allows d→d transitions to be monitored. These transitions are sensitive to the coordination geometry of the metal atom, and coupled with information provided by the ligand-to-metal charge transfer bands, can allow assignment of both the coordinating ligands and the metal binding geometry. In the following three examples of Co^{2+}, Ni^{2+} and Fe^{2+}, a maximum metal binding stoichiometry of 7 metal atoms has been determined spectroscopically. The spectral data for the binding of Co^{2+} to metallothionein demonstrates that the protein enforces a distorted tetrahedral arrangement in which the α-domain has more tetrahedral character than the β-domain (*18-21*). The spectroscopic data for Ni^{2+} binding to metallothionein does not have distinct d→d transitions, however, the spectrum was similar to Ni^{2+} bound to azurin, and this suggests a tetrahedral coordination. Fe^{2+} has also been shown to bind in a tetrahedral manner, with a d→d transition in the near infrared

region (*22*). While these metals may not be naturally associated with the protein, their spectroscopic characteristics are useful in determining the flexibility of the protein in accommodating different metals.

2.3.2 Circular Dichroism (CD) spectroscopy

CD spectroscopy is an extremely valuable method used to measure the difference in absorption between left- and right-circularly polarized light caused by chirality in the chromophore as a function of the wavelength of light used. This method is highly sensitive to conformations of optically active chiral molecules. Traditionally in biochemistry, the CD technique has been used to determine the extent of secondary structure of a protein, such as α-helices, β-sheets and turns in the protein, or the status of complexation based on the relative differential absorbance of the amino acids in the peptide chain. In this manner the effects of denaturing agents, temperature, potential ligands and mutations can be readily and reliably monitored.

In MT much greater structural sensitivity is found in the CD spectrum, because the metals that bind form structurally significant binding sites that exhibit specific chirality and cause the protein to fold into a predefined structure (Figure 2-2). These chiral structures are composed of the metal ion and the thiolate donor atoms of the cysteine residues. The ligand to metal charge transfer transitions in MTs are easy to measure above 230 nm because they occur in the region of the electronic spectrum devoid of the usual transitions associated with aromatic amino acids. This window region has allowed detailed spectroscopic analyses of the metalation reactions of MT to be carried out for the d^{10} metals that are otherwise chromophorically-silent. The CD spectrum of MT to the red of 220 nm is completely dependent on the binding of metal ions.

Possibly the first CD spectrum of MT was published for Zn,Cd-βα-MT (*23*). In subsequent studies of the rabbit liver Cd_7-βα-MT-2a, it was reported that the morphology of the CD spectrum resembled a derivative shape with the cross-over point aligned with the 250 nm band of the $S \rightarrow Cd^{2+}$ ligand-to-metal charge transfer (*12*, *24-25*). The origin of this morphology was explained by Stillman *et al.* as resulting from exciton coupling between pairs of Cd^{2+} ions in the α-domain through the interpretation of CD spectral changes that took place following the titration of Cd^{2+} into rabbit liver Zn_7-βα-MT-2a

(*12*). That this CD band envelope represented a specific metalated structure was again demonstrated when the supermetalated Cd_5-α-hMT-1a was formed (*26*). Figure 2-4 shows the titration of human Cd_3-β-MT-1a with excess Cd^{2+} to form the Cd_4-β-MT-1a species, also the associated ESI-MS and ^{113}Cd NMR support the formation of a new species. It is in this way that CD data may act as a fingerprint for the determination of specific metalated species in MT.

Because of the utility of the CD technique, CD spectroscopic studies have been reported for a wide variety of metals (*11*), including Ag-MT (*27-28*), Cu-MT (*6, 24, 29-31*), Zn-MT (*6, 12, 25, 31-32*), Cd-MT (*6, 12, 24-25, 29*), and Hg-MT (*8, 33-34*). In this thesis, CD spectroscopy is used to investigate changes in the chirality of both the isolated β-domain and full MT protein upon binding of an additional Cd^{2+} ion to form Cd_4-β-rhMT (Chapter 5) and Cd_8-βα-rhMT (Chapter 6), respectively.

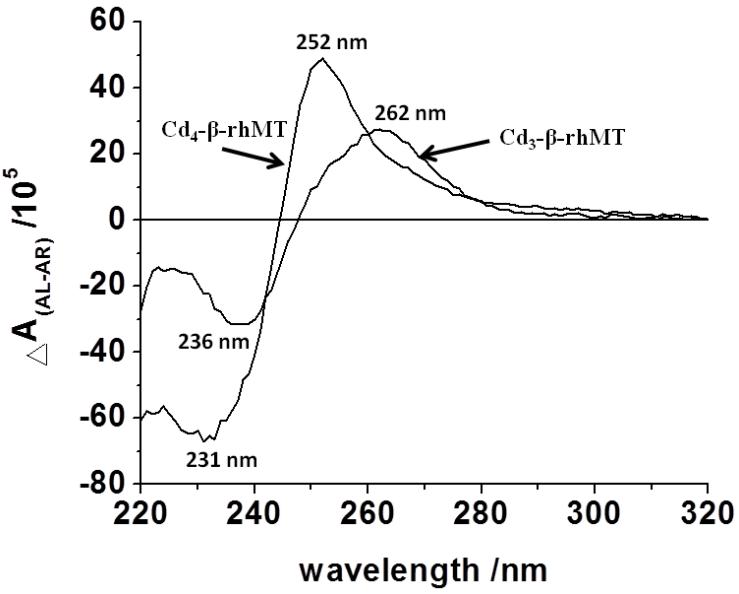

Figure 2-4 Circular dichroism spectral changes observed upon titrating human Cd_3-β-rhMT with an additional 4.4 molar equivalents of Cd^{2+} to form Cd_4-β-rhMT. Adapted from Sutherland *et al.*(35).

2.3.3 Nuclear Magnetic Resonance (NMR) Spectroscopy

NMR spectroscopy is one of the most powerful techniques used to analyze the structure and dynamics of metalloproteins. It should be noted that MT has been described as being notoriously difficult to crystallize, and much of our structural

knowledge is the result of many NMR-based studies. Structures based on analyses of the NMR data have been reported from several mammalian sources. These structures provide the absolute connectivities of all atoms and their spatial relationship within the metal-thiolate core. Specifically, structural studies of metallothionein have focused largely on $^{111/113}$Cd binding. There are several advantages to using Cd^{2+} to study the metalation of metallothionein including the natural presence of Cd^{2+} in metallothionein (*36*), Cd^{2+} having a similar coordination geometry to Zn^{2+}, and enhanced resistance to oxidation due to Cd^{2+} having a high affinity for thiolates.

Both isotopes ($^{111/113}$Cd) have a spin of ½: ^{111}Cd has a natural abundance of 12.75% but a relative sensitivity to ^{1}H (^{1}H = 1) of only 9.54×10^{-3}, while ^{113}Cd has a natural abundance of 12.26% and a relative sensitivity of 1.09×10^{-2}. The increased relative sensitivity of ^{113}Cd compared with ^{111}Cd makes the former isotope more widely used. The chemical shift range of ^{113}Cd has been recorded for a number of structurally characterized ^{113}Cd-substituted metalloproteins (*37*). With a chemical shift range of roughly 900 ppm (relative to 0.1 M $Cd(ClO_4)_2$), each ^{113}Cd is extremely sensitive to the coordinating ligands: heptacoordinate oxygen ligands are the most shielded, while tetrathiolate ligands are the most deshielding.

Enrichment with ^{113}Cd leads to an eight-fold enhancement of sample sensitivity over those measurements based upon natural abundance ^{113}Cd. This enhancement allows for data acquisition on low concentration (mM) samples in a reasonable amount of time. Samples can be prepared by demetalation at low pH, followed by removal of metal ions using gel filtration, and finally, remetalation using isotopically enriched $^{113}CdCl_2$. It should be stressed at this point that the high concentrations of a typical NMR sample have been reported to cause dimerization. Further complicating this issue are reports suggesting that demetalation through the use of strong acid leads to structural changes in metallothionein itself. As such, NMR spectral data should be correlated with other spectroscopic techniques (above), as well as spectrometric techniques, such as ESI-MS (below), which do not necessarily rely on either acid-induced demetalation or the large concentrations necessary for this technique (*38-40*).

Through an analysis of both the 1-D ^{113}Cd-NMR chemical shifts and splitting patterns, the structures of the polynuclear clusters within MT were determined. These experiments

identified the coordinating ligands as cysteinyl-thiolates and formulated the polynuclear centers as Cd_3S_9 and Cd_4S_{11}, corresponding to the β-domain and α-domain, respectively (*41-44*). While 1-D ^{113}Cd-NMR spectroscopy provides key information regarding the number of Cd^{2+} ions bound and their respective coordinating ligands, these experiments are resource intensive, requiring several days of acquisition.

A newer NMR method that is being used extensively in MT studies is Heteronuclear Single Quantum Coherence (HSQC), which provides increased sensitivity by using easily observed nuclei, such as ^{1}H, to obtain NMR information on insensitive nuclei, such as ^{113}Cd. A ^{1}H{^{113}Cd} HSQC experiments polarizes a ^{1}H nuclei and transfers that polarization to ^{113}Cd J-coupled nuclei. The signal is then allowed to evolve, and the polarization is transferred back to the ^{1}H nuclei, where acquisition occurs. A sensitivity increase of $\gamma_{1H}/\gamma_{113Cd}$, where γ is the magnetogyric ratio of the nuclei in question, is theoretically possible. ^{1}H nuclei have a magnetogyric ratio, γ_{1H}, of 267 radians/Tesla and ^{113}Cd nuclei have a magnetogyric ratio, γ_{113Cd}, of 59.6 radians/Tesla. From this combination of nuclei one can theoretically expect an additional 4.5-fold increase in sensitivity. Additionally, it may be possible to determine some of the terminal and bridging cysteine residues, where terminal coordination defines a cysteine residue bound to a single Cd^{2+} ion. The experiment may also provide some discriminatory evidence towards either a one- or two-domain model. Perhaps most importantly, good quality spectra are possible within a 12 hr period, as opposed to the much longer timescales of the ^{113}Cd 1-D NMR.

In this thesis, both 1-D and 2-D NMR spectroscopies are used to investigate Cd_3- and Cd_4-β-rhMT 1a (Chapter 5) and Cd_7- and Cd_8-βα-rhMT 1a (Chapter 6). Specifically, 1-D NMR spectroscopy provides the number of unique Cd^{2+} ions, while 2-D NMR spectroscopy is used to determine the identity of different Cd^{2+} ion. In both cases, the chemical shift provides information about the identity of the coordinating ligands.

2.3.4 Electrospray Ionization Mass Spectrometry (ESI-MS)

Electrospray ionization mass spectrometry (ESI-MS) measures the mass-to-charge ratio (*m/z*) of analytes, and because the ionization method allows the infusion of the analyte directly from solution, this method has become critical to many metallothionein

binding experiments. Unique to this technique is its ability to determine not only the number of metals bound but also the types of metals bound, which allows for a direct correlation between the spectroscopy and speciation of a sample. A brief description of the technique, followed by how data is interpreted, will allow for a better understanding of its usefulness in studying the complex metal binding properties of metallothioneins.

In the ESI-MS experiment, a sample in solution is introduced, under atmospheric pressure, into the tip of the electrospray capillary (Figure 2-5). This tip is electrically charged to several thousand volts and causes the solution to accumulate positive charge. Enrichment of the tip with positive ions leads to the formation of a Taylor cone, which ejects small positively charged droplets. Solvent evaporation decreases the radius of the droplet, while the charge remains constant. When Coulombic forces, due to the nearness of positively charges ions, overcome the surface tension, fission of the droplet occurs. Evaporation-fission events repeat until very small charged droplets are produced. Eventual formation of the multiply charged protein is thought to occur via the charged residue model (CRM) (*45-46*). The CRM mechanism of gas phase ion formation states that the small highly charged droplet will evaporate to dryness leaving any unpaired ions as adducts to the protein. Since each droplet will have varying numbers of charges, a distribution of mass-to-charge ratios will be observed. The charge state distribution is directly related to both the number of basic sites on the protein, as well as the size of the protein, as such any alterations to this size, or site exposure, through folding or through denaturation, will lead to changes in the charge state distribution.

Charged proteins are separated by differences in the *m/z* ratio; common analyzers include the quadrupole and time-of-flight mass analyzers, allowing detection of species even with very similar *m/z* values. The ESI-MS technique allows for the introduction of samples in aqueous solution and at physiological pH. Folding experiments can be conducted, in which the charge state distribution can be directly related to changes in sample conditions, such as pH or metal added, and changes in metalation status can be monitored by mass changes. By knowing the concentration of protein, from spectroscopic techniques, accurate quantification is possible through a comparison of the deconvoluted peaks. This, however, assumes that all species in solution ionize at the same rate, and may not always be true.

In the case of MT, metal induced folding experiments may be performed by the addition of small aliquots of metal ions to apo-MT (*17*, *47*). In this way both the number of metals bound and changes in the folding of the protein may be observed. For example, Figure 2-6 compares the ESI-mass spectral data for metal-free (apo-) MT 1a recorded when 0 and 7.3 eq. Cd^{2+} have been added to solution. It is immediately obvious that apo-MT possesses a greater number of charge states (+8 to +5) than Cd_7-MT (+6 and +5) and indicates that a folding event has occurred. The speciation of MT in solution may also be observed from the deconvoluted spectra, Figure 2-6 (right). These spectra are the result of the analysis of the *m/z* data, and allow slight shifts in the charge state of the protein to be interpreted as the relative populations of differently metalated species. Consequently, the folding of the protein is the result of metalation and has decreased the overall volume of space occupied by MT and/or the solvent exposed residues.

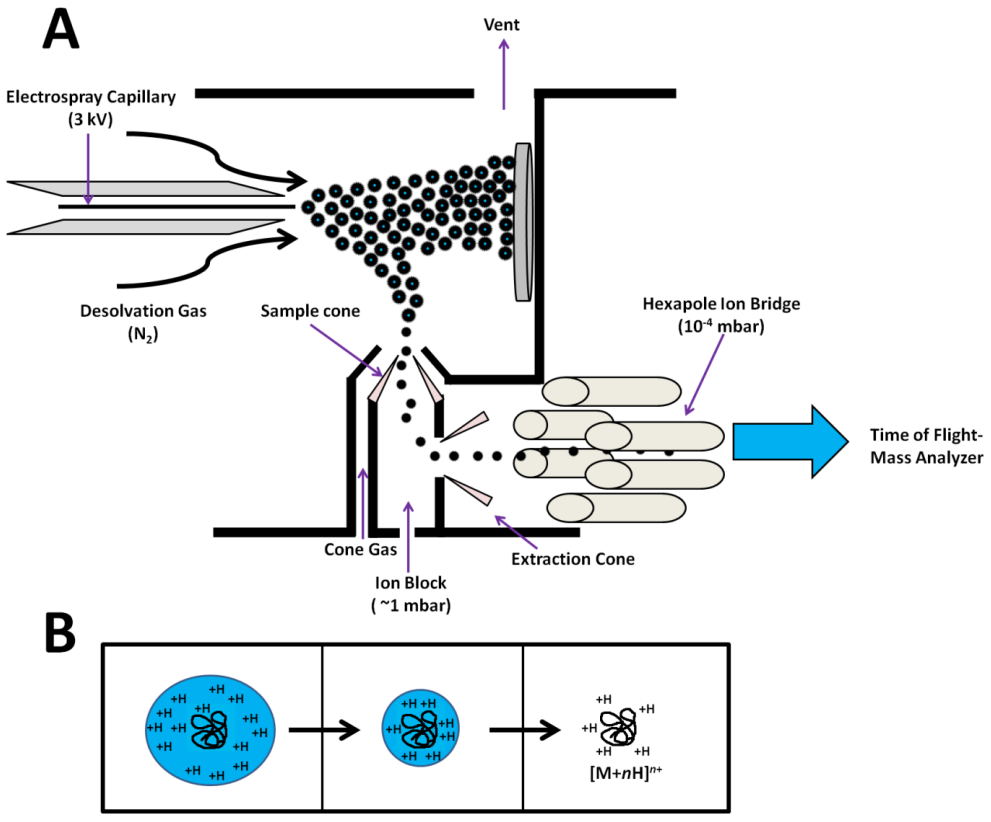

Figure 2-5. Electrospray ionization mass spectrometer. (A) Instrumental configuration of the electrospray ionization mass spectrometer. Depicted is the 'Z-spray' configuration of Waters Micromass ESI-MS operating in positive ion mode. (B) The charged residue model for analyte desolvation, where evaporation leads to the deposition of unpaired protons on the surface of the protein.

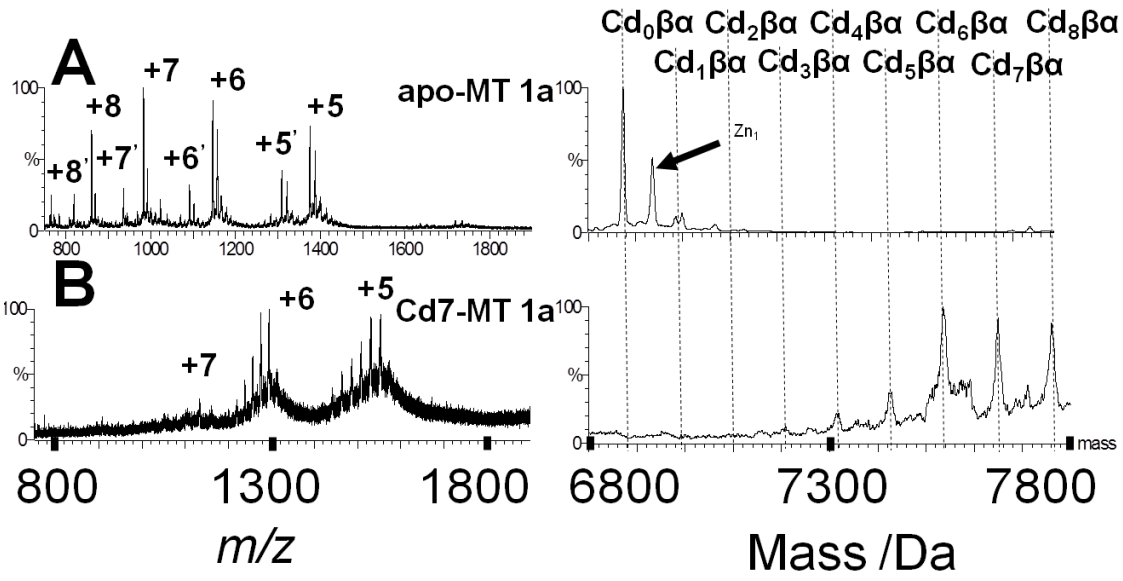

Figure 2-6. **ESI mass spectra recorded during the titration of MT with Cd^{2+}.** (A) metal-free (apo)-MT 1a at 0 eq. Cd^{2+} added to solution and (B) $Cd_{6/7/8}$-MT 1a at 7.3 eq. Cd^{2+} added to solution. Charge states +5' to +8' correspond to a less prevalent truncated species.

In this thesis, mass spectrometric analysis of MT and its isolated domains is present in all Chapters. Specifically in the Chapters 3 and 4, metal binding reactions of MT 1a under equilibrium conditions is used to determine both the mechanism of metal binding and the relative affinity of the isolated domains. A great strength of this technique is in allowing the correlation of spectroscopic data with speciation in solution. In Chapters 5 and 6, ESI-MS is used to rationalize distinct changes in the spectroscopy of β-rhMT 1a and βα-rhMT 1a.

2.3.5 Computational modeling

MT is notoriously difficult to crystallize and while structural information has been made available in the form of NMR data, these studies require a complete backbone assignment of the protein. The particular isoform studied in this thesis, isoform 1a, has not had a complete backbone assignment performed. Consequently, a complete structure for either Cd_4-β- (Chapter 5) or Cd_8-βα-rhMT 1a (Chapter 6) is not possible at this time. In order to circumvent this problem, the work included in this thesis has produced tentative models based upon the modified crystal structure of MT isoform 2 reported by

Chan *et al*. (*16*). This thesis has used both molecular mechanics and molecular dynamics to produce the qualitative structures of supermetalated MT and below is a brief description of the computational techniques used.

Molecular mechanics (MM) uses Newtonian physics to model molecular system. All atoms in the system are treated as hard spheres with a defined radius and the bonds between these atoms are treated as a series of springs with associated lengths and force constants. As an empirical technique, MM relies upon experimental data to construct the force field necessary to calculate the structure of the molecule. The CACHE system used for all calculations is based upon parameters published by Allinger for the MM force field directly for all elements, except metals (*48*). The total energy of the system is given by the following equation:

$$E_{\text{total}} = E_{\text{bonding}} + E_{\text{theta}} + E_{\text{phi}} + E_{\text{improp}} + E_{\text{elec}} + E_{\text{vdw}} + E_{\text{H-bond}}$$

The above terms describe the energies involved in the bond, angles, dihedral angles, improper torsions, electrostatic potential, van der Waals interactions, and hydrogen bonding, respectively. Common force fields used for biological molecules are Allinger's MM2/3/4 (*48-52*), CHARMM (*53*) and AMBER (*54-55*). However in bioinorganic chemistry, the presence of metal ions necessitates modification of the above force fields to account for their presence. Thus the difficulty lies in obtaining an accurate force field for the metal ion, specifically the metal-thiolate bonds found in metallothionein. The force field used in this study was specifically tailored by Chan *et al.* to take into account the cadmium-thiolate bonds present in MT (*16, 56*)**.**

Molecular dynamics (MD) uses a classical mechanics approach to simulate the motion of the atoms as a function of time according to the temperature and the calculated forces exerted on the atoms. This method allows the user to search for energy minima by injecting energy directly into the bonds, causing motion. At every time-step of the dynamic simulation, the potential energy is calculated using molecular mechanics (MM/MD). Conformational slices can be extracted and structurally relaxed by MM. The lowest energy conformer of the supermetalated Cd_4-β- and Cd_8-βα-rhMT is presented in both Chapter 5 and 6.

2.4 References

1. Rigby-Duncan, K. E., and Stillman, M. J. (2006) Metal-dependent protein folding: Metalation of metallothionein, *J. Inorg. Biochem. 100*, 2101-2107.
2. Rigby, K. E., Chan, J., Mackie, J., and Stillman, M. J. (2006) Molecular dynamics study on the folding and metalation of the individual domains of metallothionein, *Proteins: Struct. Funct. Bioinf. 62*, 159-172.
3. Kagi, J. H. R. (1993) *Evolution, structure and chemical activity of class I metallothioneins: An overview*, Birkhauser-Verlag, Berlin.
4. Kojima, Y. (1991) *Introduction [2] Definitions and nomenclature of metallothioneins*, Vol. 205, Academic Press, Inc., San Diego.
5. Kagi, J. H. R., Vasak, M., Lerch, K., Gilg, D. E. O., Hunziker, P., Bernhard, W. R., and Good, M. (1984) Structure of mammalian metallothionein, *Environ. Health Perspect. 54*, 93-103.
6. Presta, A., Green, A. R., Zelazowski, A., and Stillman, M. J. (1995) Copper binding to rabbit liver metallothionein: Formation of a continuum of copper(I)-thiolate stoichiometric species, *Eur. J. Biochem. 227*, 226-240.
7. Zelazowski, A. J., Szymanska, J. A., Law, A. Y. C., and Stillman, M. J. (1984) Spectroscopic properties of the α fragment of metallothionein, *J. Biol. Chem. 259*, 12960-12963.
8. Leiva-Presa, A., Capdevila, M., and Gonzalez-Duarte, P. (2004) Mercury(II) binding to metallothioneins: Variables governing the formation and structural features of the mammalian Hg-MT species, *Eur. J. Biochem. 271*, 4872-4880.
9. Bofill, R., Palacios, O., Capdevila, M., Cols, N., Gonzalez-Duarte, R., Atrian, S., and Gonzalez-Duarte, P. (1999) A new insight into the Ag^{+} and Cu^{+} binding sites in the metallothionein β domain, *J. Inorg. Biochem. 73*, 57-64.
10. Vasak, M., Kagi, J. H. R., and Hill, H. A. O. (1981) Zinc(II), cadmium(II), and mercury(II) thiolate transitions in metallothionein, *Biochemistry 20*, 2852-2856.
11. Stillman, M. J. (1995) Metallothioneins, *Coord. Chem. Rev. 144*, 461-511.
12. Stillman, M. J., Cai, W., and Zelazowski, A. J. (1987) Cadmium binding to metallothioneins: Domain specificity in reactions of α and β fragments, apometallothionein, and zinc metallothionein with Cd^{2+}, *J. Biol. Chem. 262*, 4538-4548.
13. Kagi, J. H. R., and Vallee, B. L. (1961) Metallothionein: A cadmium and zinc-containing protein from equine renal cortex, *J. Biol. Chem. 236*, 2435-2442.
14. Zhang, B. L., Sun, W. Y., and Tang, W. X. (1997) Determination of the association constant of platinum(II) to metallothionein, *J. Inorg. Biochem. 65*, 295-298.
15. Willner, H., Vasak, M., and Kagi, J. H. R. (1987) Cadmium-thiolate clusters in metallothionein: Spectrophotometric and spectropolarimetric features, *Biochemistry 26*, 6287-6292.
16. Chan, J., Huang, Z., Watt, I., Kille, P., and Stillman, M. J. (2007) Characterization of the conformational changes in recombinant human metallothioneins using ESI-MS and molecular modeling, *Can. J. Chem. 85*, 898-912.

17. Sutherland, D. E. K., and Stillman, M. J. (2008) Noncooperative cadmium(II) binding to human metallothionein 1a, *Biochem. Biophys. Res. Commun. 372*, 840-844.
18. Vasak, M., Kagi, J. H. R., Holmquist, B., and Vallee, B. L. (1981) Spectral studies of cobalt(II)- and nickel(II)-metallothionein, *Biochemistry 20*, 6659-6664.
19. Vasak, M. (1980) Spectroscopic studies on cobalt(II) metallothionein: Evidence for pseudotetrahedral metal coordination, *J. Am. Chem. Soc.* ***102***, 3953-3955.
20. Good, M., Hollenstein, R., and Vasak, M. (1991) Metal selectivity of clusters in rabbit liver metallothionein, *Eur. J. Biochem. 197*, 655-659.
21. Vasak, M., and Kagi, J. H. R. (1981) Metal thiolate clusters in cobalt(II)-metallothionein, *Proc. Natl. Acad. Sci. USA 78*, 6709-6713.
22. Good, M., and Vasak, M. (1986) Iron(II)-substituted metallothionein: Evidence for the existence of iron-thiolate clusters, *Biochemistry 25*, 8353-8356.
23. Weser, U., Rupp, H., Donay, F., Linnemann, F., Voelter, W., Voetsch, W., and Jung, G. (1973) Characterisation of Cd, Zn-thionein (metallothionein) isolated from rat and chicken liver, *Eur. J. Biochem. 39*, 127-140.
24. Stillman, M. J., and Szymanska, J. A. (1984) Absorption, circular dichroism, magnetic circular dichroism and emission study of rat kidney Cd,Cu-metallothionein, *Biophys. Chem. 19*, 163-169.
25. Stillman, M. J., and Zelazowski, A. J. (1988) Domain specificity in metal binding to metallothionein. A circular dichroism and magnetic circular dichroism study of cadmium and zinc binding at temperature extremes, *J. Biol. Chem. 263*, 6128-6133.
26. Rigby-Duncan, K. E., Kirby, C. W., and Stillman, M. J. (2008) Metal exchange in metallothioneins – a novel structurally significant Cd_5 species in the alpha domain of human metallothionein 1a, *FEBS J. 275*, 2227-2239.
27. Zelazowski, A. J., Gasyna, Z., and Stillman, M. J. (1989) Silver binding to rabbit liver metallothionein. Circular dichroism and emission study of silver-thiolate cluster formation with apometallothionein and the α and β fragments, *J. Biol. Chem. 264*, 17091-17099.
28. Zelazowski, A. J., and Stillman, M. J. (1992) Silver binding to rabbit liver zinc metallothionein and zinc α and β fragments. Formation of silver metallothionein with Ag(I):protein ratios of 6,12 and 18 observed using circular dichroism spectroscopy, *Inorg. Chem. 31*, 3363-3370.
29. Vaher, M., Romero-Isart, N., Vasak, M., and Palumaa, P. (2001) Reactivity of Cd_7-metallothionein with Cu(II) ions: Evidence for a cooperative formation of Cd_3,$Cu(I)_5$-metallothionein, *J. Inorg. Biochem. 83*, 1-6.
30. Roschitzki, B., and Vasak, M. (2002) A distinct Cu_4-thiolate cluster of human metallothionein-3 is located in the N-terminal domain, *J. Biol. Inorg. Chem. 7*, 611-616.
31. Meloni, G., Sonois, V., Delaine, T., Guilloreau, L., Gillet, A., Teissie, J., Faller, P., and Vasak, M. (2008) Metal swap between Zn_7-metallothionein-3 and amyloid-β-Cu protects against amyloid-β toxicity, *Nat. Chem. Biol. 4*, 366-372.
32. Meloni, G., Polanski, T., Braun, O., and Vasak, M. (2009) Effects of Zn^{2+}, Ca^{2+}, and Mg^{2+} on the structure of Zn_7metallothionein-3: Evidence for an additional zinc binding site, *Biochemistry 48*, 5700-5707.

33. Lu, W., Zelazowski, A. J., and Stillman, M. J. (1993) Mercury binding to metallothioneins: Formation of the Hg_{18}-MT species, *Inorg. Chem. 32*, 919-926.
34. Lu, W., and Stillman, M. J. (1993) Mercury-thiolate clusters in metallothionein. Analysis of circular dichroism spectra of complexes formed between α-metallothionein, apometallothionein, zinc metallothionein, and cadmium metallothionein and Hg^{2+}, *J. Am. Chem. Soc. 115*, 3291-3299.
35. Sutherland, D. E. K., Willans, M. J., and Stillman, M. J. (2010) Supermetalation of the β domain of human metallothionein 1a, *Biochemistry 49*, 3593-3601.
36. Margoshes, M., and Vallee, B. L. (1957) A cadmium protein from equine kidney cortex, *J. Am. Chem. Soc. 79*, 4813-4814.
37. Oz, G., Pountney, D. L., and Armitage, I. M. (1998) NMR spectroscopic studies of I = 1/2 metal ions in biological systems, *Biochem. Cell Biol. 76*, 223-234.
38. Ejnik, J. W., Munoz, A., DeRose, E., Shaw-III, C. F., and Petering, D. H. (2003) Structural consequences of metallothionein dimerization: solution structure of the isolated Cd_4-α-domain and comparison with the holoprotein dimer, *Biochemistry 42*, 8403-8410.
39. Gan, T., Munoz, A., Shaw-III, C. F., and Petering, D. H. (1995) Reaction of $^{111}Cd_7$-metallothionein with EDTA. A reappraisal., *J. Biol. Chem. 270*, 5339-5345.
40. Namdarghanbari, M. A., Meeusen, J., Bachowski, G., Giebel, N., Johnson, J., and Petering, D. H. (2010) Reaction of the zinc sensor FluoZin-3 with Zn_7-metallothionein: Inquiry into the existence of a proposed weak binding site, *J. Inorg. Biochem. 104*, 224-231.
41. Sadler, P. J., Bakka, A., and Beynon, P. J. (1978) ^{113}Cd nuclear magnetic resonance of metallothionien: Non-equivalent CdS_4 sites, *FEBS Lett. 94*, 315-318.
42. Otvos, J. D., and Armitage, I. M. (1979) ^{113}Cd NMR of metallothionein: direct evidence for the existence of polynuclear metal binding sites, *J. Am. Chem. Soc. 101*, 7734-7736.
43. Otvos, J. D., and Armitage, I. M. (1980) Structure of the metal clusters in rabbit liver metallothionein, *Proc. Natl. Acad. Sci. USA 77*, 7094-7098.
44. Boulanger, Y., and Armitage, I. M. (1982) ^{113}Cd nmr study of the metal cluster structure of human liver metallothionein, *J. Inorg. Biochem. 17*, 147-153.
45. Felitsyn, N., Peschke, M., and Kebarle, P. (2002) Origin and number of charges observed on multiply-protonated native proteins produced by ESI, *Int. J. Mass Spectrom. 219*, 39-62.
46. Kebarle, P., and Verkerk, U. H. (2009) Electrospray: From ions in solution to ions in the gas phase, what we know now, *Mass Spectrom. Rev. 28*, 898-917.
47. Rigby-Duncan, K. E., and Stillman, M. J. (2007) Evidence for noncooperative metal binding to the α domain of human metallothionein, *FEBS J. 274*, 2253-2261.
48. Allinger, N. L. (1977) Conformational analysis. 130. MM2. A hydrocarbon force field utilizing V_1 and V_2 torsional terms, *J. Am. Chem. Soc. 99*, 8127-8134.
49. Lii, J.-H., and Allinger, N. L. (1989) Molecular mechanics. The MM3 force field for hydrocarbons. 2. Vibrational frequencies and thermodynamics, *J. Am. Chem. Soc. 111*, 8566-8575.

50. Lii, J.-H., and Allinger, N. L. (1989) Molecular mechanics. The MM3 force field for hydrocarbons. 3. The van der Waals' potentials and crystal data for aliphatic and aromatic hydrocarbons, *J. Am. Chem. Soc. 111*, 8576-8582.
51. Allinger, N. L., Yuh, Y. H., and Lii, J.-H. (1989) Molecular mechanics. The MM3 force field for hydrocarbons. 1, *J. Am. Chem. Soc. 23*, 8551-8566.
52. Allinger, N. L., Chen, K., and Lii, J.-H. (1996) An improved force field (MM4) for saturated hydrocarbons, *J. Comput. Chem. 17*, 642-668.
53. Brooks, B. R., Brooks-III, C. L., Mackerell-Jr., A. D., Nilsson, L., Petrella, R. J., Roux, B., Won, Y., Archontis, G., Bartels, C., Boresch, S., Caflisch, A., Caves, L., Cui, Q., Dinner, A. R., Feig, M., Fischer, S., Gao, J., Hodoscek, M., Im, W., Kuczera, K., Lazaridis, T., Ma, J., Ovchinnikov, V., Paci, E., Pastor, R. W., Post, C. B., Pu, J. Z., Schaefer, M., Tidor, B., Venable, R. M., Woodcock, H. L., Wu, X., Yang, W., York, D. M., and Karplus, M. (2009) CHARMM: The biomolecular simulation program, *J. Comput. Chem. 30*, 1545-1614.
54. Ponder, J. W., and Case, D. A. (2003) Force fields for protein simulations, *Adv. Protein Chem. 66*, 27-85.
55. Case, D. A., Cheatham, T. E., Darden, T., Gohlke, H., Luo, R., Merz, K. M., Onufriev, A., Simmerling, C., Wang, B., and Woods, R. J. (2005) The amber biomolecular simulation programs, *J. Comput. Chem. 26*, 1668-1688.
56. Chan, J., Merrifield, M. E., Soldatov, A. V., and Stillman, M. J. (2005) XAFS spectral analysis of the cadmium coordination geometry in cadmium thiolate clusters in metallothionein, *Inorg. Chem. 44*, 4923-4933.

Chapter 3. Noncooperative Cadmium binding to human MT 1a[3]

3.1 Introduction

Metallothionein (MT) is a ubiquitous metalloprotein found in bacteria, mammals and invertebrates (*1-3*). Characteristic features of MT include its small size, high cysteine content, and lack of aromatic amino acids. Although the exact *in vivo* function of MT is unknown, it has been implicated as a metallochaperone involved in essential zinc and copper homeostasis, as a detoxifying agent of toxic metals, and as a protective agent against oxidative stress (*4-7*). The most well characterized member of the MT family is mammalian MT and structural analysis of its fully metalated form by NMR and X-ray crystallography have shown it to contain two separate metal binding domains: the N-terminal β-domain with 9 cysteine residues capable of binding three Cd^{2+}/Zn^{2+}, or 6 Cu^{+} and the C-terminal α-domain with 11 cysteine residues capable of binding four Cd^{2+}/Zn^{2+} or 6 Cu^{+} (*8-11*). Both the isolated β- and α-domain encapsulate a metal thiolate core as shown in Figure 3-1, and the metalation chemistry of each is thought to be independent. Specifically, the β-domain of MT has been shown to have a preference for Cu^{+} coordination, while the α-domain has been shown to have a preference for Zn^{2+}/Cd^{2+} coordination. In this manner, MT is thought to be able to separate the redox active Cu^{+} chemistry from the redox inactive Zn^{2+} chemistry.

While Cu-MT has been isolated from a number of sources including, fetal liver (*12-13*), bovine calf liver (*14*), rat kidney (*15*), brain specific MT-3 (*16*), as well as patients suffering from Wilson's disease (*17*), it is the zinc form that is most commonly found in healthy adult mammals. These observations have led to a long association of MT with zinc homeostasis. Specifically, MT is thought to act as a robust metallochaperone, capable of donating Zn^{2+} ions to apo-enzymes and accepting Zn^{2+} in cases of excess. Indeed metal exchange experiments have been conducted in which Zn^{2+} from Zn_7-βα-MT

---

[3]A version of this work has been published:

has been transferred to Zn-dependent enzymes, for example, m-aconitase (*18*), carbonic anhydrase (*19*), and the prototypical transcription factor, Gal4 (*20*). Removal of Zn^{2+} from the zinc finger-containing transcription factor Sp1 demonstrates that MT may also act as a Zn^{2+} acceptor (*21*). Thus this natural association of MT with the biologically essential Zn^{2+} and Cu^{+} has suggested that one of the functions of MT is the maintenance of metal ion homeostasis. To support this view a recent report by Krezel & Maret demonstrated the presence of three sets of binding affinities (*22*): four Zn^{2+} ions that bind strongly (logK = 11.8), 2 with intermediate affinity (logK~10) and finally a single weakly bound Zn^{2+} (logK = 7.7). Thus MT is able to act as a dynamic metallochaperone capable of binding and donating Zn^{2+} ions over a range of concentrations.

Several MT polymorphisms have been linked to the longevity of certain human groups, with both low Zn-MT levels and satisfactory Zn^{2+} bioavailability being good markers for human health (*23*). Mutations of MT-1a (Asn27Thr) have also been associated with diabetes type 2 and cardiovascular complications (*24-25*), where nitric oxide, an oxidizing agent, was used to determine the availability of Zn^{2+} from Zn-MT. Exposure of the mutant MT to nitric oxide, resulted in less Zn^{2+} release compared to the wild-type, suggesting that either the mutant is inherently less reactive, or that a large pool of partially oxidized MT exists. In both cases, the mechanism of metalation, and the potential for partially metalated species taking part in cellular chemistry has significant consequences in the understanding of the relationship between Zn^{2+} bioavailability, MT and the overall health of an individual.

Specifically, if the mutant is inherently less reactive to NO, then one would predict the mutation has affected the most weakly bound Zn^{2+} ion. However, this mutation may have also affected the stability of the protein leading to the accumulation of partially oxidized MT, where loss of Zn^{2+} ions from weakly bound sites has led to an accumulation of stronger binding sites. These strong binding sites would decrease cellular availability of Zn^{2+} and impede the health of the individual. It should be made clear that while this was an *in vivo* study and no information about the metal loading of the mutant MT is available, the final result of the individual is the same: only tightly bound Zn^{2+} exists and cannot be released easily either because of an increase in the stability of a weaker binding site, or partial oxidation and subsequent loss of a weaker

binding site. In either case, MT impacts pathogenesis through both Zn buffering and antioxidant dysfunction, which in turn rely on the metalation status *in vivo*. It is clear that knowledge of the mechanism of metalation is needed to establish the metal status *in vivo*, which will aid in determining the exact involvement of MT in these disorders.

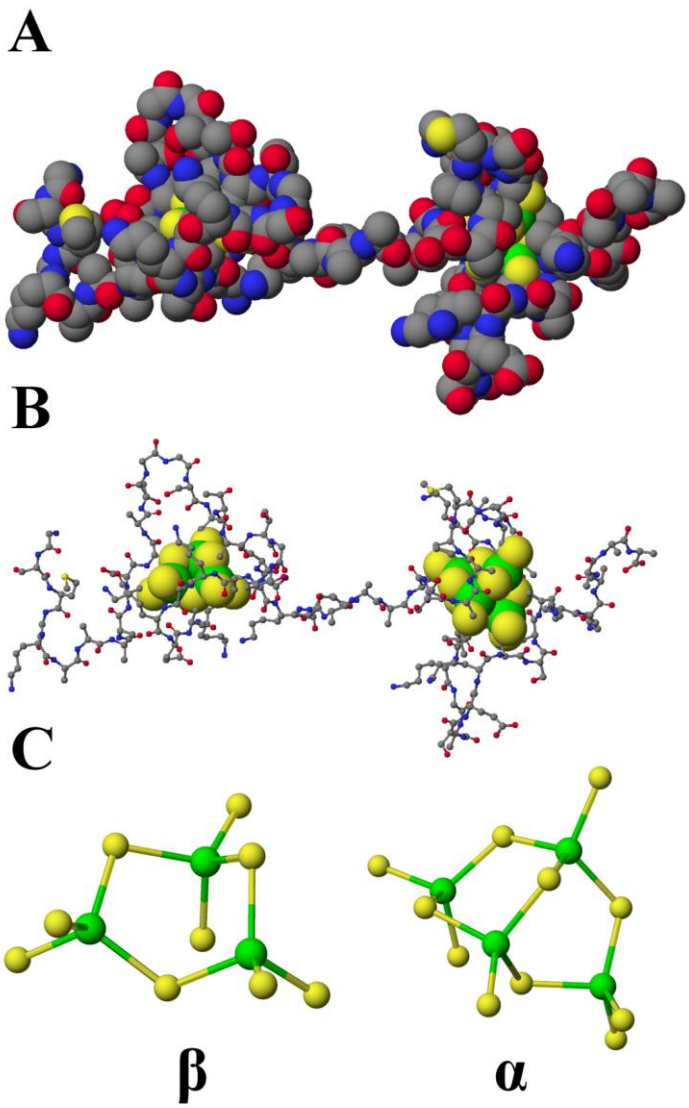

Figure 3-1. **Molecular model structure of Cd_7-βα-rhMT.** A) space filling; B) Ball-and-stick with the domains in space filling form; C) Ball and stick models of Cd_3-β- (left) and Cd_4-α- (right) rhMT cadmium-cysteinyl-thiolate clusters. Cysteinyl sulphurs are coloured yellow, while cadmium atoms are coloured green. Data of Chan *et al.* (26).

Surprisingly, while the stoichiometric ratios of 3 (β) and 4 (α) for Zn^{2+}/Cd^{2+} ions are well known, there has been considerable debate regarding the mechanism of MT

metalation. It has been frequently proposed that the mechanism occurs in a cooperative fashion, that is, the binding of one metal facilitates the binding of the next metal (*27-28*). In this mechanism, one would expect only the metal free (apo-MT) and fully metalated (holo-MT) forms to be relevant. Several experiments support this viewpoint. Most notably in an NMR titration of apo-MT with $^{113}Cd^{2+}$, the appearance of four ^{113}Cd-NMR peaks associated with the α-domain could be clearly observed at 2.8 equivalents of $^{113}Cd^{2+}$ per MT molecule, and the remaining 3 peaks, associated with the β-domain, appeared at 5.3 equivalents of $^{113}Cd^{2+}$ per MT molecule (*28*). It should be noted that at 2.8 equivalents of Cd^{2+} per MT molecule, a broad peak is observed at 685 ppm and could be the result of chemical exchange or overlap of peaks in the sample.

Contrary to a cooperative mechanism of metalation, a noncooperative mechanism is also possible in which metalation events occur independently of each other (*29-31*). In this alternate hypothesis, it would be expected that apo-MT, partially metalated MT and completely metalated MT would coexist. In this situation, the mechanism of MT metalation determines the number of possible physiologically relevant structures that can be present in the cell. Several studies support this alternative mechanism of metalation including Zn_7-MT titration, where chelator agents were used to determine the presence of three distinct binding sites with log(K) affinities of 11.8, ~10 and 7.7 (*22*). In addition, S-nitrosylation studies of brain-specific MT-3, as monitored by NMR spectroscopy, demonstrated the persistence of two α-domain-Cd^{2+} atoms, even in the presence of excess nitric oxide (*32*). If the mechanism of metalation were cooperative then in the first case, one would predict increasing log(K) affinities as metalation progressed, and in the latter case oxidation would lead to a destabilization of partially metalated β- and α- clusters. In addition, enhanced resistance to S-nitrosylation has been reported in MT-1a mutants (Asn27Thr) (*24-25*). These results may be reasonably interpreted if a noncooperative mechanism is in effect; however this has not been proven experimentally to date.

A recent report has provided convincing evidence for noncooperative binding of cadmium to the isolated α-domain of human MT-1a (*33*) but not the complete protein or the isolated β-domain. Determination of the mechanism of the β-domain and the complete protein is important, because in a recent paper by Palumaa *et al.* (*34*) the authors comment that while the brain-specific MT-3 exhibits noncooperative binding, β–

MT domains from other species bind cooperatively. For this reason, we have studied the step-wise metalation of the isolated β-domain and the two-domain βα human protein so that the metalation properties of this human protein can be firmly established.

This chapter provides the necessary data establishing unambiguously the noncooperative nature of cadmium binding to both the isolated domains and the combined βα-MT protein (βα-rhMT) of human MT-1a. Section 3.2 describes the experimental details used to study the mechanism of metalation. Mass spectrometric results are presented in section 3.3 and, finally section 3.4 discusses these results in the context of current research and its implications. Briefly, the dominant metalation state (1-3 for β- and 1-7 for βα-) was directly dependent on the stoichiometric ratio of Cd^{2+} added, and interestingly, titration of apo-MT (β or βα) with excess $CdSO_4$ yielded supermetalated (metalation in excess of the normal maximum levels) species for the β- and full-MT protein not previously reported.

3.2 Experimental Methods

In this section, the details of the protein preparation protocol for the metal-binding studies (Section 3.2.1) and the instrumental parameters (Section 3.2.2) will be described, as well as a detailed account of the experimental design for the metalation of apo-β- and apo-βα-rhMT 1a with Cd^{2+} at pH 9.4 and 8.4, respectively (Section 3.2.3).

3.2.1 Protein preparation for metal binding studies

Chemicals

$CdSO_4$ (J.T. Baker Chemical Company). All chemicals used in this study were of the highest-grade purity from commercial sources. All solutions were made with $>14 M\Omega cm^{-1}$ deionized water (Barnstead Nanopure Infinity). Protein purification steps were performed on Hi Trap SP ion exchange columns, fine G-25 Sephadex (Amersham Biosciences) and a stirred ultrafiltration cell (Amicon Bioseparations/Millipore) with a YM-3 membrane (3000 MWCO).

Protein preparation

The expression and purification methods have been previously described in detail in chapter 2. The β-rhMT and βα-rhMT proteins used in this study were based on the 38-

residue and 72-residue sequences, respectively: β-rhMT MGKAAAACSC ATGGSCTCTG SCKCKECKCN SCKKAAAA, βα-rhMT MGKAAAACSC ATGGSCTCTG SCKCKECKCN SCKKAAAACC SCCPMSCAKC AQGCVCKGAS EKCSCCKKAA AA. There are 9 and 20 cysteine residues present in β-rhMT and βα-rhMT, respectively, and no disulfide bonds. The expression system included, for stability purposes, an N-terminal S-tag (MKETAAAKFE RQHMDSPDLG TLVPRGS). Recombinant β-rhMT was expressed in BL21(DE3) Escherichia coli (E. coli.), while βα-rhMT was expressed in ER2566 E. coli.. Both cell lines were transformed using the pET29a plasmid. Removal of S-tag was performed using a Thrombin CleanCleave^{TM} Kit (Sigma). To impede oxidation of the cysteine residues to disulfide bonds, all protein samples were argon saturated and rigorously evacuated.

A general description of the demetalation procedure can be found in chapter 2 (Section 2.2.6). In this experiment, concentrated formic acid was used to lower the pH of the MT sample to 2 with concomitant demetalation. Previously bound Cd^{2+} ions were removed by buffer exchange using a G-25 (Sephadex) column into deoxygenated di-H_2O pH adjusted to 2.7. The solution was evacuated, septum capped and backfilled with argon.

Small aliquots of both the apo-β- and apo-βα-rhMT 1a were remetalated using Cd^{2+} and their concentrations were determined to be 18.0 and 18.4 μM from the ligand-to-metal charge transfer band (LMCT band) centered at 250 nm ($\varepsilon_{250\beta}$ = 36,000 and $\varepsilon_{250\beta\alpha}$ = 89,000 $M^{-1}cm^{-1}$). Cadmium solutions were prepared as the sulfate salt in di-H_2O to a final concentration of 7.1 mM as determined by atomic absorption spectroscopy (AAS).

3.2.2 Mass spectrometric measurements

ESI-MS procedures.

All data were collected on an electrospray ionization time-of-flight (ESI-TOF) mass spectrometer (Waters Micromass Inc.) in the positive ion mode. NaI was used as the calibrant, because of its ability to form salt clusters that cover the *m/z* range of the protein. The scan conditions for the spectrometer were: capillary, +3000.0 V; sample cone, 15 V; extraction cone, 10 V; RF lens, 450 V; desolvation temperature, 20.0 °C; source temperature, 80.0 °C; cone gas flow, 52 Lhr^{-1}; and desolvation gas flow, 514 Lhr^{-1}. The *m/z* range was 500.0-2000.0; the scan mode was continuum, with a scan time of 2.4 s

and an interscan delay of 0.10 s. Spectra were constructed and deconvoluted using the MASSLYNX v.4.0 software package.

3.2.3 Metalation of apo-β- and apo-βα-rhMT 1a with Cd^{2+}

The pH of the apo-β- and apo-βα-rhMT 1a solutions were raised to 9.4 and 8.4, respectively, through the stepwise addition of concentrated NH_4OH. This stepwise addition was initially monitored through the use of pHydrion® pH paper (Micro Essential Laboratory, Inc.) and immediately following the titration, the pH was determined using a pH meter (Accumet Basic AB15, Fisher Scientific, Ottawa, ON, Canada) with an Accumet Semimicro pH electrode.

After the addition of each aliquot of Cd^{2+}, the solution was thoroughly mixed and allowed to equilibrate for 5 min. Mass spectra were then acquired of the MT solution. Following the ESI-MS titration, AAS was used to calibrate the exact equivalents added to solution at each step of the titration.

3.3 Results

In this section, the ESI mass spectral results for the titration of the isolated apo-β-domain and full MT 1a protein with Cd^{2+} are outlined. Specifically, the effects of metalation on the isolated β-domain (Section 3.3.1), the full MT protein (Section 3.3.2) and an analysis of the deconvoluted mass spectral data as a function of Cd^{2+} added to solution (Section 3.3.3).

3.3.1 Metalation of apo-β-rhMT 1a with Cd^{2+} at pH 9.4

The mass spectra recorded during the titration of apo-β-rhMT are shown in Figure 3-2. The data clearly show that stepwise addition of Cd^{2+} to the initially metal-free protein results in the formation of partially-metalated ($\beta<3$ Cd^{2+}) species until saturation occurs with the fully metalated species at 2.8 equivalents Cd^{2+} added to solution. It should be noted that there is some error in the measurement of Cd^{2+} added to solution and that 2.8 equivalents represents complete metalation, either because of an overestimation of the protein content or an underestimation of the Cd^{2+} added to solution. In Figure 3-2, the observed charge states (A-E) and their corresponding deconvoluted spectra are shown as

a function of increasing concentration of Cd^{2+}. Cleavage of the S-tag leaves the residues GS attached to the N-terminal of the protein. Theoretical mass values for β-rhMT are as follows: apo-β-rhMT 3753.46 Da, Cd_1 3863.85 Da, Cd_2 3974.24 Da, Cd_3 4084.63 Da and Cd_4 4195.02 Da.

In more detail, Figure 3-2 shows the bound-metal speciation for β-rhMT as a function of the number of Cd ions added at pH 9.4. One Zn^{2+} is bound to about 25% of the total protein. The binding persists until the Zn^{2+} is displaced at the Cd_3 point, (D). Surprisingly, addition of five molar excess led to the quantitative formation of a new species Cd_4-β-rhMT forms (E). Metal free apo-β-rhMT exhibits significant intensity in charge states corresponding to +5, +4, and +3 at the 0 Cd^{2+} added point (A1). The +5 charge state intensity is no longer apparent when Cd_1-β-rhMT forms. The loss of the +5 charge state clearly indicates some degree of folding has occurred as a result of the conformational changes required following binding of just the first Cd^{2+} or the Zn^{2+} to the apo-β-rhMT to form Cd_1-β-rhMT or Zn_1-β-rhMT (B1). After the disappearance of the +5 charge state, there is very little change in the charge state distribution with further additions of Cd^{2+}, indicating that the most significant folding occurs upon binding of the first metal ion.

3.3.2 Metalation of apo-βα-rhMT 1a with Cd^{2+} at pH 9.4

The mass spectra recorded during the titration of apo-βα-rhMT Cd^{2+} are shown in Figure 3-3. As in the case of apo-β-rhMT 1a, the data show that stepwise addition of Cd^{2+} to the initially metal-free protein species results in the formation of partially-saturated (βα- <7 Cd^{2+}) metalated species until saturation occurs with the fully metalated species, which forms when stoichiometric amounts of Cd^{2+} are added. In Figure 3-3, the observed charge states (A-E) and the corresponding deconvoluted spectra are shown as a function of increasing concentration of Cd^{2+}. Cleavage of the S-tag leaves the residues GS attached to the N-terminal of the protein. However, the mass spectra show that several amino acids of βα-rhMT were truncated either during the cleavage, or in the mass spectrometer itself producing two different species: one in which the N-terminal G residue and C-terminal AA residues were truncated, and a second in which the N-terminal GSMGK as well as A from either the N-terminal or C-terminal were truncated.

None of the highly conserved cysteine residues were truncated. By assuming both species of βα-rhMT are equivalently ionized, the first species is more prevalent. Theoretical mass values for the predominant βα-rhMT species are as follows: apo-βα-rhMT 6874.37 Da, Cd_1 6984.76 Da, Cd_2 7095.15 Da, Cd_3 7205.54 Da, Cd_4 7315.93 Da, Cd_5 7426.32 Da, Cd_6 7536.71 Da, Cd_7 7647.10 Da and Cd_8 7757.49 Da.

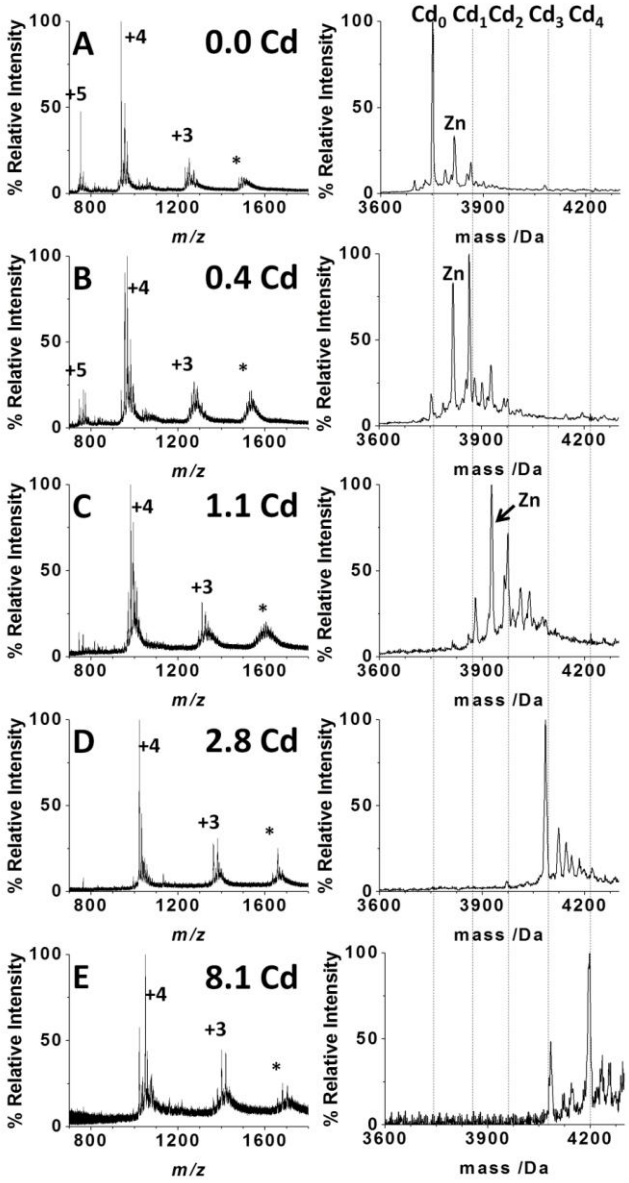

Figure 3-2. ESI mass spectral titration of apo-β-rhMT with $CdSO_4$. The protein concentration was 18.0 μM and a pH of 9.4. Mass spectral data (Left) and the corresponding deconvolutions (Right) were recorded as aliquots of Cd^{2+} (7.1 mM) were titrated into the solution at 22 °C. The * refers to a +5 m/z minority species corresponding to slight dimer formation of β-rhMT.

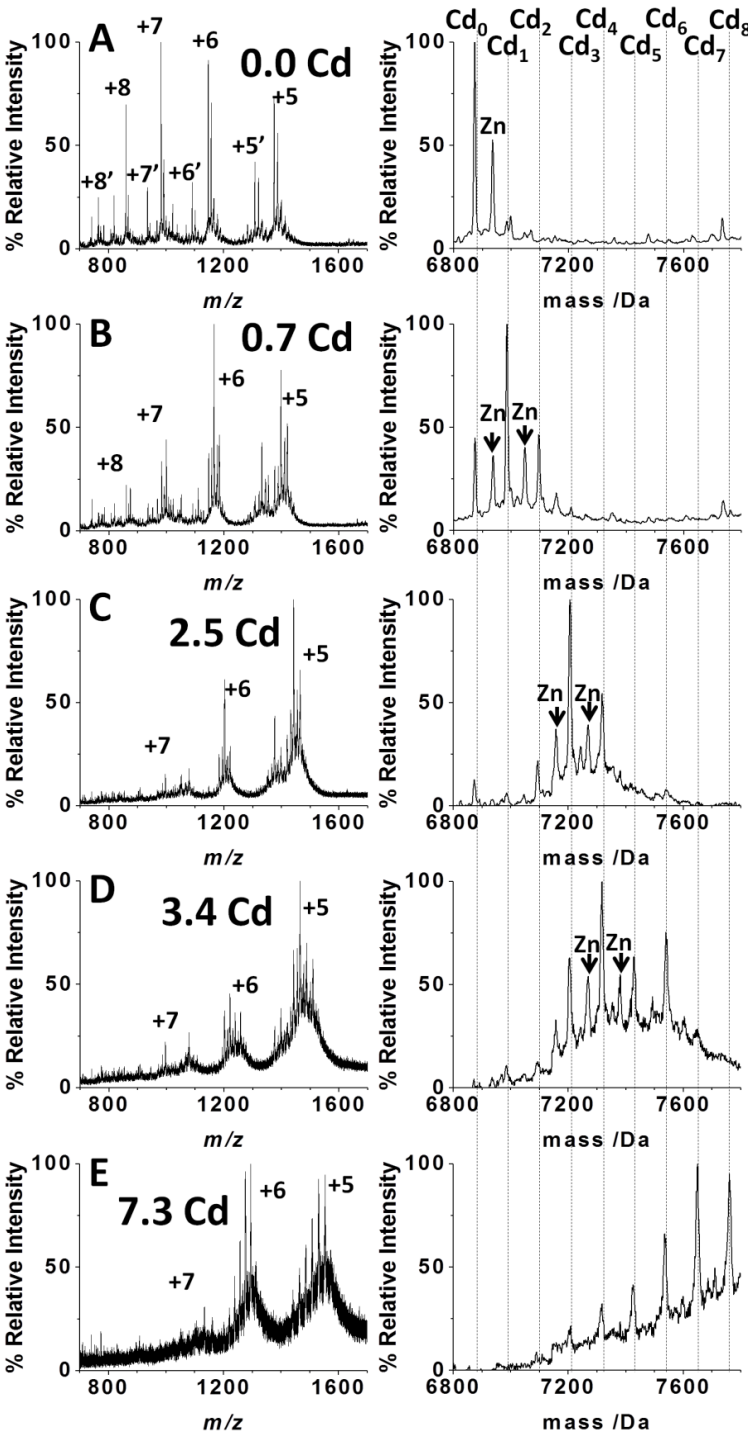

Figure 3-3. ESI mass spectral titration of apo-βα-rhMT with $CdSO_4$. The protein concentration was 18.4 μM and a pH of 8.4. Mass spectral data (Left) and the corresponding deconvolutions (Right) were recorded as aliquots of Cd^{2+} (7.1 mM) were titrated into the solution at 22 °C. Two sets of m/z refer to the presence of two βα-rhMT species, see text.

Cd-loading of the two-domain protein is shown in Figure 3-3 with the metal-speciation in βα-rhMT measured as a function of added Cd^{2+}. Cd-species from 1 to 8 at pH 8.4 are observed with stoichiometric addition of Cd^{2+}. A single Zn^{2+} persists in 25% of the protein as the Zn_1-βα-rhMT species in (A). The Zn^{2+} is only displaced when Cd_7-species forms. The important feature in Figure 3-3 is the step-wise increases in Cd^{2+}-loading as a function of added Cd^{2+} and the appearance of Cd_8-βα-rhMT with excess added Cd^{2+}. Apo-βα-rhMT (A) exhibits charge states corresponding to +8, +7, +6, and +5 (+5' to +8' correspond to the less prevalent truncated βα-rhMT species). Addition of 1 Cd^{2+}, data in (B), causes a significant reduction in the intensity of the +8 and +7 charge states, again, indicating that a conformational change takes place reducing the exposed basic amino acids. Complete loss of the +8 charge state occurs with formation of Cd_2-βα-rhMT, which corresponds to the complete loss of apo-βα-rhMT species. As the titration proceeds, up to 7 equivalents of Cd^{2+} are added, the intensity of +6 relative to +5 increases. This reversal in trend in the charge state intensity indicates an increase in volume of the structure. The deconvoluted spectra in (E) show that this corresponds to the emergence of Cd_8-βα-rhMT. The appearance of the lower mass signals at the end of the titration, Cd_3/Cd_4/Cd_5-βα-rhMT, are due to the presence of metalated, truncated βα-rhMT.

3.3.3 Relative abundance of apo-β- and apo-βα-rhMT 1a with Cd^{2+}

Assembled in Figure 3-4 are the relative abundances of each metalated protein species shown in Figure 3-2 and 3-3. Because there is a small fraction of Zn^{2+} bound, it has shown that Zn^{2+} and Cd^{2+} bind isomorphously, all Zn^{2+} species are counted as if Cd^{2+} were bound (*35*). Of course, Cd^{2+} binds with a greater K_F and so displaces the Zn^{2+} when no other binding sites are available in the noncooperative model, as observed here. The value of Figure 3-4 is that it clearly demonstrates that partial metalation occurs; hence the extent of metalation is directly dependent on the amount of metal in solution. At low equivalents of metal only partially metalated species are observed and addition of excess Cd^{2+} to β-rhMT and βα-rhMT lead to the formation of Cd_4-β-rhMT and Cd_8-βα-rhMT, respectively.

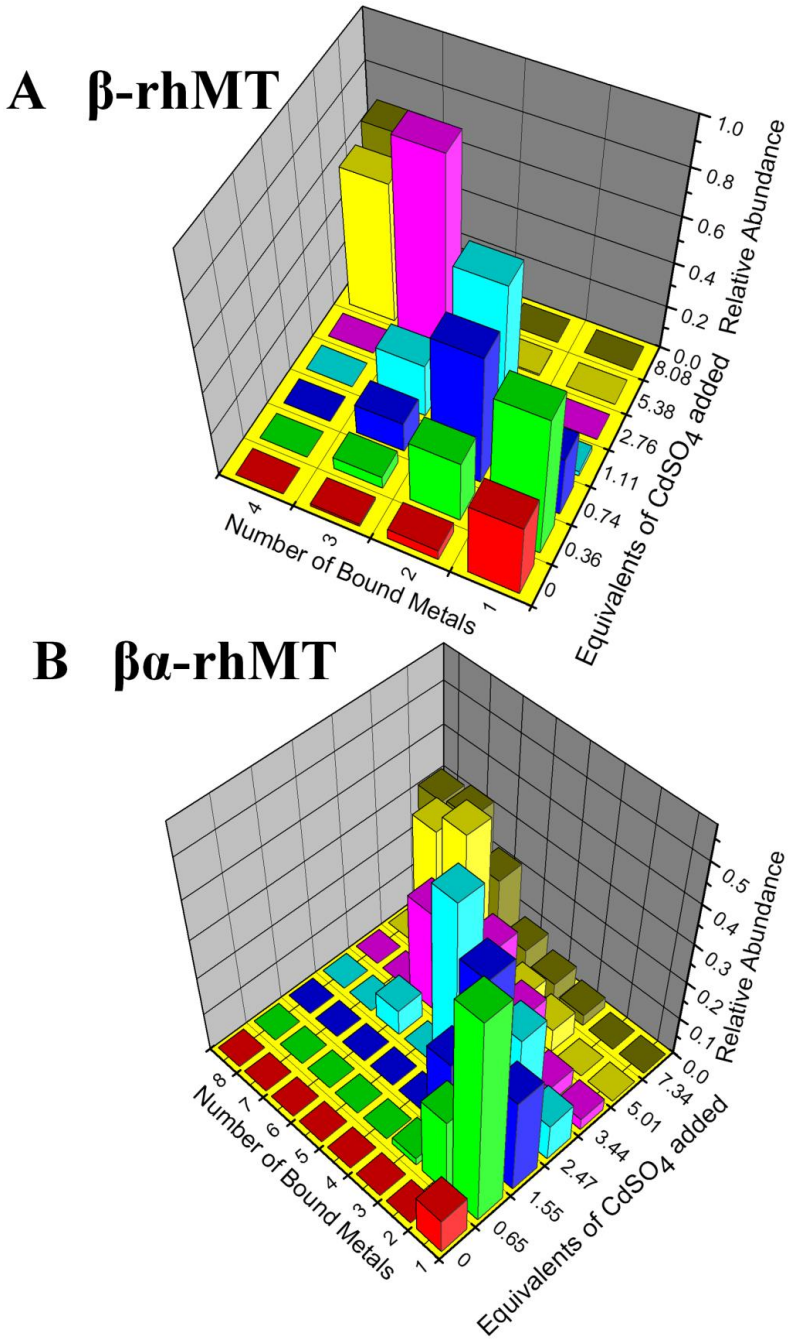

Figure 3-4. The metalation state as a function of Cd^{2+} added. This plot assumes that the binding of zinc and cadmium are equivalent and treats them interchangeably. (A) refers to the metalation of β-rhMT, whereas (B) refers to the metalation of βα-rhMT. The second βα-rhMT truncation, accounts for 13% of total signal, which must be spread over several species, no adjustment was made to metal speciation.

3.4 Discussion

3.4.1 Cooperative versus noncooperative metalation of metallothionein

Mammalian metallothioneins bind metals in metal-cysteinyl-thiolate clusters with stoichiometries dependent on the associated metal: Cd_7-MT, Zn_7-MT, Ag_{12}-MT, Cu_{12}-MT, Hg_{18}-MT, and As_6-MT (*9, 11, 36-38*). The details of the metal binding mechanisms are important because of implications in the possible metalation status of the protein *in vivo*, especially, whether partially metalated species exist under normal conditions. There are two overall mechanisms (i) a cooperative mechanism in which only the metal-free (apo-MT) and the metal-saturated (holo-MT) are significantly populated and a noncooperative mechanism, which would allow for the presence of partially metalated species that could potentially serve a biological function, such as controlling the bioavailability of zinc (*4, 22*). Previous attempts to determine the mechanism of metalation have relied on techniques that do not produce direct evidence for the absence/presence of intermediate species (*28-31*) or may be more sensitive to specific species, for example, the CD spectrum of Cd_4-α-domain dominates the spectrum compared with the partially metalated Cd_{1-3} (*33*). ESI-MS data reported over several years, and the specific recent results for the metalation of the α-domain of rhMT 1a (*33, 39*) show that ESI-MS data exhibit the discriminating power required to detect and quantify the presence of partially metalated metallothioneins.

Cooperative metalation

A cooperative mechanism of metalation implies that the binding of one metal ion, for example Cd^{2+}, affects the binding of subsequent metal ions. There are two cases of cooperative metalation: positive cooperativity, where the binding of one ligand facilitates the binding of subsequent ligands ($K_{n+1} > K_n$, where n is the number of ligands bound), and negative cooperativity, where the binding of one ligand hinders the binding of subsequent ligands ($K_n > K_{n+1}$, where n is the number of ligands bound). The traditional view of MT is that metalation occurs in a positive cooperative fashion with only the fully metalated (holo-) and metal free (apo-) MT taking part in cellular chemistry. As such,

research of the metalation properties of MT have focused primarily on the metal free, and fully metalated forms.

Noncooperative metalation

A noncooperative mechanism of metalation implies that the each binding event is independent of the others. In this model, one would expect the binding affinity to decrease as a function of metals bound, because as each metalation site becomes occupied the number of available sites decreases. Kinetic experiments involving As^{3+} binding to MT have supported the noncooperative mechanism of metalation. Specifically, by studying the ESI-mass spectral metalation of the triple MT mutants (βββ- and ααα-rhMT) and comparing it to the isolated β- and α-domains, as well as the full MT 1a protein, it was shown that the rate of metalation is directly dependent upon the number of available sites. This experiment was possible, because metalation of MT with As^{3+} occurs on the order of minutes to hours. Unlike As^{3+}, Cd^{2+} metalation is complete in the 4 ms of the dead time of a stopped-flow machine, and ESI-mass spectral data on the metalation of MT with Cd^{2+} is not currently available. Recent ESI-mass spectral studies of the isolated α-domain of MT-1 by Rigby and Stillman, and full MT-3 protein by Palumaa *et al.* have shown that partially metalated Cd-MT species are in fact stable and that the dominant metalation state is directly dependent on the equivalents of Cd^{2+} added to solution. These results support a noncooperative mechanism of metalation. However, in the former case no metalation data are available without the metalation properties of the isolated β-domain and the full MT protein no mechanism can be conclusively supported.

3.4.2 Noncooperative metalation: ESI-mass spectral evidence

Many of the previous MT metalation experiments were based on optical techniques and included CD, EPR, and UV spectroscopy. These techniques, while sensitive to the metal-thiolate bond, provide an average of the metalation state of MT, and consequently do not have the discriminating power necessary to determine the mechanism of metalation. ESI-mass spectrometry, a unique technique in that it is able to simultaneously determine the number and type of metals bound to the protein. In addition, by monitoring changes to the charge state profile, protein folding information

may also be extracted. Recently, ESI-MS has been extensively used to analyze the metalation of MT through both the kinetics of metal binding and the discovery of a new low affinity binding site. Specifically, the metalation of the isolated α-domain of human MT-1a and the full MT-3 both support a noncooperative mechanism of metalation.

The present study demonstrates that the partially metalated species of the isolated β-domain and the two-domain protein of MT 1a are stable. Following the step-wise addition of 1 to 4 (β) or 1 to 7 (βα) equivalents of Cd^{2+}, all metalated species are observed ranging from apo-MT to holo-MT depending on the amount of Cd^{2+} added, Figure 3-2 and 3-3. When combined with the kinetics of As^{3+} metalation and the stability of the partially metalated species in the α-domain of MT 1a, we can now conclusively say that both the isolated domains and full protein of metallothionein isoform 1a bind metals in a noncooperative manner. It is very likely that noncooperative metalation applies to all metals capable of binding metallothionein although this has yet to be proven. Significantly, a noncooperative mechanism allows for partially metalated and metal exchange intermediates to be stable and, therefore, to be able to take part in cellular chemistry.

In addition to the metalation status, information from the charge state populations, specifically changes in these populations, provides conformational information about the protein. These charge state distributions are directly dependent on both the number of basic sites and size of the protein. As such, any alterations to this size, or site exposure, through folding or through denaturation, will lead to changes in the charge state distribution. Higher charge states correspond to a more open, solvent exposed, conformation, while lower charge states correspond to more closed, solvent unexposed, conformation.

The ESI-mass spectral data presented in Figures 3-2 and 3-3 show that the addition of the first metal ion to both β-rhMT and βα-rhMT result in loss of intensity in the highest charge states, +5 for the β-domain and +8 for the full protein, which indicates that binding of this first metal leads to significant folding of the protein. The lack of change in the distribution of the intensity in the charge states with further Cd^{2+} addition up to 3 (β) or 7 (βα) indicates the first metal locks the structure in place and that, unexpectedly, further metalation does not require significant rearrangement of the polypeptide backbone

to occur. This compares well the α-domain of MT 1a, which upon binding the first Cd^{2+} ion losses the +7 and +6 charge states after which there is very little change to the charge state spectra.

The dominant charge state of both fully metalated Cd_3-β-rhMT and Cd_4-α-rhMT is +4, while the dominant charge state of the full MT protein is +6. One would predict that the dominant charge state of the full MT protein would be the sum of the isolated domains. This prediction is based upon the traditional view of the individual domains acting in isolation of each other and is supported by a number of NMR studies, most convincingly the almost identical location of the ^{113}Cd-NMR peaks associated with the isolated α-domain when compared to the full MT protein (*10*). However, contrary to this traditional view, the dominant charge state of the fully folded MT protein is in fact +6 and is significantly lower than the expected charge state of +8. This finding would suggest that there is, in fact, some domain-domain interactions, which act to attenuate to total charge that the protein is capable of holding. These domain-domain interactions, while not well characterized may be critical in the equilibration of metal ions within each domain and may help to explain the metal-ion preference of each domain (Zn^{2+} and Cd^{2+} in the α-domain and Cu^{+} in the β-domain) (*40*-*41*).

3.4.3 Implications of a noncooperative mechanism of metalation

The most significant consequence of a noncooperative mechanism of metalation is the prospect of the existence of stable partially metalated MT species. For example, a recent isolation of partially oxidized cardiac-specific MT from overexpressing transgenic mice was somewhat surprising because in a cooperative mechanism partial oxidation of the MT protein would act to labilize the remaining metal ions and facilitate complete oxidation (*42*). Prior to this study, isolation of partially metalated MT could be interpreted as an artifact of purification and of no biological relevance. However, this data establishes a noncooperative mechanism of metalation, which allows for the stability of partially metalated intermediates. Under this mechanism, partially metalated MT is likely to have several free thiol groups that can oxidize without interfering with the remaining thiol-bound metal ions.

The traditional functions of MT include the protective roles as a buffering agent against both toxic metal exposure and oxidative stress. In both cases, interaction of MT with the insult leads to a release of naturally bound Zn^{2+}, which coordinates to metal-regulatory transcription factor 1 (MTF-1). Zn-MTF-1 translocates to the nucleus and upregulates MT, allowing the cell to deal with the insult. In the former case, MT has been shown to protect an organism against a wide range of metals including Cd^{2+}, Hg^{2+} and As^{3+} (*43-44*). In the latter case, exposure of MT to oxidizing agents, such as H_2O_2, facilitates the oxidation of cysteine thiols to disulfide bonds (*45*).

A significant exception to this pattern of protection is methylmercury ($MeHg^+$) (*46*). The neurotoxicity of $MeHg^+$ is well known and the expression of MT has been shown to protect an organism against it. However induction of MT *in vivo* and *in vitro* with $MeHg^+$ using both astrocytes and neurons has not been possible (*43-44*). An analysis of the binding affinities suggests that $MeHg^+$, binding thiols with an association constant ranging from 10^{15} to 10^{23} (*46*), would be able to effectively outcompete zinc, which has an association constant ranging from 10^7 to 10^{12} (*22*). Taken together, these results suggest that while at equilibrium $MeHg^+$ should be able to displace Zn^{2+} from Zn-MT, in a cellular environment it is not able to effectively compete. It has, however, been shown that a pretreatment of the cell with either zinc or cadmium, both known to induce MT-1 and -2, is capable of aiding in metal-induced resistance to neurotoxicity (*47-48*). A noncooperative mechanism is critical since it affords stability to partially metalated species in the cellular environment. These partially metalated species, having several non-coordinating thiols, would likely be more susceptible to $MeHg^+$ binding. Without the necessity for Zn^{2+} to dissociate from MT, $MeHg^+$ coordination acts to sequester the toxic metal insult and is likely the cause of the observed resistance.

3.4.4 Supermetalation: Cd_4-β-rhMT 1a and Cd_8-βα-rhMT 1a

Supermetalated forms of metallothionein were also observed for both the β- and the βα-proteins studied, where we define supermetalation as metalation in excess of traditionally measured values. In the case of Cd_3-β-rhMT and Cd_7-βα-rhMT, addition of excess Cd^{2+} led to the formation of Cd_4-β-rhMT and Cd_8-βα-rhMT, respectively. These results complement well with the previously discovered supermetalated Cd_5-α-rhMT,

which was postulated to be a metal-exchange intermediate essential for MT's ability to maintain metal ion homeostasis (*39*).

Supermetalation of the β-domain has been previously postulated following analysis of CD and UV-visible absorption spectral data (*49*). Capdevila *et al.* have postulated from their spectral data, with excess Cd^{2+}, that Cd_4-β-rhMT subsequently unwound to form Cd_9-β-rhMT in a cooperative manner. It was proposed the unwinding required addition of 9 excess equivalents of Cd^{2+}. The ESI-MS data described here demonstrates that the mechanism is noncooperative for metalation of apo-β-rhMT to Cd_3-β-rhMT, Figure 3-2, and subsequently excess Cd^{2+} forms only Cd_4-β-rhMT.

Interestingly, based on the supermetalated data of the isolated domains we would predict that supermetalation of the full MT protein would lead to the formation of Cd_9-βα-rhMT and not Cd_8-βα-rhMT. Based solely on the ESI-mass spectral evidence two possibilities exist: 1) supermetalation of one of the two domains inhibits supermetalation of the other, or 2) coordination of the additional Cd^{2+} metal ion requires cysteine residues from both domains. Meloni and Vasak recently determined that there exists an eighth metal ion binding site in MT-3 (*50*). In the case of MT-3, the formation of supermetalated Cd_8-βα-hMT-3 results in a decrease in the Stoke's radius of the protein, which suggests the mutual approach of the two domains. Based on both this data, and the existence of Cd_8-βα-rhMT and not Cd_9-βα-rhMT in our ESI-mass spectra titration, we predict that supermetalation involves both domains.

3.5 Conclusion

In summary, addition of Cd^{2+} to β-rhMT and βα-rhMT results in noncooperative binding of to both. It can now be conclusively stated that the metalation of MT 1a with Cd^{2+} occurs in a noncooperative manner for both the isolated domains and the full MT protein. It was also shown that addition of excess Cd^{2+} to Cd_3-β-rhMT and Cd_7-βα-rhMT leads to the formation of Cd_4-β-rhMT and Cd_8-βα-rhMT, respectively. This result was surprising, since previous supermetalation studies of the isolated α-domain have also shown an additional Cd^{2+} ion is capable of binding to form Cd_5-α-rhMT and one would predict that supermetalation of the full MT protein would be merely the sum of the supermetalated isolated domains (Cd_9-βα-rhMT). Based on ESI-mass spectral evidence,

it is unclear if the additional Cd^{2+} ion coordinates to a single domain in Cd_7-βα-rhMT or involves both domains. The model of metal binding in metallothionein is now clearly more complex than previously thought, with the existence of partially- as well as super-metalated species. With the elucidation of noncooperative metalation of mammalian metallothionein, determination of both the presence and function of intermediate species are now possible.

3.6 References

1. Kagi, J. H. R., and Vallee, B. L. (1960) Metallothionein: A cadmium- and zinc-containing protein from equine renal cortex, *J. Biol. Chem. 235*, 3460-3465.
2. Robinson, N. J., Gupta, A., Fordham-Skelton, A. P., Croy, R. R. D., Whitton, B. A., and Huckle, J. W. (1990) Prokaryotic metallothionein gene characterization and expression: chromosome crawling by ligation-mediated PCR, *Proc. R. Soc. Lond. B 242*, 241-247.
3. Sturzenbaum, S. R., Kille, P., and Morgan, A. J. (1998) The identification, cloning and characterization of earthworm metallothionein, *FEBS Lett. 431*, 437-442.
4. Krezel, A., and Maret, W. (2008) Thionein/metallothionein control Zn(II) availability and the activity of enzymes, *J. Biol. Inorg. Chem. 13*, 401-409.
5. Kang, Y. J. (2006) Metallothionein redox cycle and function, *Exp. Biol. Med. 231*, 1459-1467.
6. Shaw-III, C. F., Stillman, M. J., and Suzuki, K. T. (1991) Metallothioneins: An overview of metal-thiolate complex formation in metallothioneins, In *Metallothioneins: Synthesis, structure and properties of metallothioneins, phytochelatins and metal-thiolate complexes* (Stillman, M. J., III, C. F. S., and Suzuki, K. T., Eds.), pp 1-13, VCH Publishers, Inc., New York.
7. Maret, W. (2008) Metallothionein redox biology in the cytoprotective and cytotoxic functions of zinc, *Exp. Gerontol. 43*, 363-369.
8. Wagner, G., Frey, M. H., Neuhaus, D., Worgotter, E., Braun, W., Vasak, M., Kagi, J. H. R., and Wuthrich, K. (1987) Spatial structure of rabbit liver metallothionein-2 in solution by NMR, In *Metallothionein II* (Kagi, J. H. R., and Kojima, Y., Eds.), pp 149-157, Birkhauser Verlag Basel, Basel.
9. Braun, W., Vasak, M., Robbins, A. H., Stout, C. D., Wagner, G., Kagi, J. H. R., and Wuthrich, K. (1992) Comparison of the NMR solution structure and the x-ray crystal structure of rat metallothionein-2, *Proc. Natl. Acad. Sci. U.S.A 89*, 10124-10128.
10. Boulanger, Y., Armitage, I. M., Miklossy, K.-A., and Winge, D. R. (1982) ^{113}Cd NMR study of a metallothionein fragment: Evidence for a two-domain structure, *J. Biol. Chem. 257*, 13717-13719.
11. Robbins, A. H., McRee, D. E., Williamson, M., Collett, S. A., Xuong, N. H., Furey, W. F., Wang, B. C., and Stout, C. D. (1991) Refined crystal structure of Cd, Zn metallothionein at 2.0 Å resolution, *J. Mol. Biol. 221*, 1269-1293.

12. Ryden, L., and Deutsch, H. F. (1978) Preparation and properties of the major copper-binding component in human fetal liver: Its identification as metallothionein, *J. Biol. Chem. 253*, 519-524.
13. Hartmann, H. J., and Weser, U. (1977) Copper-thionein from fetal bovine liver, *Biochim. Biophys. Acta 491*, 211-222.
14. Briggs, R. W., and Armitage, I. M. (1982) Evidence for site-selective metal binding in calf liver metallothionein, *J. Biol. Chem. 257*, 1259-1262.
15. Szymanska, J. A., Zelazowski, A. J., and Stillman, M. J. (1983) Spectroscopic characterization of rat kidney Hg,Cu-metallothionein, *Biochem. Biophys. Res. Commun. 115*, 167-173.
16. Uchida, Y., Takio, K., Titani, K., Ihara, Y., and Tomonaga, M. (1991) The growth inhibitory factor that is deficient in the alzheimer's disease brain is a 68 amino acid metallothionein-like protein, *Neuron 337-347*.
17. Stillman, M. J., Gasyna, Z., and Zelazowski, A. J. (1989) A luminescence probe for metallothionein in liver tissue: Emission intensity measured directly from copper metallothionein induced in rat liver, *FEBS Lett. 257*, 283-286.
18. Feng, W., Cai, J., Pierce, W. M., Franklin, R. B., Maret, W., Benz, F. W., and Kang, Y. J. (2005) Metallothionein transfers zinc to mitochondrial aconitase through a direct interaction in mouse hearts, *Biochem. Biophys. Res. Commun. 332*, 853-858.
19. Mason, A. Z., Perico, N., Moeller, R., Thrippleton, K., Potter, T., and Lloyd, D. (2004) Metal donation and apo-metalloenzyme activation by stable isotoopically labeled metallothionein, *Mar. Environ. Res. 58*, 371-375.
20. Maret, W., Larsen, K. S., and Vallee, B. L. (1997) Coordination dynamics of biological zinc "clusters" in metallothioneins and in the DNA-binding domain of the transcription factor Gal4, *Proc. Natl. Acad. Sci. U.S.A 94*, 2233-2237.
21. Zeng, J., Heuchel, R., Schaffner, W., and Kagi, J. H. R. (1991) Thionein (apometallothionein) can modulate DNA binding and transcription activation by zinc finger containing factor Sp1, *FEBS Lett. 279*, 310-312.
22. Krezel, A., and Maret, W. (2007) Dual nanomolar and picomolar Zn(II) binding properties of metallothionein, *J. Am. Chem. Soc. 129*, 10911-10921.
23. Mocchegiani, E., Giacconi, R., Muti, E., Cipriano, C., Costarelli, L., Tesei, S., Gasparini, N., and Malavolta, M. (2007) Zinc-bound metallothioneins and immune plasticity: Lessons from very old mice and humans, *Immun. Ageing 4*, doi:10.1186/1742-4933-1184-1187.
24. Giacconi, R., Bonfigli, A. R., Testa, R., Sirolla, C., Cipriano, C., Marra, M., Muti, E., Malavolta, M., Costarelli, L., Piacenza, F., Tesei, S., and Mocchegiani, E. (2008) +647 A/C and +1245 MT1A polymorphisms in the susceptibility of diabetes mellitus and cardiovascular complications, *Mol. Gen. Metab. 94*, 98-104.
25. Maret, W. (2008) A role for metallothionein in the pathogenesis of diabetes and its cardiovascular complications, *Mol. Gen. Metab. 94*, 1-3.
26. Chan, J., Huang, Z., Watt, I., Kille, P., and Stillman, M. J. (2007) Characterization of the conformational changes in recombinant human metallothioneins using ESI-MS and molecular modeling, *Can. J. Chem. 85*, 898-912.

27. Gehrig, P. M., You, C., Dallinger, R., Gruber, C., Brouwer, M., Kagi, J. H. R., and Hunziker, P. E. (2000) Electrospray ionization mass spectrometry of zinc, cadmium, and copper metallothioneins: Evidence for metal-binding cooperativity, *Protein Sci. 9*, 395-402.
28. Good, M., Hollenstein, R., Sadler, P. J., and Vasak, M. (1988) ^{113}Cd NMR studies on metal-thiolate cluster formation in rabbit Cd(II)-metallothionein: Evidence for a pH dependence, *Biochemistry 27*, 7163-7166.
29. Vasak, M., and Kagi, J. H. R. (1981) Metal thiolate clusters in cobalt(II)-metallothionein, *Proc. Natl. Acad. Sci. U.S.A 78*, 6709-6713.
30. Willner, H., Vasak, M., and Kagi, J. H. R. (1987) Cadmium-thiolate clusters in metallothionein: Spectrophotometric and spectropolarimetric features, *Biochemistry 26*, 6287-6292.
31. Bernhard, W. R., Vasak, M., and Kagi, J. H. R. (1986) Cadmium binding and metal cluster formation in metallothionein: A differential modification study, *Biochemistry 25*, 1975-1980.
32. Wang, H., Li, H., Cai, B., Huang, Z.-X., and Sun, H. (2008) The effect of nitric oxide on metal release from metallothionein-3: gradual unfolding of the protein, *J. Biol. Inorg. Chem. 13*, 411-419.
33. Rigby-Duncan, K. E., and Stillman, M. J. (2007) Evidence for noncooperative metal binding to the α domain of human metallothionein, *FEBS J. 274*, 2253-2261.
34. Palumaa, P., Eriste, E., Njunkova, O., Pokras, L., Jornvall, H., and Sillard, R. (2002) Brain-specific metallothionein-3 has higher metal-binding capacity than ubiquitous metallothioneins and binds metals noncooperatively, *Biochemistry 41*, 6158-6163.
35. Palumaa, P., Njunkova, O., Pokras, L., Eriste, E., Jornvall, H., and Sillard, R. (2002) Evidence for non-isostructural replacement of Zn^{2+} and Cd^{2+} in the β-domain of brain-specific metallothionein-3, *FEBS Lett. 527*, 76-80.
36. Lu, W., Zelazowski, A. J., and Stillman, M. J. (1993) Mercury binding to metallothioneins: Formation of the Hg_{18}-MT species, *Inorg. Chem. 32*, 919-926.
37. Nielson, K. B., Atkin, C. L., and Winge, D. R. (1985) Distinct metal-binding configurations in metallothionein, *J. Biol. Chem. 260*, 5342-5350.
38. Ngu, T. T., and Stillman, M. J. (2006) Arsenic binding to human metallothionein, *J. Am. Chem. Soc. 128*, 12473-12483.
39. Rigby-Duncan, K. E., Kirby, C. W., and Stillman, M. J. (2008) Metal exchange in metallothioneins - a novel structurally significant Cd_5 species in the alpha domain of human metallothionein 1a *FEBS J. 275*, 2227-2239.
40. Good, M., Hollenstein, R., and Vasak, M. (1991) Metal selectivity of clusters in rabbit liver metallothionein, *Eur. J. Biochem. 197*, 655-659.
41. Green, A. R., Presta, A., Gasyna, Z., and Stillman, M. J. (1994) Luminescent probe of copper-thiolate cluster formation within mammalian metallothionein, *Inorg. Chem. 33*, 4159-4168.
42. Feng, W., Benz, F. W., Cai, J., Pierce, W. M., and Kang, Y. J. (2006) Metallothionein disulfides are present in metallothionein-overexpressing

transgenic mouse heart and increase under conditions of oxidative stress, *J. Biol. Chem. 281*, 681-687.

43. Kramer, K. K., Zoelle, J. T., and Klaassen, C. D. (1996) Induction of metallothionein mRNA and protein in primary murine neuron cultures, *Toxicol. Appl. Pharmacol. 141*, 1-7.
44. Kramer, K. K., Liu, J., Choudhuri, S., and Klaassen, C. D. (1996) Induction of metallothionein mRNA and protein in murine astrocyte cultures, *Toxicol. Appl. Pharmacol. 136*, 94-100.
45. Zhang, B., Georgiev, O., Hagmann, M., Gunes, C., Cramer, M., Faller, P., Vasak, M., and Schaffner, W. (2003) Activity of metal-responsive transcription factor 1 by toxic heavy metals and H_2O_2 in vitro is modulated by metallothionein, *Mol. Cell. Biol. 23*, 8471-8485.
46. West, A. K., Hidalgo, J., Eddins, D., Levin, E. D., and Aschner, M. (2008) Metallothionein in the central nervous system: Roles in protection, regeneration and cognition, *Neurotoxicology 29*, 488-502.
47. Aschner, M., Conklin, D. R., Yao, C. P., Allen, J. W., and Tan, K. H. (1998) Induction of astrocyte metallothioneins (MTs) by zinc confers resistance against the acute cytotoxic effects of methylmercury on cell swelling, Na^+ uptake, and K^+ release, *Brain Res. 813*, 254-261.
48. Rising, L., Vitarella, D., Kimelberg, H. K., and Aschner, M. (1995) Metallothionein induction in neonatal rat primary astrocyte cultures protects against methylmercury cytotoxicity, *J. Neurochem. 65*, 1562-1568.
49. Capdevila, M., Cols, N., Romero-Isart, N., Gonzalez-Duarte, R., Atrian, S., and Gonzalez-Duarte, P. (1997) Recombinant synthesis of mouse Zn_3-β and Zn_4-α metallothionein 1 domains and characterization of their cadmium(II) binding capacity, *Cell. Mol. Life Sci. 53*, 681-688.
50. Meloni, G., Polanski, T., Braun, O., and Vasak, M. (2009) Effects of Zn^{2+}, Ca^{2+}, and Mg^{2+} on the structure of Zn_7metallothionein-3: Evidence for an additional zinc binding site, *Biochemistry 48*, 5700-5707.

Chapter 4. Single domain MT: Evidence for the onset of clustered metal binding domains[4]

4.1 Introduction

Metallothionein (MT) is a small cysteine rich protein found in all organisms. MT coordinates a variety of metals including the biologically essential Zn^{2+} and Cu^{+}, as well as toxic Cd^{2+}, Hg^{2+} and As^{3+} (*1-2*). These metal ions are capable of coordinating in a number of geometries, including digonal, trigonal, and tetrahedral (*3*). For Zn^{2+} and Cd^{2+} tetrahedral coordination by a mixture of terminal (binding to only a single metal-ion) and bridging cysteine residues (Cys) is critical to the metal binding site structure. As a consequence, we find 'magic numbers' for metal binding, formally defined as the stoichiometric ratios that appear to represent stable saturated clusters, that range from 7 to 18 metal ions per MT protein (*4*). While the exact *in vivo* functions of MT are unknown, MT has been implicated in toxic metal detoxification, metal ion homeostasis and as a protective agent against oxidative stress. All of these processes rely on MT's dynamic ability to bind and release metal ions within the cellular environment. The key to understanding the different roles of MTs is in a precise description of the metalation reactions – this allows a definitive description of the allowed metalation states possible for MTs and therefore an assessment of the functional metalation states. In previous studies, 7 Zn^{2+} is known as the 'fully metalated' state, while loss of 1 or 2 Zn^{2+} ions meant the protein had available binding sites and the cysteine residues not bound to Zn^{2+} would be exposed to oxidation. The result presented here show that the 5 Zn^{2+} metalation state is the protective level leaving no accessible cysteine residues.

The most well characterized members of the MT family are the mammalian MTs (Figure 4-1), for which X-ray diffraction and NMR studies of the fully metalated protein show that metal ions form two essentially isolated and distinct metal-thiolate clustered binding domains using the 20 cysteine residues of the protein. The N-terminal β-domain is capable of binding 3 Zn^{2+} , 3 Cd^{2+} or 6 Cu^{+} metal ions using 9 cysteine residues, while

[4] A version of this work is in preparation
D.E.K. Sutherland, K.L. Summers and M.J. Stillman (2012).

the C-terminal α-domain is capable of binding 4 Zn^{2+} , 4 Cd^{2+} or 6 Cu^{+} metal ions using 11 cysteine residues (*5-7*). The current view of these domains is that each acts as an effectively isolated metal-thiolate cluster. This view has been supported by a number of NMR studies of mammalian MT, where no inter-domain peaks associated with the nuclear overhauser effect (NOEs) were found (*7-8*). Since NOEs are a through space phenomenon it has been inferred that the two domains are not physically near one another. The sole exception to this observation is supermetalation of MT, where addition of excess Cd^{2+} results in formation of a single Cd_8Cys_{20} 'super-domain' (*9-10*). Based on a combination of electrospray ionization mass spectrometry (ESI-MS) and absorption, circular dichroism and NMR spectroscopy it was determined that the addition of the 8^{th} Cd^{2+} ion resulted in rearrangement of all 8 Cd^{2+} ions to form a single clustered Cd_8-S_{20}-βα-rhMT domain.

One important feature in many of the MT's studied is the existence of multiple, often 2, isolated domains that are reported to coordinate both different numbers and different types of metal ions. It has been suggested that the existence of the two domain structure present in many MTs allows the protein to function simultaneously in both Zn^{2+} and Cu^{+} chemistries (*11-12*). The potential for MT to be able to spatially separate metal ion chemistry into different domains has significant consequences for our understanding of the role of MT in metal ion homeostasis and as a protective agent against oxidative stress. For instance, MT-3 has been proposed to play an important role in maintaining the balance of metals in the brain (*13*) and it has been reported to be downregulated in patients with Alzheimer's disease. A recent paper has shown that Zn_7-βα-MT 3 is capable of metal exchange with the copper bound amyloid-β-peptide ($A\beta_{1\text{-}40}$-Cu^{2+}) (*14*). The exchange reaction and subsequent reduction to Cu^{+} leads to the formation of Cu_4Zn_4-βα-MT 3. This process eliminates the production of reactive oxygen species and related toxic effects, and it is thought to somewhat protect the individual from Alzheimer's disease. While the exact structure of this Cu_4-motif is not known, it has been reported as a stable folding intermediate leading towards the complete metalation of MT (Cu_{12}-βα-MT) (*15*).

Currently, little is known about the exact mechanism of the metalation of MT. However, it has been demonstrated through ESI-MS that MT binds Cd^{2+} and As^{3+} in a

noncooperative manner, meaning that in addition to apo- and holo-MT, partially metalated species may also exist *in vivo (2, 16-18).* Furthermore these partially metalated species may be critical in the metal-exchange reactions necessary for maintenance of metal-ion homeostasis.

While the fully metalated proteins have been studied in detail by numerous methods, there are few studies that specifically focus on the metal binding reaction to the apo-metal-free protein other than the recent As^{3+} kinetic data (*2, 18*). A key feature of the conclusions from those As^{3+} data was that each As^{3+} ion was bound to exactly 3 cysteinyl thiolates, meaning that no clustering took place.

With the noncooperative mechanism of metalation recently established, it is now crucial to determine the structural features of MT in the early stages of metalation (before the protein is saturated) with Zn^{2+}, the key biologically significant metal. The importance of determining the 'holding point' for MT, that is the minimum 'safe' metalation point against oxidative stress, is to answer the question of what is the naturally-metalated state and the effects expected from demetalation when MT is part of a redox cycle.

In this chapter, we report on a series of Zn^{2+} competition experiments performed using the metal-free isolated fragments apo-β- and apo-α- and the metal-free full protein apo-βα-rhMT 1a. Individual titrations of both the isolated domains and the full MT protein demonstrated that Zn^{2+} metalation occurs in a noncooperative manner. Competition experiments using the very slight differences in the formation constants (K_F) introduced by co-metallating the isolated fragments containing the individual β- and α-domains, and the isolated domains and the full MT protein probe the metalation reaction in detail not previously reported. The data show that K_F is sensitive to the metalation status and particularly to the onset of clustering. We interpret the ESI-MS results to indicate that initial metalation of MT does not occur in a domain specific manner, rather the availability of up to 20 cysteines means that Zn^{2+} up to and including 5 bind tetrahedrally to four terminal cysteinyl thiolates (each cysteine residue coordinates only a single metal ion) that do not bridge in a ‘beaded necklace’-like fashion. Only then does clustering take place via bridging interactions and a concomitant reduction in K_F for those sites. The subsequent metalation of the full protein to Zn_6- and Zn_7-βα-rhMT 1a requires a complete structural rearrangement, loss of the single domain structure, together with

development of the clusters associated with the formation of the more traditional Zn_3- and Zn_4-domains.

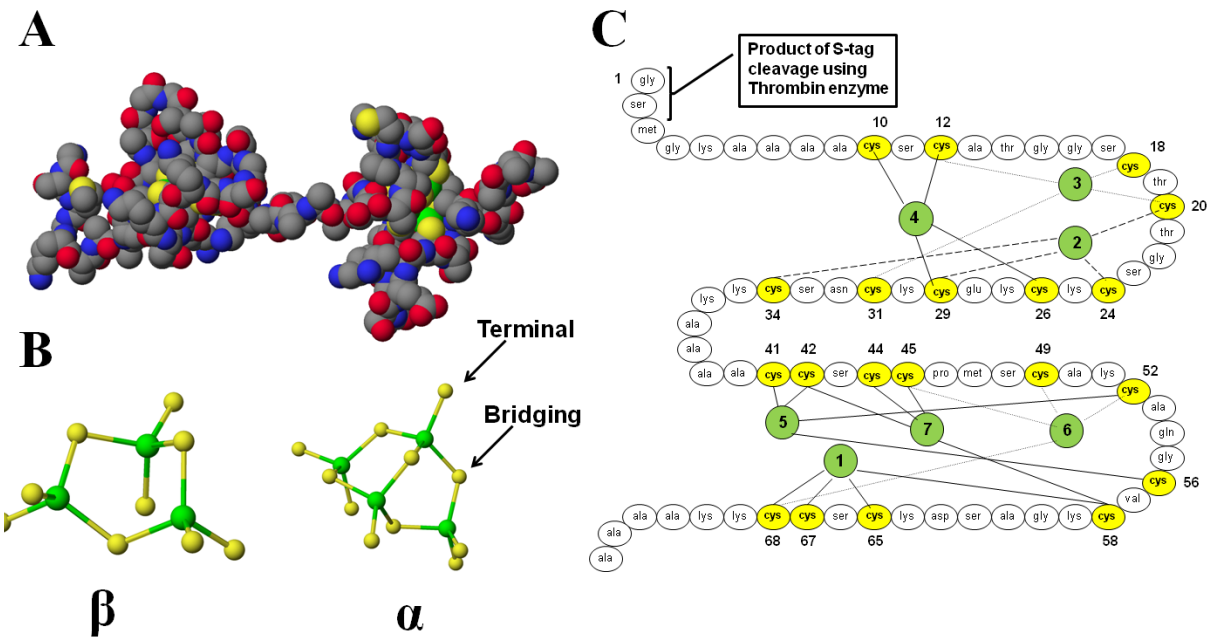

Figure 4-1. **Structure of MT 1a.** (A) A space filling structure of Cd_7-βα-rhMT 1a. The N-terminal β-domain is located on the left hand side, while the C-terminal α-domain is located on the right hand side. (B) Cadmium-cysteinyl-thiolate clusters of Cd_7-βα-rhMT 1a presented as a ball and stick model: β-domain (left) and α-domain (right). (C) A connectivity diagram of MT 1a, which shows each of the seven cadmium atoms connected to exactly four cysteine amino acids. The connectivity diagram has been renumbered from the original to accommodate the amino acids glycine and serine, both of which are a product of S-tag cleavage with thrombin, located on the N-terminal of the β-domain. Numbering of the Cd-thiolate centers is based on the NMR assignment by Messerle *et al.* (7). Data from Chan *et al.* were used to produce the molecular models seen in (A) and (B) (19).

4.2 Experimental Methods

Chemicals: cadmium sulfate (Fisher Scientific); zinc sulfate (Caledon Laboratory Chemicals); ThrombinCleanCleave™ Kit (Sigma); Tris, tris(hydroxymethyl)aminomethane (EMD Chemicals/VWR); ammonium hydroxide (Caledon Laboratory Chemicals); formic acid (Caledon Laboratory Chemicals); and hydrochloric acid (Caledon Laboratory Chemicals). All solutions were made with >16

MΩ·cm deionized water (Barnstead Nanopure Infinity). HiTrap™ SP HP ion exchange columns (Amersham Biosciences/ GE Healthcare), superfine G-25 Sephadex (Amersham Biosciences/ GE Healthcare), stirred ultrafiltration cell Model 8200 (Amicon Bioseparations/Millipore) with a YM-3 membrane (3000 MWCO) were used in protein preparation steps.

Protein preparation: The expression and purification methods have been previously reported (*19*). β-rhMT, α-rhMT and βα-rhMT 1a proteins used in this study were based on the 38-residue, 41-residue, and 72-residue sequences, respectively: β-rhMT MGKAAAACSC ATGGSCTCTG SCKCKECKCN SCKKAAAA, α-rhMT MGKAAAAC CSCCPMSCAK CAQGCVCKGA SEKCSCCKKA AAA, βα-rhMT MGKAAAACSC ATGGSCTCTG SCKCKECKCN SCKKAAAACC SCCPMSCAKC AQGCVCKGAS EKCSCCKKAA AA. There are 9, 11, and 20 cysteine residues present in β-rhMT, α-rhMT and βα-rhMT, respectively, and no disulfide bonds. The expression system included, for stability purposes, an N-terminal S-tag (MKETAAAKFE RQHMDSPDLG TLVPRGS). Recombinant proteins were expressed in BL21(DE3) *Escherichia coli*. All cell lines were transformed using the pET29a plasmid. Removal of S-tag was performed using a Thrombin CleanCleave™ Kit (Sigma). To impede oxidation of the cysteine residues to disulfide bonds, all protein samples were argon saturated and rigorously evacuated to remove any residual oxygen that may be present in the solution. Concentrated hydrochloric acid was used to demetalate protein samples, followed by desalting on a G-25 (Sephadex) column.

ESI MS procedures: Protein solutions were prepared in dilute formic acid in deionized water (pH 2.7). Final ESI MS solutions were pH adjusted using concentrated ammonium hydroxide. A small aliquot of protein was remetalated with cadmium to determined the protein concentration by UV absorption spectroscopy using the absorbance at 250 nm, which corresponds to the ligand-to-metal charge transfer transition generated by the metal-thiolate bond ($\varepsilon_{\beta 250}$= 36,000 $M^{-1}cm^{-1}$; $\varepsilon_{\alpha 250}$= 45,000 $M^{-1}cm^{-1}$; $\varepsilon_{\beta\alpha 250}$= 89,000 $M^{-1}cm^{-1}$). Zinc sulfate was prepared in deionized water. The concentration of zinc sulfate and all molar equivalents added to MT solutions were measured through calibration of the Zn^{2+} content using atomic absorption spectrometry (AAS).

All data were collected on an electrospray-ionization time-of-flight (ESI-TOF) mass spectrometer (Bruker Daltonics) in the positive ion mode. NaI was used as the calibrant. The scan conditions for the spectrometer were: end plate offset, -500V; capillary, +4200 V; nebulizer, 2.0 bar; dry gas flow, 8.0 L/min; dry temperature, 80°C; capillary exit, 180 V; skimmer 1, 22.0 V; hexapole 1, 22.5 V; hexapole RF, 600 Vpp; skimmer 2, 22 V; lens 1 transfer, 88 μs; lens 1 pre pulse storage 23 μs. The range was 500.0–3000.0 m/z, averaging 2 × 0.5 Hz. Spectra were deconvoluted using the Bruker Compass DataAnalysis software package.

Molecular Model: MM3 and MD calculations parameterized using the modified force field described by Chan *et al.* and the dielectric constant for water (78.4) were carried out to obtain the minimum-energy structure for apo-βα-rhMT 1a to Zn_7-βα-rhMT 1a (*20*). All MM3 and MD calculations and model-structure rendering were carried out using CAChe WorkSystem Pro 6.1.1 software (Fujitsu America). The original Cd_7-βα-rhMT 1a was modified to produce molecular models for Zn_5-βα-rhMT 1a (*19*). The structure was energy minimized using the MM3 calculation followed by the MD simulation at 300 K for 5000 ps.

4.3 Results

4.3.1 Noncooperative metalation of isolated apo-β and apo-α- and apo-βα-rhMT 1a by Zn^{2+}

The mass spectral data recorded during the titration apo-β-rhMT 1a, apo-α-rhMT 1a, and apo-βα-rhMT 1a with Zn^{2+} are shown in Figure 4-2 with their corresponding deconvoluted spectra (right hand columns). Stepwise metalation of apo-β-rhMT (A-E) leads to the formation of partially metalated species (Zn_1-, Zn_2-β-rhMT 1a) at substoichiometric equivalents (β < 3 Zn^{2+}). Complete metalation occurs when 3.5 equivalents of Zn^{2+}/β-rhMT 1a are added to solution. From the data it can be clearly seen that the dominant metalation state is a direct result of the number of equivalents of Zn^{2+} added to solution: at 1.7 eq. Zn^{2+} the dominant species is Zn_1-β-rhMT 1a, while at 2.6 eq. Zn^{2+} the two most abundant species are fully metalated Zn_3-β-rhMT 1a and partially metalated Zn_2-β-rhMT 1a. Metal free apo-β-rhMT 1a exhibits charge states

corresponding to 4+, 3+ and 2+ at 0.1 eq. Zn^{2+}. The most significant change in the charge state profile is the decrease in intensity of the 2+ charge state at 1.7 equivalents of Zn^{2+} added to solution. There is also a 20% decrease in the intensity of the 3+ relative to the 4+ charge state when comparing apo-β-rhMT 1a to Zn_3-β-rhMT 1a. Taken together, these results suggest that the addition of the first two metal ions stabilize a slightly more open conformation of apo-β-rhMT 1a.

Stepwise metalation of apo-α-rhMT (F-J) leads to the formation of partially metalated species (Zn_1-, Zn_2-, Zn_3-α-rhMT 1a) at substoichiometric equivalents ($\alpha < 4$ Zn^{2+}). The dominant metalation state is a direct result of the number of equivalents of Zn^{2+} added to solution: at 2.2 eq. Zn^{2+} the dominant species is Zn_1-α-rhMT 1a, while at 3.7 and 3.9 eq. Zn^{2+} the dominant species are Zn_2- and Zn_3-α-rhMT 1a, respectively. Complete metalation is observed at 4.1 eq. Zn^{2+} added to solution, however, there still exists a relatively small (~15% of total species present) population of Zn_3-α-rhMT 1a, which we attributes to slight errors in the calculation of the equivalents of Zn^{2+} added. Much like the β-domain, apo-α-rhMT 1a exhibits significant changes in the 4+, 3+ and 2+ charge state distribution when even a low stoichiometric ratio of Zn^{2+} has been added (e.g. 0.4). Also like apo-β-rhMT 1a, the 2+ and 3+ charge state decrease in intensity upon addition of one equivalent or more Zn^{2+}, relative to the 4+ charge state (compare the ESI-mass spectral data of apo-α-rhMT to Zn_4-α-rhMT). These changes in the overall charge state profile demonstrate that the metalated forms of both β- and α-rhMT, while similar to that of the apo-forms of the protein, occupy a somewhat larger volume.

The mass spectral data recorded during the titration of apo-βα-rhMT 1a with Zn^{2+} and the corresponding deconvoluted spectra are shown in Figure 4-2 (K-O). As is the case for both the β- and α-domain, stepwise metalation of apo-βα-rhMT leads to the formation of partially metalated species (from Zn_1 to Zn_6) at substoichiometric equivalents ($\beta\alpha < 7$ Zn^{2+}) confirming the noncooperative nature of the metalation reaction. The endpoint of the titration occurs after 7 equivalents of Zn^{2+} have been added to the solution. In each step of the titration, the dominant metalation state is a direct result of the number of equivalents of Zn^{2+} added to solution. Apo-βα-rhMT 1a exhibits a charge state profile that ranges from +8 to +3. The increase in the total number of charge states, as compared to the isolated domains, is because the full protein occupies a larger volume than either of

the two isolated domains. At 2.7 equivalents of Zn^{2+}, the dominant metalation states are Zn_2- and Zn_3-βα-rhMT 1a. A significant reduction in the intensity of the +7 charge state, as well as the disappearance of the +8 charge state is also observed at this point. These changes to the charge state envelope suggest that the first metal ion must significantly restrict the motion of the protein reducing its volume. Beyond 2.7 eq. Zn^{2+}, there is very little change in the +6, +5, +4 and +3 charge state distribution indicating that further metalation does not substantially alter the folding of the protein.

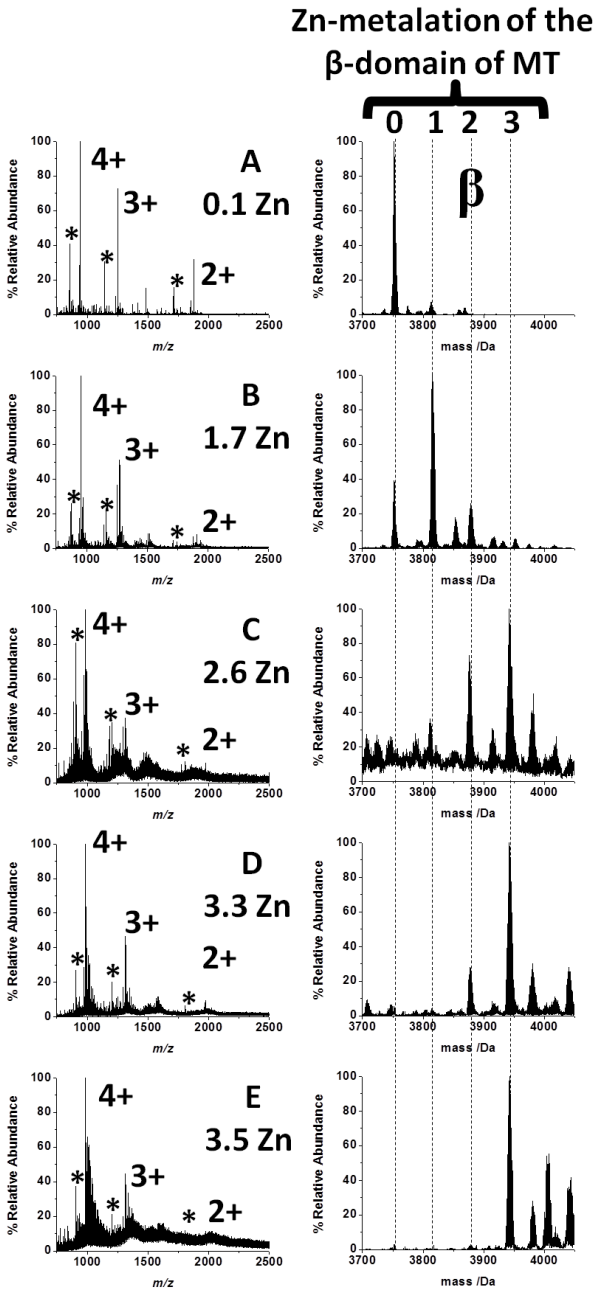
Zn-metalation of the
β-domain of MT
0 1 2 3
A
0.1 Zn
B
1.7 Zn
C
2.6 Zn
D
3.3 Zn
E
3.5 Zn
4+
3+
2+
β
% Relative Abundance
m/z
mass /Da

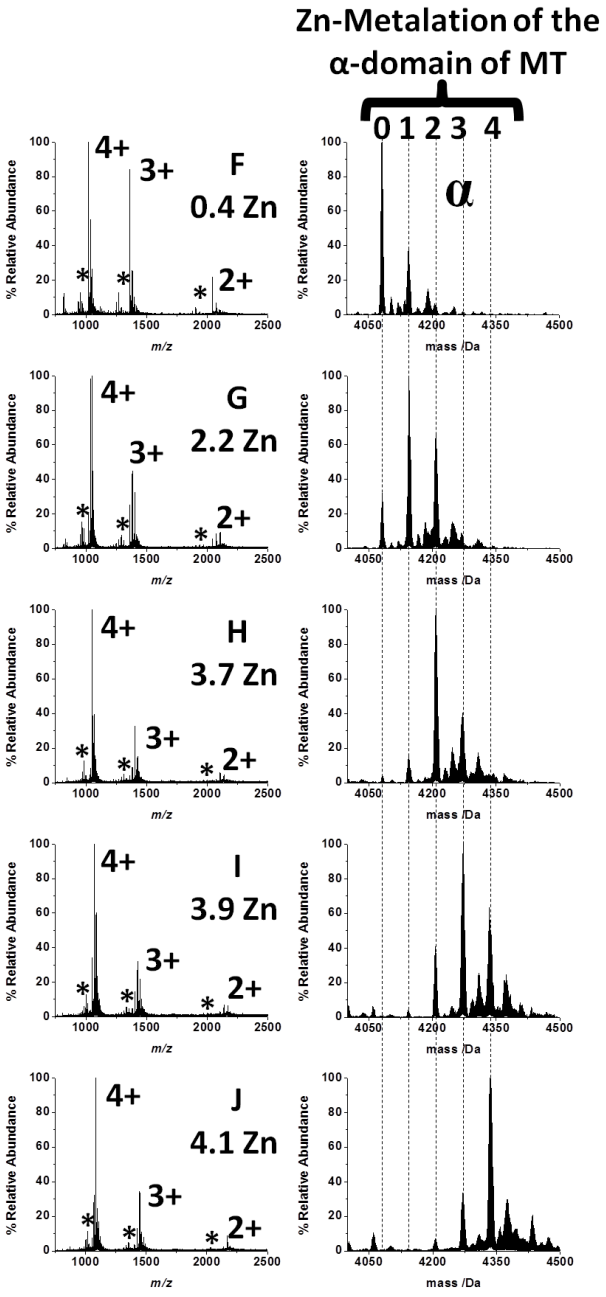
Zn-Metalation of the
α-domain of MT
0 1 2 3 4
α
F
0.4 Zn
G
2.2 Zn
H
3.7 Zn
I
3.9 Zn
J
4.1 Zn
4+
3+
2+
% Relative Abundance
m/z
mass /Da

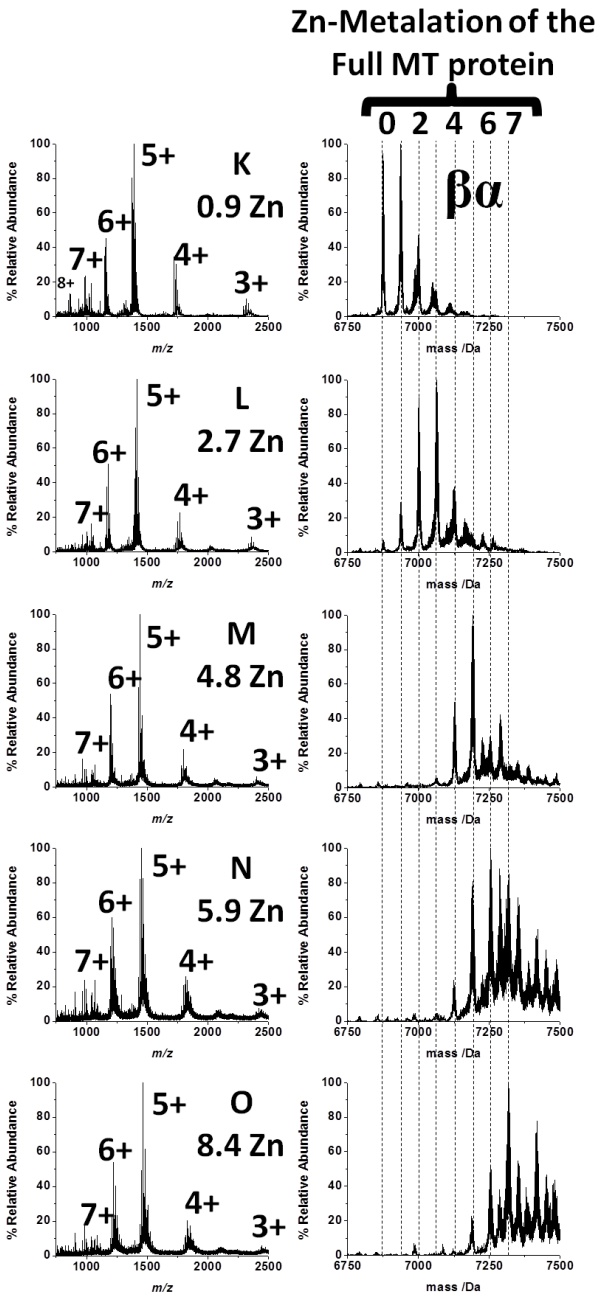

Figure 4-2. ESI mass spectra recorded during the titration of apo-β-rhMT, apo-α-rhMT and apo-βα-rhMT, with $ZnSO_4$. In each column the ESI mass spectral data (left) and their deconvolted counterparts (right) were recorded as Zn(II) was added to the solution. Dotted lines follow metal binding. (A-E) The titration of apo-β-rhMT, 29.2 μM at pH 9.2, with $ZnSO_4$. (F-J) The titration of apo-α-rhMT, 34.1 μM at pH 9.5, with $ZnSO_4$. (K-O) The titration of βα-rhMT, 29.2 μM at pH 9.1, with $ZnSO_4$.

4.3.2 Competitive metalation with Zn^{2+} of the isolated fragments containing the β- and α-domains of MT 1a

The metal binding specificity of each of the two metal binding domains of MT has been the subject of many studies. Yet, no step-wise metalation data have been published showing the development of the fully metalated protein from the metal-free apo-protein that identifies clearly any specific domain specificity for a metal. This was determined by competitively metalating both the isolated domains with Zn^{2+}. This competitive metalation experiment of the isolated β- and α-domains using Zn^{2+} was monitored with ESI-MS. The value of this technique over those previously used in competition experiments is that the exact metalation status of each domain can be monitored for all equivalents added during a single titration. This experimental setup also allows the interpretation of results in the context of a noncooperative mechanism of metalation, which allows for partial metalation and a continuum of metalated states to exist. In this way one can determine the average metalation of MT and also the exact distribution at each step of the titration. Other competition experiments, such as copper luminescent experiments (*12*), provide only an averaged measure of metalation and not the exact speciation over all sites in each domain. Consequently, it is possible to determine the relative affinity of each site in each domain for Zn^{2+} binding from the metalation status.

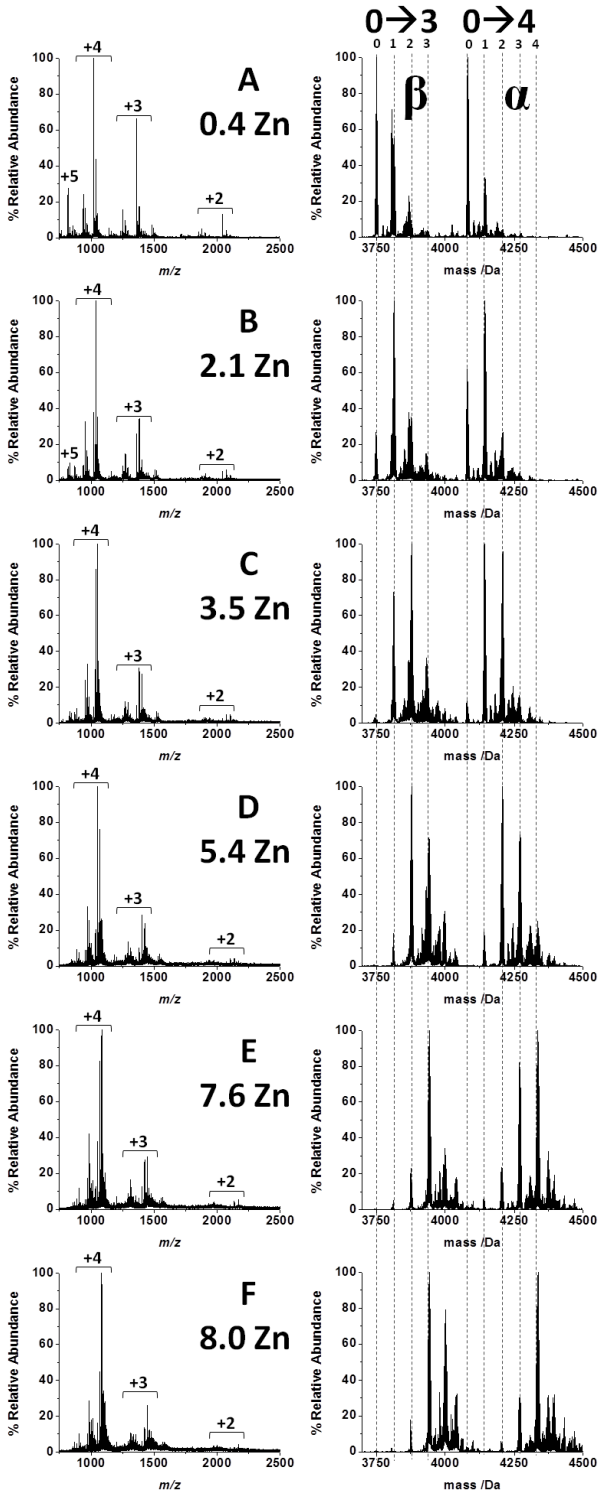

Figure 4-3. **ESI mass spectra recorded during the competitive titration of apo-β- and apo-α-rhMT with $ZnSO_4$.** Both species were at a concentration of 29.2 μM and at a pH of 9.2. ESI mass spectral data (left) and their deconvoluted counterparts (right) were recorded at Zn(II) molar equivalents of 0.4, 2.1, 3.5, 5.4, 7.6, and 8.0. Dotted lines follow metal binding in both β- and α-rhMT. The most intense species for both the β- and α-domain have been normalized to 100% relative abundance.

Figure 4-3 (A-F) shows the ESI-MS monitored competition experiment for Zn^{2+} between the isolated β- and α-domains of MT. Both domains are present in equal concentrations and their metalation status is a function of Zn^{2+} added to solution. It should be noted that there exists a slight Zn^{2+} contaminant, ~0.3 equivalents of total protein. The charge state data (left) have been deconvoluted to obtain the neutral parent species (right). Because two domains are present and each exhibits several metalation states, the charge state data are complicated and the deconvolution data fall into two sets reflecting the different chain lengths of the β and α fragments. To our knowledge this is the first report of a competition experiment in which metalation data from both domains can be monitored at the same time. Figures 4-4 and 4-5 extract and condense these data to show the information contained as function of number of Zn^{2+} equivalents added. The equivalents of Zn^{2+} added to the solution are relative to the total protein concentration of a given domain (β-domain plus α-domain). In this way, one would expect 7 molar equivalents to be necessary to fully metalate both domains. At 0.4 equivalents of Zn^{2+} added to the solution, it can be seen that metal free (apo-) β-rhMT dominates, but there also exists significant Zn_1-β-rhMT (relative abundance compared to the most abundant metalated species (RA): 70%) and Zn_2-β-rhMT (RA: 20%) present in solution. In the case of the α-domain, apo-α-rhMT dominates, but unlike the β-domain, there is very little Zn_1-α-rhMT (20%). This strongly suggests that initially metalation of the β-domain is, in fact, favored over that of the α-domain when the fragments are studied. At the 3.5 Zn^{2+} point, (Figure 4-3C) the dominant metalated species are Zn_2-β-rhMT and Zn_1-α-rhMT, respectively. The metalated profiles observed at 5.4 Zn^{2+} added (Figure 4-3D) are similar for both domains. Prior to this point in the titration, the β-domain consistently binds more Zn^{2+} than the α-domain, so this equalizing of the metalated species would suggests that the K_F for the third binding site for the β-domain, that is the conversion of the Zn_2-β-rhMT with its terminal-Cys-bonded Zn^{2+} (no bridging interactions) to the clustered Zn_3-β-rhMT, is substantially weaker than the previous two.

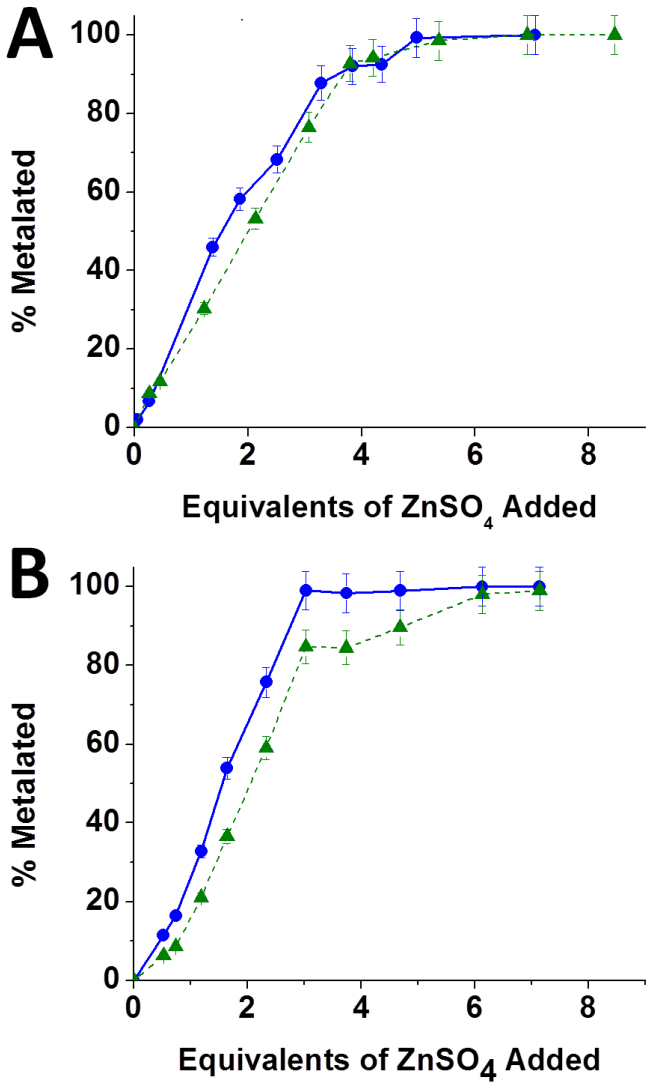

Figure 4-4. The normalized metalation properties of the β- and α-domains. (A) The % metalation of the individual isolated domains (B) The % metalation of the isolated domains present in direct competition with each other for metal ions. The associated metalation data for the β-domain is labelled with a solid line ( ), while the α-domain is labelled with a dashed lined ( ).

This interpretation is based on the uniquely rich nature of these data in which almost identical cysteine binding sites compete for the same metal. In addition, the distribution of the Zn^{2+} (1-bound, 2-bound, etc.) provides a much greater resolution of the binding pathway than a simple average and leads to the step-wise data shown below. The change in metalation status of the β-domain can be interpreted as resulting from the necessity for

the onset of cluster formation that involves three bridging cysteine residues (Fig 1B) when its 9 cysteine residues accommodate all three Zn^{2+} ions. In sharp contrast, the α-domain, with 11 cysteine residues, requires only a single shared cysteine residue to bind three Zn^{2+} ions. Complete metalation of the β-domain occurs at 7.6 Zn^{2+} added (Figure 4-3E), at which point the α-domain still exists as a mixture of Zn_2-, Zn_3- and Zn_4-α-rhMT. Complete metalation of the α-domain is observed at 8.0 eq Zn^{2+} added (Figure 4-3F) at which point 5 cysteines are bridging (Figure 4-1).

Figure 4-4 shows the normalized metalation of the fragments with the isolated domains as a function of added Zn^{2+}. In these plots, the fully metalated protein status is 100% (that is, 3 Zn^{2+} for β and 4 Zn^{2+} for α). Figure 4-4A depicts the relative metalation of the isolated domains with Zn^{2+} in the absence of any competitor - that is simply the metalation of the domains themselves. Clearly, both domains have similar metalation properties, although the β-domain has an advantage over the α-domain. The 60% mark for the β-domain represents the binding of 2 Zn^{2+} and the change in slope may be interpreted as the effect of the extensive bridging required to add the 3rd Zn^{2+}. The α domain can add 3 Zn^{2+} (75% mark) before significant bridging is required.

Figure 4-4B shows the normalized metalation of the two domains when in direct competition for the added Zn^{2+}. This Figure 4-4 demonstrates that the β-domain dominates the titration, completely metalating before the α-domain. The pause in metalation for the α domain at about the 80% mark represents the change from 3 Zn^{2+} to 4 Zn^{2+} bound. These plots highlight the importance of the competition reaction in determining the relative metalation of the two domains. The data suggest that when sufficient Zn^{2+} is added, the β domain simply competes directly with the α domain and continues to complete metalation.

4.3.3 Speciation of the β and α fragments with isolated domains-effect of domain competition

Figure 4-5 shows the relative abundances of each individual Zn-species formed during the metalation of the two isolated fragments and during the competitive metalation reaction extracted from the experimental data shown in Figures 4-2 and 4-3 above. The top row of plots (A, C, E) represent the individual Zn-loading as a function of Zn^{2+} added

for the β domain and the results of modeling the K_F's for each of the three steps. The bottom row of plots (B, D, F) represent the individual Zn-containing species as a function of Zn^{2+} added for the α domain and the results of modeling the K_F's for each of the four steps. For the isolated fragments (A, B), that is for metalation with no competitor (see Figure 4-2 A-E and F-J) we see that the increasingly metalated species coexist throughout the metalation reaction until metalation is complete at 100%. For the β domain, Zn_2- overlaps Zn_1-, followed by almost 100% formation of Zn_3-. On the other hand, the α domain metalates stepwise with even the Zn_4- species forming while a mixture of Zn_2- and Zn_3- have appreciable content.

The effect of competition for the Zn^{2+} by the two domains (C, D) is of critical importance because the two peptides offer slightly different K_F`s for the specific Zn^{2+} binding so these data allow resolution of each individual step in the metalation pathway. Clearly, the data in Figure 4-5 C and D show that the metalation steps are spread out compared with A and B - this means that there is direct competition for the Zn^{2+} as the K_F decreasing as the number of Zn^{2+} ions bound increases. For example, at the Zn^{2+} added point of 4 in (C) there is a mixture of Zn_2 (50%), Zn_1(25%), Zn_3 (25%) - compare this mixture with the Zn^{2+} added point of 2 (as the molar ratios of the Zn^{2+} added are scaled for the presence of both fragments, 4 approximately scales to 2) for the isolated domain in (A): here Zn_1 is 60%, Zn_2 is 10% and apo is still 20%. Similar data are observed for the α domain (D).

A model was produced in which the competing sites, each with their own K_F values, were metalated (Figure 4-5). The dependence of the individual metalated species on the amount of Zn^{2+} ions added to solution are shown for the β-domain, as (E), and the α-domain, as (F). The appearance and disappearance of the individual Zn-species was modeled by a series of declining K_F's for the 7 Zn^{2+}-binding steps (E,F), based upon the K_F values reported by Krezel and Maret (*21*). The model emphasizes a steeper decline in K_F when terminal Cys have been exhausted (at 2 Zn^{2+} bound for the β domain and 3 Zn^{2+} bound for the α domain) arguing that terminal coordination (a cysteine residue that does not bridge) is thermodynamically preferred as is expected and now confirmed experimentally.

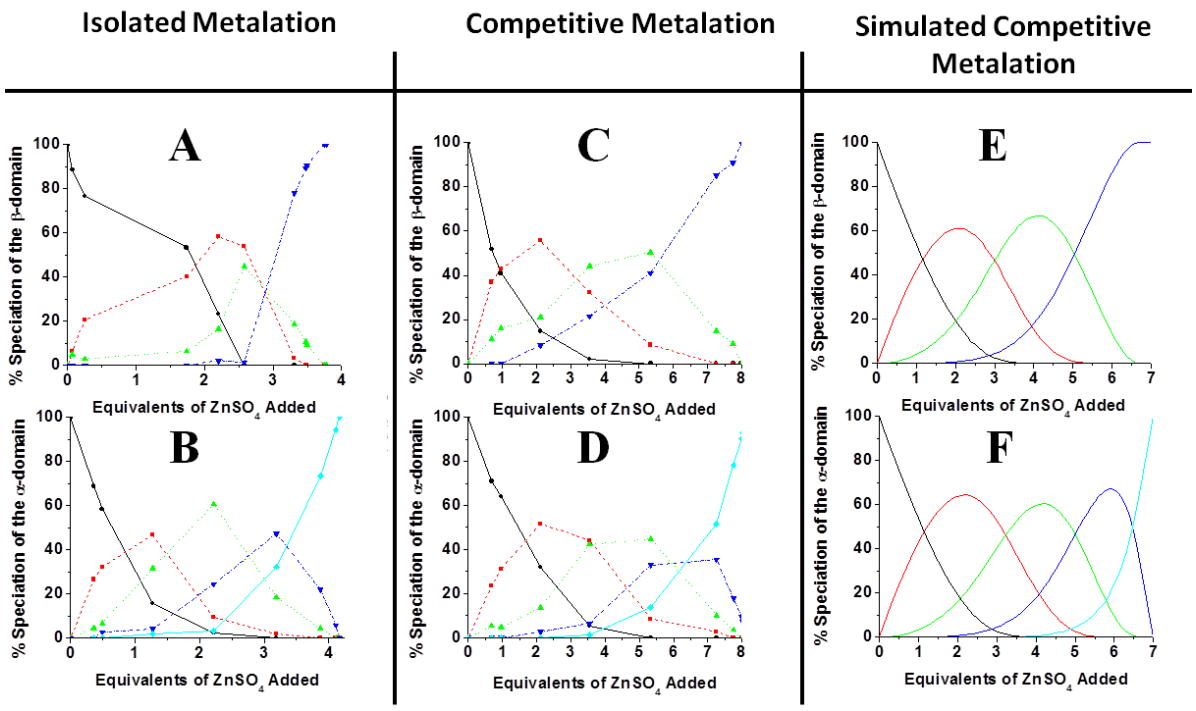

Figure 4-5. ESI-MS relative abundances for the metalation chemistry of the two isolated domains. Metalation of apo-β-rhMT (A), apo-α-rhMT (B), as well as their respective metalation under competitive conditions (C) and (D), respectively, using Zn^{2+} to form Zn_n, where n corresponds to the number of metals bound. Simulation of the metalation of both the β- and α-rhMT domains were also performed, in which the $\log_{10}(K_F)$ association constants for the α-domain were 10.4, 9.8, 9.3 and 8.6, while the β-domain was 10.4, 9.9 and 9.2. Each line corresponds to a different metalation state: Zn_0(—●—), Zn_1(- -■- -), Zn_2 (· ·▲· ·), Zn_3(-·▼·-), and Zn_4(—◆—).

4.3.4 Competitive metalation of the isolated β- and α-domains and full protein of MT 1a using Zn^{2+}

Figure 4-6 shows the experimental ESI mass spectral data when the metal-free β and α fragments are mixed with the full βα-protein and Zn^{2+} is added incrementally. This experimental arrangement allows comparison of the relative binding constants of the 14 individual Zn^{2+} binding sites spread over the two fragments and the full protein. The mass spectral data in Figure 4-6 (A-G) are complicated as there is a superposition of the charge states for each of the two fragments and the full protein for each metalated state. The deconvolution data (on the right hand side) provides greater clarity, and we have added guideline for each of the three protein species showing the metalation state. From these data further data sets can be extracted (i) the 'life' of each metalated species up to

full saturation, Figure 4-7, and (ii) the average saturation for each species as a function of added Zn^{2+} during competition, Figure 4-8. Those fractional loadings were modeled quite accurately based on the 14 K_F values, Figure 4-9.

The transient life of each metalated species in the three-protein competition experiment is shown in Figure 4-7. The data in (A), (B) and (C) are the species dependence for the isolated β-fragment, the α-fragment and the full βα-protein in the absence of competitors, as described earlier from Figure 4-5 and included here to allow direct comparison of the effect of competitive binding. Figures 4-7 (D, E, F) show that the individually metalated species exist for a wider range of added Zn^{2+}. Interestingly, Zn_1- and Zn_2- for both β- and α- form synchronously. Zn_3-β-MT is formed completely before Zn_3-α-MT and therefore, before Zn_4-α-MT. Panel (F) shows the sequential metalation of the βα-apo-MT. A number of important points can be made. First, Zn_1-, Zn_2-, and Zn_3-βα-rhMT all form when just the Zn_1- of the isolated domains forms. This is predicted by the As-analysis of Ngu, *et al.* because there are simply more available sites in the βα-MT than in the isolated domains so the K_F's of these first 3 sites of the full protein dominate. Zn_4- in (F) exists over a wide range of added Zn^{2+} (*2, 18, 22*). $Zn_{5\text{-}6\text{-}7}$ form over a relatively narrow range of added Zn^{2+} once the two domains are completely metalated.

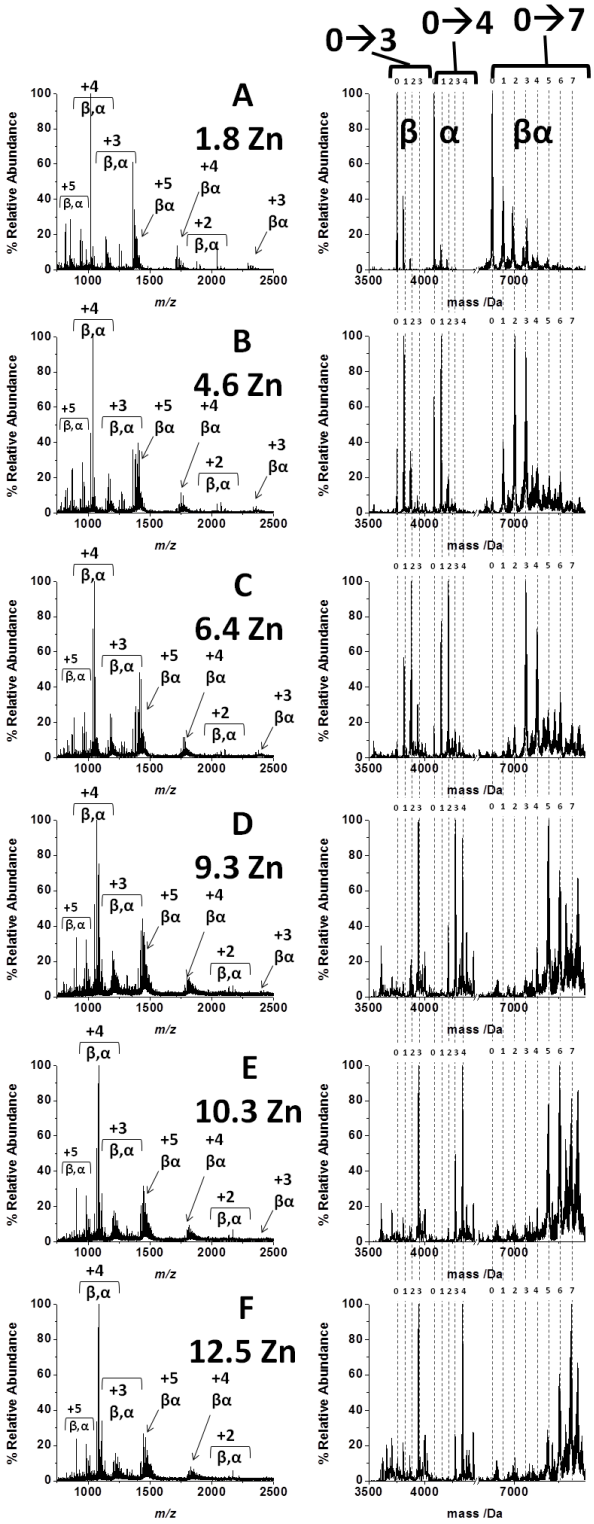

Figure 4-6. **ESI mass spectra recorded during the competitive titration of a solution containing equimolar concentrations of apo-β-, apo-α-, and apo-βα-rhMT with $ZnSO_4$ at pH 7.8.** ESI mass spectral data (left) and the deconvoluted counterparts (right) were recorded as aliquots of Zn(II) were added to the protein at molar equivalents of 1.8, 4.6, 6.4, 9.3, 10.3 and 12.5. Dotted lines follow metal binding in both β-, α- and βα-rhMT. The most intense species for both the β- and α-domain have been normalized to 100% relative abundance.

The model was applied to the 3-protein metalation (Figure 4-6) to produce Figure 4-7 as (G), (H), and (I). The traces shown are the predictions for the simultaneous formation of the metalated species based on 14 coupled K_F values. The model requires the K_F values to decline as a function of metalated number as expected for non-cooperative binding. The very close alignment of the simulation with the very complicated experimental data strongly supports the model: that there are declining K_F values and especially, a sharper reduction when the terminal Cys (cysteine residues bound to one metal ion) are exhausted for each protein and cluster formation begins using bridged Cys.

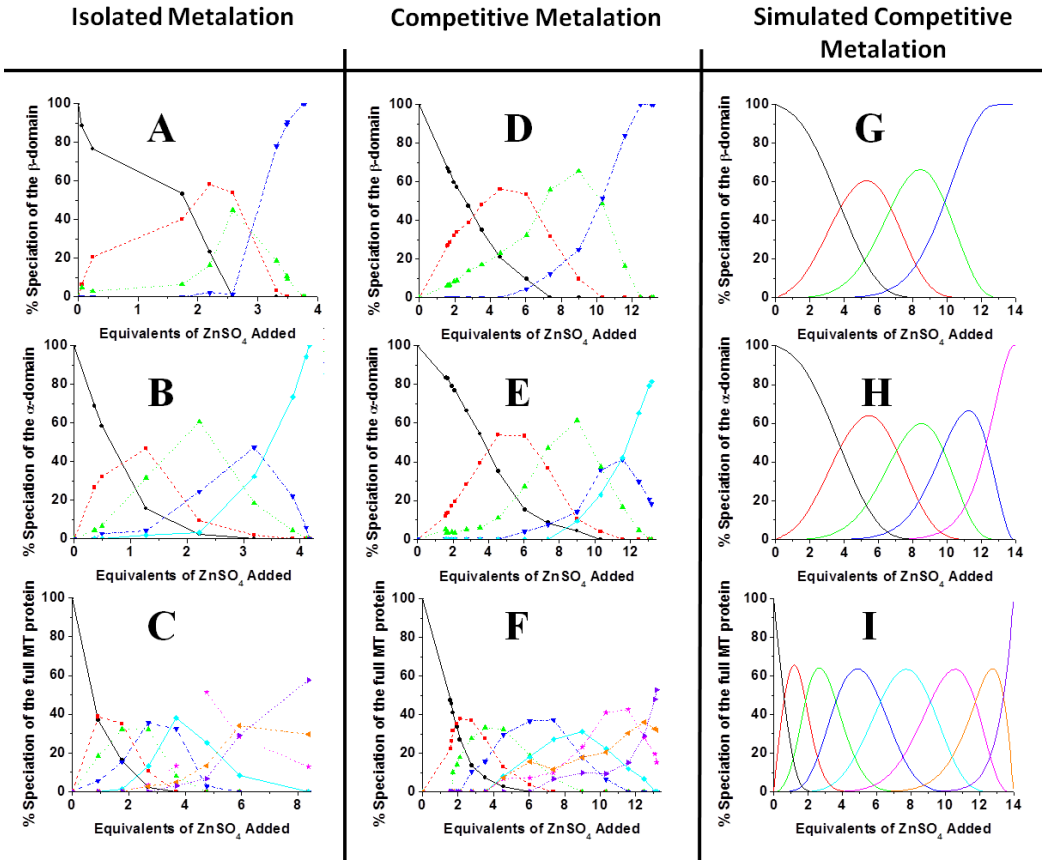

Figure 4-7. ESI MS relative abundance for the metalation chemistry of the two isolated domains and full MT protein. Metalation of apo-β-rhMT (A), apo-α-rhMT (B), apo-βα-rhMT (C), as well as their respective metalation under competitive conditions (D) and (E), and (F), respectively, using Zn^{2+} to form Zn_n, where n corresponds to the number of metals bound. A simulation of the metalation of both domains and the full MT protein was also performed, in which the $\log_{10}(K_F)$ of the association constants for the α-domain were 10.4, 9.8, 9.3 and 8.6, while for the β-domain were 10.4, 9.9 and 9.2, and finally for the full MT protein were 11.8, 11.2, 10.6, 10.0, 9.4, 8.8 and 8.2. Each line corresponds to a different metalation state: Zn_0(—●—), Zn_1(– –■– –), Zn_2(· ·▲· ·), Zn_3(– –▼– –), Zn_4(—◆—), Zn_5(·····★·····), Zn_6(– ·◀· –) and Zn_7(– – ▶– –).

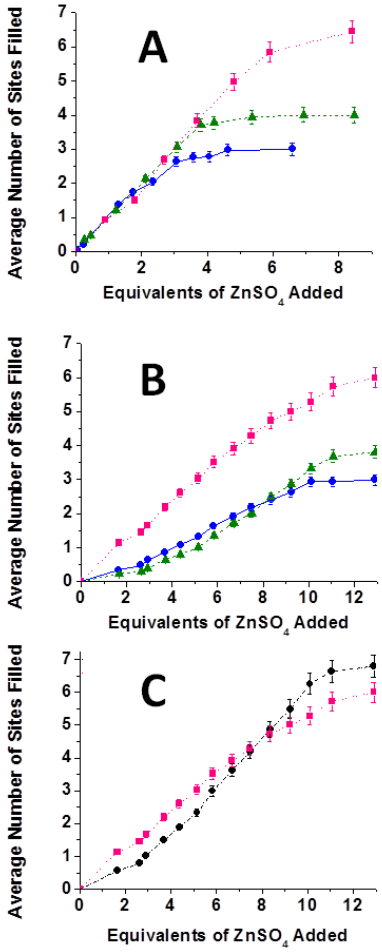

Figure 4-8. Average metalation properties of the isolated β- and α-domains and the full MT protein as a function of added Zn^{2+}. (A) The average number of metals bound to all three species: β-domain ( ), the α-domain ( ) and, finally, the full MT protein ( ) in separate solutions (based on data in Figure 4-2). (B) The average number of metals bound in the competition reaction between the isolated fragment domains and full MT protein (based on data in Figure 4-6). (C) Comparison between the sum of the average Zn^{2+} metalated states of the two isolated domains as a function of added $Zn^{2+}$when competing with the full protein ( ) and the average Zn^{2+} metalated state of the full MT protein ( ). The lines show that the full MT protein is able to outcompete the sum of the isolated domains up until it has bound 4 Zn^{2+} ions. After that point, the two isolated domains outcompete the full MT protein.

Figure 4-8 provides the average metalation data for two experiments: first metalation of the two isolated fragments and the full protein, and second the single competition experiment in which the full MT protein and the isolated fragments compete for the same

Zn^{2+} as described above. Figure 4-8A demonstrates that for metalation in the absence of a competitor, metalation of both the isolated domains and full MT protein proceeds in a similar manner initially. In isolation, the only observable change in the slope of metalation occurs at approximately the 2 molar equivalents of Zn^{2+} added to solution for the β domain, 3 for the α domain, and 5 for the full βα-protein. These changes can be interpreted as arising from the onset of cluster formation - that is the points at which cysteine residue bridging must occur for metalation to continue. However, when a competitor is present (Figure 4-8B), significant differences in the affinity of each component of the solution become apparent because now, first the β- clearly outperforms the α- domain but also, they both metalate at a lower fraction than the full protein. Figure 4-8B shows that at each molar equivalent of Zn^{2+} added to the solution up to 4, the full MT protein has bound more metal ions than the sum of the two isolated domains.

Significantly, when the metalation status of the isolated domains is summed (Figure 4-8C) so that the total of Zn^{2+} bound in sites on the isolated fragment domains can be compared directly with the Zn^{2+} bound in the full protein, we see that, in fact, the full protein dominates at added Zn^{2+} molar equivalents <8; after this point the sum of the isolated domains dominates.

This result is surprising, since it has been a traditional view of metallothionein chemistry that the two domains of mammalian MT act in isolation, and consequently that the metalation of the isolated domains should be equal to that of the full MT protein - that is the two domains in the full protein are expected to perform like the two domains in isolation. Our interpretation of this result is that the 5-Zn-species using all 20 Cys with no bridging interactions must now rearrange significantly to allow the 6^{th} Zn^{2+} to be bound. In effect this is the point at which the domain structure of the metallothionein first develops. We interpret these results to mean that at the 8 molar equivalents of Zn^{2+} added point the full MT protein must have a significant drop in the value of K_F for further metalation (the 6^{th} and 7^{th} Zn^{2+}) compared with K_F (Zn_3-β-) and K_F ($Zn_{3\text{-}4}$-α-). Based on the distribution of Zn^{2+} at this stage in the metalation profile (Figure 4-6 F) it is likely that a Zn_5-βα-rhMT 1a species using all 20 cysteine residues exists and must significantly rearrange to allow a 6^{th} Zn^{2+} ion to bind.

The experimental data in Figure 4-8B and 4-8C were modeled based on the K_F values determined by Krezel and Maret (*21*) and extrapolated following the trends reported by Ngu *et al. (2, 18)*. Figure 4-9 shows the results of this modeling. The calculated metalation not only predicts the crossover in metalation loading between the full protein and the sum of the two isolated domains correctly simulated but also the unusual trends between 0 and 4 molar equivalents of Zn^{2+} added to solution. Most importantly, the K_F values used for this model are based on the assumption that the requirement for bridging Cys leads to a significant decrease in K_F for each step after 5 Zn^{2+} have bound to all 20 cysteines in a terminal fashion (bound to only one metal ion). Most significantly, the data show that it is the 6th Zn^{2+} ion that forces the two domain structure to form.

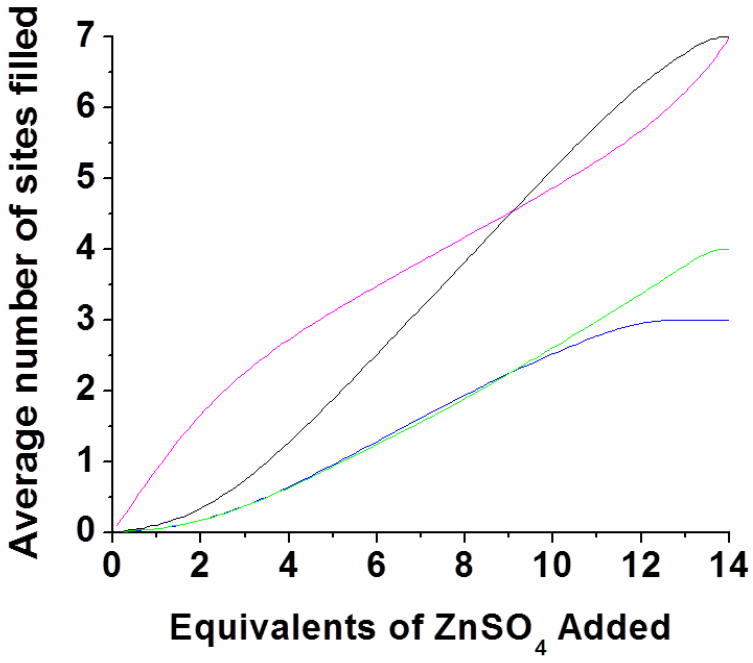

Figure 4-9. A model of the average metalation properties of the β- and α-domains and the full MT protein as a function of added Zn^{2+}. The calculated average number of metals bound to all three species taken from Figure 4-7 (G, H, I): β-domain (blue), the α-domain (green) and finally the full MT protein (magenta), as well as the sum of the average Zn^{2+} metalated states of the two domains (black). The modeled lines are based upon $\log_{10}(K_F)$ values for the α-domain of 10.4, 9.8, 9.3 and 8.6, while for the β-domain of 10.4, 9.9 and 9.2, and finally for the full MT protein of 11.8, 11.2, 10.6, 10.0, 9.4, 8.8 and 8.2. Significantly, the full MT protein outcompetes the sum of the isolated domains in the first part of the titration (<8.5 equivalents of Zn^{2+} added to solution), while after this point the sum of the isolated domains dominates. In addition, the crossover between the modeled full MT and sum of the isolated domains is at an average number of metals bound of 4.5.

4.4 Discussion

To understand the role of metal binding in MT, a large number of metalation, demetalation and metal replacement experiments have been reported under both equilibrium and kinetic conditions (*1-2, 18, 23-24*). Several of these studies have used competitive chelators to determine the affinity of MT for its metal ions (*21*, *25*). To date no single experiment has studied the simultaneous competition reaction between the β- and α-domains and the full MT protein yet one of the most important questions about the metalation properties of metallothioneins concerns the role of the two domains. ESI mass spectrometric studies have focused on both the mechanism of metalation of MT, determined for Cd^{2+}, As^{3+} and Bi^{3+}, and the kinetics of metalation, specifically As^{3+} metalation (17-18, 26-27).

In the study described here, we have used the very similar K_F values of the Zn^{2+} binding sites in the isolated fragments containing the β and α domains to compete for the incoming Zn^{2+} binding to the two-domain, βα-full protein. We show in the data presented in this study the discriminating power of ESI-mass spectrometry to provide both simultaneous and detailed information about all three species and their respective dynamic metalation states. By using both the full MT protein and its isolated fragments as competitors, the relative metal binding affinity of each species is shown. These results are important, since they provide insight into the possible structures that exist and take part in cellular chemistry.

Initially the metalation properties of the isolated fragments and full protein were determined separately (Figure 4-2). Through an analysis of the changes in the charge state profile, and their respective deconvoluted spectra, the effect of metals on protein folding can be determined. The two isolated domains both possess similar charge state envelopes throughout the titration, with a slight increase in size upon binding of the first Zn^{2+} ion following which the charge state distributions remains constant with the 4+ state dominating both fragments when fully metalated with Zn^{2+}. The prominent charge state for the apo-two-domain βα-MT is 5+ with about equal contributions from 6+ and 4+. Metalation results in an increase in 6+ and a reduction in 4+ suggesting that the apo- and metalated proteins are of similar, but not identical, volume. Additionally, the data in Figure 4-2 show clearly that Zn^{2+} metalation takes place step-wise. These results are

fundamental because they establish that metalation of MT and its fragments using the biologically relevant Zn^{2+} occur in a noncooperative manner.

Under a noncooperative mechanism of metalation, partially metalated species may be stable and able to take part in cellular chemistry. Consequently, instances in which partially metalated forms of the protein have been purified could in fact represent the biologically relevant *in vivo* forms of the protein. For example, mouse heart MT has been isolated from the organism in a partially oxidized form, where the formation of disulfide bonds has been implicated in zinc release necessary to combat the oxidative pressures (*28*). The twenty cysteine residues present in mammalian MT have long made it an attractive agent to combat oxidative stress with concomitant formation of disulfide bonds (*29*). Under this new mechanism of metalation, MT can now be understood to combat oxidative stress in a dynamic way, where progressive oxidation of MT leads to the sequential release of Zn^{2+} ions and eventually complete oxidation (or thionin formation). This released Zn^{2+} can then bind to the metal response element binding transcription factor 1 (MTF-1) (*30*). Zn-MTF-1 leads to an upregulation of MT, and other associated proteins, thus combating the oxidative stress.

The competition experiments provide a detailed view of the Zn^{2+} binding because the distribution of the Zn^{2+} between sites is governed by the relative magnitudes of K_F. Our interpretation of the data presented here is that when the isolated β- and α-domains compete for metals, the β-domain preferentially binds the first Zn^{2+} ion added to solution. There appears to be a decrease in the affinity of the β-domain, relative to the α-domain, for the third Zn^{2+} ion to form Zn_3-β-rhMT (Figure 4-3). This decrease in relative affinity is likely the result of the 3 bridging interactions necessary to form Zn_3Cys_9 in the β-domain, whereas the α-domain only requires 1 bridging interaction to form Zn_3Cys_{11}. This result was surprising, because Cd-NMR metalation studies by Good *et al.* using rabbit liver MT 2 suggested that the α-domain binds the first four Cd^{2+} ions, after which, any additional metal ions populate the β-domain (*31*). This paper also showed the presence of a broad ^{113}Cd-NMR signal centered at 684 ppm. This peak, which was not identified, could be the result of submetalated species (Cd_{1-3}-rlMT 2), in which the abundance of free cysteinyl-thiols allows for tetrahedral coordination to terminal thiols for all Cd^{2+} ions. In NMR studies, the signals associated with the α-domain are

significantly more intense than those associated with the β-domain, which is due to an increase in fluctionality of the β-domain. It could be that these weaker signals of Cd_3-cluster could not be detected leading to the conclusion that the α-domain clusters first (*32*). Based on our interpretation, we modeled the competition reaction for the two isolated domains. Figure 4-5 E and F shows the formation of the individual metalated states. The model very closely matches the experimental data and supports the formation of the Zn-β species with at least similar $K_{F(n)}$ values for n=1 and 2 compared with the α-domain.

The more challenging experiment allowed for all three species to compete for the Zn^{2+}. This pitted the relative values of 14 Zn^{2+} sites with 14 distinct K_F values. The ESI-MS data allow for the first time the observation of all the metalated species simultaneously. Significantly, and fundamental to the conclusions of this paper, the data show that the full protein exhibits higher relative K_F values for the first 4-5 Zn^{2+} than the isolated domains. The K_F values of all three proteins are essentially in balance and therefore equal when the fifth Zn^{2+} ion binds to the βα-MT (Figures 4-7 and 4-8). After this point, the isolated fragments metalate at the expense of the full protein.

In previous metalation studies, ^{113}Cd-NMR data have shown that the chemical shifts observed for the α-domain of MT are not affected by either the digestion of the β-domain by subtilisin (*33*) or the identity of the metal ions in the β-domain (either Cd^{2+} or Cu^{+}) (*11*). In addition, MT structures have been determined from several sources and in no case were interdomain NOEs observed (*7-8, 34*). Not until very recently has this view been challenged with reports of metalation in excess of traditional levels forming a single Cd_8Cys_{20} cluster (*9-10, 35-36*).

Previous metal binding studies of β-, α-, and βα-MT with arsenic by Ngu *et al.* demonstrated the affinity of MT for metal ions is directly dependent on the number of still-available binding sites (*2, 18, 22*). The same trend is observed here with initial metalation of MT by Zn^{2+} being dominated by the full protein and not the isolated domains that individually contain fewer metal binding sites. These results are critical because they show that 1) there is no domain preference for Zn^{2+} until terminal thiolates bridge, 2) bridging interactions lead to a significant decrease in the K_F values observed, 3) K_F are directly proportional to the number of available binding sites.

From our results, we can see that the proposal by Ngu *et al.* is followed up to the 4-5 Zn^{2+} added point, afterwhich the sum of the zinc bound by the isolated domains exceeds that in the full MT protein (*2, 18, 22*). The key species is the formation of Zn_5-βα-rhMT. Binding of the fifth Zn^{2+} ion can only occur in one location, thus locking a submetalated MT structure that consists of solely terminal Cys thiols. Additional metalation to Zn_6-βα-rhMT requires bridging interactions that must occur and lead to the eventual formation of the traditional Zn_7-βα-rhMT, where neither domain interacts. The significant decrease in K_F (Zn_6, Zn_7) past Zn_5-βα-rhMT, compared to the sum of the two domains, is strong evidence for the existence of a single domain up to the Zn_5- point and the complete rearrangement of the binding site to the conventional, two-domain structure for Zn_6- and Zn_7-. Unlike the two isolated domains, the full MT protein contains a total of 20 cysteine residues, which could potentially bind 5 Zn^{2+} ions without any bridging interactions. If this is the case, then a metal binding 'islet of stability' should exist for Zn_5-βα-rhMT, where K_F for the conversion of Zn_5-βα-rhMT to Zn_6-βα-rhMT is sufficiently low to allow near quantitative formation of Zn_5-βα-rhMT. The presence of Zn_5-βα-rhMT would help to explain inconsistencies observed between the activity of the isolated fragments and the full protein. For example, the recovery of mice whose cortex had been cryoinjured occurred at different rates when exposed to either of the isolated domains, or the full protein (*37*). In fact, maximal recovery was only observed for the full protein, while the isolated α-domain demonstrated some detrimental effects. If the metalation properties and related functions are simply the sum of the two domains, then it is odd that the *in vivo* recovery rates were not merely the summation of the two isolated clusters.

Because Zn^{2+} is spectroscopically silent, it is difficult to determine the exact metalation state that leads to cluster formation spectroscopically (*38-40*). However, Co^{2+} with its rich spectroscopic properties has been extensively used to mimic Zn^{2+} binding to MT because of its characteristic tetrahedral coordination with thiols. Uniquely, the electron paramagnetic resonance **(**EPR) spectroscopic intensity of Co^{2+} is directly related to not only the number of Co^{2+} atoms present in MT, but also to the number of nonclustered Co^{2+} centers (*39*). In seminal work by Vasak and Kagi, MT was titrated with Co^{2+} and the EPR signal measured. Analysis of the data when plotted as a function of added Co^{2+} showed an increase in the number of free spins until 4 molar equivalents

of Co^{2+} had been added, after which it was proposed that antiferromagnetic coupling led to a decrease in the signal intensity reaching near zero at the 7 added Co^{2+} point. These data were interpreted as cluster formation occurring after 4 metal ions have been added. We have mimicked the EPR experiment using our data that shows the exact distribution of metals in nonclustered (up to 5 Zn^{2+} bound) and clustered (6 and 7 Zn^{2+} bound) binding sites assigning a spin to the nonbridging Zn^{2+} ions in a Co^{2+} fashion, while cancelling the spins when clustering occurs (Figure 4-10). We should note that the ESI-mass spectral data provide the exact speciation and fraction making up the average loading, information absent in the Co-binding experiments where the average was assumed to represent a single speciation. We used the following rules to simulate the observed magnetic moment: Zn_1- through Zn_5-MT are formed without any bridging interactions, and consequently increase the EPR signal, after which the formation Zn_6- and Zn_7-MT require four and eight bridging interactions, respectively, and consequently decrease the signal due to antiferromagnetic coupling. The simulated EPR data, Figure 4-10, closely resemble the original Co^{2+} data with identical maxima at 4. Interestingly by using these rules, our data also show maximal intensity at an average of four filled binding sites. While we would intuitively predict 5 molar equivalents would be necessary for maximal intensity, the noncooperative nature of metalation requires that some M_6-MT must also exist at this metal loading. In the Co^{2+} titration, this species would greatly decrease the signal intensity. We suggest that the close similarity between our modeled data and the original Co^{2+} data, supports our interpretation of the ESI-MS data that clustering does not occur until the 6^{th} metal ion is added and that Zn_5-rhMT is a single domain species that does not involve bridging Cys.

A recent paper by Krezel and Maret demonstrated the presence of three sets of binding affinities: four Zn^{2+} ions that bind strongly (logK = 11.8), two with intermediate affinity (logK~10) and finally a single weakly bound Zn^{2+} (logK = 7.7) (*21*). The strong affinity sites were interpreted as binding to the α-domain and the weaker sites to the β-domain. The data presented here suggest that the large K_F's are associated with Zn_1-Zn_4 formation and the two smaller values with Zn_5 and Zn_6, and finally the weakest is associated with Zn_7. For the modeling presented herein (Figure 4-5, 4-7, 4-9), we have based our modeling calculations on these previously reported association constants. However, in

addition to these values, we have also incorporated the metalation work by Ngu *et al.*, which states the affinity for metal ions is directly related to the number of available binding sites (*2, 18, 22*). The final result is a series of association constants that decrease as the number of Zn^{2+} ions bound increases, and is related to the maximum and minimum previously determined association constants. These differences in affinity suggest that under oxidative stress, MT may lose metal ions in order to deactivate the toxic insult.

MT is often cited as a protective agent against oxidative stress, where the balance of metalated MT to metal free MT mediates the redox chemistry of the cell (*29, 41-42*). This view however, does not take into account the noncooperative nature of the metalation of metallothionein. It is likely that the average metal load of MT is what dictates the oxidative environment of the cell. DFT calculations of the reactivity of polynuclear zinc-thiolate sites have shown the mononuclear $ZnCys_4$ moiety to be more nucleophilic than either of the two fully metalated Zn_3Cys_9- and Zn_4Cys_{11}-clusters (*43*). Given this information and the work presented here, even though Zn_5-βα-rhMT possesses no free thiol groups, it should be able to take part in cellular chemistry as a protecting agent against oxidative stress.

Figure 4-11 shows the results of a series of molecular dynamics calculations that illustrate the structural changes that occur during the progressive metalation by Zn^{2+} of apo-βα-rhMT to the intermediate Zn_5-βα-rhMT, and finally Zn_7-βα-rhMT. In the case of apo-βα-rhMT (A), the minimized (5,000 ps) structure resembles that reported by Rigby *et al.* showing a collapse of the traditional dumbbell shape of metalated MT into a more globular structure with the free thiols of the 20 cysteines aligned on the surface (*44-46*). Tetrahedral Zn^{2+} coordination by terminal Cys was arranged for the first five Zn^{2+} ions forming a single 5-Zn-20-S_{CYS} binding domain. The significant feature of the model is that with 5 Zn^{2+} all 20 Cys are terminal ligands, yet despite the lack of cluster formation the overall three-dimensional structure of the protein closely resembles that of the fully metalated protein with 7 Zn^{2+}. The ramification of this is many techniques will not detect the change from non-clustered to the clustered domains as a function of metalation status.

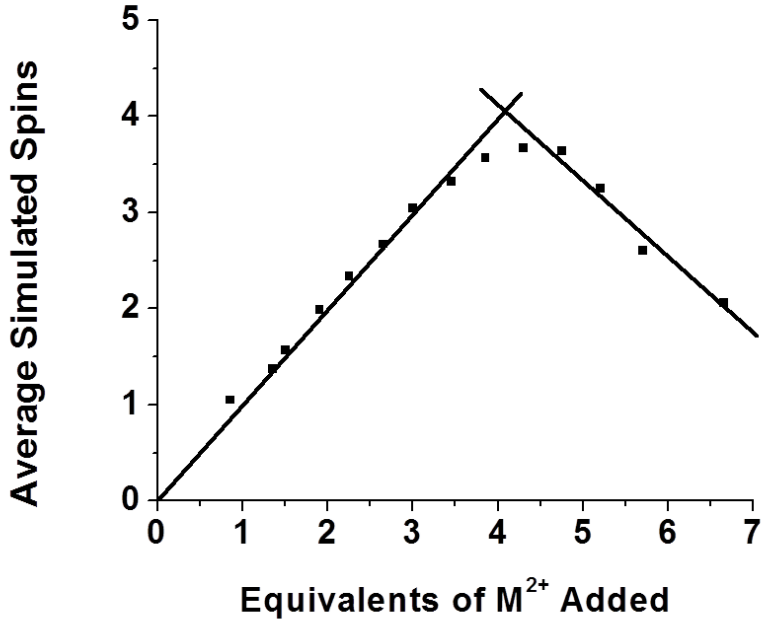

Figure 4-10. Simulated EPR titration. Simulated spin magnitude calculated by assuming the Zn^{2+} have the same spin as Co^{2+}. Metal ion speciation was obtained from the titration of MT with Zn^{2+} based on the data shown in Figure 4-2. The average number of simulated spins was determined from the following rules: 1) From M_1-βα-rhMT to M_5-βα-rhMT, the number of metal ions present is equal to the number of unpaired spins; 2) the number of spins associated with the M_6-βα-rhMT species is equal to that of M_5-βα-rhMT minus 4 due to the bridging interactions required for clustering of the α-domain; 3) formation of M_7-βα-rhMT leads to a complete spin pairing as a result of full clustering of both domains. In the original Co^{2+} titration of MT the loss of signal was associated with antiferromagnetic coupling required for cluster formation (39).

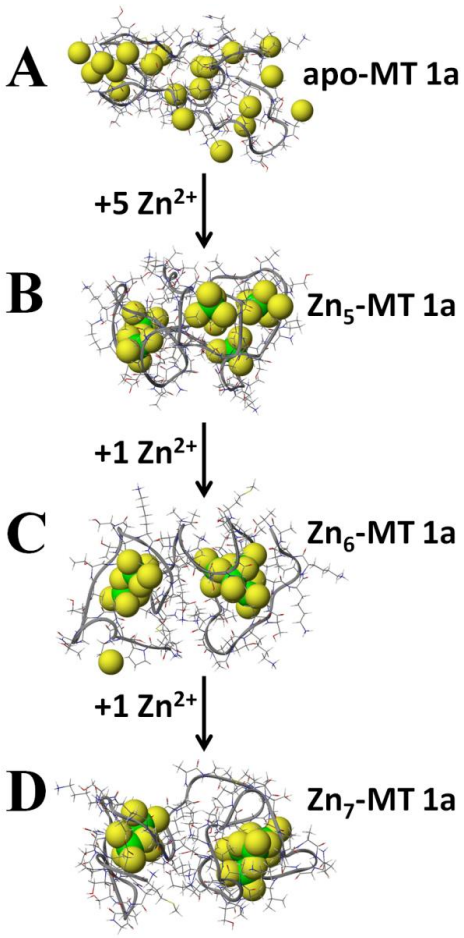

Figure 4-11. **Molecular models of the metalation of MT from apo- to Zn_7.** Ribbons show the backbone, with the zinc atoms represented as green spheres and sulfur atoms as yellow spheres. The N-terminal β domain is located on the left hand side, while the C-terminal α domain is located on the right-hand side. (A) Metal-free, apo- βα-rhMT showing an essentially spherical structure with the cysteinyl sulfurs on the outside. (B) The single domain Zn_5-βα-rhMT structure. The structure was created by assigning a single Zn^{2+} ion to every 4 consecutive cysteine residues with respect to the sequence. (C) Development of the two-domain structure with cluster formation in the α domain (right lobe) in Zn_6-βα-rhMT; (D) Formation of the filled two-domain cluster structure with addition of the 7^{th} Zn^{2+} into the β domain in Zn_7-βα-rhMT. Structures were calculated using a locally modified force-field with MM3/MD methods for molecular modeling (20). Minimization of the structures was carried out for 5000 ps at 300 K. The conformer with the lowest energy is presented above. The initial structure of the Cd_7-βα-rhMT 1a, modified for all subsequent structures, was provided by Chan *et al.* (19).

It is interesting to note that even when there are no bridging Cys present, the model of Zn_5-βα-rhMT shows that the two Zn^{2+} bonded to the β-domain Cys (ie within residues 1-

36, Figure 4-1) and the three Zn^{2+} bonded to the α-domain Cys (ie within residues 37-74) are spatially close to one another. This likely facilitates cluster formation upon further metalation to the more traditional two-isolated domains of Zn_7-βα-rhMT.

4.5 Conclusion

In this study, we demonstrate that Zn^{2+} metalation occurs in a noncooperative manner in the same way as for Cd^{2+} and As^{3+} reported previously for the human MT 1a protein. Further, in detailed studies of the metalation reaction itself, we show that with the onset of cluster formation, which is defined by the use of bridging Cys thiolate ligands rather than terminal Cys, that there is a significant decrease in the Zn^{2+} binding affinity to MT and its domains for further metalation. The switch from terminal to bridging Cys to accommodate an increase in Zn^{2+} in the binding sites reduces the binding affinity. The individual metalated states can be identified and followed in the ESI-mass spectral data and in competition experiments in which the two isolated fragments compete for the same metal as the full protein, that the full MT protein has a superior ability to initially bind Zn^{2+} ($Zn^{2+} \leq 4$) but upon binding of the fifth metal ion, the sum of Zn^{2+}-bound to the isolated domains dominates. These mass spectral data allow us to conclude for the full MT protein that the decreasing association constants necessary for a noncooperative mechanism of metalation allow formation of a stable Zn_5-βα-rhMT species, which contains no bridging interactions. This is a single binding site domain and is mechanistically a key member of the metalation pathway from apo-MT to the fully metalated Zn_7-MT. Our recently published study on the supermetalation of MT 1a, where addition of an 8^{th} Cd^{2+} ion leads to the coalescence of the two domains to form one 'super-domain' (*9*), suggests a fundamentally altered view of the metalation properties of MT from that of maintaining two-domains, regardless of metal depletion, to a new structural characterization of MT, where MT exists as a flexible, single domain protein during initial metalation (≤5 eq.) and metalation in excess of traditional levels.

4.6 References

1. Nielson, K. B., Atkin, C. L., and Winge, D. R. (1985) Distinct metal-binding configurations in metallothionein, *J. Biol. Chem. 260*, 5342-5350.

2. Ngu, T. T., and Stillman, M. J. (2006) Arsenic binding to human metallothionein, *J. Am. Chem. Soc. 128*, 12473-12483.
3. Stillman, M. J. (1995) Metallothioneins, *Coord. Chem. Rev. 144*, 461-511.
4. Sutherland, D. E. K., and Stillman, M. J. (2011) The "magic numbers" of metallothionein, *Metallomics 3*, 444-463.
5. Robbins, A. H., McRee, D. E., Williamson, M., Collett, S. A., Xuong, N. H., Furey, W. F., Wang, B. C., and Stout, C. D. (1991) Refined crystal structure of Cd, Zn metallothionein at 2.0 Å resolution, *J. Mol. Biol. 221*, 1269-1293.
6. Messerle, B. A., Schaffer, A., Vasak, M., Kagi, J. H. R., and Wuthrich, K. (1992) Comparison of the solution conformations of human [Zn_7]-metallothionein-2 and [Cd_7]-metallothionein-2 using nuclear magnetic resonance spectroscopy, *J. Mol. Biol. 225*, 433-443.
7. Messerle, B. A., Schaffer, A., Vasak, M., Kagi, J. H. R., and Wuthrich, K. (1990) Three-dimensional structure of human [$^{113}Cd_7$]metallothionein-2 in solution determined by nuclear magnetic resonance spectroscopy, *J. Mol. Biol. 214*, 765-779.
8. Zangger, K., Oz, G., Otvos, J. D., and Armitage, I. M. (1999) Three-dimensional solution structure of mouse [Cd_7]-metallothionein-1 by homonuclear and heteronuclear NMR spectroscopy, *Protein Sci. 8*, 2630-2638.
9. Sutherland, D. E. K., Willans, M. J., and Stillman, M. J. (2012) Single domain metallothioneins: Supermetalation of human MT 1a, *J. Am. Chem. Soc. 134*, 3290-3299.
10. Meloni, G., Polanski, T., Braun, O., and Vasak, M. (2009) Effects of Zn^{2+}, Ca^{2+}, and Mg^{2+} on the structure of Zn_7metallothionein-3: Evidence for an additional zinc binding site, *Biochemistry 48*, 5700-5707.
11. Briggs, R. W., and Armitage, I. M. (1982) Evidence for site-selective metal binding in calf liver metallothionein, *J. Biol. Chem. 257*, 1259-1262.
12. Salgado, M. T., and Stillman, M. J. (2004) Cu^{+} distribution in metallothionein fragments, *Biochem. Biophys. Res. Commun. 318*, 73-80.
13. Meloni, G., Faller, P., and Vasak, M. (2007) Redox silencing of copper in metal-linked neurodegenerative disorders: Reaction of Zn_7metallothionein-3 with Cu^{2+} ions, *J. Biol. Chem. 282*, 16068-16078.
14. Meloni, G., Sonois, V., Delaine, T., Guilloreau, L., Gillet, A., Teissie, J., Faller, P., and Vasak, M. (2008) Metal swap between Zn_7-metallothionein-3 and amyloid-b-Cu protects against amyloid-b toxicity, *Nat. Chem. Biol. 4*, 366-372.
15. Jensen, L. T., Peltier, J. M., and Winge, D. R. (1998) Identification of a four copper folding intermediate in mammalian copper metallothionein by electrospray ionization mass spectrometry, *J. Biol. Inorg. Chem. 3*, 627-631.
16. Palumaa, P., Eriste, E., Njunkova, O., Pokras, L., Jornvall, H., and Sillard, R. (2002) Brain-specific metallothionein-3 has higher metal-binding capacity than ubiquitous metallothioneins and binds metals noncooperatively, *Biochemistry 41*, 6158-6163.
17. Sutherland, D. E. K., and Stillman, M. J. (2008) Noncooperative cadmium(II) binding to human metallothionein 1a, *Biochem. Biophys. Res. Commun. 372*, 840-844.

18. Ngu, T. T., Easton, A., and Stillman, M. J. (2008) Kinetic analysis of arsenic - metalation of human metallothionein: Significance of the two-domain structure, *J. Am. Chem. Soc. 130*, 17016-17028.
19. Chan, J., Huang, Z., Watt, I., Kille, P., and Stillman, M. J. (2007) Characterization of the conformational changes in recombinant human metallothioneins using ESI-MS and molecular modeling, *Can. J. Chem. 85*, 898-912.
20. Chan, J., Merrifield, M. E., Soldatov, A. V., and Stillman, M. J. (2005) XAFS spectral analysis of the cadmium coordination geometry in cadmium thiolate clusters in metallothionein, *Inorg. Chem. 44*, 4923-4933.
21. Krezel, A., and Maret, W. (2007) Dual nanomolar and picomolar Zn(II) binding properties of metallothionein, *J. Am. Chem. Soc. 129*, 10911-10921.
22. Ngu, T. T., Lee, J. A., Rushton, M. K., and Stillman, M. J. (2009) Arsenic metalation of seaweed *Fucus vesiculosus* metallothionein: The importance of the interdomain linker in metallothionein, *Biochemistry 48*, 8806-8816.
23. Ejnik, J., Robinson, J., Zhu, J., Forsterling, H., Shaw-III, C. F., and Petering, D. H. (2002) Folding pathway of apo-metallothionein induced by Zn^{2+}, Cd^{2+} and Co^{2+}, *J. Inorg. Biochem. 88*, 144-152.
24. Ejnik, J., Shaw-III, C. F., and Petering, D. H. (2010) Mechanism of cadmium ion substitution in mammalian zinc metallothionein and metallothionein a domain: Kinetic and structural studies, *Inorg. Chem. 49*, 6525-6534.
25. Li, T.-Y., Kraker, A. J., Shaw-III, C. F., and Petering, D. H. (1980) Ligand substitution reactions of metallothioneins with EDTA and apo-carbonic anhydrase, *Proc. Natl. Acad. Sci. U.S.A 77*, 6334-6338.
26. Rigby-Duncan, K. E., and Stillman, M. J. (2007) Evidence for noncooperative metal binding to the a domain of human metallothionein, *FEBS J. 274*, 2253-2261.
27. Ngu, T. T., Krecisz, S., and Stillman, M. J. (2010) Bismuth binding studies to the human metallothionein using electrospray mass spectrometry, *Biochem. Biophys. Res. Commun. 396*, 206-212.
28. Feng, W., Benz, F. W., Cai, J., Pierce, W. M., and Kang, Y. J. (2006) Metallothionein disulfides are present in metallothionein-overexpressing transgenic mouse heart and increase under conditions of oxidative stress, *J. Biol. Chem. 281*, 681-687.
29. Kang, Y. J. (2006) Metallothionein redox cycle and function, *Exp. Biol. Med. 231*, 1459-1467.
30. Chen, X., Chu, M., and Giedroc, D. P. (1999) MRE-binding transcription factor-1: Weak zinc-binding finger domains 5 and 6 modulate the structure, affinity, and specificity of the metal-response element complex, *Biochemistry 38*, 12915-12925.
31. Good, M., Hollenstein, R., Sadler, P. J., and Vasak, M. (1988) ^{113}Cd NMR studies on metal-thiolate cluster formation in rabbit Cd(II)-metallothionein: Evidence for a pH dependence, *Biochemistry 27*, 7163-7166.
32. Otvos, J. D., and Armitage, I. M. (1980) Structure of the metal clusters in rabbit liver metallothionein, *Proc. Natl. Acad. Sci. U.S.A 77*, 7094-7098.

33. Boulanger, Y., Armitage, I. M., Miklossy, K.-A., and Winge, D. R. (1982) ^{113}Cd NMR study of a metallothionein fragment: Evidence for a two-domain structure, *J. Biol. Chem. 257*, 13717-13719.
34. Wang, H., Zhang, Q., Cai, B., Li, H., Sze, K.-H., Huang, Z.-X., Wu, H.-M., and Sun, H. (2006) Solution structure and dynamics of human metallothionein-3 (MT-3), *FEBS Lett. 580*, 795-800.
35. Rigby-Duncan, K. E., Kirby, C. W., and Stillman, M. J. (2008) Metal exchange in metallothioneins - a novel structurally significant Cd_5 species in the alpha domain of human metallothionein 1a *FEBS J. 275*, 2227-2239.
36. Sutherland, D. E. K., Willans, M. J., and Stillman, M. J. (2010) Supermetalation of the b domain of human metallothionein 1a, *Biochemistry 49*, 3593-3601.
37. Manso, Y., Serra, M., Comes, G., Giralt, M., Carrasco, J., Cols, N., Vasak, M., Gonzalez-Duarte, P., and Hidalgo, J. (2010) The comparison of mouse full metallothionein-1 versus a and b domains and metallothionein-1-to-3 mutation following traumatic brain injury reveals different biological motifs, *J. Neurosci. Res. 88*, 1708-1718.
38. Good, M., Hollenstein, R., and Vasak, M. (1991) Metal selectivity of clusters in rabbit liver metallothionein, *Eur. J. Biochem. 197*, 655-659.
39. Vasak, M., and Kagi, J. H. R. (1981) Metal thiolate clusters in cobalt(II)-metallothionein, *Proc. Natl. Acad. Sci. U.S.A 78*, 6709-6713.
40. Vasak, M., Kagi, J. H. R., Holmquist, B., and Vallee, B. L. (1981) Spectral studies of cobalt(II)- and nickel(II)-metallothionein, *Biochemistry 20*, 6659-6664.
41. Krezel, A., and Maret, W. (2007) Different redox states of metallothionein/thionein in biological tissue, *Biochem. J. 402*, 551-558.
42. Petering, D. H., Zhu, J., Krezoski, S., Meeusen, J., Kiekenbush, C., Krull, S., Specher, T., and Dughish, M. (2006) Apo-metallothionein emerging as a major player in the cellular activities of metallothionein, *Exp. Biol. Med. 231*, 1528-1534.
43. Ohanessian, G., Picot, D., and Frison, G. (2011) Reactivity of polynuclear zinc-thiolate sites, *Int. J. Quantum Chem. 111*, 1239-1247.
44. Rigby, K. E., and Stillman, M. J. (2004) Structural studies of metal-free metallothionein, *Biochem. Biophys. Res. Commun. 325*, 1271-1278.
45. Rigby, K. E., Chan, J., Mackie, J., and Stillman, M. J. (2006) Molecular dynamics study on the folding and metalation of the individual domains of metallothionein, *Proteins Struct. Funct. Bioinf. 62*, 159-172.
46. Rigby-Duncan, K. E., and Stillman, M. J. (2006) Metal-dependent protein folding: Metalation of metallothionein, *J. Inorg. Biochem. 100*, 2101-2107.

Chapter 5. Supermetalation of the beta domain of human MT 1a[5]

5.1 Introduction

Metallothionein (MT), first characterized in 1957 (*1*), is a cysteine rich protein implicated in heavy metal detoxification, metal ion homeostasis and protection against oxidative stress (*2-3*). However, despite half a century of intensive research, specific roles for MT in living organisms are still largely unknown. One of the reasons for the uncertainty of function is that until very recently the mechanism of metalation of metallothionein was thought to proceed in a cooperative manner (*4-5*), in which the binding of one metal acts to facilitate the binding of subsequent metals. Under this model the only structures of biological significance would be the fully metalated or completely demetalated species, and any partially metalated species would likely be too unstable to have a specific role. However, new studies have shown metalation to occur in a noncoooperative manner for Cd^{2+} and Zn^{2+} (*6-8*), as well as As^{3+} (*9-10*). Most significantly, a noncooperative mechanism allows for partially metalated and metal exchange intermediates to be stable and, therefore, to be able to take part in cellular chemistry.

To further complicate matters recent papers have proposed the existence of supermetalated forms of metallothionein, that is proteins where metalation is in excess of normal maximum levels, calling into question the so-called "magic numbers" of metal binding (*11-12*). Supermetalated forms have been reported for a single additional cadmium ion binding to both the isolated α domain of human MT-1a (Cd_5-α-rhMT 1a) (*13*) and the full human MT-3 protein (Cd_8-βα-hMT 3) (*14*). Because the cadmium ions in MT-1 and -2 isomorphously replace zinc ions, these results suggest that this additional metal site may be involved with metal ion homeostasis and may be considered as a model for metal-exchange intermediates. In addition, the supermetalated site may also be

[5]A version of this work has been published:

connected with the mechanism for binding of incoming metals with binding affinities greater than the resident zinc, for example the essential copper(I) and the toxic cadmium(II). To account for the supermetalation of hMT-3, Meloni *et al.* have proposed the involvement of both the α and β domains in stabilizing the additional metal ion (*14*). However, previous studies involving the oxidation of hMT-3 with nitric oxide (*15*), as well as the lack of long range interdomain peaks associated with the nuclear overhauser effect (NOEs) in the solution structure of hMT-3 (*16*), in fact suggest that little domain interaction is involved. Taken together, these metalation properties emphasize the need for precise information on the specific properties of the individual domains in defining the function of MT as a whole.

The many members of the metallothionein family have each developed unique metal-binding sites and domain structures, with different metal binding properties. Mammalian metallothionein consists of a total of 20 cysteine residues (9 in the N-terminal β domain capable of binding 3 Zn^{2+}/Cd^{2+} and 11 in the C-terminal α domain capable of binding 4 Zn^{2+} or Cd^{2+}) (*17*). While the seaweed *Fucus vesiculosus* contains a total of 16 cysteine residues (7 in an as yet uncharacterized N-terminal γ domain and 9 in the C-terminal β domain, both able to bind 3 Zn^{2+} or Cd^{2+}) (*18*). Each of these proteins uses the thiolate sulfur of cysteine residues to coordinate the bound metals. Other coordinating amino acids have also been identified, with bacterial metallothionein SmtA binding four Zn^{2+} atoms through 9 cysteine and 2 histidine residues (*19*). Furthermore, the Zn^{2+} atom coordinated to the two histidine residues was inert to metal exchange and it was postulated that this stable metal allowed maintenance of the structure during metal depletion. Recently the C-terminal β_E domain of *Tricium aestivum*, a common wheat consisting of a two metal-thiolate domain structure with 17 cysteine residues (6 in the N-terminal domain capable of binding 2 Zn^{2+} or Cd^{2+} and 11 in the β_E domain capable of binding 4 Zn^{2+} or Cd^{2+}), was found to have both a traditional β like domain and a fourth zinc coordinated to two cysteine and two histidine residues in close proximity (*20*). Of significant interest is human metallothionein-3 (hMT-3) with approximately 70% sequence homology with hMT-2, is expressed predominantly in the central nervous system and inhibits neuronal growth (*21*). The addition of a single threonine (Thr5) in a TCPCP motif (*22*), and a glutamate-rich hexapeptide (*23*) near the C-terminal have been

shown to be critical to the function and the labilization of Zn^{2+} atoms, respectively. Interestingly, Romero-Isart *et al.* were able to engineer neuronal activity of hMT-3 into hMT-1 by addition of the TCPCP inset, which suggests the two isoforms may only differ in the slight cluster arrangements brought about by 3 distinct mutations (*22*). Analysis of the isolated domains demonstrated that the ability to inhibit neuronal growth resides in the β domain alone, and that this ability results from its unique sequence suggesting preferential interaction with target proteins (*24*). These β domain centered protein-protein interactions have not been well characterized due to a general lack of information available about this domain for all metallothionein isoforms.

Human metallothionein 1a, Figure 5-1A, consists of two independent domains each encapsulating a metal-thiolate core, Figure 5-1B. The sequence of the cleaved recombinant β domain human metallothionein 1a (β-rhMT 1a), shown in Figure 5-1C, with cadmium atoms coloured green and cysteine residues yellow, contains both a glycine and serine residue from the thrombin cleavage reaction. This fragment encompasses residues starting from Cys5 to Lys31 of human metallothionein 1a. Numbering of the cadmium-thiolate core is cross referenced to the original naming conventions based on the order of the NMR bands in the mammalian MT 2a spectra (*25*), while numbering the cysteine residues has been adjusted to accommodate both the additional amino acids from thrombin cleavage (res. 1 and 2), as well as a series of amino acids meant to aid in protein expression (res. 3 to res. 9). The β-MT polypeptide backbone wrapping of the metal-thiolate core proceeds in a right-handed manner, as opposed to the left-handed wrapping of α-MT. While properties of the α metal binding site, Cd_4-α-rhMT, have been well documented through structural studies of both the isolated domain (*8, 25*) and as part of the whole protein (*17*), far less structural information has been reported for the isolated β metal binding site, Cd_3-β-rhMT. Analysis of the NMR data for β-rhMT in human metallothionein suggested that fluctionality causes a decrease in intensity of the 1D ^{113}Cd signals. Further compounding this problem is the inability of metallothionein to readily crystallize. To date, only two crystal structures have been reported, including rat Cd_5Zn_2-MT 2 and much later a Cu_8-yeast metallothionein (*17, 26*). In order to determine such basic *in vivo* data as protein

binding partners and metalation status, the complete metalation properties of β-MT must be fully characterized, particularly when one considers the β-centered reactions in hMT 3.

The metal transfer function in MT has been well documented with Zn(II) transfer taking place from the fully metalated Zn_7-βα-MT to m-aconitase (*27*), carbonic anhydrase (*28*), and the prototypical transcription factor, Gal4 (*29*). These studies have shown the importance of protein-protein interactions. However, no zinc-exchange intermediate has been characterized that provides insight into the actual mechanism of metal transfer.

In this study, we present evidence that the isolated β domain of human metallothionein 1a, Cd_3-β-rhMT 1a, is capable of binding an additional cadmium atom forming Cd_4-β-rhMT 1a. Exact metal speciation was monitored using ESI-mass spectrometry (ESI-MS), which allowed for a direct correlation between the number of cadmium atoms bound to the protein and changes observed in the UV and CD spectroscopies. To ensure that the metal was interacting directly with the metal-thiolate cluster, both direct and indirect ^{113}Cd NMR spectroscopy was used. Addition of excess Cd^{2+}, in the form of solid $^{113}CdCl_2$, produced four cadmium signals in the range of 600-700 ppm, which corresponds to the chemical shift region expected for cadmium bound to the thiolates. When considering these results in the context of the supermetalated Cd_5-α-rhMT 1a (*13*) and Cd_8-βα-hMT 3 (*14*), two possible scenarios arise: 1) both domains, when present, work in concert to accept an additional cadmium atom or 2) both domains are individually capable of supermetalation. In either case, supermetalation must be fully characterized to understand its chemical implications that will have consequences at a cellular level.

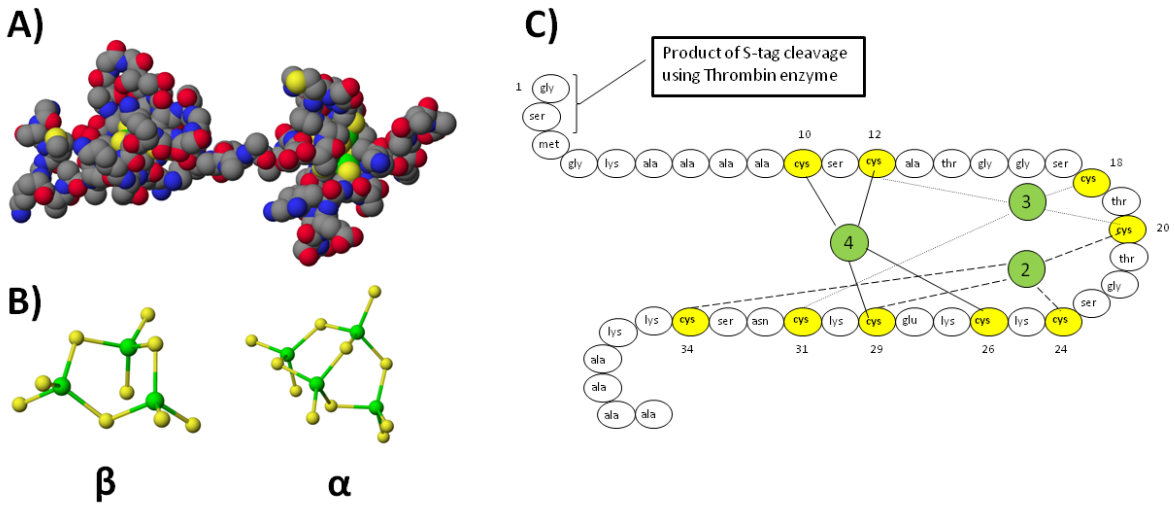

Figure 5-1. Molecular model of MT. (A) A space filling structure of Cd_7-βα-rhMT 1a calculated using molecular modeling. The N-terminal β-domain is located on the left hand side, while the C-terminal α-domain is located on the right hand side. (B) The cadmium-cysteinyl-thiolate clusters of Cd_7-βα-rhMT 1a presented as a ball and stick model: β-domain (left) and α-domain (right). (C) A connectivity diagram of the β-domain of human metallothionein 1a, which shows that each of the three cadmium atoms is connected to exactly four cysteine amino acids. The connectivity diagram has been renumbered to allow for the amino acids glycine and serine, a product of S-tag cleavage with thrombin, located on the N-terminal of the domain. Numbering of the Cd-thiolate centers is based on the NMR assignment by Messerle *et al.* (30). Molecular modeling data from Chan *et al.* (31).

5.2 Experimental Methods

5.2.1 Chemicals

Chemicals used: cadmium sulfate (Fisher Scientific); cadmium(113) chloride (Trace Sciences International Inc.); deuterium oxide (Cambridge Isotopes Laboratories, Inc.); *tris*(2-carboxyethyl)phosphine (PIERCE); ThrombinCleanCleave™ Kit (Sigma) Tris buffer, tris(hydroxymethyl)aminomethane (EMD Chemicals/VWR); ammonium formate buffer (JT Baker); ammonium hydroxide (Caledon Laboratory Chemicals); formic acid (Caledon Laboratory Chemicals); and hydrochloric acid (Caledon Laboratory Chemicals). All solutions were made with >16 MΩcm deionized water (Barnstead Nanopure Infinity). HiTrap™ SP HP ion exchange columns (Amersham Biosciences/GE

Healthcare), superfine G-25 Sephadex (Amersham Biosciences/GE Healthcare), stirred ultrafiltration cell Model 8010 and 8200 (Amicon Bioseparations/Millipore) with YM-3 membrane (3,000 MWCO) were used in the protein purification steps.

5.2.2 Protein sample preparation for CD spectroscopic and ESI mass spectrometric studies

The recombinant Cd_3-β-rhMT 1a was prepared by over-expression in *E. coli* as described in detail in Chapter 2. A solution of Cd_3-β-rhMT 1a was prepared in 5 mM ammonium formate (pH 9.0) to a concentration of 24.4 μM for CD, UV spectroscopic and ESI-mass spectrometric studies. The protein concentrations was confirmed by UV absorption spectroscopy using the absorbance at 250 nm, which corresponds to the ligand-to-metal charge transfer transition generated by the metal-thiolate bond (ε_{250} = 36,000 $M^{-1}cm^{-1}$). To ensure accuracy, all measurements were performed on the same sample for a given excess molar equivalents excess of Cd^{2+}. Cadmium sulfate was prepared in H_2O to a final concentration of 11.4 mM. The concentrations of both the cadmium sulfate solution and the cadmium content of all β-rhMT 1a solutions were determined through calibration of Cd^{2+} content using atomic absorption spectroscopy (AAS).

5.2.3 Protein sample preparation for NMR spectroscopic studies

β-rhMT 1a NMR samples were prepared by pooling protein from five-4 L recombinant preparations following thrombin-cleavage of the S-tag. The natural abundance of NMR active ^{113}Cd is 12.75%, consequently an eight-fold enhancement of signal can be achieved by isotopic enrichment of the NMR sample. To that end, pooled Cd_3-β-rhMT 1a of natural $^{113}Cd^{2+}$ abundance was demetalated using formic acid. The protein was then desalted on a G-25 Sephadex column into deionized water, which had been adjusted to a pH =2.7 using formic acid, to remove the natural abundance Cd^{2+}. To impede the oxidation of the protein, *tris*(2-carboxyethyl)phosphine (TCEP) was added to the solution. Isotopically enriched Cadmium(113) chloride (> 95%) was then added to the solution followed by neutralization using ammonium hydroxide with concomitant metal binding of $^{113}Cd^{2+}$ to the protein. The solution was then concentrated to 10 mL and

desalted into 10 mM ammonium formate buffer using a G-25 Sephadex column at pH 7.5 in order to remove any excess cadmium(113). Concentration and D_2O exchange was performed using stirred ultrafiltration cell models 8200 and 8010, respectively. The final protein concentration was determined to be 7-8 mM based on UV absorption spectroscopy using the 250-nm peak (ε_{250} = 36,000 $M^{-1}cm^{-1}$). The sample was Ar-saturated and sealed in a 5 mm NMR tube for analysis. Following acquisition of $^{113}Cd_{3/4}$-β-rhMT excess cadmium(113) was added as a solid to produce $^{113}Cd_4$-β-rhMT 1a used for both the 1D and 2D NMR spectra.

5.2.4 Experimental details for the titration of excess Cd^{2+} into a sample of Cd_3-β-rhMT 1a

CD and UV absorption spectroscopy and ESI mass spectrometry

Spectra were acquired for the Cd_3-β-rhMT 1a solution (24.4 μM) in 5 mM ammonium formate buffer (pH 9.0) and for a solution from the same stock of Cd_3-β-rhMT 1a to which 4.4 excess molar equivalent of Cd^{2+} were added, forming (as we show in the ESI-Mass spectral data) Cd_4-β-rhMT 1a.

5.2.5 Instrumental parameters

CD spectroscopy

CD spectra were acquired on a Jasco J810 spectropolarimeter in a 1-cm quartz cuvette at room temperature (22 °C) and recorded using Spectra Manager v.1.52.01 (Jasco) software. The wavelength range of 200-350 nm was scanned continuously at a rate of 60 nm/min with a band width of 2 nm. The spectral data were organized and plotted using Origin® v.7.0383. The CD spectra are expressed in the units of ΔA.

UV absorption spectroscopy

UV spectra were acquired on a Cary 5G UV-Vis-NIR spectrophotometer (Varian Canada, Mississauga, ON, Canada) in a 1-cm quartz cuvette at room temperature (22 °C) and recorded using the Cary Win UV Scan software application. The wavelength range of 200-350 nm was scanned continuously. All spectra were baseline corrected. The spectral data were organized and plotted using Origin® v.7.0383.

ESI mass spectrometry

ESI-MS measurements were carried out after the UV absorption and CD spectroscopic experiments had been completed. Mass spectra were acquired on a Micromass LCT electrospray-ionization time-of-flight (ESI-TOF) mass spectrometer (Waters Micromass) at room temperature (22 °C) and recorded using the Mass Lynx software package v. 4.0. The ESI-TOF was calibrated with a solution of NaI. The scan conditions for the spectrometer were: capillary, 3000.0 V; sample cone, 15.0 V; extraction cone, 10.0 V; RF lens, 450.0 V; desolvation temperature, 20.0 ^{o}C; source temperature, 80.0 ^{o}C; nebulizer gas flow, 53 L/hr; and desolvation gas flow, 548 L/h. The m/z range was 500.0 to 3000.0, the scan mode was continuum, and interscan delay was 0.10 s. Max Ent 1 from the Mass Lynx v.4.0 software package (Waters Micromass, Mississauga, ON, Canada) was used for spectra reconstruction program.

NMR spectroscopy

All NMR spectra were acquired on a Varian Inova 600 NMR spectrometer ($\nu_L(^1H)$ = 599.44 MHz, $\nu_L(^{113}Cd)$ = 132.99 MHz) using Varian's VNMRJ 2.2D software with Chempack 3.0 add-on. The ^{113}Cd chemical shifts were referenced with respect to an external 1.0 M solution of $CdSO_4$ in D_2O ($\delta(^{113}Cd)$ = 0.0 ppm), while ^{1}H chemical shifts were internally referenced to TMS ($\delta(^1H)$ = 0.0 ppm) based on the ^{2}H frequency of the deuterated solvent.

Direct-detect 1D $^{113}Cd\{^1H\}$ NMR spectra were acquired using a Varian broad-band 5.0mm HX probe, a spectral range from 540 to 740 ppm, and WALTZ-16 ^{1}H decoupling during acquisition only. For $Cd_{3/4}$-β-rhMT 1a, a total of 93 000 transients were accumulated using a 1s relaxation delay and a 16.2 μs 90-degree pulse width with a 1.234 s acquisition time at 10 °C. The data were processed using a line-broadening of 10 Hz. For Cd_4-β-rhMT 1a, a total of 84 000 transients were accumulated using a 2s relaxation delay and a 10.8 μs 60-degree pulse width with a 0.587 s acquisition time at 25 °C. The data were processed using a line-broadening of 20 Hz.

Indirect 2D ^{1}H-^{113}Cd HSQC NMR spectra were acquired using a Varian indirect-detection 5.0 mm HCX probe, a ^{113}Cd spectral range from 540 to 740 ppm, a ^{1}H spectral range from -0.4 to 4.8 ppm, a 0.15 s acquisition time, and a 1 s relaxation delay. Water suppression was achieved using a selective 1 s presaturation pulse at a power of 4 dB. In the indirect ^{113}Cd dimension the data was zero-filled to 1024 total points, and a Gaussian

weighting function was applied. In the direct ^{1}H dimension, the data were zero-filled to 1024 points and a Gaussian weighting function was applied. For $Cd_{3/4}$-β-rhMT 1a, a total of 84 transients were accumulated for each of the 128 increments, a forward linear prediction of 128 points in ^{113}Cd dimension, and the $^{3}J(^{113}Cd,^{1}H)$ value was set to 60 Hz at 30 °C. For Cd_4-β-rhMT, a total of 44 transients were accumulated for each of the 256 increments, a forward linear prediction of 256 points in ^{113}Cd dimension, and the $^{3}J(^{113}Cd,^{1}H)$ value was set to 67 Hz at 25 °C.

5.3 Results

5.3.1 Supermetalation of β-rhMT 1a studied by ESI-mass spectrometry and CD and UV absorption spectroscopies

To determine the effect of the fourth metal on the overall fold of the isolated β domain, analysis with both CD and UV absorption spectroscopy, coupled with metal speciation provided by ESI-MS, was carried out. These techniques allowed us to directly correlate the number of metals bound and observed spectroscopic changes in solution. The protein used in this set of experiments was taken directly after purification and desalted into an ESI-MS compatible buffer. This was done to avoid structural changes that may occur upon acid induced demetalation and to demonstrate that the additional low affinity site for Cd^{2+} is not the result of high concentrations found in the NMR experiment (*32*).

A solution of Cd_3-β-rhMT 1a (Figure 5-2A) was initially measured. Addition of 4.4 excess molar equivalents of Cd^{2+} produced a solution with a composition of 10% Cd_3- β-rhMT 1a and 90% Cd_4-β-rhMT 1a (Figure 5-2B). The mass of apo-β-rhMT 1a is 3754 Da (spectra not shown), giving the theoretical masses of Cd_3-β-rhMT 1a and Cd_4-β-rhMT 1a as 4085 Da and 4195 Da, respectively, which compare well with the experimental masses of 4085 Da and 4197 Da, respectively. Because of the weaker binding of the fourth Cd^{2+} atom to the protein, we attribute this residual 10% Cd_3-β-rhMT 1a to MS induced dissociation of the metal. An approximate equilibrium binding constant of 6.0 ± 0.8 x 10^4 M^{-1} was determined, using the ratio of Cd_3/Cd_4 based on an ESI-MS titration of apo-β-rhMT for the low affinity site by ESI-MS, a value that is several orders of

magnitude less than previously reported binding constants for normal binding of both Cd^{2+}, $6.0x10^{21} – 10^{25.6}$ M^{-1} (*33*-*34*), and Zn^{2+}, $5.0x10^{7} – 6.3x10^{11}$ M^{-1} (*35*).

To determine the location of the fourth cadmium ion, whether it was either attached to the cluster or existed as an adduct to other opportunistic amino acids, the UV absorption and CD spectra for both Cd_3-β-rhMT 1a and Cd_4-β-rhMT 1a were measured. While the UV spectra did not change significantly (Figure 5-2C), the CD spectra measured for these species (Figure 5-2D) showed drastic changes in the extrema. Maxima and minima at 262 and 236 nm, respectively, were observed for Cd_3-β-rhMT 1a, while Cd_4-β-rhMT 1a exhibited maxima and minima of 252 nm and 231 nm, respectively. For Cd_3-β-rhMT 1a the maximum at 262 nm was broad suggesting that the traditional structure is flexible and exists as a mixture of conformations.

Upon addition of excess Cd^{2+} to solution, the maximum blue shifted to 252 nm and the intensity increased by 60%. The increase in intensity may be attributed to a decrease in the conformational flexibility of the protein, while the blue shift can be associated with a breaking of the exciton coupling between the three Cd^{2+} of the system as observed when Cd_5-α-rhMT 1a is formed (*13*). The breaking of exciton coupling strongly suggests that the fourth Cd^{2+} atom is involved in the metal-thiolate cluster. A previous analysis of the β domain using mouse MT-1 demonstrated CD spectral changes between 3 and 12 equivalents of Cd^{2+} (*36*), which the author argued was the result of a Cd_9-rhβ-MT 1, but which we postulate to be supermetalated Cd_4-β-rhMT 1.

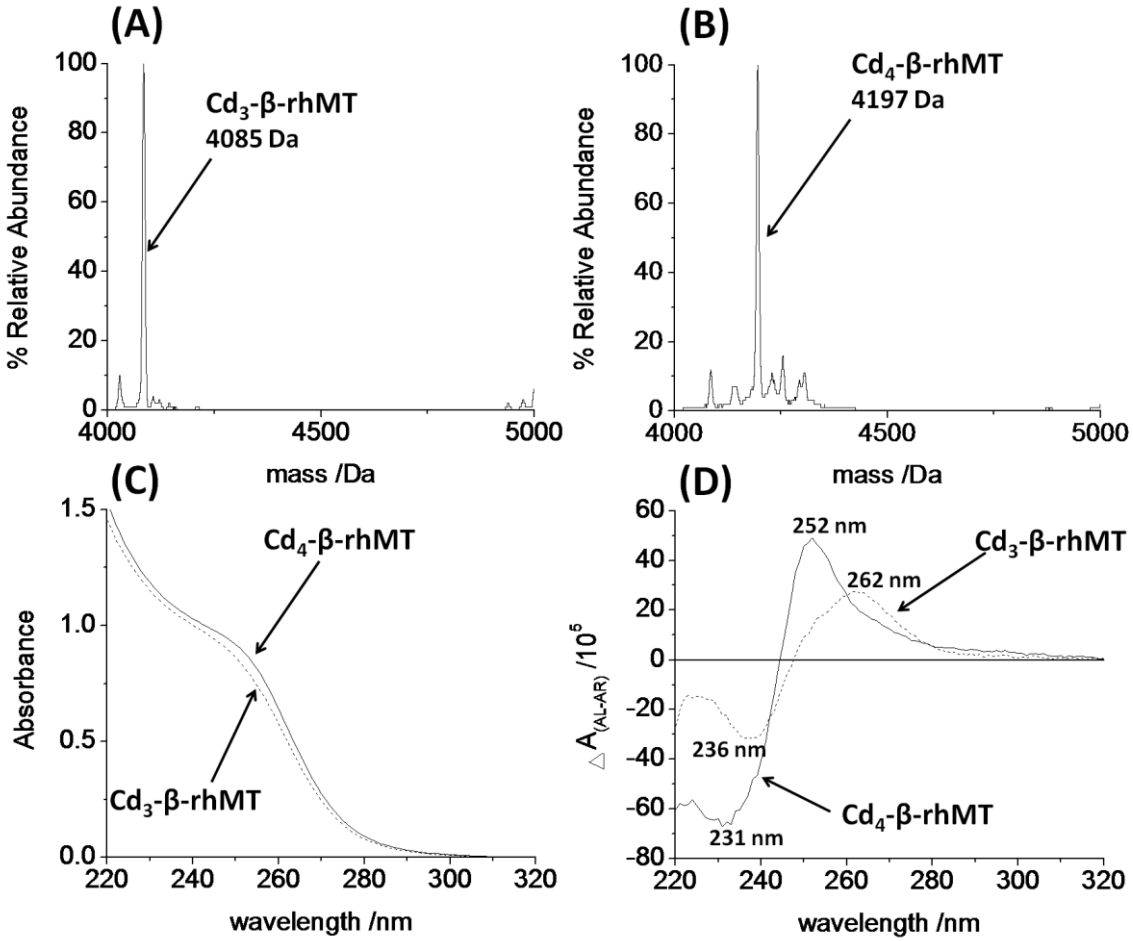

Figure 5-2. ESI-MS deconvoluted spectra, UV-absorption and CD spectra of Cd_3-β-rhMT 1a and the supermetalated Cd_4-β-rhMT 1a. (A) ESI-MS deconvoluted spectrum of Cd_3-β-rhMT 1a, showing the mass equal to the apo-protein with 3 Cd^{2+}; (B) ESI-MS deconvoluted spectrum of supermetalated Cd_4-β-rhMT 1a formed following the addition of 4.4 molar equivalents of $CdSO_4$ to the Cd_3-β-rhMT 1a, showing the additional mass from 1 extra Cd^{2+}. (C) UV absorption and (D) CD spectral changes observed for Cd_3-β-rhMT 1a and the supermetalated Cd_4-β-rhMT 1a formed following the addition of 4.4 molar equivalents of $CdSO_4$ to the Cd_3-β-rhMT 1a. To ensure accurate speciation, the same samples of Cd_3-β-rhMT 1a and Cd_4-β-rhMT 1a were used in all experiments. All experiments were carried out in 5 mM ammonium formate buffer, at pH 9.0, and at 22 ^{o}C.

5.3.2 One dimensional ^{113}Cd NMR spectroscopy of Cd_3-β-rhMT 1a and Cd_4-β-rhMT 1a

Direct 1D $^{113}Cd[^{1}H]$ NMR spectroscopy was used for a mixture of $Cd_{3/4}$-β-rhMT 1a, a result of a slight excess of Cd^{2+} to increase resistance to oxidation, and a pure sample of Cd_4-β-rhMT 1a in order to determine relative speciation of the individual metal binding

sites as well as the type of coordinating ligands through chemical shift data. Samples were isotopically enriched with $^{113}CdCl_2$ in 10 mM ammonium formate pH 7.4, following demetalation with formic acid, in order to enhance the NMR signal. Signals observed for $Cd_{3/4}$-β-rhMT 1a (Figure 5-3A) include 687.9, 674.0, 644.7, 634.5, 629.9, 616.7 and 601.3 ppm, while the observed signals for the pure Cd_4-β-rhMT 1a (Figure 5-3B) are 688.8, 650.3, 635.9 and 602.5 ppm. The chemical shift range of all the peaks is between 600 and 700 ppm, which overlaps significantly with the region expected for tetrahedral cadmium-thiolate clusters (*37*), traditional of metallothioneins, as well as both trigonal cadmium thiolate and tetrahedral cadmium-thiolate clusters where a single sulfur has been replaced by water (*38*). By comparing the signals from both sets of data, the peaks for Cd_3-β-rhMT 1a can be identified as 674.0, 629.9 and 616.7 ppm. Previous NMR work on human liver MT 1 have shown chemical shifts of 670.5, 652.0 and 645.8 ppm for the β domain (*25*); the differences in the chemical shifts are most likely due to the lack of the α domain as well as differences in sample conditions.

Direct detection of ^{113}Cd in the binding site allows one to infer the fluctionality of the individual metal ions. Analysis of the spectrum in Figure 5-3A shows that peaks attributed to Cd_3-β-rhMT 1a species, with the exception of 674.0 ppm, are significantly less intense than those we attribute to Cd_4-β-rhMT 1a. Previous NMR studies involving both domains, has suggested that the α domain is less fluctional than the β domain leading to sharper peaks of greater intensity (*25*). Upon addition of excess $^{113}Cd^{2+}$ to solution, the observed chemical shifts of Cd_3-β-rhMT 1a almost completely disappear with an increase in intensity of the peaks assigned to Cd_4-β-rhMT 1a suggesting an overall reduction in the fluctionality of Cd_4-β-rhMT 1a compared to Cd_3-β-rhMT 1a. There is a slight chemical shift in each of the four peaks, with the most significant shift being a total of 5.6 ppm involving the movement of 644.7 ppm to 650.3 ppm, attributed to the increase in chloride ions from $^{113}CdCl_2$ (*39*). This peak is also noticeably broader and less intense than the other three, which are of comparable size, suggesting that this binding site is more solvent exposed and fluctional. The increase in fluctionality and solvent exposure of just this site would make this Cd^{2+} site the most likely candidate for the metal-exchange intermediate, allowing both the solvent and acceptor/donor proteins access to the metal. The sharpness of the spectral lines further supports the interpretation

of CD spectroscopic data that the maxima blue shift between Cd_3-β-rhMT 1a and Cd_4-β-rhMT 1a, with an increase in intensity of 60%, is the result of a reduction in the fluctionality of the domain overall.

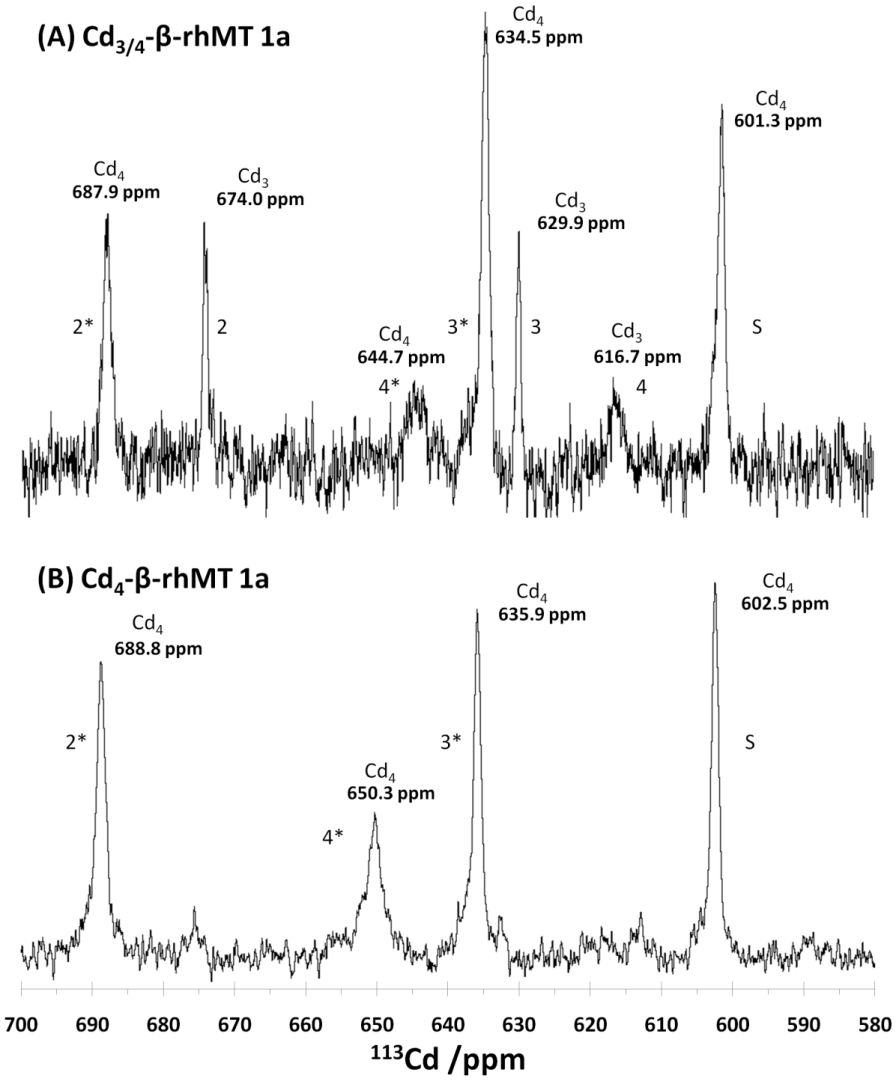

Figure 5-3. Direct 1D $^{113}Cd[^1H]$ NMR spectrum (133 MHz) of (A) mixture of Cd_3-β-rhMT 1a and Cd_4-β-rhMT 1a and (B) Cd_4-β-rhMT 1a formed by addition of excess $^{113}CdCl_2$. Slight shifts in the ppm values of Cd_4-β-rhMT 1a were observed between the mixture and the pure supermetalated sample. This shift is attributed to the addition of chloride ions from $^{113}CdCl_2$, to the solution and is most pronounced in the least intense Cd_4-β-rhMT 1a signal at 644.7 ppm, with a total shift of 5.6 ppm downfield. The $Cd_{3/4}$-β-rhMT was prepared in 10 mM ammonium formate pH 7.4 and buffer exchanged into 90% D_2O. Subsequent addition of solid $^{113}CdCl_2$ to $Cd_{3/4}$-β-rhMT 1a led to the formation of Cd_4-β-rhMT 1a. Spectra of $Cd_{3/4}$-β-rhMT 1a and Cd_4-β-rhMT 1a were acquired at 10 °C and 25 °C, respectively.

5.3.3 Two dimensional $^{1}H[^{113}Cd]$HSQC NMR spectroscopy of both Cd_3- and Cd_4-β-rhMT 1a

Indirect $^{1}H[^{113}Cd]$ HSQC NMR spectroscopy was used for both $Cd_{3/4}$-β-rhMT 1a and Cd_4-β-rhMT 1a (Figure 5-4). Analysis of the β protons of the cysteine residues allowed determination of peak relatedness as well as a tentative assignment of the metal-thiolate connectivity. Peaks were interpreted as related based on similarity in both the ^{1}H and ^{113}Cd chemical shifts. Chemical shifts in the β protons of the cysteine were observed for all metal sites existing in both Cd_3-β-rhMT and Cd_4-β-rhMT and it is likely these are the result of the structural changes necessary for the accommodation of a fourth cadmium atom in the β metal-thiolate cluster. In Figure 5-4, peak 2* possessed intense signals observable at both the 2.3 and 2.8 ppm in the ^{1}H dimension, both signals overlapped well with peaks assigned to 2. Similarity in both the ^{1}H profile as well as their closeness in the ^{113}Cd chemical shift range suggests that they are related. Peaks 3 and 3*, from Cd_3-β-rhMT 1a and Cd_4-β-rhMT 1a, were interpreted as related with both similar peak shape and profile from 2.4 to 3.5 ppm. A chemical shift disturbance of a β proton from peaks 3 and 3* is observed in the 3.2 to 3.4 ^{1}H range with a slight downfield shift that can be seen in the Cd_4-β-rhMT 1a compared to Cd_3-β-rhMT 1a. Assignment of the cadmium center associated with peaks 4 and 4* was based on the significant similarity in the β protons region. Additionally, these peaks are equally broad and have comparable intensities in the 1D $^{113}Cd[^{1}H]$ NMR spectrum (Figure 5-3a). The new signal, S, is attributed to the supermetalated site and is significantly upfield from all other cadmium peaks. At 602.5 ppm, this peak may represent a tetrahedral geometry coordinating either four thiolates or three thiolates and a single water molecule/chloride ion.

Assignment of the HSQC spectrum for Cd_3-β-rhMT 1a shows three bridging cysteine residues (Figure 5-4a), as one would expect from the connectivity (Figure 5-1). Upon addition of excess cadmium, an additional two bridging interactions are observed. Interestingly, the new metal appears to coordinate with all other metal centers at the expense of bridging interactions within the original cluster. It is this loss of original bridging interactions that may explain the loss of exciton coupling in CD spectroscopy without any significant change in the ligand-to-metal charge transfer band observed in UV spectroscopy (Figure 5-2).

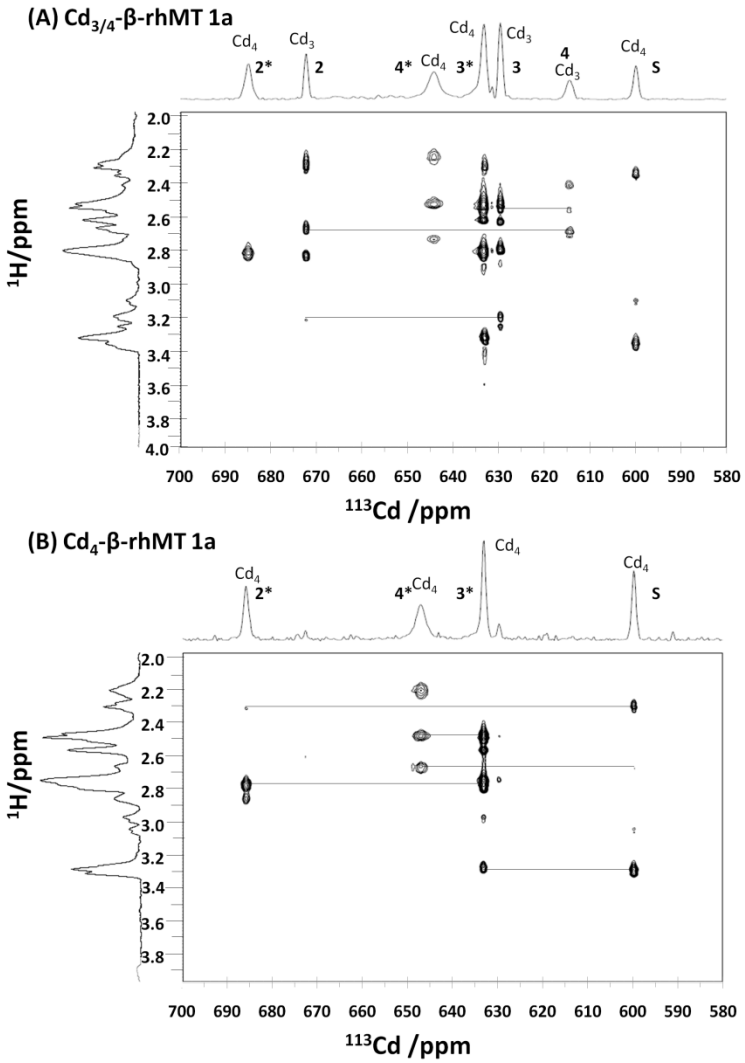

Figure 5-4. Indirect 2D $^{1}H[^{113}Cd]$ HSQC NMR spectra of (A) Mixture of Cd_3-β-rhMT 1a and Cd_4-β-rhMT 1a and (B) Cd_4-β-rhMT 1a produced upon addition of excess $^{113}CdCl_2$. The spectra were recorded in the ^{1}H chemical shift range of -0.4 – 4.8 ppm and the ^{113}Cd range of 540-740 ppm (^{3}J = 60 Hz and 67 Hz) for Cd_3-β-rhMT 1a and Cd_4-β-rhMT 1a, respectively. Spectra (A) was recorded at 30 °C, while spectra (B) was recorded at 25 °C. Both spectra were acquired using an inverse single axis z-gradient HCX probe with X tuned to ^{113}Cd. These spectra were used to aid in the correlating Cd_3-β-rhMT 1a peaks with Cd_4-β-rhMT peaks 1a.

5.4 Discussion

It has been proposed over the last 50 years that the various different metallothioneins perform many critical functions concerned with metal homeostasis, metal exchange, and recently cellular redox status. In the present study, analysis of the spectroscopic data from metalation of the β domain of human metallothionein 1a has shown that a supermetalated form of the domain exists, the extra metal ion is located in the metal thiolate cluster and we propose that this supermetalated form, with a distorted cluster, may be a model of the metal exchange intermediate.

5.4.1 Location of the fourth Cd^{2+} ion in Cd_4-β-rhMT 1a

Prior to this report it was unclear whether an additional metal was bound to the protein metal-thiolate core, or if the protein was somehow bound to other ligands. The coupling of both spectroscopic and spectrometric analyses clearly demonstrates that this additional Cd^{2+} ion is coordinated to the metal-thiolate core and that this coordination leads to a significant rearrangement of the cluster. It is this fourth Cd^{2+} ion that breaks the symmetry of the cluster, as monitored through a loss of exciton coupling (Figure 5-2).

Both direct and indirect ^{113}Cd NMR spectroscopy confirm coordination of the fourth Cd^{2+} ion to the metal thiolate core and provide tentative connectivities for the Cd_3- and Cd_4-β-rhMT 1a clusters. Interestingly, an increase in the number of bridging interactions from 3 to 5 was observed. The newly coordinated metal bridges with all three of the original metals at the cost of cluster symmetry explaining the change in the CD spectrum. We propose an increase in bridging interactions, which is based upon an addition of proton-cadmium J-coupling seen as Cd_3-βα-rhMT is converted to Cd_4-βα-rhMT. Expansion of the protein cluster, may be critical for the functions of metal ion homeostasis and toxic metal detoxification because formation of these new bonds may be the first step in metal insertion, followed by expulsion of one of the originally coordinated metals.

5.4.2 The proposed mechanism of metal ion homeostasis

An insertion-expulsion mechanism would allow Cd^{2+}, which binds several orders of magnitude more tightly than Zn^{2+}, to exchange with Zn^{2+} bound metallothionein

simultaneous acting to sequester toxic Cd^{2+} and releasing free Zn^{2+} into the cellular environment. The net effect would be upregulation of metallothionein allowing an organism to effectively combat toxic metal exposure. A regulator of metallothionein transcription, the metal-responsive-element-binding transcription factor-1 (MTF-1), has been shown to upregulate metallothionein upon binding to Zn^{2+} (*40*). MTF-1 has been implicated in cellular responses including toxic metal detoxification and oxidative stress, both of which are implicated functions of metallothionein. The metal binding site of this transcription factor includes six Cys2His2 zinc fingers making it exceptionally sensitive to an organism's zinc load. For this reason supermetalation, in the context of toxic metals, may be a critical transient species in the regulation of transcription of the protein. An incoming toxic metal, such as cadmium, could coordinate in a supermetalated position allowing both sequestration of the toxic metal and release of a zinc ion. This zinc ion would consequently lead to the upregulation of MT, through the zinc binding motifs of MTF-1, allowing an organism to effectively combat toxic metals. Through this mechanism, supermetalation of metallothionein, the organism would be able to control cellular metal load.

5.4.3 Reports of supermetalated metallothionein in the literature

Supermetalation has now been reported in the α domain, Cd_5-α-rhMT 1a, the β domain, Cd_4-β-rhMT 1a and the full MT protein, Cd_8-βα-rhMT 1a, of human metallothionein 1a (*7-8, 31*). In the case of the α domain of human MT-1, analysis of ^{113}Cd NMR spectra provided data suggesting that the supermetalated form, Cd_5-α-rhMT 1a, included two bridging interactions through a crevice located on the α domain (*13*). ESI-MS titrations have also provided evidence that a supermetalated Cd_8-βα-rhMT 1a may exist in a dynamic equilibrium with Cd_7-βα-rhMT (*7*). Chan *et al.* attributed supermetalation of the full protein to supermetalation of the α domain, with the β domain remaining intact (*31*). Currently no competition experiments between the two isolated domains have been performed that would allow the determination of the relative affinity of Cd^{2+} to form supermetalated species, however the NMR chemical shifts would suggest that supermetalation first occurs in the β domain. By comparison, supermetalation of the α domain produces a peak at 224 ppm, while supermetalation of the β domain produces a

peak at 602 ppm. The dramatic difference in peak locations suggests that there are more cysteine residues coordinating the Cd^{2+} involved in the supermetalated β domain than there are in the α domain. These cysteine residues would act to stabilize the supermetalated structure, leading to an increase in the affinity of the β domain for Cd^{2+}/Zn^{2+} metal ions.

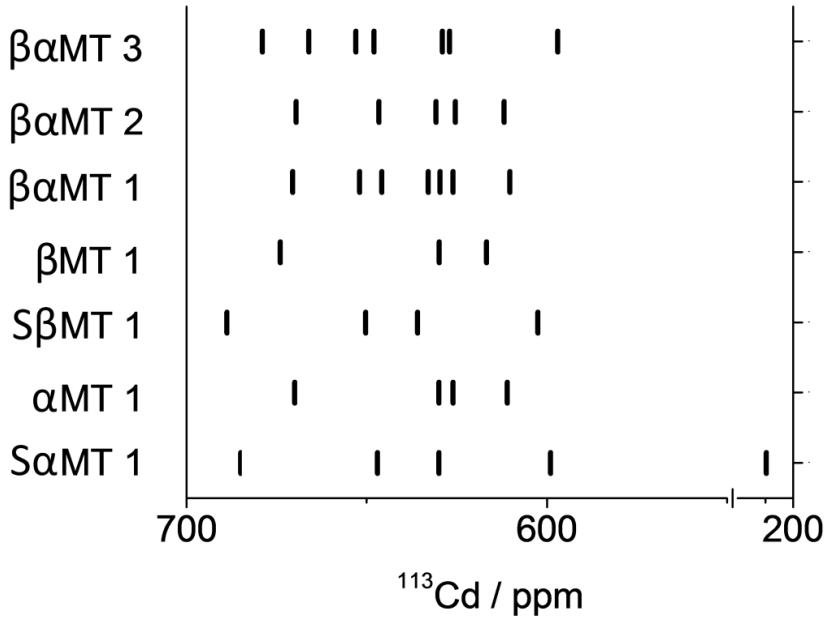

Figure 5-5. **Comparison of the ^{113}Cd NMR resonances for the human MTs**: Cd_7-βα-MT 3 (16), Cd_7-βα-MT 2 (25), Cd_7-βα-MT 1 (25), supermetalated Cd_4-β-rhMT 1a (this work), Cd_3-β-rhMT 1a (this work), Cd_4-α-rhMT 1a (13), and supermetalated Cd_5-α-rhMT 1a (13).

Supermetalation of the brain specific MT-3 to produce Cd_8-βα-MT 3 has also been observed (*14*). Unlike supermetalation of MT-1, Meloni *et al.* have suggested that both domains bridge together to accommodate the eighth cadmium atom. Interestingly, comparison of the metallothionein isoforms MT-2 and MT-3 demonstrated that while MT-3 was capable of accepting an additional metal ion, MT-2 was not. However, both MT-1 and MT-2 are more closely related than MT-3, the former having diverged before distinction of the mammalian orders while the latter, more structurally distinct, evolved much earlier (*41*). Surprisingly Romero-Isart *et al.* demonstrated the ability to confer neuroinhibitory MT-3 activity onto MT-1, through a series of mutations to the β domain (*22*). We postulate that supermetalation, a property only observed in distantly related

MT-1 and MT-3, may be a factor that leads to the differentiation of each isoform into specific functions in cellular chemistry.

One important aspect, which must be examined further, is the exact location of the low affinity binding site(s) on the Cd_8-βα-MT (1 or 2) protein. Figure 5-5 compares the NMR spectral data for human Cd_7-βα-MT 1, 2 and 3, the two isolated fragments of Cd_3-β-rhMT 1a and Cd_4-α-rhMT 1a, and the supermetalated species, Cd_4-β-rhMT 1a and Cd_5-α-rhMT 1a. The value of this figure is to show how the extra metal for the β domain described here exhibits a typical ^{113}Cd NMR spectral signature that falls within the range of MT data. Indeed, it is possible that the Cd_7-βα-MT 1 spectrum may contain a small fraction of Cd_4-β-MT as indicated by an overlap of the NMR signals of the Cd_4-β-MT 1a with those of Cd_7-βα-MT 1. On the other hand, the fifth Cd^{2+} in the Cd_5-α-rhMT 1a results in a resonance in the region well away from the tetrahedral thiolates. Two possibilities exist for the location of the low affinity sites on Cd_8-βα-MT: 1) each domain is independently capable of binding an additional metal ion, as supported by supermetalation of the isolated β and α domains of MT-1, or 2) the two domains work in concert to bind this additional metal, as supported by the decrease in the Stokes radius of MT-3 upon supermetalation, which is consistent with the close approach of both clusters. It is probable that supermetalation of metallothionein is isoform specific, related to cellular function and mechanisms of metalation must be determined on a case-by-case basis. Answers to these questions in the future will have consequences for metal ion homeostasis, as well as toxic metal detoxification and could possibly lead to an assignment of a specific function for each of the metallothionein isoforms.

5.5 Conclusion

In this study, the β domain of recombinant human MT 1a, which is known to coordinate 3 Cd^{2+} ions through 9 cysteine residues, was shown to be able to coordinate an additional Cd^{2+} ion to form Cd_4-β-rhMT 1a using a combination of CD, UV and NMR spectroscopy, as well as ESI-mass spectrometry. The CD spectrum of the Cd_4-β-rhMT 1a showed a sharp monophasic peak centered at 252 nm as compared to the derivative-shaped spectrum of the Cd_3-β-rhMT 1a species with a maximum at 262 nm (+) and a minium at 236 nm (-). This change in the CD maximum indicates a disruption of the

exciton coupling between the original 3 Cd^{2+} ions. The ESI-mass spectrum showed an increase in mass corresponding to a single Cd^{2+} ion upon the addition of 4.4 molar equivalents excess to a solution of Cd_3-β-rhMT 1a further confirming the existence of this low affinity binding site.

Both direct and indirect ^{113}Cd NMR spectroscopic techniques were used to probe the coordination environment of the additional Cd^{2+} ion. The signal detected in the 1-D NMR spectrum associated with the supermetalated Cd^{2+} ion was located at 602 ppm. This location is typical of both trigonal cadmium thiolate and tetrahedral cadmium-thiolate clusters where a single sulfur ligand has been replaced by water (*38*). Evidence from the 2-D NMR spectra suggest that binding of the additional Cd^{2+} ion significantly perturbs the cluster leading to an increase of bridging interactions from 3 to 5. These enhanced interactions are likely the cause of the loss of exciton coupling observed in the CD spectrum as Cd_3-β-rhMT 1a is converted into Cd_4-β-rhMT 1a. Based upon the significant difference between the NMR chemical shift range of the supermetalated peak in Cd_4-β- and Cd_5-α-rhMT 1a (602 ppm vs. 224 ppm respectively), it is likely that supermetalation of the β-domain dominants the full MT protein. Future research will involve the characterization of supermetalated Cd_8-βα-rhMT 1a to determine the exact location of this additional Cd^{2+} ion.

5.6 References

1. Margoshes, M., and Vallee, B. L. (1957) A cadmium protein from equine kidney cortex, *J. Am. Chem. Soc. 79*, 4813-4814.
2. Maret, W. (2008) A role for metallothionein in the pathogenesis of diabetes and its cardiovascular complications, *Mol. Gen. Metab. 94*, 1-3.
3. Kang, Y. J. (2006) Metallothionein redox cycle and function, *Exp. Biol. Med. 231*, 1459-1467.
4. Good, M., Hollenstein, R., Sadler, P. J., and Vasak, M. (1988) ^{113}Cd NMR studies on metal-thiolate cluster formation in rabbit Cd(II)-metallothionein: Evidence for a pH dependence, *Biochemistry 27*, 7163-7166.
5. Gehrig, P. M., You, C., Dallinger, R., Gruber, C., Brouwer, M., Kagi, J. H. R., and Hunziker, P. E. (2000) Electrospray ionization mass spectrometry of zinc, cadmium, and copper metallothioneins: Evidence for metal-binding cooperativity, *Protein Sci. 9*, 395-402.
6. Palumaa, P., Eriste, E., Njunkova, O., Pokras, L., Jornvall, H., and Sillard, R. (2002) Brain-specific metallothionein-3 has higher metal-binding capacity than

ubiquitous metallothioneins and binds metals noncooperatively, *Biochemistry 41*, 6158-6163.

7. Sutherland, D. E. K., and Stillman, M. J. (2008) Noncooperative cadmium(II) binding to human metallothionein 1a, *Biochem. Biophys. Res. Commun. 372*, 840-844.
8. Duncan, K. E. R., and Stillman, M. J. (2007) Evidence for noncooperative metal binding to the α domain of human metallothionein, *FEBS J. 274*, 2253-2261.
9. Ngu, T. T., Easton, A., and Stillman, M. J. (2008) Kinetic analysis of arsenic - metalation of human metallothionein: Significance of the two-domain structure, *J. Am. Chem. Soc. 130*, 17016-17028.
10. Ngu, T. T., Lee, J. A., Rushton, M. K., and Stillman, M. J. (2009) Arsenic metalation of seaweed *Fucus vesiculosus* metallothionein: The importance of the interdomain linker in metallothionein, *Biochemistry 48*, 8806-8816.
11. Sutherland, D. E. K., and Stillman, M. J. (2011) The "magic numbers" of metallothionein, *Metallomics 3*, 444-463.
12. Nielson, K. B., Atkin, C. L., and Winge, D. R. (1985) Distinct metal-binding configurations in metallothionein, *J. Biol. Chem. 260*, 5342-5350.
13. Rigby-Duncan, K. E., Kirby, C. W., and Stillman, M. J. (2008) Metal exchange in metallothioneins - a novel structurally significant Cd_5 species in the alpha domain of human metallothionein 1a *FEBS J. 275*, 2227-2239.
14. Meloni, G., Polanski, T., Braun, O., and Vasak, M. (2009) Effects of Zn^{2+}, Ca^{2+}, and Mg^{2+} on the structure of Zn_7metallothionein-3: Evidence for an additional zinc binding site, *Biochemistry 48*, 5700-5707.
15. Wang, H., Li, H., Cai, B., Huang, Z.-X., and Sun, H. (2008) The effect of nitric oxide on metal release from metallothionein-3: gradual unfolding of the protein, *J. Biol. Inorg. Chem. 13*, 411-419.
16. Wang, H., Zhang, Q., Cai, B., Li, H., Sze, K.-H., Huang, Z.-X., Wu, H.-M., and Sun, H. (2006) Solution structure and dynamics of human metallothionein-3 (MT-3), *FEBS Lett. 580*, 795-800.
17. Braun, W., Vasak, M., Robbins, A. H., Stout, C. D., Wagner, G., Kagi, J. H. R., and Wuthrich, K. (1992) Comparison of the NMR solution structure and the x-ray crystal structure of rat metallothionein-2, *Proc. Natl. Acad. Sci. U.S.A 89*, 10124-10128.
18. Morris, C. A., Nicolaus, B., Sampson, V., Harwood, J. L., and Kille, P. (1999) Identification and characterization of a recombinant metallothionein protein from a marine alga, *Fucus vesiculosus*, *Biochem. J. 338*, 553-560.
19. Leszczyszyn, O. I., Evans, C. D., Keiper, S. E., Warren, G. Z. L., and Blindauer, C. A. (2007) Differential reactivity of individual zinc ions in clusters from bacterial metallothioneins, *Inorg. Chim. Acta 360*, 3-13.
20. Peroza, E. A., Schmucki, R., Guntert, P., Freisinger, E., and Zerbe, O. (2009) The β_E-domain of wheat E_c-1 metallothionein: a metal-binding domain with a distinctive structure *J. Mol. Biol. 387*, 207-218.
21. Uchida, Y., Takio, K., Titani, K., Ihara, Y., and Tomonaga, M. (1991) The growth inhibitory factor that is deficient in the alzheimer's disease brain is a 68 amino acid metallothionein-like protein, *Neuron 337-347*.

22. Romero-Isart, N., Jensen, L. T., Zerbe, O., Winge, D. R., and Vasak, M. (2002) Engineering of metallothionein-3 neuroinhibitory activity into the inactive isoform metallothionein-1, *J. Biol. Chem. 277*, 37023-37028.
23. Zheng, Q., Yang, W.-M., Yu, W.-H., Cai, B., Teng, X.-C., Xie, Y., Sun, H.-Z., Zhang, M.-J., and Huang, Z.-X. (2003) The effect of the EAAEAE insert on the property of human metallothionein-3, *Protein Eng. 16*, 865-870.
24. Sewell, A. K., Jensen, L. T., Erickson, J. C., Palmiter, R. D., and Winge, D. R. (1995) Bioactivity of metallothionein-3 correlates with its novel β domain sequence rather than metal binding properties, *Biochemistry 34*, 4740-4747.
25. Boulanger, Y., and Armitage, I. M. (1982) ^{113}Cd NMR study of the metal cluster structure of human liver metallothionein, *J. Biol. Inorg. Chem. 17*, 147-153.
26. Calderone, V., Dolderer, B., Hartmann, H.-J., Echner, H., Luchinat, C., Bianco, C. D., Mangani, S., and Weser, U. (2005) The crystal structure of yeast copper thionein: The solution of a long-lasting enigma, *Proc. Natl. Acad. Sci. U.S.A 102*, 51-56.
27. Feng, W., Cai, J., Pierce, W. M., Franklin, R. B., Maret, W., Benz, F. W., and Kang, Y. J. (2005) Metallothionein transfers zinc to mitochondrial aconitase through a direct interaction in mouse hearts, *Biochem. Biophys. Res. Commun. 332*, 853-858.
28. Mason, A. Z., Perico, N., Moeller, R., Thrippleton, K., Potter, T., and Lloyd, D. (2004) Metal donation and apo-metalloenzyme activation by stable isotoopically labeled metallothionein, *Mar. Environ. Res. 58*, 371-375.
29. Maret, W., Larsen, K. S., and Vallee, B. L. (1997) Coordination dynamics of biological zinc "clusters" in metallothioneins and in the DNA-binding domain of the transcription factor Gal4, *Proc. Natl. Acad. Sci. U.S.A 94*, 2233-2237.
30. Messerle, B. A., Schaffer, A., Vasak, M., Kagi, J. H. R., and Wuthrich, K. (1990) Three-dimensional Structure of Human [$^{113}Cd_7$]Metallothionein-2 in Solution Determined by Nuclear Magnetic Resonance Spectroscopy, *J. Mol. Biol. 214*, 765-779.
31. Chan, J., Huang, Z., Watt, I., Kille, P., and Stillman, M. J. (2007) Characterization of the conformational changes in recombinant human metallothioneins using ESI-MS and molecular modeling, *Can. J. Chem. 85*, 898-912.
32. Ejnik, J. W., Munoz, A., DeRose, E., III, C. F. S., and Petering, D. H. (2003) Structural consequences of metallothionein dimerization: Solution structure of the isolated Cd_4-α-domain and comparison with the holoprotein dimer, *Biochemistry 42*, 8403-8410.
33. Zhang, B. L., Sun, W. Y., and Tang, W. X. (1997) Determination of the association constant of platinum(II) to metallothionein, *J. Inorg. Biochem. 65*, 295-298.
34. Kagi, J. H. R., and Vallee, B. L. (1961) Metallothionein: a cadmium and zinc-containing protein from equine renal cortex, *J. Biol. Chem. 236*, 2435-2442.
35. Krezel, A., and Maret, W. (2007) Dual nanomolar and picomolar Zn(II) binding properties of metallothionein, *J. Am. Chem. Soc. 129*, 10911-10921.
36. Capdevila, M., Cols, N., Romero-Isart, N., Gonzalez-Duarte, R., Atrian, S., and Gonzalez-Duarte, P. (1997) Recombinant synthesis of mouse Zn_3-β and Zn_4-α

metallothionein 1 domains and characterization of their cadmium(II) binding capacity, *Cell. Mol. Life Sci. 53*, 681-688.

37. Ellis, P. D. (1983) Cadmium-113 magnetic resonance spectroscopy, *Science 221*, 1141-1146.
38. Iranzo, O., Jakusch, T., Lee, K.-H., Hemmingsen, L., and Pecoraro, V. L. (2009) The correlation of ^{113}Cd NMR and ^{111m}Cd PAC spectroscopies provides a powerful approach for the characterization of the structure of Cd^{II}-substituted Zn^{II} protein, *Chem. Eur. J. 15*, 3761-3772.
39. Villarreal, L., Tio, L., Atrian, S., and Capdevila, M. (2005) Influence of chloride ligands on the structure of Zn- and Cd-metallothionein species, *Arch. Biochem. Biophys. 435*, 331-335.
40. Laity, J. H., and Andrews, G. K. (2007) Understanding the mechanisms of zinc-sensing by metal-response element binding transcription factor-1 (MTF-1), *Arch. Biochem. Biophys. 463*, 201-210.
41. Kagi, J. H. R. (1993) Evolution, structure and chemical acitivity of class I metallothioneins: An overview., In *Metallothionein III: Biological roles and medical implications* (Suzuki, K. T., Imura, N., and Kimura, M., Eds.), Birkhauser-Verlag, Berlin.

Chapter 6. Single domain metallothioneins: Supermetalation of human MT 1a[6]

6.1 Introduction

Metallothioneins (MTs), first isolated by Margoshes and Vallee in 1957 (*1*), are a family of small metalloproteins characterized by their high cysteine content, absence of disulfide bonds, and a lack of aromatic amino acids (*2*). MT is ubiquitous to living organisms and since its discovery, members of the MT family have been isolated from a wide range of sources including all animal phyla, fungi, plants, as well as cyanobacteria (*3-6*). Owing to the significant number of cysteine residues in the sequence (~30% of all amino acids) (*7*), the function(s) of MT have been postulated to include toxic metal detoxification, protection against oxidative stress and as a metallochaperone involved in the metal ion homeostasis of essential Zn^{2+} and Cu^{+} (*8*). However, despite more than sixty years of intense research, the exact *in vivo* role(s) of MT are still largely unknown.

Mammalian MTs are the most well studied members of the MT family and consist of 20 cysteine residues that act to encapsulate two metal-thiolate cores. Figure 6-1A shows a space filling model of human MT 1a coordinated to 7 Cd^{2+} ions, Cd_7-βα-rhMT 1a (mammalian isoforms other than 1a will be noted specifically). In the X-ray structure of rat liver MT 2 (Zn_2Cd_5-MT 2) (*9*), and NMR studies from other variants (*10-11*), the metal ions exist with two independent domains: an N-terminal β-domain and a C-terminal α-domain. The β-domain is capable of binding 3 Zn^{2+} or Cd^{2+} ions through 9 cysteine residues, while the α-domain is capable of binding 4 Zn^{2+} or Cd^{2+} ions through 11 cysteine residues (Figure 6-1B). Significantly, the structural data has only been reported from metal-saturated proteins. It is important to note that both Zn^{2+} and Cd^{2+} bind to metallothionein in an isostructural manner, and that the overall molecular architecture of the protein, when coordinated to either Zn^{2+} or Cd^{2+}, is identical (*11*). The

---

[6] A version of this work has been published:

sequence of the cleaved recombinant βα-rhMT coordinated to seven divalent metal ions is shown in Figure 6-1C, with the metal ions colored green and cysteine residues colored yellow. The numbering of the cadmium-thiolate core is cross referenced to the original naming conventions based on the order of the NMR bands in the mammalian Cd_7-MT 2a spectra (*10*), while the numbering of the cysteine residues has been adjusted to accommodate both the additional amino acids from thrombin cleavage (residues 1 and 2) and a series of amino acids meant to aid in protein expression (residues 3-9).

Mammalian MT can be subdivided into four distinct subfamilies (MT-1, -2, -3 and -4), each of which contain twenty cysteine residues coordinating seven divalent metals. However, different patterns of expression suggest specific *in vivo* roles for each subfamily. For example, both MT-1 and -2, found in abundance in the liver and kidneys, are induced by a number of stimuli, including metal ions, glucocorticoids, cytokines and oxidative stress (*3, 12-13*), while MT-3, found primarily in the central nervous system (*14*), and MT-4, found in stratified squamous epithelial tissues, are more tightly controlled (*15*). These differences in expression, both causal and spatial, of the MT subfamilies are likely the result of the unique biological functions of each member. In fact, it has been shown that disruption of the natural expression of MT-3, through ectopic expression in mice, has led to the development of pancreatic acinar cell necrosis and death (*16*). These results highlight the fact that a dysregulation in the expression of MT can lead to a diseased state and eventual death. However, little is known regarding the structural differences of these MT subfamilies that must underlie their functional differences.

One reason for the difficulty in determining structure-function relationships for MT is that it is notoriously difficult to crystallize. To date only two X-ray structures have been reported: the first from rat (*9*), Cd_5Zn_2-MT 2, and the second from yeast (*17*), Cu_8-MT. In the first case, both cadmium and zinc metal centers were tetrahedrally coordinated by four thiolate groups into two distinct binding domains, while in the second case a combination of both trigonal and digonal coordination was observed for a single domain Cu-thiolate cluster. Much of the structural information known for mammalian MT is a result of the many NMR-based studies (*10, 18-21*). While NMR studies can provide the solution structure of MT, analysis has been limited to the spin ½ nuclei, namely ^{111}Cd and

^{113}Cd. Unfortunately, because of an absence of interdomain peaks associated with the nuclear overhauser effect (NOEs), NMR studies can only provide the absolute connectivities of atoms in a specific domain and their spatial relationship within that domain's metal-thiolate core. While the X-ray structure of the rat liver Zn_2Cd_5-MT 2 did provide the alignment of the interdomain linkage, the lack of interdomain NOEs has led to the assumption that both domains essentially act independently of each other. Further, subsequent studies have also generally assumed that the metal-based chemistry of each domain must also be independent and significantly that MT will adopt a two domain structure at all metal loading levels.

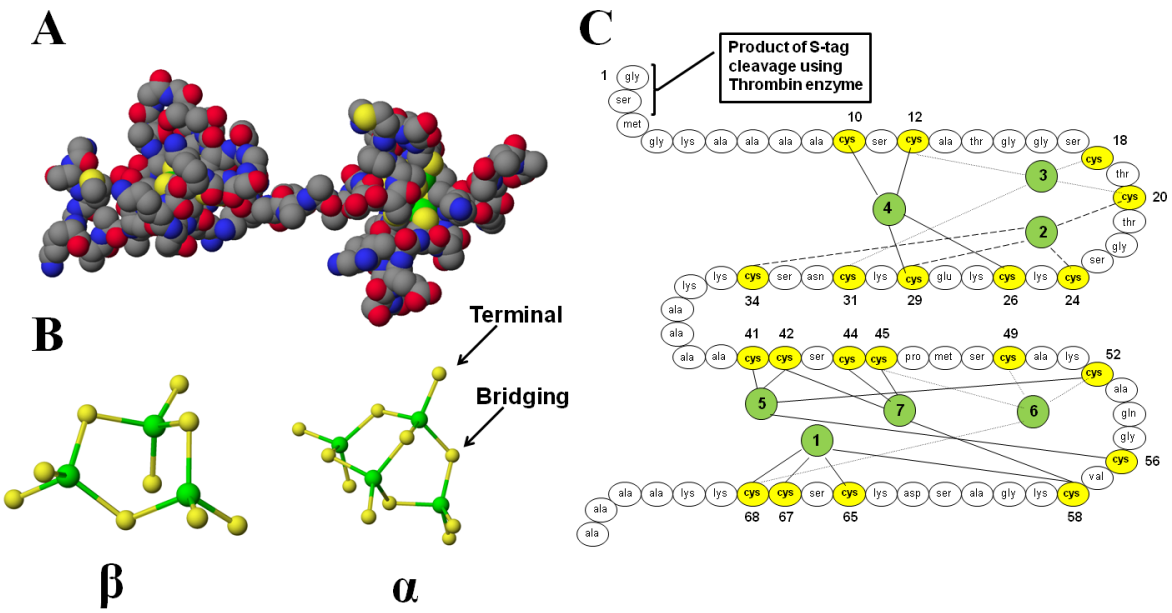

Figure 6-1. Molecular model of MT. (A) A space filling structure of Cd_7-βα-rhMT 1a. The N-terminal β-domain is located on the left hand side, while the C-terminal α-domain is located on the right hand side. (B) Cadmium-cysteinyl-thiolate clusters of Cd_7-βα-rhMT 1a presented as a ball and stick model: β-domain (left) and α-domain (right). (C) A connectivity diagram of MT 1a, which shows that each of the seven cadmium atoms is connected to exactly four cysteine amino acids. The connectivity diagram has been renumbered to accommodate the amino acids glycine and serine, both of which are a product of S-tag cleavage with Thrombin, located on the N-terminal of the β-domain. Numbering of the Cd-thiolate centers is based on the NMR assignment by Messerle *et al.* (10). Molecular modeling data from Chan *et al.* (22).

The assumption of domain independence has significant consequences for the metal exchange properties of metallothionein. Specifically, the β-domain of MT has been associated with a preference for Cu^+ coordination, while the α-domain has been

associated with a preference for Zn^{2+} or Cd^{2+} coordination (*23-25*). The question remains, however, if the domains do not interact with one another, then how does the metal binding reaction reach equilibrium? This problem is further complicated by the fact that MT is capable of binding a very wide range of metals, with differing geometries that are dependent on the stoichiometries of the associated metal, for example As_6-MT, Cd_7- or Zn_7-MT, Cu_{12}- or Ag_{12}-MT, and Hg_{18}-MT (*26-29*). A recent study with As-MT has shown that As^{3+} distribution between the full protein and the domain fragments occurred by protein-protein interactions, and not by an dissociative-associative mechanism (*30*). While not conclusive, these results support the existence of domain-domain interactions as the driving force behind metal-ion equilibration.

Another reason for the difficulty in determining the function of MT is that until recently, MT was thought to coordinate metals in a cooperative fashion, where the binding of one metal facilitates the binding of subsequent metals (*31*). However, recent studies have shown that metalation of MT by Cd^{2+}, Zn^{2+}, As^{3+}, and Bi^{3+} occurs in a noncooperative fashion (*26, 32-36*). A noncooperative mechanism allows for partially metalated, as well as metal exchange intermediates, to be stable and able to take part in cellular chemistry. Significantly, Krezel and Maret have shown from their competition experiments that there exist at least three classes of Zn^{2+} binding site, with log K values of 11.8, ~10 and 7.7 corresponding to the binding of four, two and one metal ion, respectively (*37*). This range of binding affinities shows that MT can act as a dynamic metallochaperone, capable of donating and accepting metal ions over a range of cellular concentrations.

Finally MT has been shown to bind metals in excess of traditional levels. These supermetalated states have been reported for both of the isolated α- and β-domains forming Cd_5-α-rhMT (*38*) and Cd_4-β-rhMT (*39*), respectively. This level of metalation has also been reported in human MT-3, Cd_8-βα-hMT 3 (*40*). In the case of MT-1 and MT-2, Cd^{2+} ions are known to isomorphously replace Zn^{2+} ions (*41*), which suggests the involvement of these supermetalated structures in the metal-exchange reactions that must occur for the binding of incoming metals with binding affinities greater than that of the resident zinc, for example, the essential Cu^{+} and the toxic Cd^{2+}. Indeed, metal transfer reactions in MT have been well documented, for example the Zn^{2+} transfer of fully

metalated Zn_7-βα-MT to m-aconitase (*42*), carbonic anhydrase (*43*), and the prototypical transcription factor Gal4 (*44*). Interestingly, a recent study involving the incubation of $A\beta_{1-40}$-Cu^{2+}, a producer of reactive oxygen critical to Alzheimer's disease, with Zn_7-βα-MT 3 demonstrated that MT readily exchanged Zn^{2+} for Cu^{2+}, with subsequent reduction to Cu^{+} and coordination to the remaining reduced thiols, thereby deactivating the $A\beta_{1-40}$-peptide (*45*). While these studies highlight the importance of protein-protein interactions, no exchange intermediates have been characterized that provide insight into the actual mechanism of metal transfer.

In this paper, we present evidence that human metallothionein, Cd_7-βα-rhMT, is capable of binding an additional cadmium atom to form Cd_8-βα-rhMT. Exact metal speciation was monitored using ESI-mass spectrometry (ESI-MS), which allowed for a direct correlation between the number of cadmium atoms bound to the protein and observed changes in the UV absorption and CD spectra. Direct and indirect ^{113}Cd NMR spectroscopies were used to ensure that the incoming metal was structurally significant and involved direct interaction with the metal-thiolate cluster. Possible implications of these results with respect to metal ion homeostasis and metal ion domain selectivity are discussed both of which have significant consequences for the *in vivo* function of MT in an organism.

6.2 Experimental Methods

6.2.1 Chemicals

Cadmium sulfate (Fisher Scientific); cadmium(113) chloride (Trace Sciences International Inc.); deuterium oxide (Cambridge Isotopes Laboratories, Inc.); *tris*(2-carboxyethyl)phosphine (PIERCE); ThrombinCleanCleave™ Kit (Sigma) Tris buffer, tris(hydroxymethyl)aminomethane (EMD Chemicals/VWR); ammonium formate buffer (JT Baker); ammonium hydroxide (Caledon Laboratory Chemicals); formic acid (Caledon Laboratory Chemicals); and hydrochloric acid (Caledon Laboratory Chemicals). All solutions were made with >16 M Ω cm^{-1} deionized water (Barnstead Nanopure Infinity). HiTrap™ SP HP ion exchange columns (Amersham Biosciences/GE Healthcare), superfine G-25 Sephadex (Amersham Biosciences/GE Healthcare), stirred

ultrafiltration cell Model 8010 and 8200 (Amicon Bioseparations/Millipore) with YM-3 membrane (3,000 MWCO) were used in the protein purification steps.

6.2.2 Protein sample preparation for CD spectroscopic and ESI mass spectrometric studies

The expression and purification of recombinant βα-rhMT has been previously reported (*22*) and is described in detail in Chapter 2. The βα-rhMT used in this study was based on the 72-residue sequence MGKAAAACSC ATGGSCTCTG SCKCKECKCN SCKKAAAACC SCCPMSCAKC AQGCVCKGAS EKCSCCKKAA AA with no disulfide bonds present in the system. The expression system included, for stability purposes, an N-terminal S-tag (MKETAAAKFE RQHMDSPDLG TLVPRGS). Recombinant βα-rhMT 1a was expressed in BL21(DE3) *Escherichia coli* (*E. coli*) transformed using the pET29a plasmid. Removal of S-tag was performed using a Thrombin CleanCleave^{TM} Kit. To impede oxidation of the cysteine residues to disulfide bonds, all protein samples were rigorously evacuated and then argon saturated to remove any residual oxygen that may be present in the solution.

6.2.3 Protein sample preparation for NMR spectroscopic studies

Samples of Cd-bound βα-rhMT for NMR analysis were prepared by pooling protein product from five 4 L recombinant preparations following thrombin-cleavage of the S-tag. The $^{113}Cd_7$-βα-rhMT used for acquisition of all NMR spectra was prepared by addition of concentrated formic acid to demetalate the protein, followed by desalting on a G-25 Sephadex column at which point *tris*(2-carboxyethyl)phosphine (TCEP) was added to the solution to impede oxidation. Isotopically pure (>95%) cadmium(113) chloride was added to the solution followed by neutralization using ammonium hydroxide. The solution was then concentrated to 10 mL and desalted into 10 mM ammonium formate buffer using a G-25 Sephadex column at pH 7.5 in order to remove any excess cadmium(113). Concentration, and D_2O exchange to 30% total volume, was performed using Amicon stirred ultrafiltration cell models 8200 and 8010, respectively. The final protein concentration was determined to be 5.3 mM based on UV absorption spectroscopy using the 250-nm peak (ε_{250} = 89,000 $M^{-1}cm^{-1}$). The buffer used for this

sample was 5 mM ammonium formate (pH 8.3). The sample was Ar-saturated and sealed in a 5 mm NMR tube for analysis. Following acquisition of $^{113}Cd_{7/8}$-βα-rhMT excess cadmium(113) was added to produce $^{113}Cd_8$-βα-rhMT, which was used for both the 1D and 2D NMR spectra.

6.2.4 Experimental details for the titration of excess Cd^{2+} into a sample of Cd_8-βα-rhMT 1a

CD and UV absorption spectroscopy and ESI mass spectrometry

All protein concentrations were confirmed by UV absorption spectroscopy using the absorbance at 250 nm, which corresponds to the ligand-to-metal charge transfer transition generated by the metal-thiolate bond (ε_{250}= 89 000 $M^{-1}cm^{-1}$).

CD spectra were recorded on a Jasco J810 spectropolarimeter in a 1 cm quartz cuvette at room temperature (22 °C) using Spectra Manager version 1.52.01 (Jasco). The wavelength range of 200-350 nm was scanned continuously at a rate of 50 nm/min with a bandwidth of 2 nm. The spectral data were organized and plotted using Origin version 7.0383. The CD spectra are expressed in units of ΔA. For the CD titration a solution of Cd_7-βα-rhMT was prepared in 5 mM ammonium formate (pH 8.1) to a concentration of 7.8 μM. This solution was then titrated in a stepwise manner with increasing amounts of Cd^{2+} using both 0.17 mM and 1.02 mM $CdSO_4$ in order to produce a solution of Cd_8-βα-rhMT 1a.

UV absorption spectra were recorded on a Cary 5G UV–vis–NIR spectrophotometer (Varian) in a 1 mm quartz cuvette at room temperature (22 °C) using the Cary Win UV Scan software application. The wavelength range of 200-350 nm was scanned continuously. All spectra were baseline-corrected. The spectral data were organized and plotted using Origin version 7.0383. The sample was measured in a 5 mM ammonium formate buffer at pH 8.1 with a protein concentration of 28 μM. This same sample was used in the ESI-MS titration. The extinction coefficient used for Cd_8-βα-rhMT 1a was 89 000 $M^{-1}cm^{-1}$

ESI-MS spectra were recorded on a micrOTOF II MS (Bruker). The operating parameters were as follows: End plate offset -500 V; Capillary 4200 V; Nebulizer 2.0 Bar; Dry gas 8 L/min; Dry temperature 80 °C; Capillary exit 180 V; Hexapole RF 600

Vpp; Mass range 500 to 3000 m/z. Spectra were acquired as a rolling average of 2×0.5 Hz. A solution of Cd_7-βα-rhMT was prepared in 5 mM ammonium formate (pH 8.1) to a concentration of 27.0 μM for MS measurements of Cd_7-βα-rhMT and Cd_8-βα-rhMT.

6.2.5 Instrumental parameters

CD spectroscopy

CD spectra were recorded on a Jasco J810 spectropolarimeter in a 1 cm quartz cuvette at room temperature (22 °C) using Spectra Manager version 1.52.01 (Jasco). The wavelength range of 200-350 nm was scanned continuously at a rate of 50 nm/min with a bandwidth of 2 nm. The spectral data were organized and plotted using Origin version 7.0383. The CD spectra are expressed in units of ΔA. For the CD titration a solution of Cd_7-βα-rhMT was prepared in 5 mM ammonium formate (pH 8.1) to a concentration of 7.8 μM. This solution was then titrated in a stepwise manner with increasing amounts of Cd^{2+} using both 0.17 mM and 1.02 mM $CdSO_4$ in order to produce a solution of Cd_8-βα-rhMT 1a.

UV absorption spectroscopy

UV absorption spectra were recorded on a Cary 5G UV–vis–NIR spectrophotometer (Varian) in a 1 mm quartz cuvette at room temperature (22 °C) using the Cary Win UV Scan software application. The wavelength range of 200-350 nm was scanned continuously. All spectra were baseline-corrected. The spectral data were organized and plotted using Origin version 7.0383. The sample was measured in a 5 mM ammonium formate buffer at pH 8.1 with a protein concentration of 28 μM. This same sample was used in the ESI-MS titration. The extinction coefficient used for Cd_8-βα-rhMT 1a was 89 000 $M^{-1}cm^{-1}$.

ESI mass spectrometry

ESI-MS spectra were recorded on a micrOTOF II MS (Bruker). The operating parameters were as follows: End plate offset -500 V; Capillary 4200 V; Nebulizer 2.0 Bar; Dry gas 8 L/min; Dry temperature 80 °C; Capillary exit 180 V; Hexapole RF 600 Vpp; Mass range 500 to 3000 m/z. Spectra were acquired as a rolling average of 2×0.5 Hz. A solution of Cd_7-βα-rhMT was prepared in 5 mM ammonium formate (pH 8.1) to a concentration of 27.0 μM for MS measurements of Cd_7-βα-rhMT and Cd_8-βα-rhMT.

NMR spectroscopy

All NMR spectra were acquired on a Varian Inova 600 NMR spectrometer ($\nu_L(^1H)$ = 599.44 MHz, $\nu_L(^{113}Cd)$ = 132.99 MHz) using Varian's VNMRJ 2.2D software with Chempack 3.0 add-on. The ^{113}Cd chemical shifts were referenced with respect to an external 1.0 M solution of $CdSO_4$ in D_2O ($\delta(^{113}Cd)$ = 0.0 ppm), while ^1H chemical shifts were internally referenced to TMS ($\delta(^1H)$ = 0.0 ppm) based on the ^2H frequency of the deuterated solvent.

Direct-detect 1D $^{113}Cd\{^1H\}$ NMR spectra were acquired using a Varian broad-band 5.0 mm HX probe, a spectral range from 540 to 720 ppm, and WALTZ-16 ^1H decoupling during acquisition only. For $Cd_{7/8}$-βα-rhMT 1a, a total of 39 000 transients were accumulated, while Cd_8-βα-rhMT 1a had a total of 30 176 transients accumulated. Both used a 7 s relaxation delay and a 5.33 μs 60-degree pulse width with a 0.684 s acquisition time at room temperature. The data were processed using a line-broadening of 10 Hz.

Indirect 2D ^1H-^{113}Cd HSQC NMR spectra were acquired using a Varian indirect-detection 5.0 mm HCX probe, a ^{113}Cd spectral range from 540 to 720 ppm, a ^1H spectral range from -0.5 to 10 ppm, a 0.291s acquisition time, and a 2s relaxation delay. Water suppression was achieved using a selective 2s presaturation pulse at a power of 13 dB. In the indirect ^{113}Cd dimension the data was zero-filled to 1024 total points, and a Gaussian weighting function was applied. In the direct ^1H dimension, the data were zero-filled to 1024 points and a Gaussian weighting function was applied. For both $Cd_{7/8}$-βα-rhMT 1a and Cd_8-βα-rhMT 1a, a total of 80 transients were accumulated for each of the 128 increments, a forward linear prediction of 128 points in ^{113}Cd dimension, and the $^3J(^{113}Cd,^1H)$ value was set to 67 Hz at room temperature.

Molecular Model

MM3/MD calculations parameterized using the modified force field described by Chan *et al.* and the dielectric constant for water (78.4) were carried out to obtain the minimum-energy structure of Cd_8-βα-rhMT 1a (46). All MM3/MD calculations and model-structure rendering were carried out using CAChe WorkSystem Pro 6.1.1 Software (Fujitsu America). The original Cd_7-βα-rhMT 1a was modified using CAChe to produce molecular models for Cd_8-βα-rhMT 1a. The structure was energy-minimized as follows: 1) the structure was energy minimized using the MM3 calculation followed by

the MD simulation at 500 K for 1000 ps. 2) The lowest structure was taken and again minimized at 300K for 5000 ps.

6.3 Results

6.3.1 Supermetalation of βα-rhMT 1a studied by ESI-mass spectrometry and CD and UV absorption spectroscopies

To determine the effect of the 8th metal on the overall fold of the protein, analysis with both CD and UV absorption spectroscopy, coupled with metal speciation provided by ESI-MS, were used. These techniques correlate the number of metals bound to the observed spectroscopic changes in solution. The protein used in these experiments was taken directly after purification and desalted into an ESI-MS compatible buffer. This was carried out in order to avoid structural changes that may occur upon acid induced demetalation and to demonstrate that the additional low affinity site for Cd^{2+} is not the result of high concentrations found in the NMR experiment (*47*).

A solution of Cd_7-βα-rhMT (Figure 6-2A) was initially measured. Addition of 2.8 excess molar equivalents of Cd^{2+} quantitatively converted Cd_7-βα-rhMT to Cd_8-βα-rhMT (Figure 6-2B). In the MS spectra, two sets of truncated βα-rhMT were detected: one in which the N-terminal G residue and C-terminal AA residues were truncated, and a second in which the N-terminal GSMGK as well as A from either the N-terminal or C-terminal were truncated. None of the metal-binding cysteine residues were affected. This truncation has been previously reported, and it does not affect the metal binding properties of the protein (*32*). The former truncation is of greater intensity and was used for all metal binding analyses. The theoretical *m/z* values of Cd_7-βα-rhMT are 1275.5 *m/z* for +6, 1530.4 *m/z* for +5 and 1912.7 m/z for +4, while the theoretical mass is 7,647 Da. These theoretical data are essentially identical to the experimental results of 1275.8 *m/z* for +6, 1530.6 *m/z* for +5 and 1913.2 m/z for +4 and a mass of 7,649 Da. The theoretical *m/z* values of Cd_8-βα-rhMT are 1293.9 *m/z* for +6, 1552.5 *m/z* for +5 and 1940.4 *m/z* for +4, while the theoretical mass is 7,757 Da. These theoretical values also compare well with the experimental results of 1294.5 *m/z* for +6, 1552.8 *m/z* for +5 and 1940.7 m/z for +4 and a mass of 7,759 Da. Of significance, is that the conversion of Cd_7-

βα-rhMT into Cd_8-βα-rhMT leads to an increase in the relative intensity of the +6 charge state from 38% to 55% and a decrease in the absolute intensity of the +5 charge state. These changes in intensity may be attributed to an increase in the overall volume of the protein necessary to accommodate the binding the 8^{th} Cd^{2+} ion (*48-49*).

The effect of the addition of the 8^{th} cadmium ion was also analyzed using both UV absorption and CD spectroscopy to determine the effects of this additional ion on the metal-thiolate cores. The UV absorption spectrum did not change significantly upon formation of Cd_8-βα-rhMT (Figure 6-2C). This was observed previously for the formation of the supermetalated Cd_4-β-rhMT and Cd_5-α-rhMT (*38-39*). The lack of change in the UV absorption profile with the addition of an 8^{th} Cd^{2+} ion is likely related to the necessity for the formation of only bridging interactions.

Addition of 1 molar equivalent Cd^{2+} led to significant changes in the CD spectrum (Figure 6-2D). The original maxima and minima of 260 and 239 nm observed for Cd_7-βα-rhMT were replaced by maxima and minima of 252 nm and 238 nm, respectively. Significant reduction in the intensity of the maxima located at 225 nm was also observed. Two isodichroic points are observed throughout the titration at 260 and 241 nm and provide evidence for the direct conversion of Cd_7-βα-rhMT to Cd_8-βα-rhMT. For Cd_7-βα-rhMT the maximum at 260 nm was broad suggesting that the traditional structure is flexible and exists as a mixture of conformations. However, upon supermetalation of Cd_7-βα-rhMT to form Cd_8-βα-rhMT the maximum blue shifted to 252 nm and the intensity increased by 50%. The increase in intensity may be attributed to a decrease in the conformational flexibility of the protein, while the blue shift can be associated with the metal ion directly interacting with the metal-thiolate core. These changes to the CD envelope provide strong evidence that the 8^{th} Cd^{2+} atom coordinates to both the β- and α-domain.

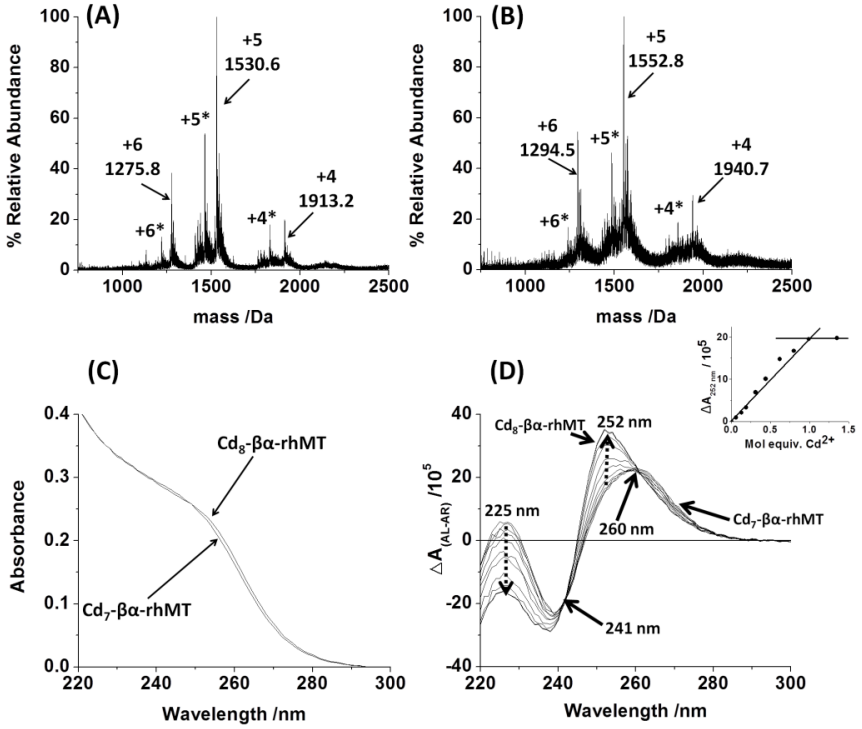

Figure 6-2. **Spectrometric and spectroscopic evidence for the existence of Cd_8-βα-rhMT.** ESI-MS spectra of (A) Cd_7-βα-rhMT and (B) Cd_8-βα-rhMT with 0.0 and 2.8 excess molar equivalents of $CdSO_4$, respectively. The charge states marked with an asterisk(*) are the result of a small fraction of truncated protein. (C) UV absorption spectra of Cd_7-βα-rhMT and Cd_8-βα-rhMT with 0.0 and 2.8 excess molar equivalents of $CdSO_4$, respectively. (D) CD spectral changes observed during the incremental titration of Cd_7-βα-rhMT with $CdSO_4$ to form Cd_8-βα-rhMT. Aliquots of $CdSO_4$ were added to solution in mole equivalents (based on the whole protein) of 0.00, 0.03, 0.06, 0.13, 0.19, 0.44, 0.62, 0.80, 0.99 and 1.35. The inset (D) shows the change in absorbance at 252 nm as a function of Cd^{2+} added to solution. Past the addition of one molar equivalent Cd^{2+}, there is no change in the CD spectrum.

The inset in the CD titration (Figure 6-2D) shows that no change in the absorbance at 252 nm is observed after a single molar equivalent of Cd^{2+} has been added to solution of Cd_7rhMT. We interpret the maxima at 252 nm to be exclusively the result of the Cd_8-βα-rhMT species. Cd_7-βα-rhMT binds the additional Cd^{2+} ion with a significantly greater affinity than either Cd_3-β-rhMT or Cd_4-α-rhMT binds the additional Cd^{2+} to form their respective supermetalated species (*38*-*39*).

6.3.2 One dimensional ^{113}Cd NMR spectroscopy of Cd_7- and Cd_8-βα-rhMT 1a

Direct 1D $^{113}Cd[^1H]$ NMR spectra were measured for a mixture of $Cd_{7/8}$-βα-rhMT, a result of a slight excess of Cd^{2+} to increase resistance to oxidation, and a pure sample of Cd_8-βα-rhMT in order to determine the relative speciation of the individual metal binding sites as well as the type of coordinating ligands through chemical shift data. In the $Cd_{7/8}$-βα-rhMT spectrum, peaks 1, 5, 5', 6 and 7 correspond to the α-domain, while peaks 2, 3 and 4 correspond to the β-domain (*50*). Signals observed for $Cd_{7/8}$-βα-rhMT (Figure 6-3A) include resonances at 673, 668, 650, 647, 631, 629 and 621 ppm, where the resonances at 673, 631, 629 and 621 ppm result from the α-domain and 668, 650 and 647 ppm result from the β-domain. An additional peak labeled(*) and located at 680 ppm has been previously observed and is likely the result of the presence of some metal-based heterogeneity in the Cd_7-βα-rhMT. This assignment is based, in part, on previous NMR work of human liver Cd-MT 1 by Boulanger and Armitage (*50*). The observed signals for the pure Cd_8-βα-rhMT (Figure 6-3B) are 690, 647, 637 and 595 ppm. The chemical shift range of all the peaks is between 590 and 700 ppm, which overlaps significantly with the region expected for tetrahedral cadmium-thiolate clusters (*51*). This region is commonly found for the NMR spectra of Cd-metallothioneins, as well as both trigonal cadmium thiolate and tetrahedral cadmium-thiolate clusters where a single sulfur has been replaced by water, or opportunistic chloride ion (*52*). No signals in the range of 200 to 250 nm were observed, which had been previously observed for supermetalated Cd_5-α-rhMT (*38*).

Direct detection of ^{113}Cd in the binding site allows one to infer the fluctionality of the individual metal sites. Analysis of the spectrum in Figure 6-3A shows that resonances attributed to the β-cluster are significantly less intense than those attributed to the α-cluster. Previous NMR studies involving both domains have shown the α-domain is less fluctional than the β domain leading to sharper peaks of greater intensity for the α-domain (*50*). Addition of excess $^{113}Cd^{2+}$ eliminates the spectral complexity associated with the two isolated domains. The loss of all seven unique Cd^{2+} signals associated with the Cd_7-MT and the formation of four unique peaks, strongly suggests that the addition of the singular Cd^{2+} to Cd_7-βα-rhMT leads to the loss of the isolated clusters in favor of a

coalesced, single domain of a 'super cluster'. While all four peaks are of similar size, and intensity, the signal located at 647 ppm is slightly broader and less intense. This suggests that the metal-ion associated with this binding site is more solvent exposed and fluxional. Consequently, it is likely that this smaller broader peak is the most likely candidate for the site of metal loss in the metal-exchange intermediate, allowing both the solvent and acceptor/donor proteins access to the metal-ion. The sharpness of the spectral lines further supports the interpretation of CD spectroscopic data that the maxima blue shift between Cd_7-βα-rhMT and Cd_8-βα-rhMT, with an increase in intensity of 50%, is the result of a reduction in the fluctionality of the protein.

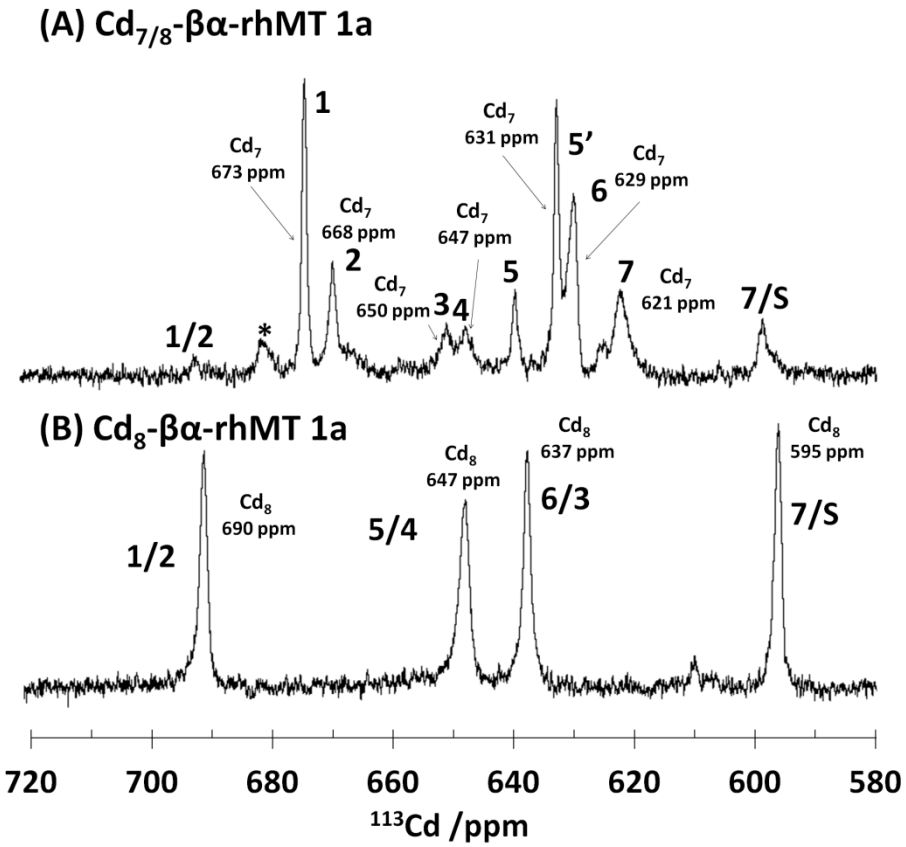

Figure 6-3. Direct 1D $^{113}Cd[^1H]$ NMR spectrum (133 MHz) of (A) a mixture of Cd_7-βα-rhMT and Cd_8-βα-rhMT and (B) Cd_8-βα-rhMT formed by addition of excess $^{113}CdCl_2$. The $Cd_{7/8}$-βα-rhMT was prepared in 5 mM ammonium formate pH 8.3 and buffer exchanged into 30% D_2O. Because of the slight excess of $^{113}Cd^{2+}$, a portion of the sample has been converted to Cd_8-βα-rhMT leading to the formation of additional peaks at 682 and 595 ppm. Subsequent addition of crystalline $^{113}CdCl_2$ to $Cd_{7/8}$-βα-rhMT led to the formation of Cd_8-βα-rhMT, which greatly simplifies the spectra reducing it to 4 peaks. Spectra of $Cd_{7/8}$-β-rhMT and Cd_8-β-rhMT were acquired at room temperature.

6.3.3 Two dimensional $^{1}H[^{113}Cd]$HSQC NMR spectroscopy of both Cd_7- and Cd_8-βα-rhMT 1a

Indirect $^{1}H[^{113}Cd]$ HSQC NMR spectra were measured for both Cd_7-βα-rhMT and Cd_8-βα-rhMT (Figure 6-4). Analysis of the β protons of the cysteine residues allowed determination of peak relatedness. Peaks were interpreted as related based on similarity in both the ^{1}H and ^{113}Cd chemical shifts. In the case of Cd_7-βα-rhMT (Figure 6-4A), both signals 1 and 2 have the same overall profile as those of the isolated domains, and are attributed to the α- and β-domain, respectively. Signals 3 and 4 result from the remaining two cadmium ions found in the β-domain and are significantly downfield compared to their counterparts found in the isolated domains (isolated β-domain 630 and 616 ppm compared with the full protein 650 and 647 ppm) (*39*). We interpret this difference as the result of the effect of the α-domain on the chemical shifts of the β-domain. Signals 5 and 5' are both attributed to the same cadmium atom found in the α-domain and have a similar cysteine β proton profile. Signals 6 and 7 both correspond to α-domain and have similar chemical shifts to those of the isolated α-domain (isolated α-domain 626 and 611 ppm compared with the full protein 629 and 621 ppm) (*38*).

The loss of cluster identity when Cd_7- is converted into Cd_8-βα-rhMT (Figure 6-4B) significantly simplifies the spectra and the addition of the 8^{th} metal ion results in dramatic changes to the β proton profile of all peaks. These changes indicate that there are significant structural rearrangements taking place to accommodate all metal ions. Interestingly, no signal was observed in the 245-215 ppm region that had previously been assigned to the supermetalated $Cd(RS)_2(OH_2)_4$ of the α-domain. This suggests that the supermetalated cadmium ion found in Cd_8-βα-rhMT is directly coordinated to at least 3 cysteine residues. With the exception of the previously mentioned $Cd(RS)_2(OH_2)_4$, the previously reported ^{113}Cd NMR data for the supermetalated isolated domains have exactly four $^{113}Cd^{2+}$ signals located between 700-600 ppm and the tentative assignment of peak identity for the Cd_8-rhMT 1 was based upon this similarity (*38*-*39*).

Note that supermetalation of the β-domain leads to an inversion of the location of the 3 and 4 peak, such that 4 is found further downfield than 3. The β proton profile of Cd_8-βα-rhMT is somewhat more complex than either isolated domain, indicating overlap of the profiles of both domains. It should be noted at this time that there are two reasons

why we have not assigned a specific cysteine residue to each 2-D signal: the first is that signals associated with the β-domain are significantly less intense than those associated with the α-domain and their overlap further complicates the spectra, the second reason is that in order to conclusively assign the identity of the peaks, one would require a complete backbone assignment. This type of assignment has been not been carried out yet for human MT-1a.

Figure 6-5 provides a graphical comparison of the NMR data for MT isoforms 1-3, as well as the supermetalated data for both Cd-MT and its isolated domains. The value of this figure is that it shows the NMR range where MT-cadmium-thiolate clusters are found. The presence of the 8^{th} cadmium atom causes both the β- and α-domains to adopt supermetalated character. This is strong evidence that this 8^{th} cadmium atom is coordinated to Cys previously in both domains. Also important to this figure is the observation that all NMR peaks, with the exception of supermetalated Cd_5-α-rhMT, fall between 700 and 590 ppm. It can be clearly seen that Cd_8-βα-rhMT, Cd_5-α-rhMT and Cd_4-β-rhMT all exhibit nearly identical ^{113}Cd signals in the 700-590 ppm range. This was a surprising result since it had been previously thought that supermetalation of the full protein would lead to either 9 unique signals, indicative of Cd_9-βα-rhMT 1a, or alternatively would only alter the metal binding sites of one of the two domains. We interpret this overlap to mean that supermetalation of the isolated domains is in fact the result of residual metal binding capacity. This is supported by CD titrations of all three, where the isolated β- and α-domains require an excess of Cd^{2+} to supermetalate and the full protein is completely supermetalated at exactly 1 equivalent (Figure 6-2). Consequently, we propose based on these experimental results, that Cd_8-βα-rhMT 1a adopts a new MT structural motif that requires the coalescence of both domains to a single binding domain.

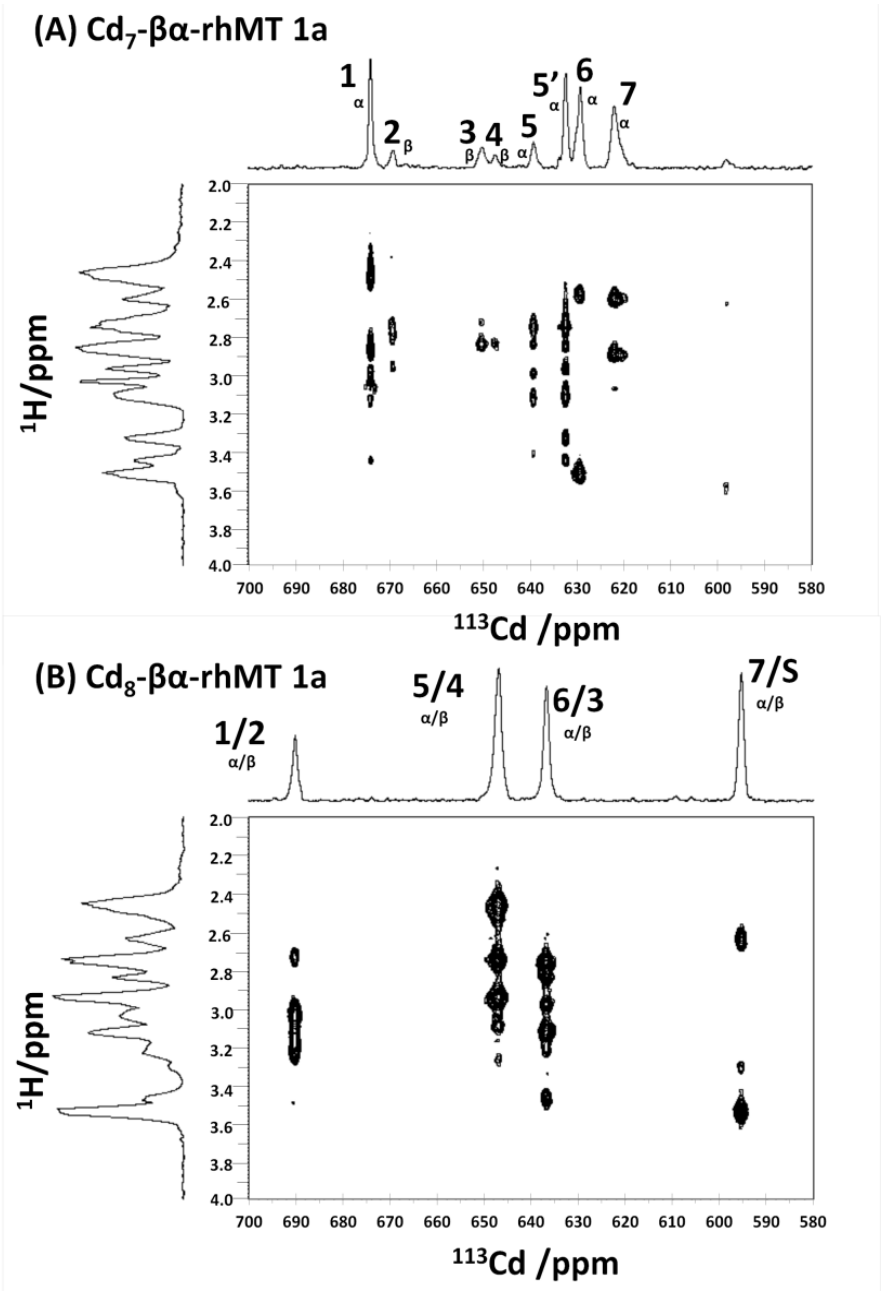

Figure 6-4. Indirect 2D $^{1}H[^{113}Cd]$ HSQC NMR of (A) Cd_7-βα-rhMT 1a and (B) Cd_8-βα-rhMT 1a formed by addition of excess $^{113}CdCl_2$. While a total of eight peaks exist for Cd_7-βα-rhMT, it can be clearly seen that 5 and 5' have similar proton profiles. This heterogeneity has been previously reported by Boulanger and Armitage and is attributed to a slight difference in two structural conformers of the protein (50). The signals in (B) are the labeled based upon the assignments of the isolated Cd_4-β-rhMT and Cd_5-α-rhMT (38-39). The peak labeled 7/S is what we consider to be the site of supermetalation and we believe that this may represent a tetrahedral geometry coordinating either four thiolates or three thiolates and a single water molecule/chloride ion.

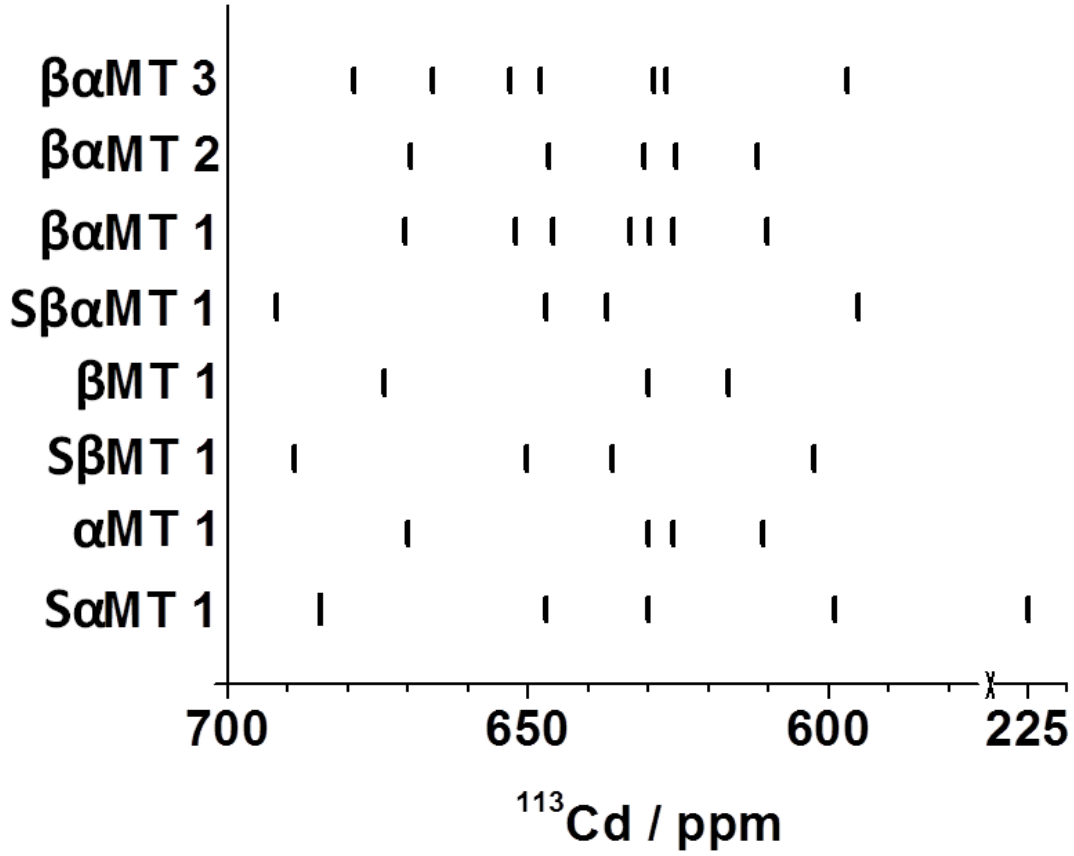

Figure 6-5. **Comparison of the ^{113}Cd NMR resonances for the human MTs**: Cd_7-βα-MT 3 (21), Cd_7-βα-MT 2 (50), Cd_7-βα-MT 1a (50), supermetalated Cd_8-βα-rhMT 1a (this work), Cd_3-β-rhMT 1a (39), supermetalated Cd_4-β-rhMT 1a, Cd_4-α-rhMT 1a and supermetalated Cd_5-α-rhMT 1a (38). Note the significant overlap in the location of signals associated with both isolated domains of MT and the full protein. The sole exception to this similarity is the presence of a single peak at 224 ppm associated with supermetalated Cd_5-α-rhMT, which is both absent from supermetalated Cd_4-β-rhMT and supermetalated Cd_8-βα-rhMT.

6.4 Discussion

For the last sixty years, MT has been proposed to be involved in metal homeostasis, toxic metal detoxification and in the protection of organisms against oxidative stress (*8*). And while it is likely that MT is involved in all three of these processes, the exact cellular function(s) have never been determined. Critical to these roles are MT's ability to act as a metallochaperone capable of coordinating incoming metal ions and exchanging them with the cellular environment. Indeed several studies have demonstrated the importance of MT in both donating to and accepting metal ions from other metalloproteins (*42-44*).

These studies have highlighted the importance of protein-protein interactions, but a metal-exchange intermediate has not been observed. Several studies have documented the preference of the β-domain for Cu^{+} ions and the α-domain for Zn^{2+}/ Cd^{2+} ions (*23, 45, 53*). Since Zn^{2+} coordination dominates mammalian MT (*54*), an incoming metal of higher binding affinity (Cd^{2+} or Cu^{+}) must either 1) coordinate in a domain specific manner, or 2) coordinate through either domain with a subsequent redistribution of metals leading to the observed metal-domain preferences. Copper luminescent studies of MT have provided evidence for a fluctional model of the protein, in which initial metalation occurs in a distributed manner, statistically across both domains, followed by a rearrangement of both clusters to their lowest energy conformers (*25, 28*). However, this model would require an intraprotein intermediate, in which both domains exchange metals with each other. To date both the β- and α-domains of fully metalated MT are considered isolated, because of both a lack of interdomain NOEs and the independence of their respective ^{113}Cd signals in NMR studies (*10, 20, 55*).

6.4.1 Location of the eighth Cd^{2+} ion in Cd_8-βα-rhMT 1a

We report here, for the first time, conclusive evidence for the presence of domain-domain interactions in fully metalated MT from experimental observation of a species in which one Cd^{2+} is proposed to bridge both domains. Formation of Cd_8-MT species results in the loss of specific α and β domain character and the formation of a single, Cd_8Cys_{20} domain. This supermetalated species provides evidence for the type of intermediate that is critically important in the metal exchange pathway necessary for the observed domain selectivity of metal ions. Implicit in this structure is the existence of a 'super domain', where both domains contribute cysteine residues to produce a single Cd_8Cys_{20} cluster in MT 1a. This supermetalated structure has been effectively 'frozen' by the higher binding constant of Cd^{2+}, compared with Zn^{2+}, and is likely critical in the metal exchange reactions necessary for MTs role as a metallochaperone.

Initial ESI-MS studies of the apo-protein of MT provided the first evidence that the Cd_7-βα-rhMT species was able to supermetalate to form Cd_8-βα-rhMT (*32*). However, prior to this report it was unclear whether this additional metal was bound to either metal-thiolate core found in the protein, or if the 8^{th} Cd^{2+} was somehow bound to other ligands.

The coupling of both spectroscopic and spectrometric analyses (Figure 6-2) demonstrates that the addition of only a single equivalent of Cd^{2+} to the fully metalated Cd_7-rhMT protein causes structural changes, which lead to a significant changes in the symmetry of the eight Cd^{2+} bound in the cluster. This rearrangement breaks the symmetry of both original clusters, observed from the simultaneous loss of exciton coupling in the CD spectrum, but with little change in the ligand-to-metal charge transfer profile. ESI-MS spectral data also show that only a single Cd^{2+} ion is found to coordinate to the protein, and further that this additional metal ion causes an increase in the relative intensity of the +6 charge state compared with the +5 charge state. This suggests that the protein must adopt a significantly larger structure to accommodate the additional metal ion. The observation of two simultaneous isodichroic points during the CD titration of Cd_7-βα-rhMT with Cd^{2+} is evidence for the direct conversion of Cd_7-βα-rhMT to Cd_8-βα-rhMT with no intermediate structures (Figure 6-2D). The location of the ^{113}Cd-NMR chemical shifts demonstrates conclusively that the additional metal directly interacts with the metal-thiolate core and that this metal ion greatly simplifies the seven unique Cd^{2+} sites to four unique Cd^{2+} sites. Taken together these results demonstrate that supermetalation of MT 1a with Cd^{2+} leads solely to the formation a bridged Cd_8Cys_{20} structure as the final product of metalation.

Based on the previous stoichiometric data for the isolated supermetalated domains of Cd_4-β-MT and Cd_5-α-MT it would be reasonable to predict that the supermetalated full protein would involve 9 Cd^{2+} ions. However, only Cd_8-MT was actually formed. This now allows us to propose that the two-domain structure does not exist generally for all metal loadings, rather only for specific metal loadings. For Zn^{2+} and Cd^{2+} this would occur at 7 metals per MT protein.

In addition to Cd-hMT-1a, Cd-hMT-3 has also been confirmed to supermetalate by 1-D ^{113}Cd NMR spectroscopy (*40*). Cd-hMT-3 is primarily found in the central nervous system and, unlike MT-1a and -2, its expression is strictly controlled (*12-13*). In the central nervous system MT-3 is thought to control metal ion homeostasis and has been shown to be downregulated in some Alzheimer's patients (*14*). Unlike Cd-hMT-1a, the supermetalated NMR spectra of Cd-hMT-3 does not simplify to four peaks. Moreover, the CD spectrum of MT-3 does not exhibit a loss of exciton coupling found in the

supermetalation of MT-1a. However, the formation of supermetalated Cd-hMT-3 does result in a decrease in the Stoke's radius of this protein, which suggests the mutual approach of the two domains. We should note that neither Meloni *et al.* studying Zn_7-MT-2 using both spectroscopic and spectrometric techniques (*40*) nor Stillman *et al.* studying rabbit liver Cd_7MT 2a by CD spectroscopy (*56*) found that MT-2 was capable of supermetalation. These differences between isoforms may be critical to the cellular role of each MT isoform. It is probable that supermetalated structures of Cd-hMT-1a and -3 are different. Based on these observations, we postulate that the ability of an MT isoform to supermetalate and the subsequent structure formed from this process are factors that lead to the differentiation of each isoform (MT-1a,-2,-3 and -4) into specific functions in cellular chemistry.

6.4.2 The proposed mechanism of metal ion homeostasis

This metal exchange structure could have significant consequences for both the metal ion homeostasis and toxic meal detoxification properties of an organism. Previous studies, using CD, UV and NMR spectroscopies have shown that Cd^{2+} binding to both apo-MT or Zn_7-MT leads to the formation of Cd_7-MT with almost identical absorption and CD properties (*23, 56-57*). These experiments suggest that regardless of initial status of the MT it is capable of assuming the same conformation when fully metalated. When the protein is fully metalated, such as Zn_7-MT, the incoming metal ion must be able to coordinate and expel a previously bound Zn^{2+}. In the case of Zn_7-MT, the formation of a transient M_1Zn_7-βα-rhMT 1a can be envisioned as an exogenous Cd^{2+}, or Cu^{+}, ion coordinating to Zn_7-βα-rhMT 1a, bridging both domains with subsequent rearrangement and expulsion of a previously bound Zn^{2+} ion. The net effect would be 1) metal ion selectivity (for example, Cu^{+} in the β-domain and Zn^{2+}/Cd^{2+} in the α-domain) and 2) upregulation of metallothionein allowing an organism to effectively combat toxic metal exposure. A regulator of metallothionein transcription, the metal-responsive-element-binding transcription factor-1 (MTF-1), has been shown to upregulate metallothionein upon binding to Zn^{2+} ions (*58-59*). MTF-1 has been implicated in cellular responses including toxic metal detoxification and oxidative stress, both of which are implicated functions of metallothionein. The metal binding site of this transcription factor includes

six Cys_2His_2 zinc fingers, making it exceptionally sensitive to an organism's zinc load. Cell free transcription experiments have shown a number of stresses, including exposure to Cd^{2+}, Cu^{+} and H_2O_2 function by displacing naturally bound Zn^{2+} from MT (*60*). These free Zn^{2+} ions bind to MTF-1 leading to a translocation of MTF-1 from the cytoplasm to the nucleus where the Zn-MTF-1 interacts with metal response elements (MREs) leading to upregulation of MT. In this way, MT is capable of countering and deactivating a wide range of insults in order to return an organism to homeostatic balance.

For this reason, supermetalation, in the context of toxic metals, may be a critical transient species in the regulation of transcription of the protein. An incoming toxic metal, such as Cd^{2+}, could coordinate in a supermetalated position allowing both sequestration of the toxic metal and release of a Zn^{2+} ion. This Zn^{2+} ion would consequently lead to the upregulation of MT, through the Zn^{2+} binding motifs of MTF-1, allowing an organism to effectively combat toxic metals. Through this mechanism, supermetalation of metallothionein, the organism would be able to control cellular metal load.

Surprisingly, we did not observe any evidence for the existence of a Cd_9-βα-rhMT species, which had previously been suggested to exist based on the summation of the metalation status of the individual supermetalated β- and α-domains. These observed supermetalated states, Cd_4-β-rhMT and Cd_5-α-rhMT, are likely the result of the residual metal binding capacity necessary for both domains to work in concert to form Cd_8-βα-rhMT. Unlike other metalation studies, which reported the collapse of the two domain structure, for example Hg- and Ag-MT, supermetalation to Cd_8-βα-rhMT does not require a change in coordination number of the metal ion (*29, 61-62*).

We have calculated a tentative model based on all eight Cd^{2+} ions being tetrahedrally coordinated to four cysteine residues, which leads to a complete collapse of the two-domain structure (Figure 6-6A). While qualitative in nature, the structure presented shows how the addition of the 8^{th} Cd^{2+} ion leads to the complete loss of cluster identity (Figure 6-6B). Through supermetalation, the bridging of both domains provides the intraprotein interactions necessary for metal ion selectivity. The coordination of the 8^{th} Cd^{2+} ion in this model accounts for the absorption, CD and NMR spectral data of Cd_8-βα-

rhMT. In the case of the CD titration, supermetalation of MT essentially locks the two domains in place resulting in a loss of conformational freedom and explains increased sharpness of the Cd_8-MT spectra. In the case of the NMR spectra, the complete collapse of the Cd7-MT spectra is the result of loss of cluster identity upon binding of the 8^{th} Cd^{2+} ion.

Much current research on MT include its interaction with metal based anticancer drugs, such as cisplatin (*63*). In these cases, MT has been implicated as a cause for the development of cisplatin resistant cancers (*64-66*). Karotki and Vasak have found that the binding of Pt^{2+} to MT occurs via a two step reaction and further that the β-domain is the preferred site of coordination. In the context of supermetalation, initial coordination likely leads to a coalescence of both domains with subsequent ejection of one of the previously bound metals of the β-domain (*67*). These researchers have also characterized a previously unknown DNA-*cis*-Pt-MT ternary structure, where coordination of the DNA bound cisplatin does not lead to the release of significant Zn^{2+} in Zn_7-MT. These results suggest that coordination occurs in a site specific manner through two sets of solvent exposed cysteine residues found in the β- and α-domain (*68*). The role of supermetalation in the initial coordination of metal-based chemotherapeutics may be of significant importance for the development of future chemotherapeutics.

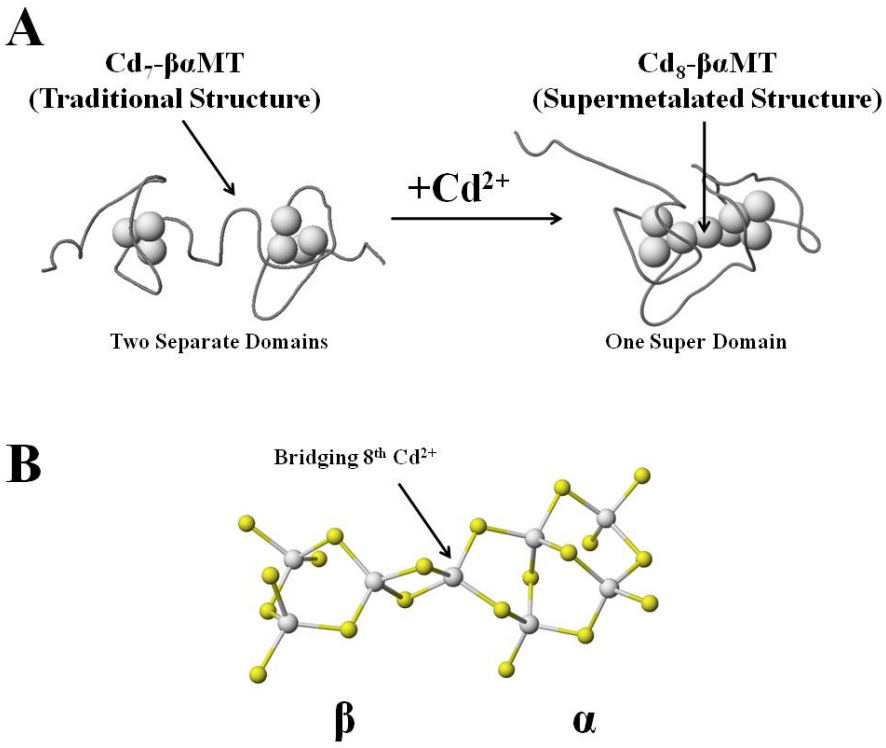

Figure 6-6. **Molecular model of a possible structure for supermetalated Cd_8-βα-rhMT 1a.** A) Ribbon structure of the backbone of Cd_7-βα-rhMT and Cd_8-βα-rhMT with the cadmium atoms represented as spheres calculated using a locally modified force-field with MM3/MD methods for molecular modeling. The N-terminal β domain is located on the left hand side, while the C-terminal α domain is located on the right-hand side. (B) The cadmium-cysteinyl-thiolate clusters of Cd_8-βα-rhMT 1a are presented as a ball-and-stick model: β domain (left) and α domain (right). The structure was created by inserting an additional Cd^{2+} ion between the two domains, and minimizing the structure in two steps: 1) 1000 ps at 500 K, and 2) 5000 ps at 300 K. The conformer with the lowest energy is presented above. The initial structure of the Cd_7-βα-rhMT 1a was provided by Chan *et al.* (22).

It is now becoming evident that MT has a significant role in the body's response to neuroinflammation (*69*). Recently, a report by Manso *et al.* has demonstrated that the full MT-1 was able to improve the performance of MT knockout mice whose cortex had been damaged through cryoinjury (*70*). Most interestingly, the authors report that exposure of the mice to the isolated MT fragments, β and α, result in markedly different recovery rates compared to the full βα-protein. While the exact mechanism of action is not known, it could be postulated that supermetalation of the full protein, which has significantly greater affinity than either of the two isolated domains, is the causative

agent in recovery. Thus full MT acts as a superior metallochaperone when compared to the isolated domains.

6.5 Conclusion

In summary, the collapse in the number of unique ^{113}Cd-NMR peaks from seven to four, the significant changes in the CD spectral envelope and the quantitative formation of Cd_8-βα-rhMT, and not Cd_9-βα-rhMT, are paradigm shifting with respect to the structural motifs in metallothionein. The spectroscopic evidence reported in this paper indicate that the β- and α-clusters act in isolation under only very specific metalation conditions. The supermetalated Cd_8-rhMT 1a protein adopts a novel single domain structure suggesting that the well-known two-domain structure might be the special case in the metal-dependent structural landscape of MTs. Further, with these results we are now able to account for both the ability of MT to exchange metals with the solution and the observed metal ion selectivity of the individual domains.

6.6 References

1. Margoshes, M., and Vallee, B. L. (1957) A cadmium protein from equine kidney cortex, *J. Am. Chem. Soc. 79*, 4813-4814.
2. Kojima, Y. (1991) Definitions and Nomenclature of Metallothioneins, In *Methods in Enzymology: Metallobiochemistry Part B Metallothionein and Related Molecules* (Riordan, J. F., and Vallee, B. L., Eds.), Academic Press, Inc., San Diego.
3. Kagi, J. H. R. (1993) Evolution, structure and chemical acitivity of class I metallothioneins: An overview., In *Metallothionein III: Biological roles and medical implications* (Suzuki, K. T., Imura, N., and Kimura, M., Eds.), Birkhauser-Verlag, Berlin.
4. Blindauer, C. A., Harrison, M. D., Parkinson, J. A., Robinson, A. K., Cavet, J. S., Robinson, N. J., and Sadler, P. J. (2001) A metallothionein containing a zinc finger within a four-metal cluster protects a bacterium from zinc toxicity, *Proc. Natl. Acad. Sci. U.S.A 98*, 9593-9598.
5. Freisinger, E. (2011) Structural features of specific to plant metallothioneins, *J. Biol. Inorg. Chem. 16*, 1035-1045.
6. Zeitoun-Ghandour, S., Charnock, J. M., Hodson, M. E., Leszczyszyn, O. I., Blindauer, C. A., and Sturzenbaum, S. R. (2010) The two *Caenorhabditis elegans* metallothioneins (CeMT-1 and CeMT-2) discriminate between essential zinc and toxic cadmium, *FEBS J. 277*, 2531-2542.
7. Stillman, M. J. (1995) Metallothioneins, *Coord. Chem. Rev. 144*, 461-511.

8. Sutherland, D. E. K., and Stillman, M. J. (2011) The "magic numbers" of metallothionein, *Metallomics 3*, 444-463.
9. Robbins, A. H., McRee, D. E., Williamson, M., Collett, S. A., Xuong, N. H., Furey, W. F., Wang, B. C., and Stout, C. D. (1991) Refined crystal structure of Cd, Zn metallothionein at 2.0 Å resolution, *J. Mol. Biol. 221*, 1269-1293.
10. Messerle, B. A., Schaffer, A., Vasak, M., Kagi, J. H. R., and Wuthrich, K. (1990) Three-dimensional structure of human [$^{113}Cd_7$]metallothionein-2 in solution determined by nuclear magnetic resonance spectroscopy, *J. Mol. Biol. 214*, 765-779.
11. Messerle, B. A., Schaffer, A., Vasak, M., Kagi, J. H. R., and Wuthrich, K. (1992) Comparison of the solution conformations of human [Zn_7]-metallothionein-2 and [Cd_7]-metallothionein-2 using nuclear magnetic resonance spectroscopy, *J. Mol. Biol. 225*, 433-443.
12. Kramer, K. K., Zoelle, J. T., and Klaassen, C. D. (1996) Induction of metallothionein mRNA and protein in primary murine neuron cultures, *Toxicol. Appl. Pharmacol. 141*, 1-7.
13. Kramer, K. K., Liu, J., Choudhuri, S., and Klaassen, C. D. (1996) Induction of metallothionein mRNA and protein in murine astrocyte cultures, *Toxicol. Appl. Pharmacol. 136*, 94-100.
14. Uchida, Y., Takio, K., Titani, K., Ihara, Y., and Tomonaga, M. (1991) The growth inhibitory factor that is deficient in the alzheimer's disease brain is a 68 amino acid metallothionein-like protein, *Neuron 337-347*.
15. Quaife, C. J., Findley, S. D., Erickson, J. C., Froelick, G. J., Kelly, E. J., Zambrowicz, B. P., and Palmiter, R. D. (1994) Induction of a new metallothionein isoform (MT-IV) occurs during differentiation of stratified squamous epithelia, *Biochemistry 33*, 7250-7259.
16. Quaife, C. J., Kelly, E. J., Masters, B. A., Brinster, R. L., and Palmiter, R. D. (1998) Ectopic expression of metallothionein-III causes pancreatic acinar cell necrosis in transgenic mice, *Toxicol. Appl. Pharmacol. 148*, 148-157.
17. Calderone, V., Dolderer, B., Hartmann, H.-J., Echner, H., Luchinat, C., Bianco, C. D., Mangani, S., and Weser, U. (2005) The crystal structure of yeast copper thionein: The solution of a long-lasting enigma, *Proc. Natl. Acad. Sci. U.S.A 102*, 51-56.
18. Arseniev, A., Schultze, P., Worgotter, E., Braun, W., Wagner, G., Vasak, M., Kagi, J. H. R., and Wuthrich, K. (1988) Three-dimensional structure of rabbit liver [Cd_7]metallothionein-2a in aqueous solution determined by nuclear magnetic resonance, *J. Mol. Biol. 201*, 637-657.
19. Schultze, P., Worgotter, E., Braun, W., Wagner, G., Vasak, M., Kagi, J. H. R., and Wuthrich, K. (1988) Conformation of [Cd_7]-metallothionein-2 from rat liver in aqueous solution determined by nuclear magnetic resonance spectroscopy, *J. Mol. Biol. 203*, 251-268.
20. Zangger, K., Oz, G., Otvos, J. D., and Armitage, I. M. (1999) Three-dimensional solution structure of mouse [Cd_7]-metallothionein-1 by homonuclear and heteronuclear NMR spectroscopy, *Protein Sci. 8*, 2630-2638.

21. Wang, H., Zhang, Q., Cai, B., Li, H., Sze, K.-H., Huang, Z.-X., Wu, H.-M., and Sun, H. (2006) Solution structure and dynamics of human metallothionein-3 (MT-3), *FEBS Lett. 580*, 795-800.
22. Chan, J., Huang, Z., Watt, I., Kille, P., and Stillman, M. J. (2007) Characterization of the conformational changes in recombinant human metallothioneins using ESI-MS and molecular modeling, *Can. J. Chem. 85*, 898-912.
23. Briggs, R. W., and Armitage, I. M. (1982) Evidence for site-selective metal binding in calf liver metallothionein, *J. Biol. Chem. 257*, 1259-1262.
24. Li, H., and Otvos, J. D. (1996) ^{111}Cd NMR studies of the domain specificity of Ag^+ and Cu^+ binding to metallothionein, *Biochemistry 35*, 13929-13936.
25. Salgado, M. T., and Stillman, M. J. (2004) Cu^+ distribution in metallothionein fragments, *Biochem. Biophys. Res. Commun. 318*, 73-80.
26. Ngu, T. T., Easton, A., and Stillman, M. J. (2008) Kinetic analysis of arsenic - metalation of human metallothionein: Significance of the two-domain structure, *J. Am. Chem. Soc. 130*, 17016-17028.
27. Nielson, K. B., Atkin, C. L., and Winge, D. R. (1985) Distinct metal-binding configurations in metallothionein, *J. Biol. Chem. 260*, 5342-5350.
28. Green, A. R., Presta, A., Gasyna, Z., and Stillman, M. J. (1994) Luminescent probe of copper-thiolate cluster formation within mammalian metallothionein, *Inorg. Chem. 33*, 4159-4168.
29. Cai, W., and Stillman, M. J. (1988) Hg_{18}-metallothionein, *J. Am. Chem. Soc. 110*, 7872-7873.
30. Ngu, T. T., Dryden, M. D. M., and Stillman, M. J. (2010) Arsenic transfer between metallothionein proteins at physiological pH, *Biochem. Biophys. Res. Commun. 401*, 69-74.
31. Gehrig, P. M., You, C., Dallinger, R., Gruber, C., Brouwer, M., Kagi, J. H. R., and Hunziker, P. E. (2000) Electrospray ionization mass spectrometry of zinc, cadmium, and copper metallothioneins: Evidence for metal-binding cooperativity, *Protein Sci. 9*, 395-402.
32. Sutherland, D. E. K., and Stillman, M. J. (2008) Noncooperative cadmium(II) binding to human metallothionein 1a, *Biochem. Biophys. Res. Commun. 372*, 840-844.
33. Ngu, T. T., Krecisz, S., and Stillman, M. J. (2010) Bismuth binding studies to the human metallothionein using electrospray mass spectrometry, *Biochem. Biophys. Res. Commun. 396*, 206-212.
34. Rigby-Duncan, K. E., and Stillman, M. J. (2007) Evidence for noncooperative metal binding to the α domain of human metallothionein, *FEBS J. 274*, 2253-2261.
35. Palumaa, P., Eriste, E., Njunkova, O., Pokras, L., Jornvall, H., and Sillard, R. (2002) Brain-specific metallothionein-3 has higher metal-binding capacity than ubiquitous metallothioneins and binds metals noncooperatively, *Biochemistry 41*, 6158-6163.
36. Ngu, T. T., and Stillman, M. J. (2006) Arsenic binding to human metallothionein, *J. Am. Chem. Soc. 128*, 12473-12483.

37. Krezel, A., and Maret, W. (2007) Dual nanomolar and picomolar Zn(II) binding properties of metallothionein, *J. Am. Chem. Soc. 129*, 10911-10921.
38. Rigby-Duncan, K. E., Kirby, C. W., and Stillman, M. J. (2008) Metal exchange in metallothioneins - a novel structurally significant Cd_5 species in the alpha domain of human metallothionein 1a *FEBS J. 275*, 2227-2239.
39. Sutherland, D. E. K., Willans, M. J., and Stillman, M. J. (2010) Supermetalation of the β domain of human metallothionein 1a, *Biochemistry 49*, 3593-3601.
40. Meloni, G., Polanski, T., Braun, O., and Vasak, M. (2009) Effects of Zn^{2+}, Ca^{2+}, and Mg^{2+} on the structure of Zn_7metallothionein-3: Evidence for an additional zinc binding site, *Biochemistry 48*, 5700-5707.
41. Palumaa, P., Njunkova, O., Pokras, L., Eriste, E., Jornvall, H., and Sillard, R. (2002) Evidence for non-isostructural replacement of Zn^{2+} and Cd^{2+} in the β-domain of brain-specific metallothionein-3, *FEBS Lett. 527*, 76-80.
42. Feng, W., Cai, J., Pierce, W. M., Franklin, R. B., Maret, W., Benz, F. W., and Kang, Y. J. (2005) Metallothionein transfers zinc to mitochondrial aconitase through a direct interaction in mouse hearts, *Biochem. Biophys. Res. Commun. 332*, 853-858.
43. Mason, A. Z., Perico, N., Moeller, R., Thrippleton, K., Potter, T., and Lloyd, D. (2004) Metal donation and apo-metalloenzyme activation by stable isotopically labeled metallothionein, *Mar. Environ. Res. 58*, 371-375.
44. Maret, W., Larsen, K. S., and Vallee, B. L. (1997) Coordination dynamics of biological zinc "clusters" in metallothioneins and in the DNA-binding domain of the transcription factor Gal4, *Proc. Natl. Acad. Sci. U.S.A 94*, 2233-2237.
45. Meloni, G., Sonois, V., Delaine, T., Guilloreau, L., Gillet, A., Teissie, J., Faller, P., and Vasak, M. (2008) Metal swap between Zn_7-metallothionein-3 and amyloid-β-Cu protects against amyloid-β toxicity, *Nat. Chem. Biol. 4*, 366-372.
46. Chan, J., Merrifield, M. E., Soldatov, A. V., and Stillman, M. J. (2005) XAFS spectral analysis of the cadmium coordination geometry in cadmium thiolate clusters in metallothionein, *Inorg. Chem. 44*, 4923-4933.
47. Ejnik, J. W., Munoz, A., DeRose, E., III, C. F. S., and Petering, D. H. (2003) Structural consequences of metallothionein dimerization: Solution structure of the isolated Cd_4-α-domain and comparison with the holoprotein dimer, *Biochemistry 42*, 8403-8410.
48. Felitsyn, N., Peschke, M., and Kebarle, P. (2002) Origin and number of charges observed on multiply-protonated native proteins produced by ESI, *Int. J. Mass spectrom. 219*, 39-62.
49. Kebarle, P., and Verkerk, U. H. (2009) Electrospray: From ions in solution to ions in the gas phase, what we know now, *Mass Spectrom. Rev. 28*, 898-917.
50. Boulanger, Y., and Armitage, I. M. (1982) ^{113}Cd NMR study of the metal cluster structure of human liver metallothionein, *J. Biol. Inorg. Chem. 17*, 147-153.
51. Ellis, P. D. (1983) Cadmium-113 magnetic resonance spectroscopy, *Science 221*, 1141-1146.
52. Iranzo, O., Jakusch, T., Lee, K.-H., Hemmingsen, L., and Pecoraro, V. L. (2009) The correlation of ^{113}Cd NMR and ^{111m}Cd PAC spectroscopies provides a

powerful approach for the characterization of the structure of Cd^{II}-substituted Zn^{II} protein, *Chem. Eur. J. 15*, 3761-3772.

53. Jensen, L. T., Peltier, J. M., and Winge, D. R. (1998) Identification of a four copper folding intermediate in mammalian copper metallothionein by electrospray ionization mass spectrometry, *J. Biol. Inorg. Chem. 3*, 627-631.
54. Li, Y., and Maret, W. (2008) Human metallothionein metallomics, *J. Anal. At. Spectrom. 23*, 1055-1062.
55. Boulanger, Y., Armitage, I. M., Miklossy, K.-A., and Winge, D. R. (1982) ^{113}Cd NMR study of a metallothionein fragment: Evidence for a two-domain structure, *J. Biol. Chem. 257*, 13717-13719.
56. Stillman, M. J., Cai, W., and Zelazowski, A. J. (1987) Cadmium binding to metallothionein: Domain specificity in reactions of α and β fragments, apometallothionein, and zinc metallothionein with Cd^{2+}, *J. Biol. Chem. 262*, 4538-4548.
57. Willner, H., Vasak, M., and Kagi, J. H. R. (1987) Cadmium-thiolate clusters in metallothionein: Spectrophotometric and spectropolarimetric features, *Biochemistry 26*, 6287-6292.
58. Chen, X., Chu, M., and Giedroc, D. P. (1999) MRE-binding transcription factor-1: Weak zinc-binding finger domains 5 and 6 modulate the structure, affinity, and specificity of the metal-response element complex, *Biochemistry 38*, 12915-12925.
59. Giedroc, D. P., Chen, X., Pennella, M. A., and LiWang, A. C. (2001) Conformational heterogeneity in the C-terminal zinc fingers of human MTF-1, *J. Biol. Chem. 276*, 42322-42332.
60. Zhang, B., Georgiev, O., Hagmann, M., Gunes, C., Cramer, M., Faller, P., Vasak, M., and Schaffner, W. (2003) Activity of metal-responsive transcription factor 1 by toxic heavy metals and H_2O_2 in vitro is modulated by metallothionein, *Mol. Cell. Biol. 23*, 8471-8485.
61. Salgado, M. T., Bacher, K. L., and Stillman, M. J. (2007) Probing structural changes in the α and β domains of copper- and silver-substituted metallothionein by emission spectroscopy and electrospray ionization mass spectrometry, *J. Biol. Inorg. Chem. 12*, 294-312.
62. Palacios, O., Polec-Pawlak, K., Lobinski, R., Capdevila, M., and Gonzalez-Duarte, P. (2003) Is Ag(I) an adequate probe for Cu(I) in structural-copper-metallothionein studies?, *J. Biol. Inorg. Chem. 8*, 831-842.
63. Knipp, M. (2009) Metallothioneins and platinum(II) anti-tumor compounds, *Curr. Med. Chem. 16*, 522-537.
64. Hagrman, D., Goodisman, J., Dabrowiak, J. C., and Souid, A.-K. (2003) Kinetic study on the reaction of cisplatin with metallothionein, *Drug Metab. Dispos. 31*, 916-923.
65. Knipp, M., Karotki, A. V., Chesnov, S., Natile, G., Sadler, P. J., Brabec, V., and Vasak, M. (2007) Reaction of Zn_7Metallothionein with *cis*- and *trans*-[Pt(N-donor)$_2$Cl$_2$] anticancer complexes: *trans*-Pt^{II} complexes retain their N-donor ligands, *J. Med. Chem. 50*, 4075-4086.

66. Casini, A., Karotki, A., Gabbiani, C., Rugi, F., Vasak, M., Messori, L., and Dyson, P. J. (2009) Reactivity of an antimetastatic organometallic ruthenium compound with metallothionein-2: Relevance to the mechanism of action, *Metallomics 1*, 434-441.
67. Karotki, A. V., and Vasak, M. (2009) Reaction of human metallothionein-3 with cisplatin and transplatin, *J. Biol. Inorg. Chem. 14*, 1129-1138.
68. Karotki, A. V., and Vasak, M. (2008) Interaction of metallothionein-2 with platinum-modified 5'-guanosine monophosphate and DNA, *Biochemistry 47*, 10961-10969.
69. Manso, Y., Adlard, P. A., Carrasco, J., Vasak, M., and Hidalgo, J. (2011) Metallothionein and brain inflammation, *J. Biol. Inorg. Chem. 16*, 1103-1113.
70. Manso, Y., Serra, M., Comes, G., Giralt, M., Carrasco, J., Cols, N., Vasak, M., Gonzalez-Duarte, P., and Hidalgo, J. (2010) The comparison of mouse full metallothionein-1 versus α and β domains and metallothionein-1-to-3 mutation following traumatic brain injury reveals different biological motifs, *J. Neurosci. Res. 88*, 1708-1718.

Chapter 7. Conclusion[7]

Metallothionein is a small cysteine rich protein, which was first isolated more than sixty years ago (*1*). In that time, it has been implicated in a number of roles, including toxic metal detoxification, metal ion homeostasis, and as a protective agent against oxidative stress (*2*). MT is found in all organisms and has been isolated from a number of sources (*3*). It is therefore quite surprising that while there exists a significant body of evidence to support all three roles, the exact *in vivo* function(s) of MT and its associated binding partners is not known. Two potential reasons for this lack of specific function(s) includes: 1) an ambiguous mechanism of metalation, and 2) a lack of metal binding motifs. In the first case, the mechanism of metal binding seriously impacts both the ability of MT to act as a dynamic metallochaperone, and the biologically relevant partially metalated states of the protein. If MT were to coordinate metals in a cooperative manner, then partially metalated forms of the protein would be unstable and unlikely to take part in cellular chemistry. As such, only the fully metalated (Zn_7-MT) and apo forms of the protein are biologically relevant. Indeed to address the lack of an exact function, much research has recently focused on the metalation chemistry of the apo form of the protein (*4-7*).

MT has also been traditionally considered a two-domain protein. The structure has always been thought to contain two independent metal-binding domains: an N-terminal β-domain, which can bind 3 Zn^{2+}, Cd^{2+}, or 6 Cu^{+} ions, and a C-terminal α-domain, which can bind 4 Zn^{2+}, Cd^{2+}, or 6 Cu^{+} ions. The most well known mammalian form is Zn_7-MT (*8-10*), and Zn^{2+} is the dominant metal found in human MT. Cu^{+} is also found, particularly in fetal MT, and finally also Cd^{2+}, due to environmental exposure(*11*). But in all three cases, metalation is thought to involve two independent metal-binding domains. Most interestingly, there exists no metal-exchange intermediate to account for these metalated forms.

---

[7] A version of this work is in preparation
D.E.K. Sutherland, K.L. Summers and M.J. Stillman (2012).

The research in this thesis demonstrates that the mechanism of metalation is noncooperative (*12-14*). Consequently, partially metalated forms of the protein are stable and may take part in cellular chemistry. Information regarding the metal-binding mechanism was extracted from the analysis of the metalated states of the isolated domains, and full MT protein, in the presence of sub-stoichiometric amounts of Zn^{2+}, or Cd^{2+} (*12*). In this way detection of only the fully metalated and the metal-free protein would indicate a cooperative mechanism, while the formation of a mixture of intermediate partially metalated species would indicate a non-cooperative mechanism of metalation. The results presented in this thesis on the metalation of apo-α-, apo-β and apo-βα-rhMT 1a with sub-stoichiometric concentrations of Cd^{2+} , or Zn^{2+}, at slightly basic pH showed the formation of stable, partially-metalated domain species as detected by ESI-mass spectrometry (Chapters 3 and 4). These results unequivocally confirmed a non-cooperative metalation mechanism for both Cd^{2+} and Zn^{2+}.

The work presented here also provides evidence for the existence of at least 2 additional and previously unknown motifs of metalation. A thorough understanding of all possible metal binding motifs of MT is essential for a complete understanding of the *in vivo* functions of MT. For example, Zn_7-MT is often cited as cellular buffer against toxic metals, Cd^{2+} and Hg^{2+}. In this case, an incoming metal ion of greater affinity than the resident zinc will coordinate forming a transient M_1Zn_7-MT, where M is the incoming metal ion, with concomitant rearrangement and expulsion of the previously bound Zn^{2+} ion to form M_1Zn_6-MT. To date no known metal exchange intermediate has been discovered and it is unknown exactly how MT reaches equilibrium with the metal ions in the cell. Furthermore the mechanism by which MT can selectively isolate different metal ions into both domains (Zn^{2+} and Cd^{2+} prefer the α-domain, while Cu^{+} prefers the β-domain) is not known, but is of critical importance to the function of MT (*15-16*). This question also has practical implications since MT overexpression is thought to be a mechanism that allows cancer cells to overcome metal based chemotherapeutics, for example cisplatin (*17-19*). The only partially metalated form that has previously been described as relevant is one in which the α-domain is completely metalated (4 Zn^{2+} ions) and the β-domain is completely demetalated (0 Zn^{2+} ions) (*20*). However, with a noncooperative mechanism of metalation, all partially metalated structure may be stable,

depending on metal ion availability, and a thorough understanding of each is a prerequisite for a complete understanding of the roles of MT during Zn^{2+} deficiency. It is, therefore, highly unlikely that one domain would be filled, while the other remains empty. More likely is a reversion of the protein to a partially metalated motif, which could incorporate cysteine residues from both domains to bind the metal ions.

In this thesis, the mechanism of metal binding and the subsequent structural motifs formed in MT 1a were investigated. Three proposals naturally fall from these results: 1) The mechanism of metalation is in fact always noncooperative, meaning that the partially metalated forms of the protein are stable and could potentially take part in cellular chemistry, and 2) two additional metal binding motifs of MT exist, the first is a supermetalated form of the protein, where an eighth Cd^{2+} ion is coordinated to both domains, and the second is a submetalated form of the protein, where five Zn^{2+} ions are each coordinated to four terminal thiol groups, where terminal thiol groups defines a cysteine residue coordinated to only a single metal ion. Taken together, these results fundamentally alter our understanding of the metalation properties of the protein by not only demonstrating that, in fact, all partially metalated forms of the protein are stable and the dominant species is directly dependent on the concentration of metal ions present, but also that cluster formation occurs only upon the addition of the sixth Zn^{2+} ion and further that addition of excess Cd^{2+} leads to the formation of a novel Cd_8-MT species. This latter species is of particular interest, since the addition of Cd^{2+} to Zn_7-MT leads to the mixed metals species until 7.0 molar equivalents have been added at which point Cd_7-MT exists. We postulate that Cd_8-MT is in fact a 'frozen' metal-exchange intermediate that is observable due to the higher association constant of Cd^{2+} compared to Zn^{2+}.

In order of significance we have discussed above: Noncooperativity. This led to the understanding that partial metalation was stable and, therefore, able to take part in cellular chemistry.

Sub-saturated metalation. In Chapter 4, we demonstrated that the onset of cluster formation, which is defined by the use of bridging Cys thiolate ligands rather than terminal Cys, leads to a significant decrease in the Zn^{2+} binding affinity to MT and its domains for further metalation. The switch from terminal to bridging Cys to accommodate an increase in Zn^{2+} in the binding sites reduces the binding affinity. These

mass spectral data allow us to conclude for the full MT protein that the decreasing association constants necessary for a noncooperative mechanism of metalation allow formation of a stable Zn_5-βα-rhMT species, which contains no bridging interactions. This is a single binding site domain and is mechanistically a key member of the metalation pathway from apo-MT to the fully metalated Zn_7-MT. In addition, we have used this model to reinterpret the Co^{2+} titration of MT(*21*). By allowing for the existence of a non-clustered Zn_5-MT intermediate, we were able to reproduce the data presented by Vasak and Kagi, and more importantly, reinterpret their data in the context of a noncooperative mechanism of metalation.

Supermetalation. To date, all reports regarding the speciation of the mammalian MT protein state a maximum of seven Cd^{2+} or Zn^{2+} ions coordinating 20 cysteinyl thiolate ligands. These metal ions are divided between the β-domain (3 Cd^{2+} or Zn^{2+}) and α-domain (4 Cd^{2+} or Zn^{2+}). The work in Chapters 5 and 6, as well as a previous report By Rigby-Duncan *et al.* (*22*), have shown that human MT-1a isoform is capable of expanding its cluster to accommodate an eighth Cd^{2+} ion by the addition of 1.0 molar equivalents excess of Cd^{2+} ions to solution (Chapter 6)(*23*). Based upon the chemical shift range of the NMR spectra, the coordination geometry of this eighth site is predicted to include tetrahedral geometry coordinating cysteine residues from both domains. In addition, the breaking of exciton coupling in the CD spectra would suggest that this eighth metal ion is directly interacting with the metal-thiolate clusters of both domains. The existence of a supermetalated state for the α-domain had been previously determined (*24*). When combined with the ability of the β-domain to supermetalate, it had been previously predicted that supermetalation of the full protein would include two additional Cd^{2+} ions binding to both domains. It was therefore quite surprising that only a single Cd^{2+} ion bound to form Cd_8-MT. This result is critically important because this structure, for the first time, provides definitive evidence for the existence of domain-domain interactions. When the protein is fully metalated, such as Zn_7-MT, the incoming metal ion must be able to coordinate and expel a previously bound Zn^{2+}. These interactions provide a rationale for two important features of MT: metal ion equilibration with cellular environment, and the ability for each domain to discriminate between metal ions (Zn^{2+} and Cd^{2+} in the α-domain, and Cu^{+} in the β-domain).

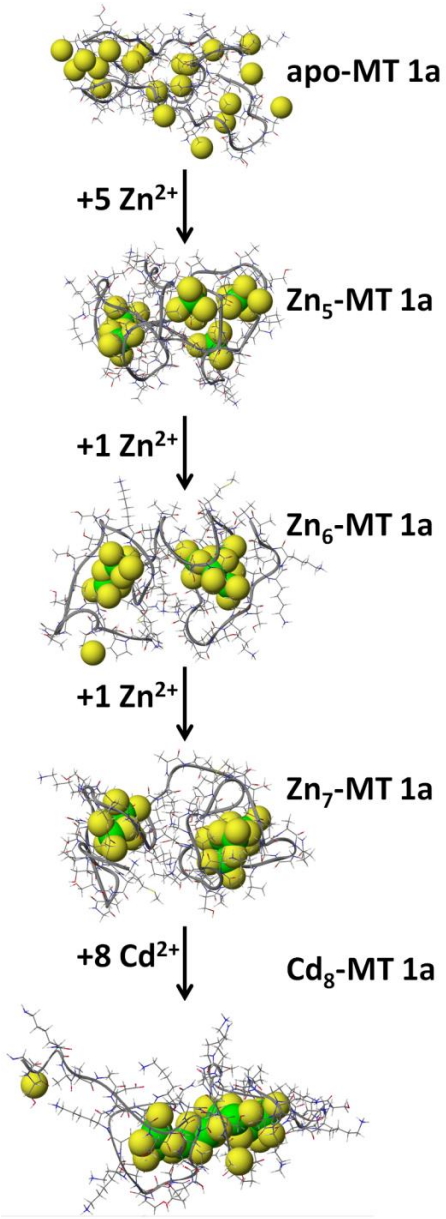

Figure 7-1. Molecular models of the metalation of apo- to Zn_7-MT, then to Cd_8-MT. The first four structures represent the sequential metalation of apo-MT using Zn^{2+}, while the last structure demonstrates the effect of the addition of 8 equivalents of Cd^{2+}. The traditional two-domain structure of MT is observed in Zn_6- and Zn_7-MT. However, prior to 6 molar equivalents of Zn^{2+} added, and following the addition of 8 molar equivalents of Cd^{2+}, the two domain structure collapses. Zn_5-MT was created by coordinating 1 Zn^{2+} ion to every 4 consecutive cysteine residues with respect to the sequence. Zn_6-MT was created by removing a Zn^{2+} ion from the β-domain of MT. Cd_8-MT was created by coordinating an additional 8^{th} Cd^{2+} ion to the exposed residues of both domains. All structures were minimized in two steps: 1) 1000 ps at 500 K, and 2) 5000 ps at 300 K. The conformer with the lowest energy is presented above. The initial structure of the Cd_7-βα-rhMT 1a was provided by Chan *et al.***(25).**

Concluding remarks. The results presented in this thesis support a paradigm altering view of MT, in which the two-domain nature of metallothionein is, in fact, the exceptional case. In the early stages of metalation, metal ions, such as Zn^{2+}, bind MT in a noncooperative manner. In the new model based on the experimental data described in this thesis, clustering, a key feature of MT, does not occur until all cysteine residues are bound terminally, that is after 5 Zn^{2+} have bound. Following this, bridging occurs to lead to the more traditional two-domain structure. Consequently, Zn_5-MT, where all twenty cysteine residues of MT are terminally coordinating five Zn^{2+} ions, will not contain any free thiol groups. MT is often considered a protective agent against oxidative stress. A metallothionein redox cycle, connecting oxidants with the redox silent Zn^{2+}, has been suggested to account for the protective role of MT in the cell. Initially a ROS oxidizes MT leading to Zn^{2+} release. This Zn^{2+} then acts to up regulates Zn-dependent proteins, through MTF-1, and subsequently reduction of MT using glutathione, or replacement with *de novo* synthesized MT and reestablishment of zinc homeostasis(*26*). With these results, one can now begin to assess the redox potential of the differently metalated versions of MT (Zn_1- to Zn_5-MT), and how metalation of all the cysteine residues, forming Zn_5-MT, affects its ability to act as a protective agent. It is possible that the subtle control of the redox activity of Zn_5-MT controls its biological activity - the change from terminal Cys to one free Cys (and therefore available SH groups) or additionally to a bridging Cys may be a low energy reaction allowing for active but controlled redox properties.

Metallothionein has also been implicated in metal-ion homeostasis, and as a protective agent against toxic metal insults (*2*). However, no metal-exchange intermediate has been isolated. The results presented in this thesis now demonstrate that MT is capable of binding an additional eighth Cd^{2+} ion to form Cd_8-MT (*23, 27*). This species is stabilized due to the higher affinity of Cd^{2+} ions for thiols, compared with Zn^{2+} ions. Unique to this structure is the bridging of both domains to coordinate the eighth metal ion. We propose that when the protein is fully metalated, such as Zn_7-MT, the incoming metal ion must be able to coordinate and expel a previously bound Zn^{2+}. In the case of Zn_7-MT, the formation of a transient M_1Zn_7-βα-rhMT 1a can be envisioned as an exogenous Cd^{2+}, or

Cu^{+}, ion coordinating to Zn_7-βα-rhMT 1a, bridging both domains with subsequent rearrangement and expulsion of a previously bound Zn^{2+} ion.

Finally, we propose a metalation chart (Figure 7-1), which begins with metal-free MT, which progressively metalates to Zn_5-MT, at which point there are no free thiols. Following this, the binding of the 6^{th} and 7^{th} Zn^{2+}'s leads to the formation of the more traditional two-domain structure. MT is capable of coordinating eight structurally unique Cd^{2+} ions leading to the formation of Cd_8-MT, where the two-domains have collapsed to form one 'super-domain.' The value of this diagram is that it shows progressive metalation of the protein, and highlights the early stages of metalation (apo- to Zn_5-MT), which are important in the protection of an organism against oxidative stress, as well as the latter stages of metalation (Zn_7- to Cd_8-MT), which are important in protecting an organism against toxic metal insult and in maintain the metal ion homeostasis of an organism.

7.1 References

1. Margoshes, M., and Vallee, B. L. (1957) A cadmium protein from equine kidney cortex, *J. Am. Chem. Soc. 79*, 4813-4814.
2. Sutherland, D. E. K., and Stillman, M. J. (2011) The "magic numbers" of metallothionein, *Metallomics 3*, 444-463.
3. Kagi, J. H. R. (1993) Evolution, structure and chemical acitivity of class I metallothioneins: An overview., In *Metallothionein III: Biological roles and medical implications* (Suzuki, K. T., Imura, N., and Kimura, M., Eds.), Birkhauser-Verlag, Berlin.
4. Rigby, K. E., Chan, J., Mackie, J., and Stillman, M. J. (2006) Molecular dynamics study on the folding and metalation of the individual domains of metallothionein, *Proteins Struct. Funct. Bioinf. 62*, 159-172.
5. Rigby-Duncan, K. E., and Stillman, M. J. (2006) Metal-dependent protein folding: Metalation of metallothionein, *J. Inorg. Biochem. 100*, 2101-2107.
6. Rigby, K. E., and Stillman, M. J. (2004) Structural studies of metal-free metallothionein, *Biochem. Biophys. Res. Commun. 325*, 1271-1278.
7. Petering, D. H., Zhu, J., Krezoski, S., Meeusen, J., Kiekenbush, C., Krull, S., Specher, T., and Dughish, M. (2006) Apo-metallothionein emerging as a major player in the cellular activities of metallothionein, *Exp. Biol. Med. 231*, 1528-1534.
8. Messerle, B. A., Schaffer, A., Vasak, M., Kagi, J. H. R., and Wuthrich, K. (1990) Three-dimensional structure of human [$^{113}Cd_7$]metallothionein-2 in solution determined by nuclear magnetic resonance spectroscopy, *J. Mol. Biol. 214*, 765-779.

9. Messerle, B. A., Schaffer, A., Vasak, M., Kagi, J. H. R., and Wuthrich, K. (1992) Comparison of the solution conformations of human [Zn_7]-metallothionein-2 and [Cd_7]-metallothionein-2 using nuclear magnetic resonance spectroscopy, *J. Mol. Biol. 225*, 433-443.
10. Robbins, A. H., McRee, D. E., Williamson, M., Collett, S. A., Xuong, N. H., Furey, W. F., Wang, B. C., and Stout, C. D. (1991) Refined crystal structure of Cd, Zn metallothionein at 2.0 Å resolution, *J. Mol. Biol. 221*, 1269-1293.
11. Li, Y., and Maret, W. (2008) Human metallothionein metallomics, *J. Anal. At. Spectrom. 23*, 1055-1062.
12. Sutherland, D. E. K., and Stillman, M. J. (2008) Noncooperative cadmium(II) binding to human metallothionein 1a, *Biochem. Biophys. Res. Commun. 372*, 840-844.
13. Rigby-Duncan, K. E., and Stillman, M. J. (2007) Evidence for noncooperative metal binding to the α domain of human metallothionein, *FEBS J. 274*, 2253-2261.
14. Palumaa, P., Eriste, E., Njunkova, O., Pokras, L., Jornvall, H., and Sillard, R. (2002) Brain-specific metallothionein-3 has higher metal-binding capacity than ubiquitous metallothioneins and binds metals noncooperatively, *Biochemistry 41*, 6158-6163.
15. Briggs, R. W., and Armitage, I. M. (1982) Evidence for site-selective metal binding in calf liver metallothionein, *J. Biol. Chem. 257*, 1259-1262.
16. Salgado, M. T., and Stillman, M. J. (2004) Cu^+ distribution in metallothionein fragments, *Biochem. Biophys. Res. Commun. 318*, 73-80.
17. Hagrman, D., Goodisman, J., Dabrowiak, J. C., and Souid, A.-K. (2003) Kinetic study on the reaction of cisplatin with metallothionein, *Drug Metab. Dispos. 31*, 916-923.
18. Karotki, A. V., and Vasak, M. (2009) Reaction of human metallothionein-3 with cisplatin and transplatin, *J. Biol. Inorg. Chem. 14*, 1129-1138.
19. Casini, A., Karotki, A., Gabbiani, C., Rugi, F., Vasak, M., Messori, L., and Dyson, P. J. (2009) Reactivity of an antimetastatic organometallic ruthenium compound with metallothionein-2: Relevance to the mechanism of action, *Metallomics 1*, 434-441.
20. Good, M., Hollenstein, R., Sadler, P. J., and Vasak, M. (1988) ^{113}Cd NMR studies on metal-thiolate cluster formation in rabbit Cd(II)-metallothionein: Evidence for a pH dependence, *Biochemistry 27*, 7163-7166.
21. Vasak, M. (1980) Spectroscopic studies on cobalt(II) metallothionein: Evidence for pseudotetrahedral metal coordination, *J. Am. Chem. Soc. 102*, 3953-3955.
22. Rigby-Duncan, K. E., Kirby, C. W., and Stillman, M. J. (2008) Metal exchange in metallothioneins - a novel structurally significant Cd_5 species in the alpha domain of human metallothionein 1a *FEBS J. 275*, 2227-2239.
23. Sutherland, D. E. K., Willans, M. J., and Stillman, M. J. (2012) Single domain metallothioneins: Supermetalation of human MT 1a, *J. Am. Chem. Soc. 134*, 3290-3299.
24. Sutherland, D. E. K., Willans, M. J., and Stillman, M. J. (2010) Supermetalation of the β domain of human metallothionein 1a, *Biochemistry 49*, 3593-3601.

25. Chan, J., Huang, Z., Watt, I., Kille, P., and Stillman, M. J. (2007) Characterization of the conformational changes in recombinant human metallothioneins using ESI-MS and molecular modeling, *Can. J. Chem. 85*, 898-912.
26. Kang, Y. J. (2006) Metallothionein redox cycle and function, *Exp. Biol. Med. 231*, 1459-1467.
27. Meloni, G., Polanski, T., Braun, O., and Vasak, M. (2009) Effects of Zn^{2+}, Ca^{2+}, and Mg^{2+} on the structure of Zn_7metallothionein-3: Evidence for an additional zinc binding site, *Biochemistry 48*, 5700-5707.

VITA

Name: Duncan Ewan Keith Sutherland

Post-Secondary Education and Degrees

Ph. D., Chemistry (September 2007 – April 2012)

The University of Western Ontario (UWO), London, Ontario, Canada

Hons. B. Sc., Biochemistry and Chemistry (September 2003 – April 2007)

The University of Western Ontario (UWO), London, Ontario, Canada (Gold Medal)

Publications

1. **Sutherland, D.E.K.,** Summers, K.L., Stillman, M.J. (**2012**) Single domain metallothioneins: Evidence for the onset of clustered metal binding domains. (In preparation)

2. **Sutherland, D.E.K.,** Summers, K.L., Stillman, M.J. (**2012**) Noncooperative metalation of metallothionein 1a and its isolated domains. (In preparation).

3. **Sutherland, D.E.K.,** Willans, M.J., Stillman, M.J. (**2012**) Single domain metallothioneins: Supermetalation of human MT 1a. *J. Am. Chem. Soc*, 134: 3290-3299.

4. **Sutherland, D.E.K.**, Stillman, M.J. (**2011**) Mammalian Metallothioneins. In Brain Diseases and Metalloproteins (Brown, D., Davies, P. Eds.) Pan Stanford Publishing, Chicago. [In Press pg. 1-58; **ISBN:** 9789814316019]

5. Kaluarachchi, H., Siebel, J.F., Kaluarachchi-Duffy, S., Krecisz, S., **Sutherland, D.E.K.**, Stillman, M.J., Zamble, D.B. (**2011**) Metal selectivity of the *Escherichia coli* nickel metallochaperone, SlyD, *Biochemistry*, 50:10666-10677.

6. **Sutherland, D.E.K.**, Stillman, M.J. (**2011**) The “magic numbers” of metallothionein, *Metallomics*, 3:444-463.
    - One of the top ten most-downloaded Metallomics articles in 2011.

7. **Sutherland, D.E.K.**, Willans, M.J., Stillman, M.J. (**2010**) Supermetalation of the β domain of human metallothionein 1a, *Biochemistry*, 49:3593-3601.

8. Xie, F., **Sutherland, D.E.K.**, Stillman, M.J., Ogawa, M.Y. (**2010**) Cu(I) binding properties of a designed metalloprotein, *J. Inorg. Biochem.*, 104: 261-267.

9. Kaluarachchi, H., **Sutherland, D.E.K.**, Young, A., Pickering, I.J., Stillman, M.J., Zamble, D.B. (**2009**) The Ni(II)-binding properties of the metallochaperone SlyD, *J. Am. Chem. Soc.*, 131:18489-18500.

10. **Sutherland, D.E.K.**, Stillman, M.J. (**2008**) Noncooperative cadmium(II) binding to human metallothionein 1a, *Biochem. Biophys. Res. Commun.*, 372: 840-844.

Honours and Awards

- Natural Sciences and Engineering Research Council (NSERC) Canada Graduate Scholarship Doctoral (May 2009-April 2012)
- Graduate Thesis Research Award (2011)
- 2004 CSC Travel Award (2009)
- SBIC Student Travel Grant (2009)
- Western Fund Ontario Graduate Scholarships (September 2008- August 2009)
- Ontario Graduate Scholarship (September 2007- August 2008)
- The University of Western Ontario Gold Medal: Biochemistry and Chemistry (2007)
- Biochemistry Summer Scholarship (2006)
- NSERC Undergraduate Student Research Award (2005-2007)
- UWO Entrance Scholarship (2003)

Related Work Experience

Teaching Assistant (September 2007 – December 2008)

Department of Chemistry, *The* University *of* Western Ontario, London, Ontario

Research Assistant (May - August 2007, NSERC USRA)

Department of Chemistry, *The* University *of* Western Ontario, London, Ontario

Supervisor: M. J. Stillman

Research Assistant (May - August 2006, Biochemistry Summer Scholarship)

Department of Biochemistry, *The* University *of* Western Ontario, London, Ontario

Supervisor: Dr. J. W. Y. Choy

Research Assistant (May - August 2005, NSERC USRA)

Department of Chemistry, *The* University *of* Western Ontario, London, Ontario

Supervisor: Dr. J. P. Guthrie

Conference Papers

1. *Supermetalation of Metallothionien 1a: Evidence for the existence of a low affinity* 8^{th} Zn^{2+}/Cd^{2+} *binding site* Sutherland, D.E.K. and Stillman, M.J., 15^{th} International Conference on Biological Inorganic Chemistry (ICBIC-15), Vancouver, BC, Canada, August 7 – 12, 2011.

2. *Supermetalation of Metallothionien 1a: Evidence for the existence of a low affinity* ^{8th} Z^{n2+}/C^{d2+} *binding site* Sutherland, D.E.K. and Stillman, M.J., The ^{3rd} Georgian Bay International Conference on Bioinorganic Chemistry, Parry Sound, ON, Canada, May 31 – June 3, 2011.

3. *Probing domain specificity using isolated metallothionein fragments* Summers, K.L., Sutherland, D.E.K. and Stillman, M.J., The 3^{rd} Georgian Bay International Conference on Bioinorganic Chemistry, Parry Sound, ON, Canada, May 31 – June 3, 2011.

4. *Acidic transition of a blue copper protein, pseudoazurin* Nihei, Y., Sutherland, D.E.K., Stillman, M.J. and Kozhuma, T., 48^{th} Annual Meeting of the Biophysical Society of Japan (BSJ48), Sendai, Miyagi Prefecture, Japan, September 20– 22, 2010.

5. *NMR Analysis of the β-domain of Human Metallothionein: Evidence for Supermetalation* Sutherland, D.E.K., Duncan, K.E.R., Willans, M.J. and Stillman, M.J., Gordon Research Seminar, Ventura, California, United States of America, February 4 – 7, 2010.

6. *Noncooperative cadmium(II) binding to human metallothionein* Sutherland, D.E.K., Duncan, K.E.R. and Stillman, M.J., 14th International Conference on Biological Inorganic Chemistry, Nagoya, Aichi Prefecture, Japan, July 15 – 30, 2009.

7. *Metalation properties of β- and βα- human metallothionein* Sutherland, D.E.K., Duncan, K.E.R. and Stillman, M.J., The 2nd Georgian Bay International Conference on Bioinorganic Chemistry, Parry Sound, ON, Canada, May 26 – 29, 2009.

8. *Noncooperative metalation in metallothioneins* Sutherland, D.E.K. and Stillman, M.J. Inorganic Discussion Week, St. Catharines, ON, Canada, Nov. 28 – 30, 2008.

9. *Metal thiolate cluster motifs in the protein metallothionein* Sutherland, D.E.K. and Stillman, M.J. Tohoku University Global Center of Excellence (COE) Summer School, Sendai, Miyagi Prefecture, Japan, August 18 – 20, 2008.

10. *Non-cooperative binding of cadmium to the beta domain of human metallothionein* Sutherland, D.E.K. and Stillman, M.J. Inorganic Discussion Week, Toronto, ON, Canada, Nov. 2 – 4, 2007.

11. *Novel Cd5- Species Formed In The Alpha Domain of Human Metallothionein 1a* Sutherland, D.E.K., Rigby Duncan, K.E., Kirby, C.W. and Stillman, M.J. The 1st Georgian Bay International Conference on Bioinorganic Chemistry, Parry Sound, ON, Canada, May 22 – 25, 2007.